BMR JOURNAL

OF AUSTRALIAN GEOLOGY & GEOPHYSICS

VOLUME 13 NUMBER 4

1993

BMR JOURNAL

OF AUSTRALIAN GEOLOGY & GEOPHYSICS

VOLUME 13 NUMBER 4 FEBRUARY 1993

CONTENTS

Editor, BMR Journal: Bernadette Hince
Cover design by Saimonne Bissett
Figures prepared by AGSO Cartographic Services Unit unless otherwise indicated
Prepared for publication by Lin Kay

AUSTRALIAN GOVERNMENT PUBLISHING SERVICE CANBERRA 1993

ISSN 0312-9608

Month of issue: February 1993

Subscriptions to the BMR Journal are available through the Australian Geological Survey Organisation (GPO Box 378, Canberra ACT 2601; tel. 06 249 9642, fax 06 257 6466) or through the Australian Government Publishing Service (Mail Order Sales, GPO Box 84, Canberra ACT 2601; tel. 06 295 4485).

Other matters concerning the Journal should be sent to the Editor, BMR Journal.

Printed in Australia by A. J. Law, Commonwealth Government Printer, Canberra

BMR Journal of Australian Geology & Geophysics, 13, 275–279

Depth phases from local earthquakes

Günter Bock[1]

Synthetic seismogram modelling and observations suggest that depth phases from local crustal earthquakes are of the type sX, where X stands for P_g, P_n, and the reflections from the crust-mantle boundary, mainly P_MP and S_MS. Depth phases of the type pX generally have much smaller amplitudes and are unlikely to stand out in seismograms. The differential times sX–X provide a very good control of focal depth. Examples of earthquakes that occurred in May and June 1991 in an area northwest of Kempsey (New South Wales) and in September 1991 near St George (Queensland) indicate that their foci were in the uppermost crust, at depths of between 2 and 3 km.

Introduction

Focal depths of Australian earthquakes are usually poorly constrained. Most, if not all earthquakes have their foci in the upper crust, at depths not deeper than about 20 km. Good depth control is normally provided by data of stations that are located close to the epicentre. This favourable condition is rarely met in Australia.

Accurate depth estimates have been obtained for large earthquakes and some of their foreshock and aftershock sequences in central and western Australia using waveform analysis of local and teleseismic seismograms and data of temporary seismic networks (Langston, 1987; Fredrich & others, 1988; Bowman & others, 1990; Choy & Bowman, 1990). Langston (1987) used the depth phase sP_g and the ratio Rg/S_g observed at distances of less than 100 km to constrain focal depths of events in the 1968 Meckering earthquake sequence. He showed that most foreshocks and aftershocks occurred within 2 km of the surface.

Most weak earthquakes in Australia usually do not attract attention far beyond the realm of routine interpretation. In the absence of reliable constraints, focal depths are often fixed to a value chosen by the interpreter. An improved knowledge of the depth distribution of earthquakes, however, is of considerable importance in seismotectonic studies of the Australian continent.

It is the purpose of this paper to discuss depth-sensitive phases from crustal earthquakes at distances to several hundred kilometres, which may provide a much improved depth control over what is possible with first arrival time data only. The successful identification of such phases is considerably aided, and in the experience of the author only possible in many cases, if digital seismograms are available. In this paper, synthetic seismograms are presented that tell us which depth-sensitive phases we may expect to see on seismograms. Examples from the Armidale (New South Wales) seismograph station, where a PC-based data logger has been successfully tested for more than a year, are then discussed.

Synthetic seismograms

Synthetic seismograms have been calculated for a shear dislocation point source using the reflectivity method of Kind (1978, 1979a). The crustal gradient model used is shown in Table 1. A crustal thickness of 33 km is assumed which is based on seismic refraction studies in the New England Orogen described by Finlayson & Collins (in press). Synthetic seismogram sections are shown (Figs 1, 2) for two different distance ranges.

Seismograms from a 3 km deep source (Fig. 1) are shown for the distance range from 70 to 140 km. A dip slip shear dislocation was assumed along a plane dipping at 45° towards the receivers. The crustal phase P_g is the first arrival followed about 0.6 s later by a second phase which, based on travel time, is the surface reflection sP_g. This is a phase which has left the focus upwards as an S wave, been converted at the surface to a P wave, and then has travelled the remaining path to the receivers as P entirely confined to the upper crust.

Following the P_g wavegroup another set of phases arrives between 2 s and 5 s reduced time. The first phase has the travel time of the Moho reflection P_MP. Its amplitude is

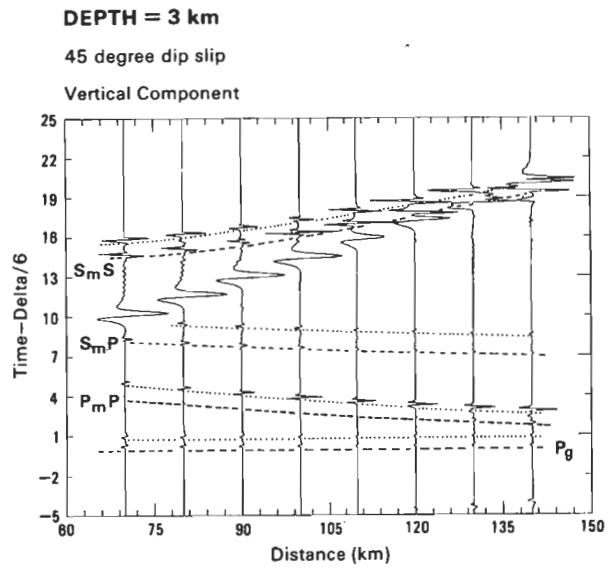

Figure 1. Synthetic seismograms for a 45° dip slip point source at 3 km depth.
The arrival times of various crustal phases have been marked by the dashed lines; the associated depth phases of type sX, where X stands for P_g, P_MP, S_MP or S_MS are marked by dotted lines.

Table 1. Crustal gradient model.

Depth (km)	*P-wave velocity (km/s)*	*S-wave velocity (km/s)*	*Density (g/cc)*	*QP*	*QS*
0	6.00	3.53	2.53	1000	444
12.5	6.00	3.53	2.53	1000	444
22	6.15	3.61	2.58	1000	444
33	6.45	3.79	2.70	1000	444
33	7.70	4.46	3.17	1000	444
45	7.80	4.50	3.21	1000	444
60	8.08	4.66	3.31	1000	444
92	8.12	4.69	3.33	1000	444

[1] GeoForschungsZentrum, Telegrafenberg A6, O-1561 Potsdam, Germany; formerly Department of Geology and Geophysics, University of New England, Armidale NSW 2351

small because P wave radiation is weak in the takeoff direction of P_MP for the 45° dip slip source used in the calculations. About 1 s after P_MP a second, large-amplitude phase arrives. Its arrival time suggests that it is the surface reflection sP_MP which leaves the focus upwards as an S wave, is converted at the surface to P, and then follows along the P_MP path to the receivers. The amplitude of P_MP is sensitive to the radiation pattern. Assuming a vertical strike slip dislocation, for example, P_MP and sP_MP reach similar amplitudes.

Another reflection from the crust-mantle boundary and associated depth phase shows up in Figure 1 between 7 s and 10 s reduced time. The earlier phase fits the travel time of S_MP while the phase arriving about 1.5 s after S_MP is the surface reflection sS_MP.

The Moho reflection S_MS and associated depth phase sS_MS shows up between 15 s and 20 s reduced time; it interferes at larger distances with the surface wave arrival R_g.

The synthetic seismogram section in Figure 2 covers the distance range from 250 to 450 km. A vertical strike slip dislocation source at 6 km depth was assumed, with the receivers located at 45° azimuth to the strike of the fault plane. The first arrivals are upper mantle phases (P_n) that are followed about 2.5 s later by a second phase which fits the travel time for the surface reflection sP_n. The phase sP_n has been discussed by other authors (Kind, 1979b; Zonno & Kind, 1984; Barbano & others, 1985), and has been used by Bock (in press) to constrain the focal depth of the 1990 Woods Reef earthquake. If sP_n can be correctly identified it provides a stringent constraint on focal depth. As noted by Bock (in press) the amplitude ratio P_n/sP_n depends strongly on the source mechanism. For a 45° dip slip source, for example, the P_n amplitude becomes quite small compared to sP_n. In this case P_n may go unnoticed, especially for weaker earthquakes, and sP_n may be picked as first arrival and erroneously interpreted as P_n.

Other depth phases in Figure 2 are associated with P_g, S_n and multiple reflections from the crust-mantle boundary.

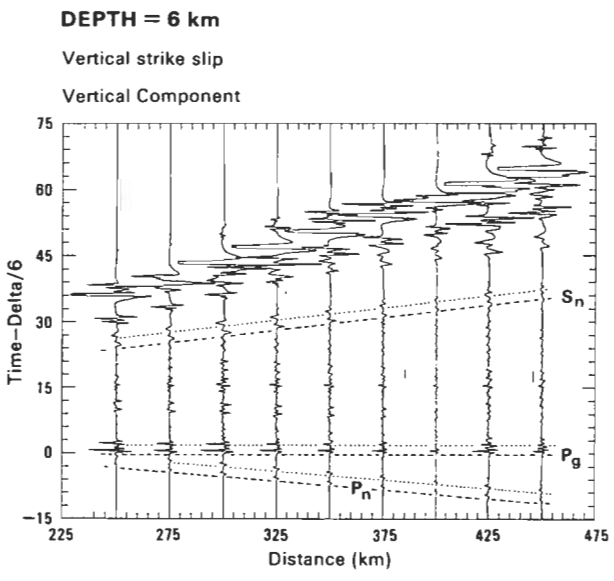

Figure 2. Synthetic seismograms for a strike slip point source along a vertical plane at 6 km depth.
Dotted lines indicate depth phases of type sX associated with P_n, P_g and S_n.

Some of these phases are identified in Figure 2. The occurrence of multiple reflections from the Moho depends on many factors such as crustal thickness, crustal velocities and sharpness of the crust-mantle transition. Their actual arrival times and amplitudes are clearly subject to regional variations. The differential times between these phases and associated depth phases however are much less dependent on regional variations in crustal structure; they are therefore well suited as depth constraint if they can be reliably identified.

Note that in all the cases discussed in this section the depth phases are of the type sX, where X stands for P_g, P_n, or reflections from the Moho. Depth phases of the type pX are unlikely to stand out with significant amplitude because the P–P reflection coefficient for the free surface is small over a range of angles of incidence (Aki & Richards, 1980, 142). The S–P reflection coefficient of the free surface, on the other hand, reaches large values particularly if the angle of incidence is near critical.

Examples

Armidale seismograph

In this section, recordings of several earthquakes that occurred in eastern Australia in 1991 are discussed with regard to the presence of depth phases. The observations are from the vertical-component, short-period Armidale seismograph which is part of the National Seismograph Network operated by the Australian Seismological Centre (ASC). The seismometer was located until September 1991 in the Cooney (COO) tunnel at 30.568°S, 151.884°E, approximately 25 km east of Armidale. In September 1991 it was shifted to a new location at Newholme, about 7 km north of Armidale (ARMA, 30.420°S, 151.628°E). A telephone line has been used to transmit the seismometer signal to the recording site in the Department of Geology and Geophysics of the University of New England where seismograms are routinely recorded as Helicorder chart records.

Since April 1991, recordings of most earthquakes have been obtained also as digital records. This was achieved by digitising the output of the demodulator at the recording site using a 12 bit analogue-digital converter (ADC) connected to an AT compatible microcomputer. A data acquisition program written in Quickbasic by Boggs (1991) is based on the comparison of short term average (STA) and long term average (LTA) values of the seismic signal as described by McEvilly & Majer (1982). If the STA exceeds the LTA by a prescribed value, an event is indicated and the data are stored with a sample frequency of 50 Hz to hard disk. The dynamic range of the digital record is of course limited by the analogue recording system. Furthermore, data are recorded over a narrow frequency band because of the filter settings for the analogue system. Therefore, the quality of the Armidale digital records is poor by comparison to those obtained from state of the art broadband seismographs. Nevertheless, the availability of a digitised copy of the analogue seismogram leads to a dramatic improvement in data quality, and much more information can be extracted from the digital records than is possible with chart recordings as demonstrated by the following examples.

The 1991 Kempsey earthquakes

The first example is from a series of three earthquakes that occurred in 1991 on May 21, 0324 Universal Coordinated

Time (UTC), May 23, 2134 UTC, and June 11, 0740 UTC. All events were recorded by the Cooney station (COO). The May 21 event was the strongest (M_L = 2.3) in the series. Its epicentre was located at 31.0°S and 152.6°E, some 25 km northwest of Kempsey (New South Wales). This location, however, is very poorly constrained.

The digital COO seismograms of the events that are shown in Figure 3 are very similar, which suggests that the two later events were located close to the first one. Several distinct phases are visible. The largest-amplitude phase is the surface wave arrival marked *Rg*. Its signal contains relatively low frequencies, and there is an indication that higher-frequency signals are superimposed on the *Rg*

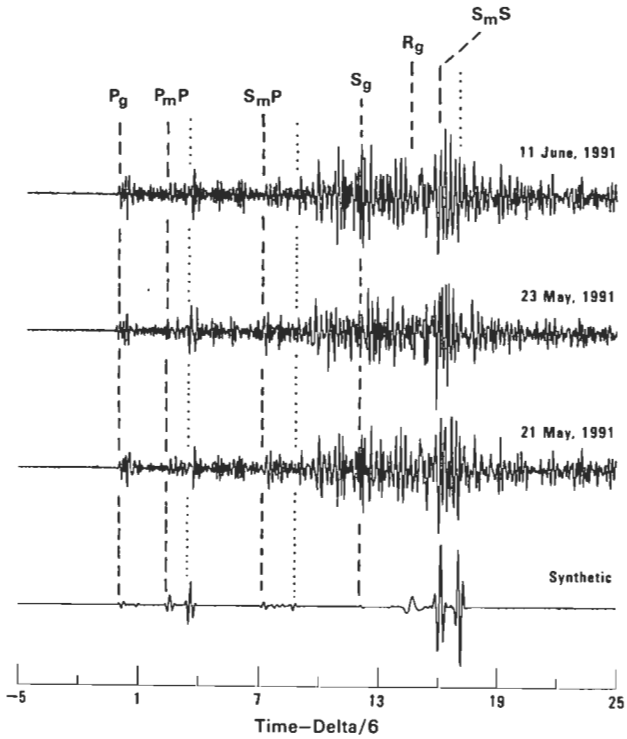

Figure 3. Observed COO seismograms (top traces) of three earthquakes that took place northwest of Kempsey in May/June 1991, and synthetic (bottom trace) calculated for the model in Table 1 and 3 km focal depth, modified with the crust–mantle boundary at 31 km depth.

wavetrain. This is confirmed by the bandpass filtered records shown in Figure 4. Based on the comparison of observed with synthetic seismograms several conclusions can be drawn.

The epicentral distance from COO was about 100 km. This follows mainly from the arrival times of *P* and *Rg*. The crustal thickness in the model used to calculate the synthetics was slightly reduced to 31 km. This provides a good fit to the arrival times of Moho reflections (Figs 3, 4). The time differences between Moho reflections and their associated depth phases suggest that focal depth was about 3 km for these events. An attempt was made to put constraints on the focal mechanism of the events using amplitudes of various phases. Note that the phase interpreted as P_MP has quite a small amplitude relative to sP_MP. Synthetic seismogram modelling suggests that this is indicative of dip slip faulting along an inclined fault plane. The amplitudes of S_MS and sS_MS, on the other hand, are

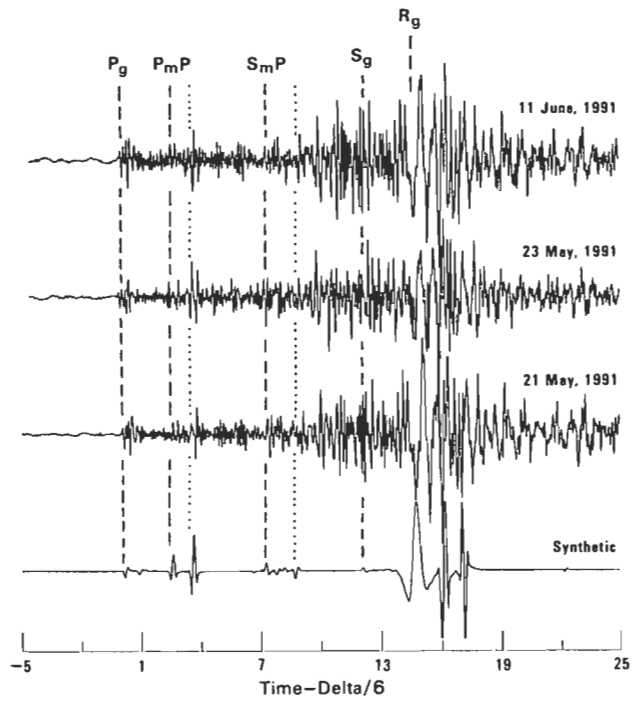

Figure 4. Bandpass filtered (2.5–11 Hz) records of the seismograms in Figure 3.

approximately equal (Fig. 4). I searched the full range of dip and strike angles of fault planes to find those that are consistent with the observed amplitudes of P_MP, sP_MP, S_MS, sS_MS, and P_g. Pure dip slip motion was assumed, and an epicentre-to-station azimuth of 300. The best fitting fault plane strikes N20°E and dips 34° to the east, with the conjugate plane striking 200° and dipping 56° to the west. The synthetic traces in Figures 3 and 4 were obtained for this fault orientation.

The September 1991 St George (Queensland) earthquakes

Two earthquakes took place northeast of St George (Queensland) in September 1991, the first one (M_L = 4.3) on Sept. 24, 0436 UTC, and the second one (M_L = 4.0) on Sept. 28, 1505 UTC. ASC located the events at 27.52°S, 149.14°E and 27.72°S, 148.98°E, respectively. Focal depths were given as 10 km for the first, and 5 km for the second event. The ARMA digital records of the events are shown in Figure 5. The epicentral distance was about 400 km. The phases P_n, P_g, and S_n are marked in Figure 5; they correlate well with the synthetic. Figure 6 shows the P_n and P_g phases at an expanded timescale. It is obvious that P_n is followed about 0.6 s later by a larger-amplitude phase. If the first phase is P_n and the second one sP_n then a focal depth of about 2 km is indicated for both events, which significantly differs from the ASC values.

The synthetic seismogram (Figs 5, 6) does not contain the high-frequency components that are present in the observed seismograms. The reflectivity method becomes computationally prohibitive for high frequencies. The point to be made here is the fact that sP_n is observable.

The epicentral area of the St George earthquakes lies in the

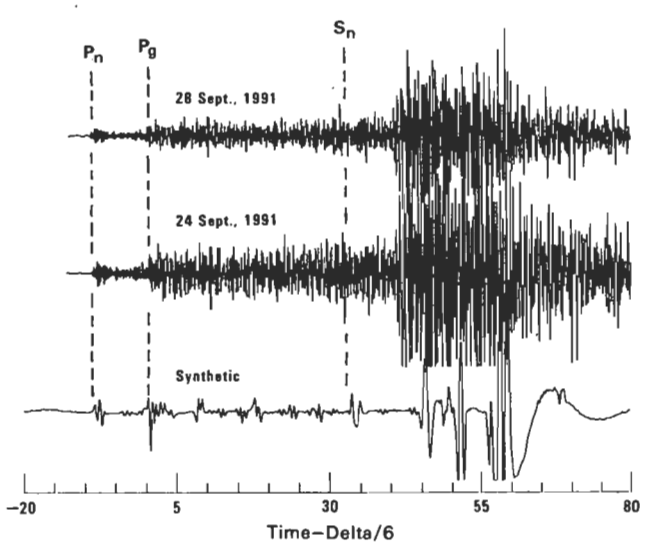

Figure 5. Observed ARMA seismograms (top traces) of the St George earthquakes that occurred in September 1991 and synthetic (bottom trace) calculated for 2 km focal depth.

Surat Basin near Riverslea. Sediment thicknesses there are about 1.5 km (Petroleum Resources Assessment and Development Subprogram, 1990). This suggests that the St George earthquakes took place near the top of the basement underlying the basin sediments. I investigated the question of whether the presumed phase sP_n could be in fact a reflection from the sediment-basement interface rather than from the surface. This however is unlikely because reasonable reflection coefficients of the sediment-basement interface are too small to produce the large-amplitude arrivals observed.

The P_g wavetrain, by comparison, is relatively complex in both observed and synthetic seismograms. It would be quite difficult to identify reliably depth phases in the P_g coda. The same applies to the Lg wavetrain. The presence of significant scattered energy following the P_g and Lg arrivals makes it impossible to identify any reflections from the Moho and associated depth phases. It is therefore concluded that, if only vertical-component records from a single station are available, the phase sP_n is probably the only useful body wave phase which allows us to put constraints on focal depth from recordings at several hundred kilometres distance.

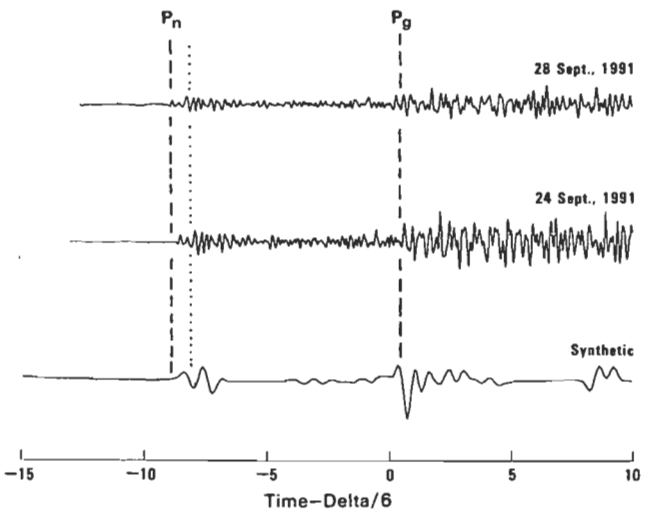

Figure 6. The P_n and P_g wavetrains of Figure 5 in close up view.

Discussion and summary

Synthetic seismograms presented in this paper suggest that a number of depth phases can be observed from local earthquakes at distances up to several hundred kilometres. At epicentral distances of about 100 km or less, reflections from the crust–mantle boundary and associated surface reflections may show up in the seismograms. To be observed over a wide distance range, the crust–mantle transition must be sharp compared with the wavelength of the signals. If the transition is smooth, observable reflections may be restricted to distances near critical. The depth phases are mainly of the type sX, where X represents the Moho reflections P_MP, S_MP, or S_MS. Depth phases of the type pX are negligible in amplitude because the P–P reflection coefficient of the free surface is much smaller than the S–P coefficient. Differential times sX–X are shown plotted against focal depth (Fig. 7) for the crustal model in Table 1.

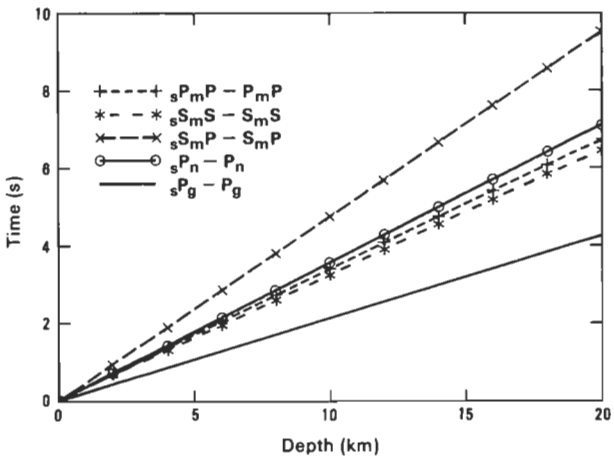

Figure 7. Differential times $sX - X$ for the phases marked in the legend box against focal depth.

Synthetic seismograms suggest that another observable depth phase may be sP_g This phase is less sensitive to focal depth than sX as the differential time $sP_g - P_g$ reaches only about half the values of the $sX - X$ times associated with Moho reflections (Fig. 7).

At epicentral distances where P_n is the first arrival, the most useful depth phase is sP_n. To be observed at single stations, the time difference $P_g - P_n$ must be large enough so that sP_n arrives well before P_g This means that the epicentral distance must be well beyond the distance at which P_g is overtaken by P_n. The differential $sP_n - P_n$ times are also shown in Figure 7.

The method of synthetic seismogram comparison has been applied to earthquakes that occurred in 1991 near Kempsey (New South Wales) and St George (Queensland). Very shallow depths between 2 and 3 km are indicated for these events, while the 1990 Woods Reef earthquake investigated in an earlier study by Bock (in press) was located at a greater depth, near 12 km. A prerequisite for the success of the method described in this paper was the availability

of digital images of the Helicorder chart recordings of the Armidale seismograph. Without this, identification of the various phases contained in the *P* wave coda would have been impossible. The usage of depth-sensitive phases as discussed in this paper and also by Langston (1987) may eventually lead to a much improved picture of the depth distribution of Australian earthquakes

Acknowledgements

I am grateful to Frank Ludbey who installed the ADC and made it work, to Russell Cuthbertson who drew my attention to the Petroleum Resources Assessment paper, and to Riki Davidson who critically read the manuscript. Marion Leiba from the Australian Seismological Centre is thanked for providing the epicentral location of the May 21 1991 Kempsey earthquake. This research was supported by an Internal Research Grant from the Department of Geology and Geophysics of the University of New England.

References

Aki, K. & Richards, P.G., 1980 — Quantitative seismology theory and methods. Vol. 1. *Freeman and Co., San Francisco.*

Barbano, M.S., Kind, R. & Zonno, G., 1985 — Focal parameters of some Friuli earthquakes (1976–1979) using complete theoretical seismograms. *Journal of Geophysics* 58, 175–182.

Bock, G., in press — The Woods Reef (New South Wales) earthquake of 14 November 1990: focal mechanism derived from amplitude ratios and synthetic seismograms. *Australian Journal of Earth Sciences.*

Boggs, D., 1991 — A computer based earthquake record acquisition system. *Department of Geology and Geophysics, University of New England, unpublished project report.*

Bowman, J.R., Gibson, G. & Jones, T., 1990 — Aftershocks of the January 22, 1988 Tennant Creek, Australia intraplate earthquakes: evidence for a complex fault geometry. *Geophysical Journal International* 100, 87–97.

Choy, G.L. & Bowman, J.R., 1990 — Rupture process of a multiple main shock sequence: analysis of teleseismic, local, and field observations of the Tennant Creek, Australia, earthquakes of January 22, 1988. *Journal of Geophysical Research* 95, 6867–6882.

Finlayson, D.M. & Collins, C.D.N., in press — Lithospheric velocity structures under New England, northeastern New South Wales — contrasts with other areas of the Tasman Orogen. *Australian Journal of Earth Sciences.*

Fredrich, J., McCaffrey, R. & Denham, D., 1988 — Source parameters of seven large Australian earthquakes determined by body waveform inversion. *Geophysical Journal* 95, 1–13.

Kind, R., 1978 — The reflectivity method for a buried source. *Journal of Geophysics* 44, 603–612.

Kind, R., 1979a — Observations of sPn from Swabian Alb earthquakes at the GRF array. *Journal of Geophysics* 45, 337–340.

Kind, R., 1979b — Extensions of the reflectivity method. *Journal of Geophysics* 45, 373–380.

Langston, C.A., 1987 — Depth of faulting during the 1968 Meckering, Australia, earthquake sequence determined from waveform analysis of local seismograms. *Journal of Geophysical Research* 92, 11561–11574.

McEvilly, T.V. & Majer, E.L., 1982 — ASP: an automated seismic processor for microearthquake networks. *Bulletin of the Seismological Society of America* 72, 303–325.

Petroleum Resources Assessment and Development Subprogram, 1990 — Petroleum Resources of Queensland (Review to June 30, 1989). *Queensland Department of Resource Industry Review Series, Department of Resource Industries, Queensland.*

Zonno, G. & Kind, R., 1984 — Depth determination of North Italian earthquakes using Gräfenberg data. *Bulletin of the Seismological Society of America* 74, 1645–1659.

BMR Journal of Australian Geology & Geophysics, 13, 281–292

Quaternary and modern environments of the Van Diemen Rise, Timor Sea, and potential effects of additional petroleum exploration activity

Ian H. Lavering[1]

Environmental baseline data are required for Australia's offshore areas before petroleum exploration. This has boosted demand for analysis and interpretation of the Quaternary evolution, modern geological processes and environmental features of the Australian continental shelf. One such area overlies the Van Diemen Rise on the Sahul Shelf in the eastern Timor Sea. Sea bottom sediments in the region are dominantly calcareous sand derived from skeletal carbonate material. A number of sinuous channel-like features cut through a series of terraces and banks which comprise the Van Diemen Rise. These features are the product of subaerial exposure and weathering of the underlying carbonate shelf during the last Quaternary glacial maximum. At about 18 000 BP sea level was ~120 m below the present shoreline, much of which was subjected to subaerial exposure and erosion. Only a narrow marine shelf existed close to the outermost edge of the present continental shelf. Shallow banks and shoals on this narrow shelf were the focus of significant coral reef growth. Calcrete concretions formed on the exposed land surface. Holocene transgression inundated the entire margin and shifted reef growth onto the shallowest parts of the flooded banks and terraces. Today sedimentation within the 50 m contour is entirely clastic and derived from wet-season river input. On the outer shelf foraminiferal calcarenites are being deposited. These become finer-grained and contain more planktonic components the greater the water depth. Silty clays and molluscan debris are accumulating in the sheltered channels between the banks and terraces of the Van Diemen Rise. Large foraminiferal and coralline algae dominate the shallow banks and rises. An assemblage dominated by *Halimeda* is growing on the outermost shelf edge banks. Seismic surveying and drilling are the main activities likely on the Van Diemen Rise. The short-term nature of these activities would cause no long-term impact on environmental conditions. They would cause minor short-term localised disturbance. Rock fragments from exploration drillsites would be dispersed by normal current and tidal action within a short period.

Introduction

Petroleum exploration and development activities in Australia have always been undertaken with an awareness of potential impact of such activity on ecosystems (cf. Warren, 1989). Environmental assessment work undertaken as part of the exploration process has included such elements as site surveys, bathymetric readings, oceanographic data, the documentation of relevant heritage sites and faunal surveys (cf. Holloway, 1988; Warren, 1989). Such surveys have gained increased public attention and the information they yield is needed to assess the effects of exploration operations on marine environments.

This paper outlines relevant Quaternary and modern features and processes which characterise that part of the Van Diemen Rise (Fig. 1) which is expected to be available for application in a future release round for exploration activity under the terms and conditions of the Petroleum (Submerged Lands) Act 1967. The area is termed 'vacant area' in Figure 1 and throughout this paper. It describes features by reference to their regional setting as well as their unique characteristics. Because of the intergrading nature of some of the sedimentological and ecological features of the Van Diemen Rise, reference is also made to relevant adjacent parts of the coastal zone.

The first regional geoscientific survey in tropical waters of the North West Shelf was undertaken in 1960-61 when the sea bottom sediments, morphology and subsurface structure were examined on the Sahul Shelf and in the Timor Trough by van Andel & Veevers (1967). An additional survey of the North West Shelf from the Sahul Shelf to North West Cape was undertaken by Jones (1973) who described sea bottom sediments of the continental shelf and upper slope, and the Quaternary geological evolution of the Australian North West margin. A similar survey was undertaken in the Arafura Sea by Jongsma (1974).

From the study of the Sahul Shelf undertaken by van Andel & Veevers (1967) several major morphological features were identified including a significant channel system present along the northern margin of the Van Diemen Rise which also separates it from the Sahul Rise to the west (Fig. 1).

[1] Petroleum Resource Assessment Program. Australian Bureau of Resource Sciences, GPO Box 378 Canberra, ACT 2601

Geomorphic features of the Van Diemen Rise

The Van Diemen Rise is overlain by water 100–>400 m deep. The central and southern parts of the area are a complex series of relatively shallow flat-topped banks (Fig. 1). Cutting through the banks are a series of sinuous channels and terraces which are the result of Late Pleistocene subaerial erosion (van Andel & Veevers, 1967; van der Kaars, 1991) (Fig. 2). Cross-correlation of such features allows for up to four base levels at which erosion and physical weathering processes have been active for short but significant periods (van Andel & Veevers, 1967). Whether the erosion results from nearshore marine, strandline or fluvially-dominated processes is not clear, although van der Kaars (1991) suggests that a relatively arid climate inferred from palynological information would favour marine or strandline processes.

Quaternary history of northern Australia

Palaeogeography

Previous shoreline positions on the Sahul Shelf west of the Van Diemen Rise at 110–130 m below sea level are identified by van Andel & Veevers (1967) and radiometrically dated by them as 18 000 BP, the period of the last glacial sea-level maximum. At that time the land area extended well across the current shelf and the present carbonate banks on the shelf edge, now at depths of 110–130 m below sea level, formed a string of islands seaward of the coastline. An area below sea level inland of the coast, the Bonaparte Depression, formed an estuarine embayment with a depth of up to about 18–28 m. This was connected to the sea by a number of narrow and sinuous channels up to 150 km long by 5 km wide. The orientation of the embayment and size of the channels connecting it

with the Timor Sea suggest that only a minor amount of seawater circulation was possible in the Bonaparte Depression. The presence of brackish-water bivalves in the embayment supports such a view (van Andel & Veevers, 1967).

Palynological data from the Timor Trough (van der Kaars, 1991) suggests that during the last glacial maximum (18 000 BP) emergent parts of the Sahul Shelf, including the Van Diemen Rise, were subject to a dry arid climate. Much of the region was covered by open grassland with

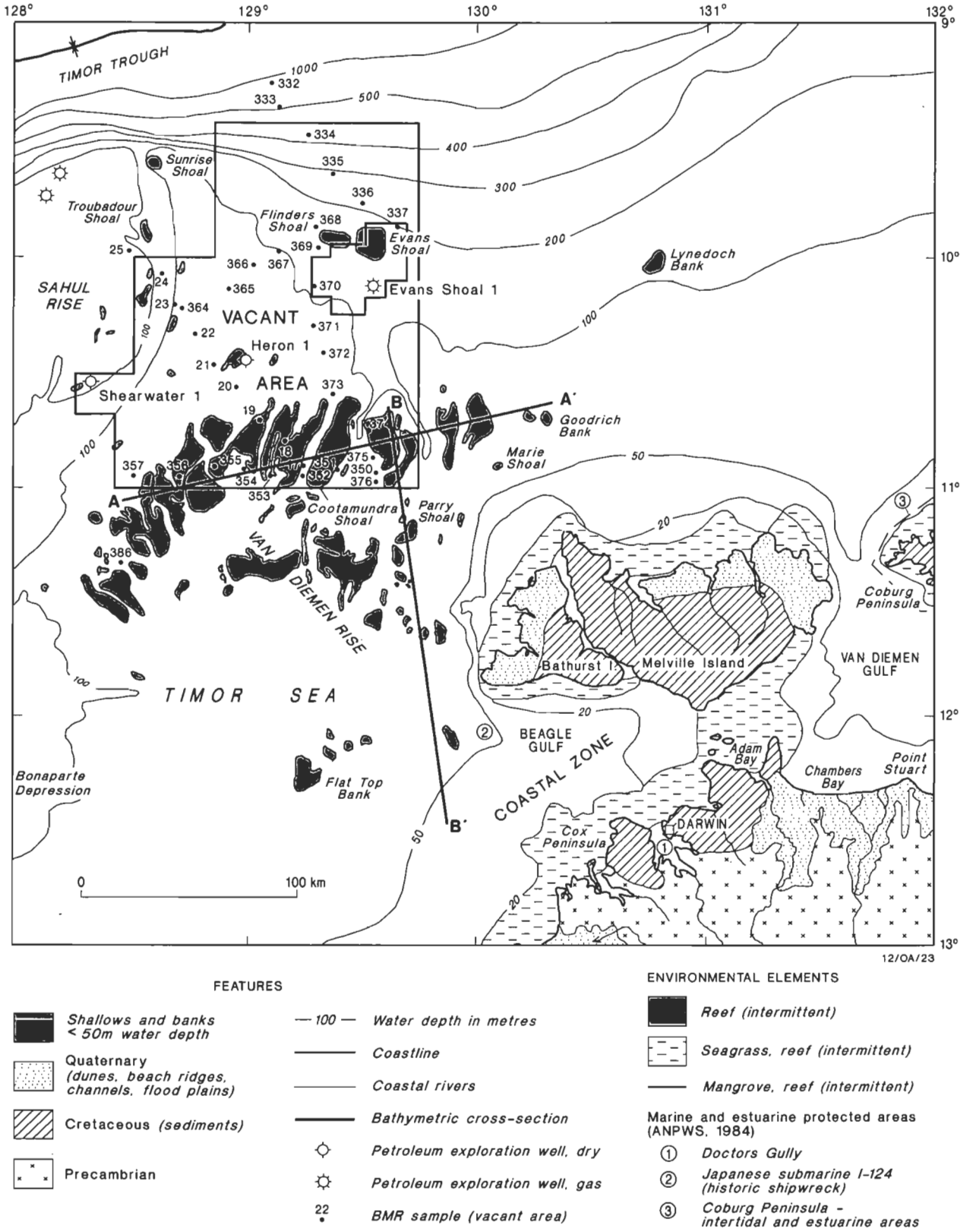

Figure 1. Location map of the Van Diemen Rise area, Timor Sea, showing bathymetry and simplified geology/geomorphology.

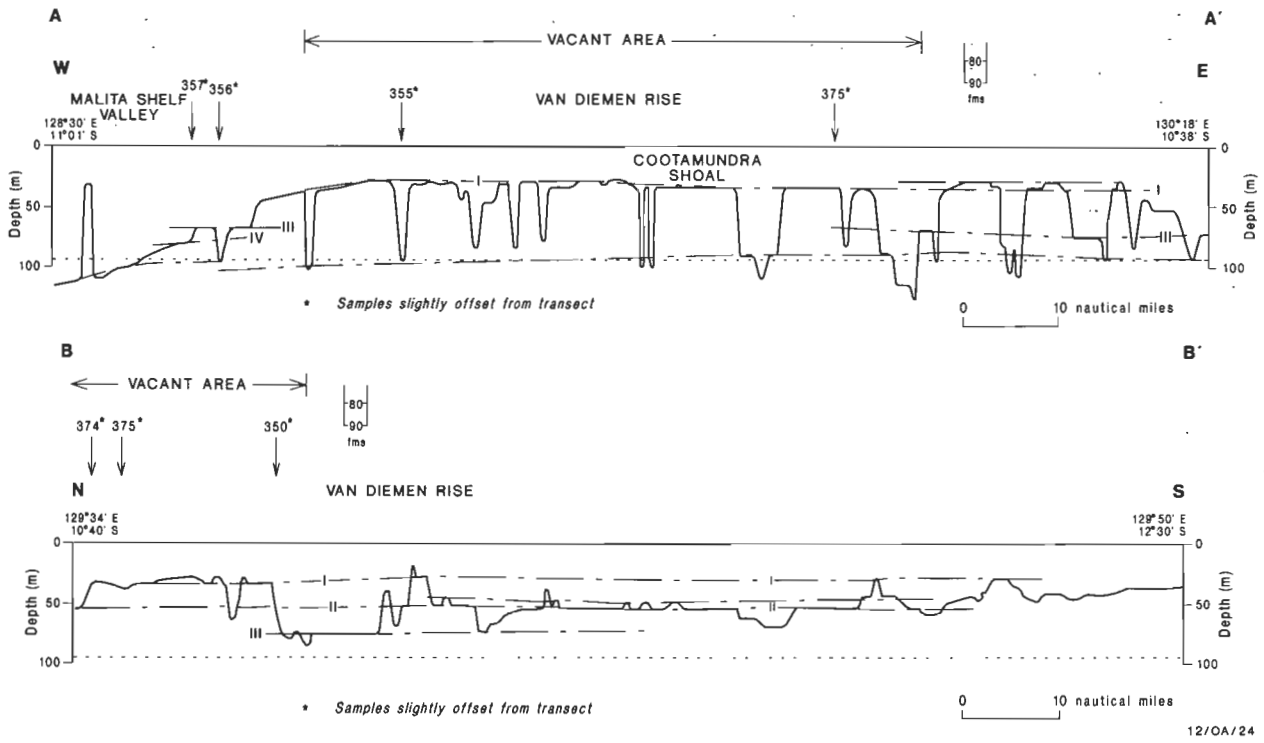

Figure 2. Cross-sections of sea bottom topography, Van Diemen Rise, Timor Sea.
Vertical exaggeration ×200.

eucalyptus woodlands in a narrow band close to the coastline (now 110–130 m subsea) and some mangrove forests in tidally-influenced estuaries.

The presence of Quaternary calcareous nodules ('calcrete') on what would have been land areas surrounding the Bonaparte Depression has been interpreted as evidence of formation in the soil profile and subsequent winnowing into fluvial lag deposits (van Andel & Veevers, 1967). After 18 000 and between 15 000 and 13 000 BP a rapid rise in sea level inundated most of the shelf, including the area surrounding the Bonaparte Embayment, to at least the level of the 55 m depth contour. Large tidal flats surrounded the embayment.

Open marine conditions followed additional inundation with banks and islands forming on the highest parts of the Van Diemen Rise. Close to the site of the present coastline sheets of quartz sand accumulated at the mouths of active drainage and river systems. Marine inundation of the Sahul Shelf appears to have facilitated the expansion of mangrove vegetation and associated supratidal chenopod salt-marsh vegetation (van der Kaars, 1991). A further rise in sea level at about 9 000 BP brought the shoreline to the 15 m depth contour with an outline similar to that of the present coast. This was followed by another rise in level to the present position.

Marine terraces

Jones (1973) correlated a wave-cut platform evident at a depth of approximately 120 m along the western part of the outer Sahul Shelf with a persistent scarp at this depth extending along the entire North West Shelf. Other features which Jones (1973), Jongsma (1974) and van Andel & Veevers (1967) attributed to strandline erosion on the North West Shelf are present at depths of 380 m and several at levels between 60 and 105 m. The 120 m scarp is correlated with the feature mapped at 102–143 m in the Timor Sea by van Andel & Veevers (1967), a scarp at 125 m in the Arafura Sea (Jongsma, 1974) and scarps at 100–150 m off the Great Barrier Reef (Maxwell, 1968). Evidence for the age of each of the features is noted by these authors.

Coastal features

Investigations of the relative ages of coastline dune systems by Lees & others (1990) suggested that they developed in an episodic fashion, with a first period of dune and chenier building between 81 000 and 171 000 BP, a second period between 8 500 and 7 000 BP and a third between 2 600 and 1 800 BP. The first date is similar to the inferred age of the oldest unconformity surface identified in offshore seismic records by Jongsma (1974). Each of the periods of dune building coincides with change to a drier climate — higher evaporation and lower precipitation. Reduced vegetation cover and seasonally persistent winds have resulted in greater dune mobility. Rising sea levels further contributed by eroding foredunes, initiating blow-outs and developing transgressive dune sequences (Lees & others, 1990).

The strandline units at Point Stuart on the coast of Van Diemens Gulf, east of Darwin, examined by Lees (1987), contain five chenier ridges which have formed in the last 1270 years. Major storms, over an 80 to 200 year frequency, appear to have built the five ridges closest to the coast. A further five ridges landwards of this set have a much lower proportion of carbonate and shelly material and differences between the two sets are explained by a major change in the pattern of sediment supply (Lees, 1987). The origin of the two distinct sets of chenier systems may be due to the switching of one river system from discharge into

Chambers Bay to Adam Bay and/or the alteration of the next river system to the east from a single channel to several discharge channels.

The dominant force forming the beach ridges at Point Stuart and others around the coastal fringes of northern Australia is storm waves whose bases reach deeper and further offshore than normal. Wave-winnowing can excavate shelly material and remove fine-grained sediments, allowing coarse-grained sediments and shelly debris to accumulate on the strandline or at storm-surge level landwards of the normal strandline (Lees, 1987, 1992).

Climate and oceanography

All of northern Australia's coastal regions have a monsoon climate, with a wet season during the northwest monsoon (summer) and a dry season from May to October during which the southeast trade winds prevail. Rainfall in the north can vary from 720 mm to 1920 mm (30 to 80 inches) a year. Mean temperatures in the wet season are in the high 20s to 30s (°C) with high humidity, down to 18–20°C in the dry season, with low humidity. Thunderstorms occur on average 85 days in summer in Darwin. The mean average evaporation rate is approximately twice the average annual rainfall (van Andel & Veevers, 1967).

The seasonality in temperature and wind regimes has a significant effect on the salinity levels in nearshore areas and water temperature. Much of the nearshore variation is related to the volume and sediment load of runoff from coastal river systems (Poiner & others, 1987). The marine coastal zone around Arnhem Land is less affected by the influx of riverine input than similar areas of the Joseph Bonaparte and Van Diemen Gulfs and Gulf of Carpentaria.

The Arafura and Timor Seas have a mean annual precipitation of 900 mm and a mean annual evaporation of 1716 mm. The southeast trade winds blow from April to November in the dry period, and monsoons from the northwest during December to March (wet season). Tropical cyclones lasting 12–24 hours occur in the period December to April. During these, wind velocities of 50–>90 knots develop, and can increase to as much as 140 knots. Squalls in the dry season rarely last longer than 3 hours and develop winds of 30–100 knots (van Andel & Veevers, 1967).

The southeast trade winds can generate moderate to rough seas, the main swell being from the southeast. During much of the monsoon season seas are calm and smooth except for the disturbance caused by tropical cyclones. Swells developed during cyclones come from the southwest, west and northwest (Division of National Mapping, 1986).

Humidity levels in major bays and coastal embayments such as the Gulf of Carpentaria and Joseph Bonaparte Gulf are high year round with an average relative humidity at 9 am of 80% in January and 70% in July (Division of National Mapping, 1986). Median annual rainfall in coastal parts of these regions is 800 mm per year with an intensity of 4 mm per hour. The year round average temperature is above 18°C (Division of National Mapping, 1986).

The seasonality in temperature and wind regimes has a significant effect on the salinity levels in nearshore areas of the Timor Sea. Such waters can vary in temperature by 10°C and have a salinity range of 12 g/kg (Poiner & others, 1987). Less variation is evident in offshore areas. Much of the nearshore variation is related to the volume and sediment load of runoff from coastal river systems. In the central part of major gulfs or embayments seasonal water temperatures vary by 5°C and have a salinity range of 3 g/kg. Water from the Coral and Arafura Seas can intrude into the Gulf of Carpentaria and Joseph Bonaparte Gulf and modify the local patterns (Poiner & others, 1987).

The sediments of the Sahul Shelf which underlie the Timor Sea are dominated by tidal influence; tidal range is 7.8 m at Wyndham in Cambridge Gulf (Lees, 1992). Associated tidal current velocities of 3.5 m/s are evident at the mouths of major tidally-influenced river systems such as the Ord River but decrease to 1.6 m/s along the inner shelf region (Lees, 1992). Tidal currents in the Timor Sea flow northeast to southwest, depending on coastline proximity and configuration. The southeasterly trade winds (April to November) drive the pattern of surface circulation but these surface circulation currents are generally weak and result in a net westward flow (Harris & others, 1991).

Sedimentation

Shelfal sedimentation

Van Andel & Veevers (1967) sampled the sea bed of the Van Diemen Rise as part of a major regional study of the Timor Sea. They collected and analysed some 35 sea bottom samples from within the Van Diemen Rise (Fig. 3). The sediments were predominantly of sand-size material, much of which consisted of skeletal carbonate. Calcarenites and clayey and silty calcarenites covered the banks, rises and channels of most of the vacant area identified in Figures 1 and 3. The coarsest calcarenites were found on the tops of banks within the Van Diemen Rise and the shelf edge banks such as Sunrise and Evans Shoals and Lynedoch Bank. The origin of such sedimentation is evident from the biofacies patterns identifed by van Andel & Veevers (1967).

Beyond shelf edge banks and towards the Timor Trough, clay and silt grade material is the dominant sea bottom sediment (van der Kaars, 1991). Some silty sand is also present on the extensive number of banks landward of (shallower than) the 200 m depth contour (van Andel & Veevers, 1967).

While carbonate comprises much of the sediment on the Van Diemen Rise it is mixed with a significant amount of fine clastic material to form calcarenite with some silty calcilutite. The sequence is part of a broad suite of calcarenite and calcilutite which is a significant feature of the outer continental shelf in the Timor Sea and parts of the Arafura Sea. The calcarenite is derived from the breakdown of skeletal and algal carbonate material deposited on the banks and rises of the outer shelf. Although such areas are now covered by water about 50 m deep, the present water depth is due to a Holocene rise in sea level, and/or additional local subsidence. Before sea level rose, the shelf area was much narrower and the banks and shoals of the outer shelf were part of a very shallow reef and carbonate bank system which fringed the shelf edge.

The coarse fraction of recent sediments deposited on the Van Diemen Rise is largely skeletal and is derived from present reefs and banks or reworked from older sequences (van Andel & Veevers, 1967). Smaller foraminifera, algal and coral colonies are the major source for the skeletal material on the shallow banks of the Van Diemen Rise and Evans Shoal.

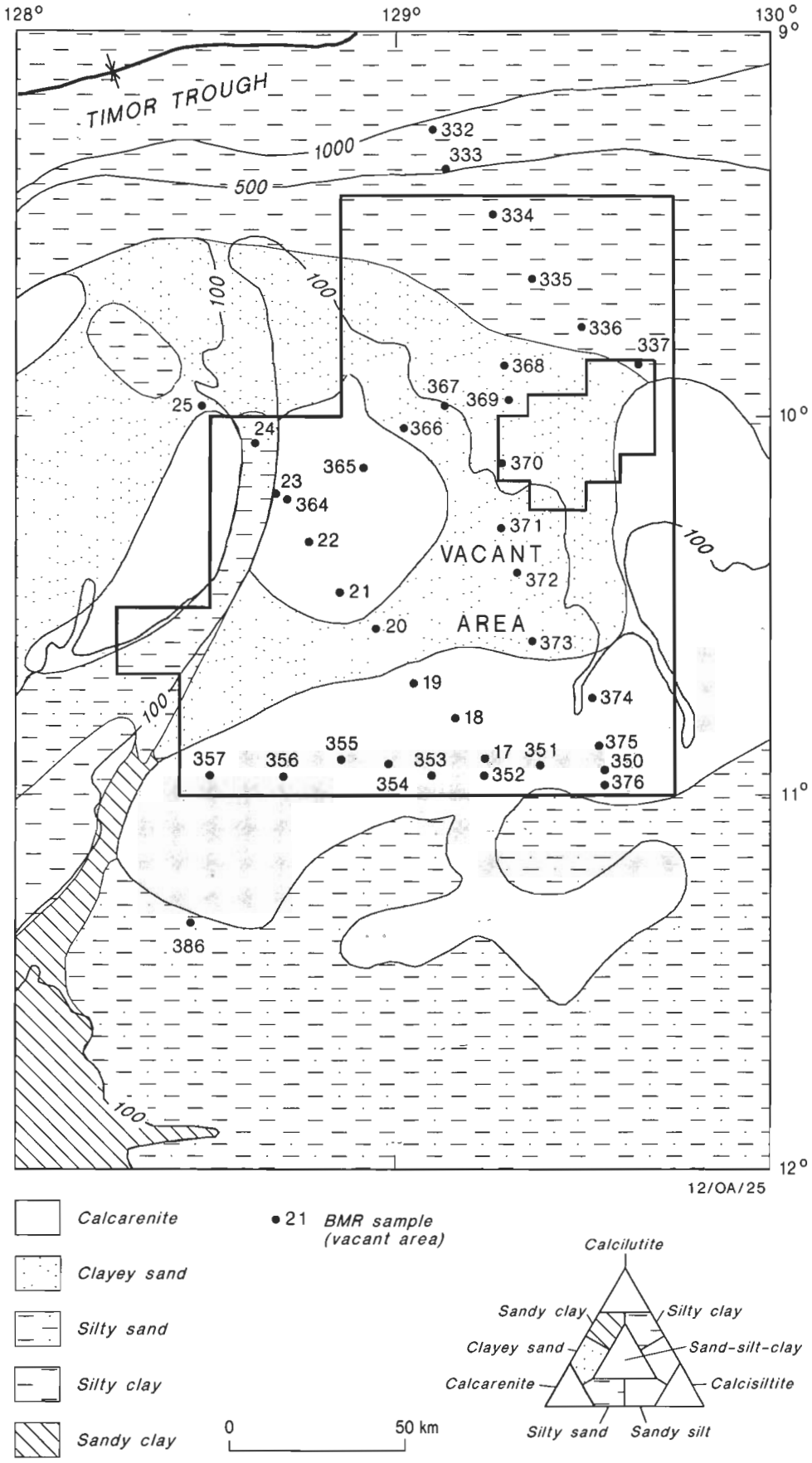

Figure 3. Lithofacies map of the Van Diemen Rise, Timor Sea.

Side scan sonar records obtained before drilling of the Evans Shoal No. 1 well (Western Mining Corporation, 1988) indicate that near the well site the sea bottom is about 102–118 m deep and comprises unconsolidated carbonate sands. The sea-bottom topography is notable in that circular depressions about 10–30 m in diameter and 1–2 m deep are widely developed across the shelf. In some cases the edges of these features exhibit a raised outer lip. The interpretation of their origin is subject to conjecture because of the lack of specific information. Fluid release in the form of biogenic or thermogenic gas is a possible reason for the development of such features, as is subsurface dewatering of semi-consolidated sediments.

Nearshore sedimentation

Each of the major features in the present day coastal zone is noted for the development of a suite of sediment types, including fluvial channel and floodplain sequences landwards of the coastal system. These comprise silt, fine sand, mud, minor gravel and alluvium sediments up to 5 m thick in meander channels, swamp depressions and even cut-off meanders. Towards the hinterland and in between such units are red sandy and mottled grey to yellow sandy soils up to 10 m thick in colluvial and eluvial environments (Hughes, 1978). These sandy soils are generally developed as a result of the erosion and dissection of Tertiary and possibly older consolidated sequences.

In coastal and offshore areas littoral, aeolian, intertidal deltaic and estuarine sand, shell and coral debris, organic rich mud and silt are being deposited in sequences up to 20 m thick. Beach and littoral strandline sands are evident on present coastlines and as low vegetated ridges. Along some shoreline and other areas Pleistocene coquina, calcarenite and conglomerate have formed in sequences up to 8 m thick (Hughes, 1978).

The modern sediments of the Timor and Arafura Seas are most extensive in the nearshore areas of less than 50 m water depth. Within these areas sediment distribution is irregular, being controlled by proximity to sediment sources and the degree of exposure to tidal and wind generated activity (Lees, 1992). The current pattern of modern sedimentation and older Quaternary units is thought to be the combined effect of sea-level fluctuations, relict deposits and subaerial, fluvial, lacustrine and marine conditions (Jones, 1987). Sea level during the past 6000 years is thought to have been relatively stable at or near its present level (Thom & Chappell, 1978).

Fluvial sediments are the major input into the Timor and Arafura Seas from the coastline and hinterland, where major river systems empty into sheltered bays and estuaries such as those in the Joseph Bonaparte Gulf and Van Diemen Gulf.

Some fine clastic (clay grade) material is deposited from suspension as a result of plumes derived from major river systems which are most active in the monsoon wet season (Lees, 1992). Analyses of the clay fraction in sediments of the Van Diemen Rise show that it is predominantly kaolinite derived from an onshore deeply weathered lateritic hinterland. Organic carbon content in the clay fraction is 0.75–1% and may reflect the input from both terrestrial and marine sources. Heavy minerals present in the minor sand fraction are largely tourmaline and zircon derived from a deeply weathered sedimentary terrain onshore (van Andel & Veevers, 1967).

Biofacies sedimentation

Samples of biological components on the Van Diemen Rise were collected and analysed by van Andel & Veevers (1967). They were classified into major biological components by means of all particles coarser than 0.062 mm (Figs 4, 5). Most particles are skeletal material. Their distribution may reflect the effect of transporting agents as well as the living habitats of the organisms.

Using the end members identified in the analysis of all samples in the Timor Sea, including those on the Van Diemen Rise, van Andel & Veevers (1967) used a correlation coefficient to measure positive and negative covariance between the various major components and the samples in which they were present (Fig. 4). The essential groupings reflected those components which are likely to be found in similar habitats and locations: corals/bryozoans, algae/forams, molluscs/echinoids. It also showed those which were not cohabitants by grouping these with a low level or negative correlation. Only the groups with a positive correlation of greater than 0.01 were statistically significant for biofacies identification (van Andel & Veevers, 1967).

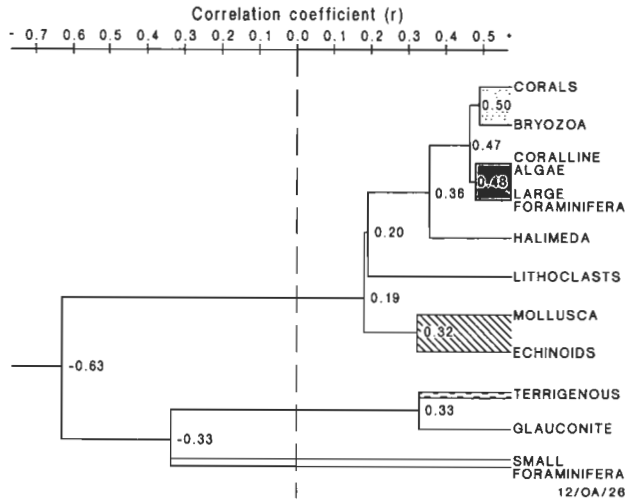

Figure 4. Dendrograph of Van Diemen Rise associations.

Halimeda clustered separately, but all other calcareous algae such as *Lithothamnium* and *Amphipora* were combined. Larger foraminifera included *Marginopora, Heterostegina, Amphistogina, Cycloclypeus, Aveolinella, Calcarina, Sorites,* Peneroplids, and large Miliolids (van Andel & Veevers, 1967). The rest were smaller foraminifera. Minor components such as ostracods, pteropods and crustaceans were not significant elements. Lithoclasts were notable and comprised calcareous and terrigenous fragments cemented by calcite.

The small foraminifera were a regional 'background' biofacies (Fig. 5) on which others appear to have been superimposed. With increasing distance from shore there was an increase in the proportion of planktonic forms in this group, which was dominant in the deep waters of the Timor Trough. The molluscan group was dominant in and around the Bonaparte Depression and may be a remnant Late Quaternary estuarine assemblage (van Andel & Veevers, 1967).

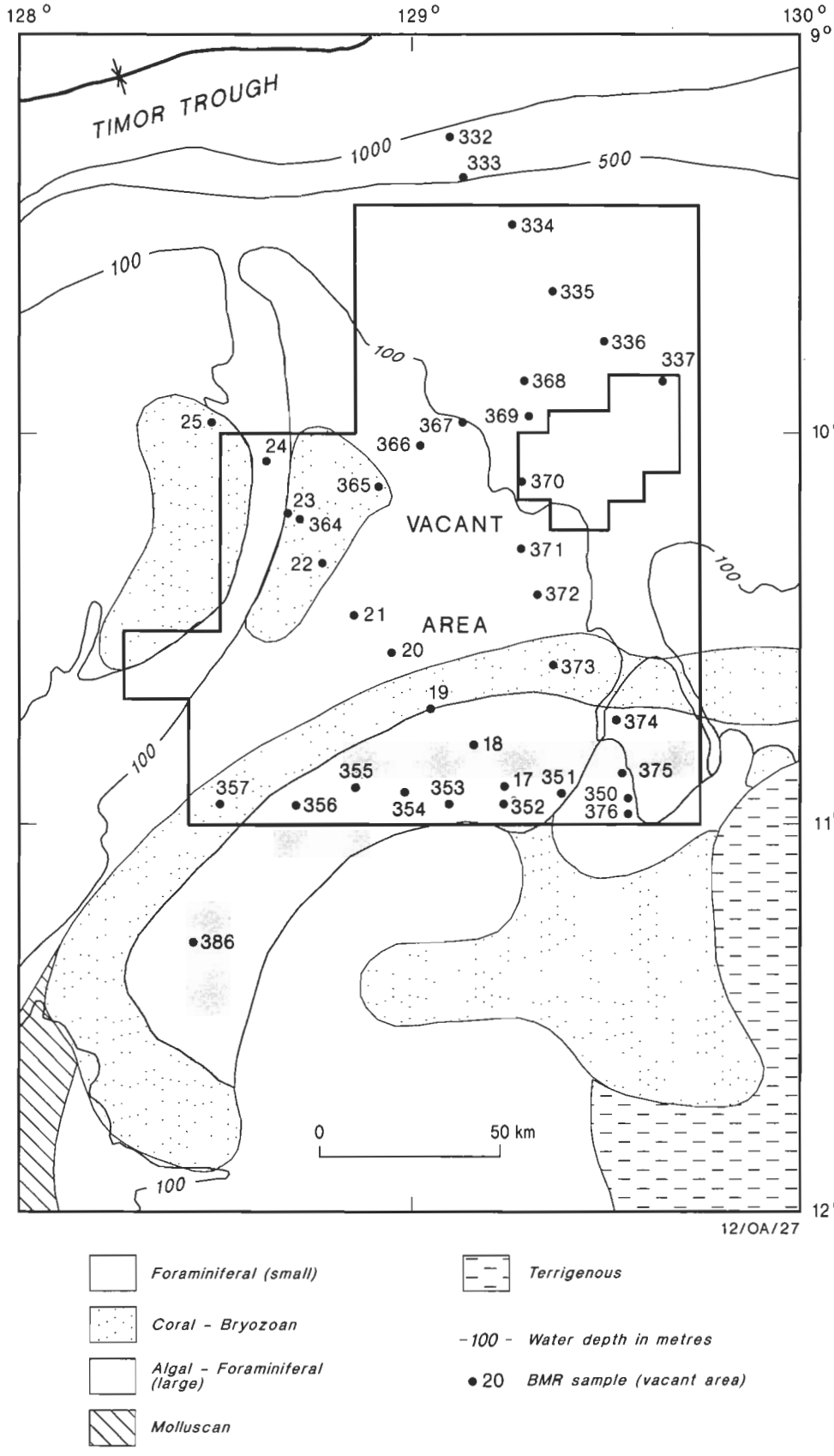

Figure 5. Biofacies map, Van Diemen Rise, Timor Sea.

The coral/bryozoan group is present on the banks and rises of the western Sahul Rise (Fig. 5) and Van Diemen Rise although it is limited to the seaward edge of the major groups of banks. The algal/foraminifera (large) group is present on the shallowest and broadest banks of the Van Diemen Rise. The terrigenous end member is limited to an area closest to the coast. It has developed as a result of the input of clastic material from major river systems during the wet season.

In additional to the biofacies evident on the seafloor of the Van Diemen Rise, other major ecological associations are present in the coastal zone. They include such features as seagrass and mangrove assemblages. For definition purposes the 'coastal area' is the area from the nearshore and intertidal region seawards to 25 nautical miles offshore or the 50 m depth contour, whatever is greater. The coastal zone extends onshore to include all landforms which are subject to coastal processes, including mobile sand dunes and chenier beach ridges (Northern Territory Department of Mines & Energy, 1991).

Three basic divisions of the coastal area are readily made, based on the dominant sedimentological processes as well as the biofacies present. The first division is the intertidal zone which includes the areas between high and low tide levels. Elements such as mangroves, salt marshes, some seagrass beds, mudflats, sand flats, sandy beaches and dune systems may also be present (Northern Territory Department of Mines & Energy, 1991).

Landwards of the intertidal areas are dunes and chenier beach-ridges, as well as low-lying areas which become water-logged during the monsoon season, including paperbark swamps and monsoonal vine thickets. Such areas comprise the supratidal zone which is a buffer between intertidal and non-marine environments.

The final element is that of subtidal zone, i.e. marine or estuarine areas below low tide level. Elements in this group are major tidally-influenced channels, coastal lagoons, coral reefs, seagrass banks and shoals, as well as marine shelf areas. A variety of cultural, social, biological, geological and geographical values are attributed to many of the coastal features of the Northern Territory (Northern Territory Department of Mines & Energy, 1991). Some might be sensitive to the impact of activities associated with exploration and development work where that activity includes dredging, drilling and seismic exploration using explosive sources.

Features which have been identified as being likely to be adversely affected by such activities include marine and estuarine protected areas, sacred sites, occupational reserves, fisheries reserves and undeclared areas. Other undeclared areas such as seagrass, mangroves, turtle or bird breeding areas, shipwrecks, recreational sites and potential aquaculture development sites are also the subject of considerable interest (Northern Territory Department of Mines & Energy, 1991). No declared protected areas are listed by the Australian National Parks and Wildlife Service (Ivanovici, 1984) on the vacant area of the Van Diemen Rise (Fig. 1).

Major habitat assemblages

Seagrass communities

Seagrass communities develop below the low tide level in estuaries, bays and the open ocean into water up to 30 m deep. They are known on the coastal fringes of the Timor Sea, Bathurst and Melville Islands, the coastline of the Cox Peninsula, the western part of the Gulf of Carpentaria and the coastal zone adjacent to the Van Diemen Rise (Fig. 1). Water clarity controls the water depth limit of seagrass development. In turbid water seagrass grows only in very shallow depths due to a low light penetration. Seagrass binds sediment particles together on the sea bed by means of a fine mat of roots. Such vegetated substrates can reduce the height of storm surges, provide a physical baffle against tidal and current flows (Hatcher & others, 1989) and encourage the settlement of benthic larvae. Seagrass assemblages can comprise depth-limited species associations which develop along open coastline areas, or mixed-species associations which are lower in diversity and reflect the less favourable conditions of intertidal areas.

Seagrass areas are important nursery grounds for juvenile tiger and endeavour prawns, the main components of the prawn catch in northern Australia (Poiner & others, 1987). The seagrass communities of the Northern Territory coastline contain similar species to those in the Gulf of Carpentaria; species of *Cymodocea, Halodule, Enhalus, Thalassia, Syringodidium* and *Halophila* are most commonly present (Poiner & others, 1987). The depth-limited communities tend to be dominated by a single species such as *Syrinodium* sp., *Thalassia testudium* and/or *Cyodocea serrulata* (Poiner & others, 1987). Stands of *Halophila ovalis* and *H. uninervis* dominate the intertidal zone of open coastline areas, whereas *C. serrulata* and *S. isoetifolium* are major species in subtidal areas (Poiner & others, 1987).

The interaction between prawn populations and seagrass communities has been closely studies in the western part of the Gulf of Carpentaria (Poiner & others, 1987). The results appear to be applicable to other parts of the Northern Territory coastline. There are four types of seagrass community — reef flat, open coastline, sheltered embayment and river mouth areas. Juvenile prawns were least well represented in the river mouth seagrass stands, most prevalent in the sheltered embayment and of intermediate numbers in the reef flat and open coastline areas (Poiner & others, 1987).

Human activities which can most seriously affect seagrass communities are the dredging and infilling of habitat areas. Significant side effects can also develop without direct disturbance because of turbidity or the resuspension of unconsolidated sediments (Hatcher & others, 1989). Increased nutrient levels in runoff from the land surface can lead to widespread mortality and habitat loss by seagrass stands. Even with only mild disturbance, changes in seagrass communities can occur and be sufficient to cause a turnover from the more diverse species assemblage typical of subtidal areas to the hardier intertidal forms which are tolerant of less favourable or high stress environments.

Reefs

In the Arafura and Timor Seas, reefs are evident on shallow banks of the continental shelf and outer shelf edge (van Andel & Veevers, 1967). Statistical analysis of all samples collected by van Andel & Veevers (1967) identifies coralline algae, larger foraminifera, *Halimeda* and the algae *Lithothamniuma* as dominant elements of bank areas (compare banks on Fig. 1 to biofacies on Fig. 5).

The dominant feature of both the Timor and Arafura Sea reefs is the drowned carbonate formations (reefs) on the outer shelf edge, the site of significant reef-building activity during the Quaternary (lower sea level). Reef-like growth on the outer shelf has generally been unable to keep pace with sea level rise during the last 20 000 years, and the focus of reef growth has spread landwards onto banks and shoals back towards the present coastline.

Reef development is also patchy because of the additional impact of regional subsidence, which has caused inundation and the submergence of most sites on the outer shelf edge. Despite the presence of mangrove, seagrass and reef communities in coastal zone and outer shelf areas of the Arafura and Timor Seas, most of the sea bottom consists of unconsolidated sediment inhabited by a limited epifauna and infauna which have been classified into the biofacies shown in Figure 5.

Mangroves

These are essentially marine tidal forests and are adapted to colonising loose wet soil types which are subject to periodic tidal submergence. On the Northern Territory coastline conditions favourable for their development are widespread, particularly in bays, tidal channels and estuaries. Minimum air temperature ultimately controls the occurrence of mangrove forests, although they are known to extend into temperate parts of the Australian coastline where local conditions are at the extreme of their range (Hatcher & others, 1989). Soil salinity, frequency of tidal inundation, sedimentation, rainfall variation and frequency of tropical cyclones contribute to the richness of species present (Smith & Duke, 1987). There is some debate over whether mangroves are the cause of sediment aggradation and accumulation or the opportunistic consequence of existing sedimentation processes. They are generally regarded as the means of stabilising sediments deposited by the prevailing physical forces rather than the cause of sedimentation.

Optimal conditions for mangrove development occur in brackish water. The theory that mangroves are important sources of outwelled dissolved nutrients has been challenged by Boto & Wellington (1988) who suggest that no net annual exchange of organic or inorganic nutrients occurs in mangroves and that they require a significant import of dissolved phosphorus for growth. They are however important areas for the development of juvenile fish and prawns (*Penaeus merguiensis* in particular; Staples & others, 1985). Mangroves in northern Australia contain an order of magnitude greater number of juvenile fish and prawn species than adjacent seagrass, bay and estuarine areas (Robertson & Duke, 1987).

A major cause of disturbance to mangroves can be the reclamation of intertidal areas for industrial or other uses. The presence of iron pyrite in the anaerobic subsoil of such areas can render them unsuitable for use in agriculture and aquaculture (Hatcher & others, 1989). There is a very close correlation between the areal extent of mangroves on the Carpentaria coast of the Northern Territory and the size of commercial prawn catches in adjacent coastal waters (Kirkwood & Somers, 1984).

Releases of crude oil into mangroves are rare but the effects can be cumulative. The speed of recovery for mangrove communities is related to the period required to degrade the crude oil; light-grade indigenous crudes would have a lower impact on such communities because of more rapid degradation (Kagi & other, 1988).

Other activities

Northern Territory coastal waters also support significant commercial and recreational fishing activities including pearl, prawn, fish and algal cultures. While potential disturbance to such activities by petroleum exploration activity is not yet evident, future disturbance should be avoided. Significant species such as dugongs, the Irrawaddy River dolphin and turtles may be present in areas of the coastal zone where there might be future exploration but they are unlikely to be present in areas of the Van Diemen Rise.

Petroleum exploration

Petroleum operations in Australia beyond coastal waters are governed by Commonwealth legislation and this, in part, is administered jointly with the States and Northern Territory. The twelve million or more square kilometres of ocean waters surrounding the continent are rich in marine life and biodiversity as well as having proven oil and gas potential.

Australian offshore petroleum exploration and production activity are undertaken subject to the provisions of Commonwealth legislation which provides for the safety of operations and protection of the environment, including the Petroleum (Submerged Lands Act) 1967, the Environment Protection (Impact of Proposals) Act 1974, the Australian Heritage Commission Act 1975, the National Parks and Wildlife Conservation Act 1975 and the Whale Protection Act 1980.

The recent releases of vacant petroleum exploration areas for application under Commonwealth legislation (Release of Offshore Petroleum Exploration Areas, Release No. 1 1992) have been accompanied by a list of special conditions. The conditions require that exploration groups wanting to drill exploration wells during the course of a permit work program supply the Commonwealth with a description of the environment, both within the permit and adjacent to it, which is likely to be affected by drilling and production. Where there is written material already available this has to be included. In addition, a description must be provided of the potential impact of drilling and production on the environment, and of proposed safeguards and standards for the protection of the environment.

Before areas are released for exploration or development proposals are approved, the Federal Minister for Resources considers advice given by Commonwealth, State and Territory energy, environmental, conservation and fisheries agencies. Using such advice the Federal Minister may require that special environmental protection operating conditions be placed on petroleum exploration or production activities. On the advice of the Federal Minister for the Environment, such activity can also be suspended pending the results of further environmental research.

The specific requirements for descriptions of the environment surrounding sites on which petroleum exploration drilling is proposed have formalised a process the industry has been undertaking for some time (Holloway, 1988; Warren, 1989). Site surveys, water temperature, current, wave, wind and tide patterns, and other oceanographic data have been evaluated as part of the process of petroleum

exploration (Holloway, 1988). The requirement for formal documentation of such information in applications to drill exploration wells has resulted in the research, interpretation and analysis of such information in the form of this paper by AGSO for use by government, the industry and the public.

The major initial feature of each recent phase of petroleum exploration activity in the Timor Sea region has been the use of seismic survey techniques which gather data on subsurface geological structure so that the petroleum potential of a region can be fully assessed. For almost 20 years such surveys have been periodically undertaken using airgun rather than explosive energy sources, a development made primarily in response to technological and safety considerations but also because of the relatively benign environmental impact of the airgun system. Advances in drilling and production technology have also been readily implemented to ensure that existing facilities and future work by the industry result in minimal disturbance and negligible damage to the natural habitats which characterise the Australian continental shelf.

Potential effects of additional exploration

Seismic surveys

The initial form of additional exploration effort likely to be undertaken in the Victoria River Downs region is seismic surveying. This would comprise towing of surveying equipment, in the form of a receiver cable and acoustic signal source, along a grid of survey lines so that the subsurface geological structure of the region might be revealed. As the activity is limited to periods of generally less than 40 days for most surveys, no persistent environmental impact would be evident. The effect of acoustic noise levels on fish and invertebrate populations is minimal unless they are within several metres of the seismic source (Neff & others, 1987). Some concerns have been raised about the disturbance effects of such acoustic noise on larger marine mammals at close range (<1 km) even though the noise from a seismic source (160 decibels at 1 metre) is less than that generated by mammals during occasional periods of vigorous activity such as 'breaching' activity by whales (230–240 decibels at 1 m; Warren, 1989).

According to Geraci & St. Aubin (1987), marine mammals and vertebrates can readily habituate to low level background noise. Marine habitats on the Australian continental shelf are, however, not without significant levels of noise associated with wind and wave movement, sea-bottom sediment transport, and the feeding and other activities of fish, bivalves, sea urchins, shrimps and crayfish (lobster) (Harris & others, 1991).

Crayfish alone are capable of generating popping, fluttering or rasping sounds with amplitudes of about 15, 9 and 40 decibels, respectively (Harris & others, 1991). Studies of fish in various habitats have measured peak noise levels of 119 decibels associated with peak migrations levels off the east coast of North America. An East Indian Ocean study indicated that daily biological choruses result in peak noise levels at least 10 decibels above background (Harris & others, 1991). Sediment transportation in the form of migrating shelfal sand waves have been observed to produce noise levels of about 140 decibels. Strong tidal currents of up to 1 m/s generate bottom noise levels of the order of 180 decibels (Harris & others, 1991).

Drilling

Exploration drilling involves controlled excavation of a subsurface bore into geological sequences which may contain natural accumulations of petroleum. Much of the hole drilled by each well bore is less than 0.25 m in diameter. Drilling is undertaken by purpose-designed vessels, whose anchoring and operation have limited local disturbance. Operational periods of less than 40 days are generally involved.

Excavation of the well bore generates rock fragments or 'cuttings' of the subsurface rock strata. These are transported from the cutting edge of a drilling assembly or 'bit' by a drilling 'mud' which is a fluid mixture of clay minerals and water. Upon reaching the surface the mud and cuttings are separated. The cuttings are size-sorted and washed before discharge to the sea bed where dispersal by local sea-bed currents occurs.

Drilling mud is recycled to the drilling assembly in order to lubricate the drill bit. Some drill mud may be present on the rock cuttings discharged to the sea bed. Minor additives in the drill mud are present to adjust its physical properties for maximum safe operating conditions. Drilling operations examined by Spies (1987) show that cuttings, traces of drill mud and additives on cuttings are rapidly diluted by wave and current activity. Limited quantities of other fluids such as treated sanitary wastes are discharged to the sea during operations, as during any normal maritime activity. Noise levels generated by exploration and production activity are limited by the relevant occupational health and safety standards and even at close range they are less than 5 decibels above background at water level (Warren, 1989).

Production

Should the results of exploratory drilling warrant it, fixed or floating structures could be installed to develop commercially any potential hydrocarbon accumulation(s). Development for such accumulations could involve drilling a number of wells from drilling/production facilities. Production, in the case of crude oil production, will usually involve the discharge of subsurface water separated from the crude oil into the sea after processing. If full processing is undertaken on the offshore facility the crude oil and other fluids are offloaded and transported. Otherwise, a pipeline connection to shore-based facilities is required. The functioning and effects of such operations are beyond the scope of this analysis. The most relevant local guide to the long term effects of such operations is the production platforms and facilities of the Gippsland Basin in Bass Strait.

Major studies of the ecological impact of production facilities are available for a range of marine habitats (Bosech & Rabalais, 1987). Ecological changes which occur are largely related to artificial reef effects or changes due to the presence on the sea bottom of cuttings. Other changes are subtle and not readily detectable without detailed sampling (Spies, 1987).

Oil releases

Climatic and oceanographic features of any part of Australia's continental margins are important in determining the impact of oil releases which largely result from maritime transport mishaps. Crude oils are mixtures of different types of hydrocarbon molecules. All but a few

Australian oils are relatively rich in low molecular weight compounds and as a result low in viscosity and high in specific gravity. They undergo rapid chemical, physical and biological alteration if released or exposed to the atmosphere or the marine environment. Processes leading to such alteration include evaporation, photo-oxidation, dissolution and emulsification (Bartha & Atlas, 1987).

The high ambient sea and air temperature patterns in the Timor Sea are such that volatile-rich indigenous crudes are likely to undergo rapid evaporation of most components within 72 hours of release. Studies by Kagi & others (1988) led them to suggest that crude oil released in open tropical waters would spread and evaporate so rapidly that the marine hazard from such releases would be minimal. Only where an oil release is chronically persistent, and temperature, wind and wave energy are very low, is it likely that release of such crude would cause significant ecological disturbance. This combination of factors is very unlikely in the Timor Sea.

The persistence of medium and higher molecular weight hydrocarbons on the sea surface, in the water column or on the sea bottom substrate causes most of the stress or toxic effects of oil on marine populations (Capuzzo, 1987). The limited quantities of such compounds and the dominance of saturated (paraffins) rather than the more toxic benzenes in Australian crude oils mean that local crudes would have a less severe impact than the more viscous and asphalt-rich Middle East or Indonesian crudes. An oil release from exploration drilling on the Van Diemen Rise would be unlikely to have a long term or chronic impact, unless the release continued for an extended period and affected some areas in a concentrated fashion.

The results of van Andel & Veevers (1967) indicated that the dominant currents in the Timor Sea operate parallel to the coast. The winds are southeasterly in the dry season and from the northwest in the monsoon. Only during the latter conditions would it be possible for remnants of a crude oil release from an exploration site to become stranded on the Van Diemen High. The required travel time of at least 5–6 days from release in the vacant area to coastal stranding is nearly twice the evaporation half-life of the heaviest fractions likely to be found in indigenous crudes. Shorter travel times caused by increased wind or current velocities would tend to decrease the evaporation half-life and result in little if any stranding. More detailed modelling of spill behaviour and movement prediction is required if the points outlined here are to be further evaluated.

Over the past 30 years of exploration and production activity a total of over 2800 million barrels of oil have been produced and more than 1000 wells drilled in Australia's offshore continental margins (Griffiths, 1991). During this activity the petroleum industry's safety and environmental record has been such that only approximately 350 barrels of crude have been accidentally released (Griffiths, 1991). In the same period and over the same area spillages of fuel oil or crude associated with maritime shipping mishaps have been an order of magnitude greater per incident. Natural seepages of crude oil are perhaps less noticeable on our continental margin but can yield even greater volumes of oil to coastline areas. An earth tremor on 7 December 1986 in the vicinity of Kangaroo Island released an estimated 7300 barrels of crude oil subsequently found on the island's beaches and coastline. Geochemical analysis of the crude confirmed that it was from a natural source (Griffiths, 1991).

Conclusions

Baseline environmental conditions in the Timor Sea, including the Van Diemen Rise, can be identified from the study by van Andel & Veevers (1967). The pattern of lithofacies, biofacies and oceanographic features identified by their study is based on data acquired in 1960–61 before any extensive petroleum exploration activities in the region. It therefore provides a useful reference with which any post-exploration patterns can be compared. Additional seismic surveys and drilling are the main activities likely to be undertaken during further evaluation of the prospectivity of the region. Available information suggests that limited, if any, long-term impact on substrate conditions of minor short-term localised disturbance is likely. Cuttings generated by drilling operations are the only significant traces of such work and these would be rapidly reworked by normal marine processes. Trace amounts of additives and drilling mud produced by exploration drilling operations would be rapidly diluted and removed by normal marine processes after drilling stops. The impact of the installation of production facilities requires further examination. Prevailing climatic conditions and the volatile nature of indigenous crudes are such that coastal strandings of oil released from exploration on the Van Diemen Rise are highly unlikely. More detailed modelling is required if the initial results outlined here are to be tested by specific modelling of spill behaviour and movement under the climatic and oceanographic regime of the Timor Sea.

Acknowledgements

The efforts of P.R. Temple, A. Williams and J. Marshall in examining draft copies of the paper are greatly appreciated. Drafting of figures was undertaken under the guidance of B. Pashley.

References

Bartha, R. & Atlas, R.M. (editors), 1987 — Transport and transformations of petroleum: biological processes. *In* Bosech, D.F. & Rabalais, N.N. (editors), Long-term environmental effects of offshore oil and gas development. *Elsevier Applied Science,* 708 pp.

Bosech, D.F. & Rabalais, N.N., 1987 — ong-term environmental effects of offshore oil and gas development. *Elsevier Applied Science.* 708 pp.

Boto, K.G. & Wellington, J.T., 1988 — Seasonal variation in concentrations and fluxes of dissolved organic and inorganic materials in a tropical, tidally-dominated mangrove waterway. *Marine Ecology Program Series* 50, 151–160.

Capuzzo, J.M., 1987 — Biological effects of petroleum hydrocarbons: assessments from experimental results. *In* Bosech, D.F. & Rabalais, N.N. (editors) Long-term environmental effects of offshore oil and gas development. *Elsevier Applied Science,* 708 pp.

Division of National Mapping, 1986 — Atlas of Australian resources. 3rd series. Volume 4 Climate. *Division of National Mapping, Department of Resources and Energy,* 60 pp.

Geraci , J.R. & St. Aubin, D.J., 1987 — Effects of offshore oil and gas development on marine mammals and turtles. *In* Bosech, D.F. & Rabalais, N.N. (editors), Long-term environmental effects of offshore oil and gas development. *Elsevier Applied Science,* 708 pp.

Griffiths, A., 1991 — Principal address — Opportunities for Australian companies. *The APEA Journal* 31(2), 27–31.

Harris, P.T., Baker, E.K. & Cole, A.R., 1991 — Physical sedimentology of the Australian continental shelf with emphasis on Late Quaternary deposits in major shipping channels, port approaches and choke points. *Ocean Sciences Institute Report* No. 51, *University of Sydney*, 505 pp.

Hatcher, B.G., Johannes, R.E. & Robertson, A.I., 1989 — Review of research relevant to the conservation of shallow tropical marine ecosystems. *Oceanography and Marine Annual Review* 27, 337–414.

Holloway, P.E., 1988 — Physical oceanography of the Exmouth Plateau Region, North-western Australia. *Australian Journal of Marine and Freshwater Research* 39, 589–606.

Hughes, R.J., 1978 — The geology and mineral occurrences of Bathurst Island, Melville Island, and Coburg Peninsula, Northern Territory. *Bureau of Mineral Resources, Geology and Geophysics, Bulletin* 177.

Ivanovici, A.M. (editor), 1984 — Inventory of declared marine and estuarine protected areas in Australian waters, Volume 2. *Australian National Parks and Wildlife Service, AGPS.*.

Jones, H.J., 1973 — Marine geology of the Northwest Australian continental shelf. *Bureau of Mineral Resources, Geology and Geophysics, Bulletin* 136.

Jones, M.R., 1987 — Surficial sediments of the Western Gulf of Carpentaria, Australia. *Australian Journal of Marine and Freshwater Research* 38, 151–167.

Jongsma, D., 1974 — Marine geology of the Arafura Sea. *Bureau of Mineral Resources, Geology and Geophysics, Bulletin* 157.

Kagi, R.I., Fisher, S.J. & Alexander, R., 1988 — Behaviour of petroleum in northern Australian waters. *In* Purcell, P.G. & Purcell, R.R. (editors), The North West Shelf, Australia. *Proceedings of Petroleum Exploration Society of Australia, Symposium, Perth, 1988.*

Kirkwood, G.P. & Somers, I.F., 1984 — Growth of two species of tiger prawn, *Penaeus esculentus* and *P. semisulcatus*, in the western Gulf of Carpentaria. *Australian Journal of Marine and Freshwater Research* 35, 703–712.

Lees, B.G., 1987 — Age structure of the Point Stuart Chenier Plain: a reassessment. *Search* 18(5), 257–259.

Lees, B.G., 1992 — The development of a chenier sequence on the Victoria Delta, Joseph Bonaparte Gulf, northern Australia. *Marine Geology* 103, 215–224.

Lees, B.G., Yanchou, L. & Head, B., 1990 — Reconnaissance thermoluminescence dating of Northern Australian coastal dune systems. *Quaternary Research* 34, 169–185.

Maxwell, W.G.H., 1968 — Atlas of the Great Barrier Reef. *Elsevier, Amsterdam.*

Neff, J.M., Rabalais, N.N. & Bosech, D.F., 1987 — Offshore oil and gas development activities potentially causing long-term environmental effects. *In* Bosech, D.F. & Rabalais, N.N. (editors), Long-term environmental effects of offshore oil and gas development. *Elsevier Applied Science*, 149–175.

Northern Territory Department of Mines and Energy, 1991 — Guidelines for mineral exploration in coastal areas of the Northern Territory. *Environmental Protection Unit, Conservation Commission of the Northern Territory, Mines Environment Directorate. Northern Territory Department of Mines and Energy*, 11 pp.

Poiner, I.R., Staples, D.J. & Kenyon, R., 1987 — Seagrass communities of the Gulf of Carpentaria, Australia. *Australian Journal of Marine and Freshwater Research* 38, 121–131.

Robertson, A.I. & Duke, N.C., 1987 — Mangroves as nursery sites: comparisons of the abundance and species composition of fish and crustaceans in mangroves and other nearshore habitats of tropical Australia. *Marine Biology* 96, 193–205

Smith, T.J. & Duke, N.C., 1987 — Physical determinants of inter-estuary variation in mangrove species richness around the tropical coastline of Australia. *Journal of Biogeography* 14, 9–19.

Spies, R.B., 1987 — The biological effects of petroleum hydrocarbons in the sea: assessments from the field and microcosms. *In* Bosech, D.F. & Rabalais, N.N. (editors), Long-term effects of offshore oil and gas development. *Elsevier Applied Science*, 708 pp.

Staples, D.J., Vance, D.J. & Heales, D.S., 1985 — Habitat requirements of juvenile penaeid prawns and their relationship to offshore fisheries. *In* Rothlisberg, B.J., Hill, B.J. & Staples, D.J. (editors), Second Australian National Prawn Seminar. *Cleveland Australia*, 47–54.

Thom, B.G. & Chappell, J., 1978 — Holocene sea level change: an interpretation. *Philosophical Transactions of the Royal Society of London* 291, 187–194.

van Andel, T.H. & Veevers, J.J., 1967 — Morphology and sediments of the Timor Sea. *Bureau of Mineral Resources, Geology and Geophysics Bulletin* 83.

van der Kaars, W.A., 1991 — Palynology of eastern Indonesian marine piston-cores: a Late Quaternary vegetational and climatic record for Australasia. *Palaeogeography, Palaeoclimatology, Palaeoecology* 85, 239–302.

Warren, R.P., 1989 — Offshore oil and gas exploration: what are the environmental effects and do they justify limitations on access to coastal waters. *The APEA Journal* 29(1), 84–95.

Western Mining Corporation, 1988 — Evans Shoal No. 1 well completion report. *Western Mining Corporation Ltd, BHP Petroleum Ltd.*

BMR Journal of Australian Geology & Geophysics, 13, 293–322

Conodonts from the Lower Ordovician Coolibah Formation, Georgina Basin, central Australia

Kathi Stait[1] & E.C. Druce[2]

The Coolibah Formation outcropping around the Toko Syncline, southeastern Georgina Basin, was sampled for conodonts during a multidisciplinary study of Georgina Basin geology by the Australian Geological Survey Organisation. Twenty-two species of conodonts belonging to 17 genera recovered from acid insoluble residues are described. *Alcoorina* and *Tokoconus* are new genera; *Alcoorina nadala*, *Bergstroemognathus kirki* and *Tokoconus wheelamanensis* are previously undescribed species. Four species remain in open nomenclature awaiting more material. The conodont faunas are grouped into three broad biostratigraphic associations, although few sections record all three. Faunas low in the Coolibah Formation are dominated by *Drepanoistodus costatus* (Abaimova) and *Scolopodus multicostatus* Barnes & Tuke, with *Diaphorodus tortus* (McTavish), *Scandodus* sp. nov. A and hyaline conical elements. The succeeding conodont association records first appearances of *Ansella fengxiangensis* (An & others), *Aurilobodus? leptosomatus* An, *Paroistodus originalis* (Sergeeva), *Protoprioniodus nyinti* Cooper, and *Triangulodus larapintinensis* (Crespin). Specimens of younger species are found in the uppermost Coolibah Formation. Examination of these associations within different sections indicates that both upper and lower contacts of the Coolibah Formation are probably diachronous. Recovered conodonts are closest in affinity to those of North China, and North and South Korea. They range in age from middle to late Arenig.

Introduction

The Coolibah Formation is part of the Cambrian to Ordovician shallow water succession in the Georgina Basin (Fig. 1). It is exposed near the rims of the northwest–southeast trending Toko Syncline which crosses the Northern

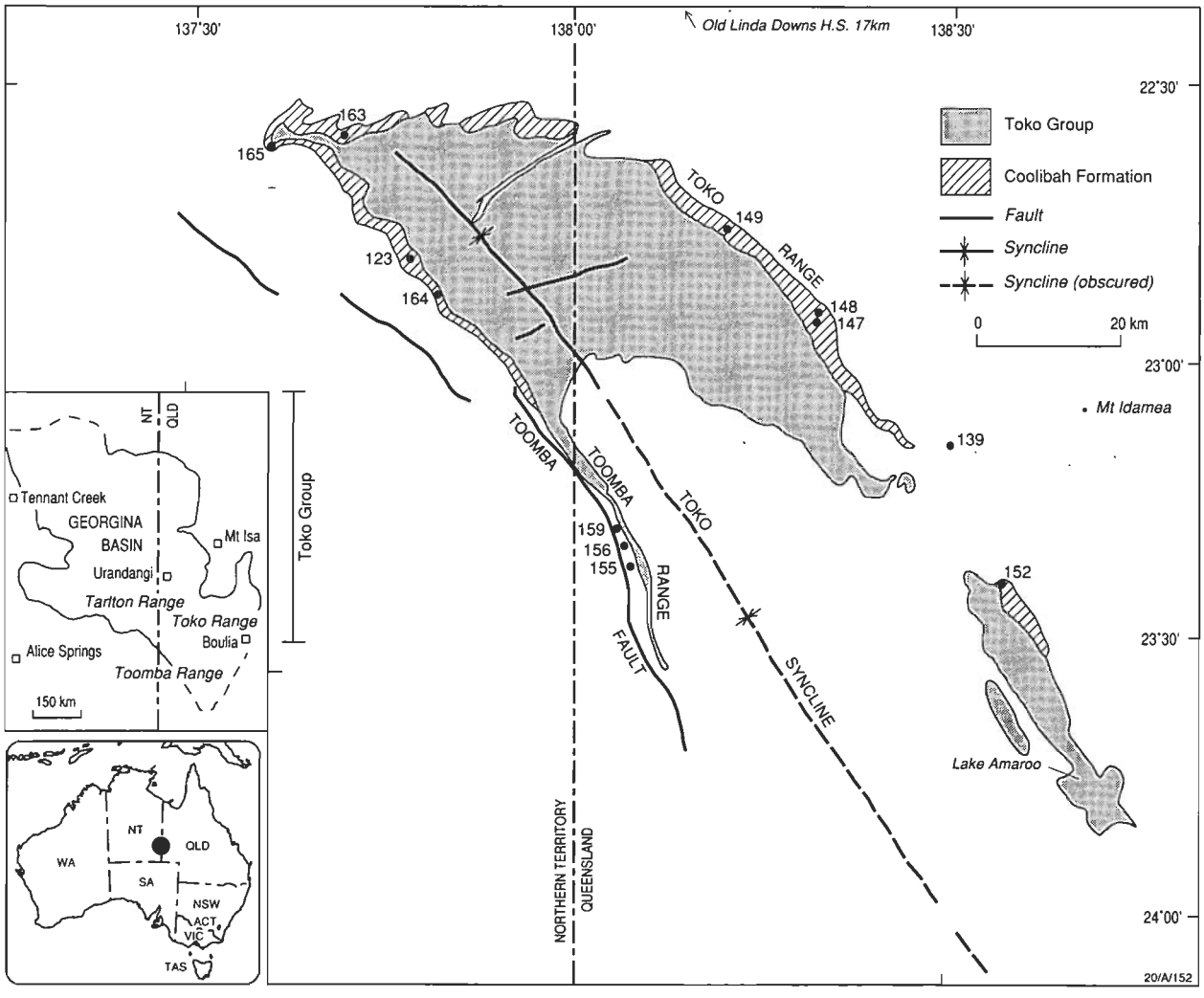

Figure 1. Coolibah Formation in southern Georgina Basin, and location of sampled sections (modified from Draper, 1980).

[1] Geology Department, University of Tasmania, GPO Box 252C, Hobart TAS 7001
[2] 8 Mildenhall Place, Fraser ACT 2615

Territory–Queensland border just north of the Tropic of Capricorn. This formation is also known in core from the Toko Range.

The Coolibah Formation is underlain by the predominantly dolomitic Kelly Creek Formation, and overlain by the carbonate-rich and clastic sequences of the Nora Formation. It comprises a variable succession of fine-grained, grey to white limestones with minor grey calcareous siltstones (Playford and Wicander, 1988). Lithologies have been more fully described in Shergold & others (1976) and Webby & others (1981).

Relationships of the Coolibah Formation with both underlying and overlying rocks are unclear. Shergold (1985) believed the Kelly Creek–Coolibah contact to be interdigitative. Others have maintained that sequences may be either conformable or disconformable (see Webby & others, 1981). Similarly, contact between the Coolibah and Nora Formations is reported to be conformable (e.g. Draper, 1980; Shergold, 1985) or unconformable, at least in places (Wade *in* Playford & Wicander, 1988).

The Coolibah Formation varies in thickness, from 7.5 m at the type locality (Fig. 2) to 110 m near the southeastern end of the Toko Range (Smith, 1972)

The precise age of the Coolibah Formation is doubtful. Its fauna and flora are largely unknown outside Australasia (e.g. Playford & Wicander, 1988) or may even, in some cases, be endemic to the Georgina Basin. Shergold & others (1976), Shergold & Druce (1980) and Nicoll & others (1992) assign an early Arenig age to this formation. Acritarchs described by Playford & Wicander (1988) range from latest Tremadoc to Llanvirn. Nautiloids from the base of the Nora Formation are late Arenig (Wade *in* Playford & Wicander, 1988). Nora Formation trilobites are largely endemic (Fortey & Shergold, 1984): the only species known with certainty from outside Australia appears to be mid Arenig (Fortey & Shergold, 1984, 350).

The lower boundary of the Coolibah Formation may be diachronous (Smith, 1972), and the implication of nautiloid distribution within the basal Nora Formation is that the Coolibah–Nora formation boundary is not isochronous (M. Wade, Queensland Museum, pers. comm., July 1991).

This study is one part of a systematic evaluation of conodont faunas throughout the Kelly Creek to Nora formations. Detailed taxonomy of these collections, in the light of improved understanding of conodont apparatuses, should clarify much of the biostratigraphic uncertainty relating to these sequences.

The following is a re-evaluation of unpublished material collected by Druce before 1970 as part of the Australian Geological Survey Organisation (then the Bureau of Mineral Resources) multidisciplinary study of Cambrian to Ordovician rocks from the southern margin of the Georgina Basin.

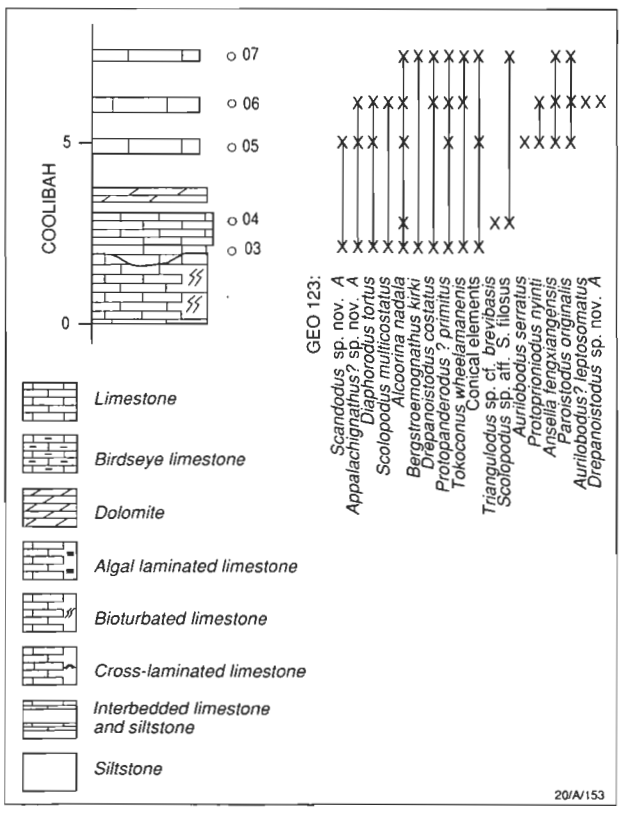

Figure 2. Stratigraphic section and associated conodont range chart, locality GEO 123, Coolibah Formation Type Section, Bloodwood Creek.
Stratigraphic thickness is measured in metres. Symbols defined here are used in Figures 311.

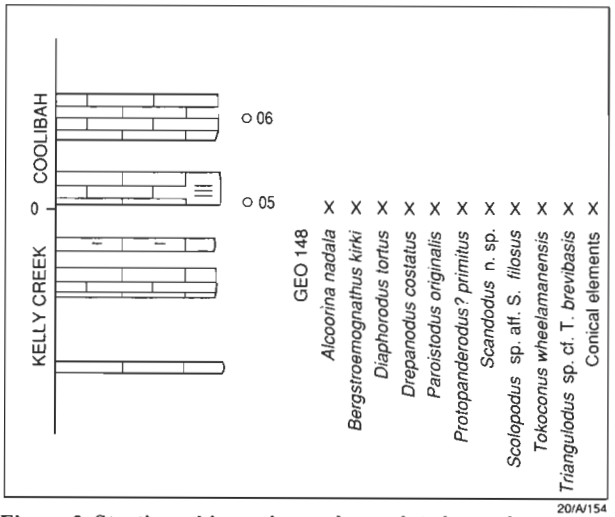

Figure 3. Stratigraphic section and associated conodont range chart, locality GEO 148, Wheelaman Creek.
Stratigraphic thickness is measured in metres. Symbols and scale as in Figure 2.

Samples are accurately located (Fig. 1) where sections were measured and collected. However, during an initial exploratory phase of geological mapping, spot samples were collected and some localities are unclear. Material from these localities was used in taxonomic evaluations, but not biostratigraphically.

Locality information

Samples were collected from sections on both eastern and western limbs of the Toko Syncline, along the Toko and Toomba ranges (Fig. 1). Each section is referred to by number, prefaced by 'GEO'. Sample numbers are composite: each refers to the section from which each sample was collected followed by a sequential number. Precise location

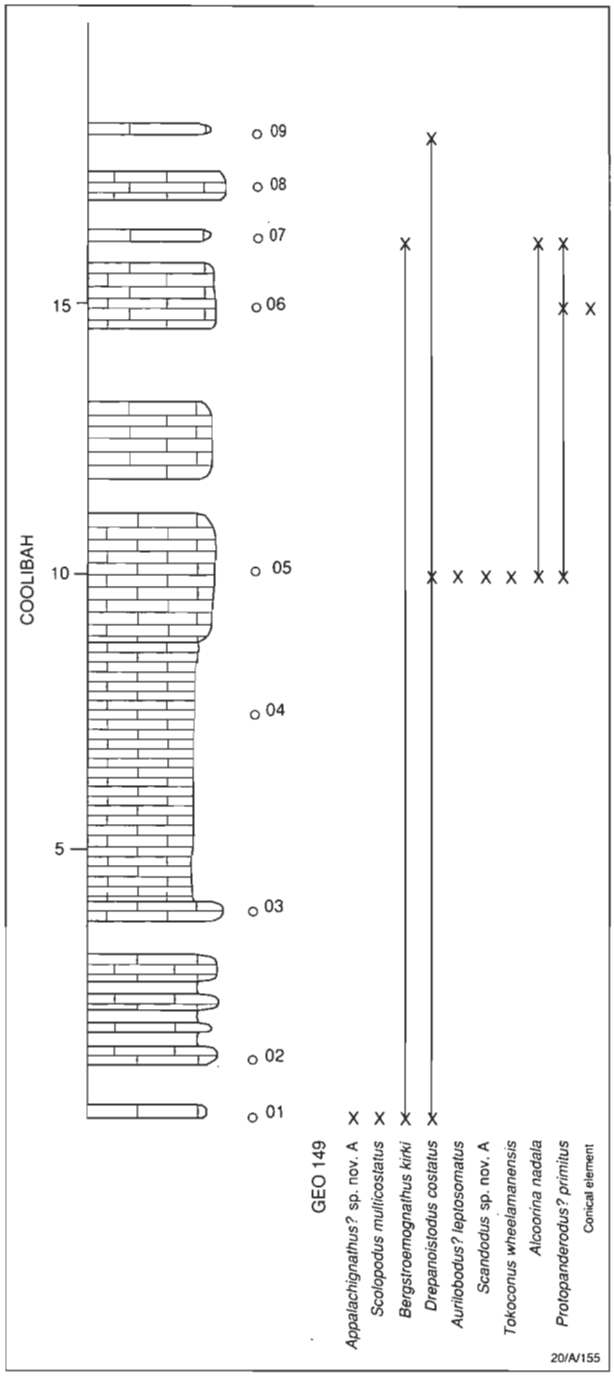

Figure 4. Stratigraphic section and associated conodont range chart, locality GEO 149, south of Linda Creek.
Stratigraphic thickness is measured in metres. Symbols and scale as in Figure 2.

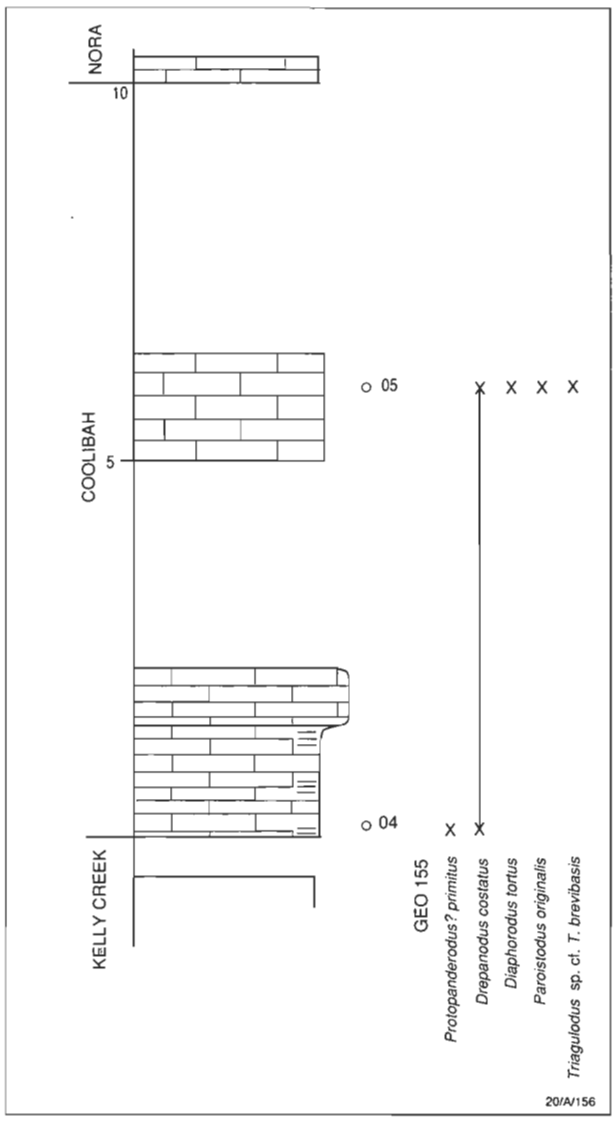

Figure 5. Stratigraphic section and associated conodont range chart, locality GEO 155, southern end of Toomba Range.
Stratigraphic thickness is measured in metres. Symbols and scale as in Figure 2.

of conodont-bearing samples is indicated on accompanying stratigraphic sections (Figs 2–10).

Grid references refer to locality of sections, as follows:

GEO 123: Coolibah Formation type section; Bloodwood Creek, grid reference 596153 on Tobermory 1:250 000 topographic sheet SF 53–12, Edition 2, Series R 502.

GEO 132: spot samples, Coolibah Formation, precise locations unknown.

GEO 139: Coolibah to Nora formations, 2 km south of Ilanama Swamp, grid reference 455?07 on Mt Whelan 1:100 000 geological sheet 6651, Preliminary Edition, September 1979.

GEO 147: Coolibah Formation, Wheelaman Creek near Wheelaman East Hut, grid reference 656144 on Glenormiston 1:250 000 geographic sheet SF 54-9 Edition 1, Series R 502.

GEO 148: Kelly Creek and Coolibah formations, Wheelaman Creek near Wheelaman East Hut, grid reference 656145 on Glenormiston 1:250 000 geographic sheet SF 54–9 Edition 1, Series R 502.

GEO 149: Coolibah Formation, south of Linda Creek, grid reference 637165 on Glenormiston 1:250 000 geographic sheet SF 54–9 Edition 1, Series R 502.

GEO 152: Kelly Creek to Coolibah formations, 10 km west of Jewlerry Waterhole, grid reference 593189 on Mt Whelan 1:100 000 geological sheet 6651, Preliminary Edition, September 1979.

GEO 155: Kelly Creek to Coolibah formations, southern end of Toomba Range, grid reference 055134 on Abudda Lakes 1:100 000 geological sheet 6551, Preliminary Edition, May 1980.

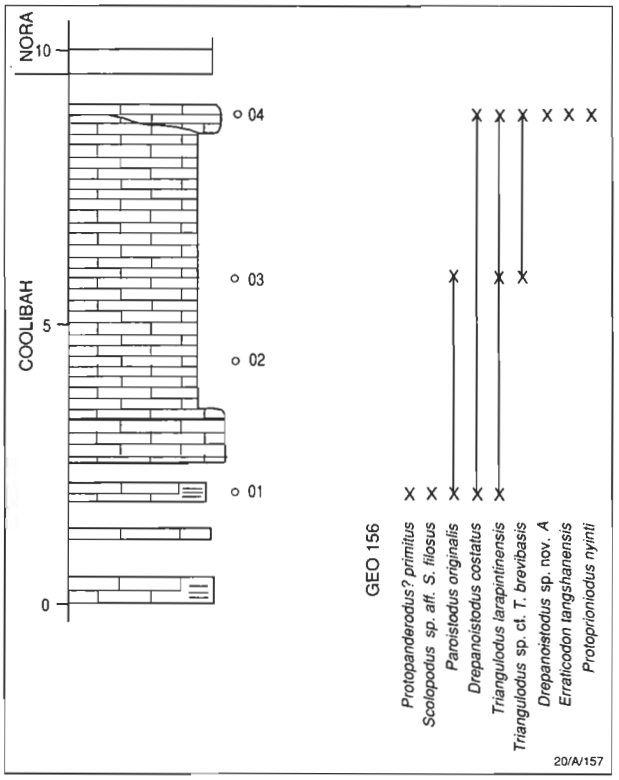

Figure 6. Stratigraphic section and associated conodont range chart, locality GEO 156, Toomba Range, near Craven's Peak. Stratigraphic thickness is measured in metres. Symbols and scale as in Figure 2.

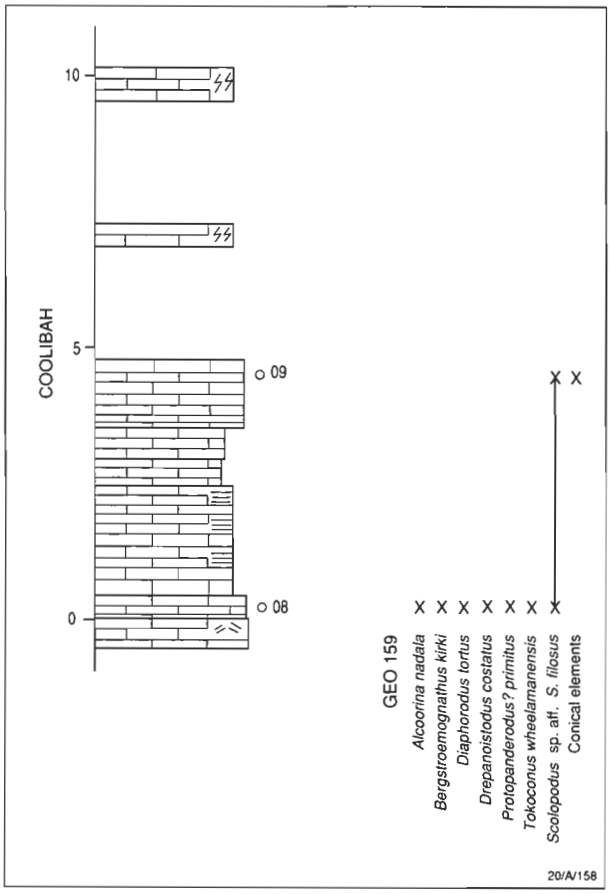

Figure 7. Stratigraphic section and associated conodont range chart, locality GEO 159, Toomba Range, west of Twin Hills. Stratigraphic thickness is measured in metres. Symbols and scale as in Figure 2.

GEO 156: Coolibah to Nora formations, on low hill near Craven's Peak, grid reference 028171 on Abudda Lakes 1:100 000 geological sheet 6551, Preliminary Edition, May 1980.

GEO 159: Kelly Creek to Coolibah Formations, west of Twin Hills, grid reference 030211 on Abudda Lakes 1:100 000 geological sheet 6551, Preliminary Edition, May 1980.

GEO 163: Coolibah Formation, Alcoora Creek, grid reference 615175 on Tobermory 1:250 000 topographic sheet SF 53–12, Edition 2, Series R 502.

GEO 164: Coolibah Formation, Halfway Dam, grid reference 606146 on Tobermory 1:250 000 topographic sheet SF 53–12, Edition 2, Series R 502.

GEO 165: Coolibah Formation, Bloodrock Creek near MarquaTobermory boundary fence, grid reference 589173 on Tobermory 1:250 000 topographic sheet SF 53–12, Edition 2, Series R 502.

TOK samples were collected from the Toko Range during early reconnaissance of the area; localities unknown.

Biostratigraphy

Ranges of Coolibah Formation conodonts are shown in Figs 2–10 plotted against lithostratigraphy of sections in which they occur.

The conodont fauna in basal strata of the Coolibah Formation generally consists of *Diaphorodus tortus* McTavish, *Scolopodus multicostatus* Barnes & Tuke, *Alcoorina nadala* gen. et sp. nov., *Bergstroemognathus kirki* sp. nov., *Drepanoistodus costatus* (Abaimova), *Protopanderodus? primitus* Cooper, *Tokoconus wheelamanensis* gen. et sp. nov., with new species of *Scandodus* Lindström and *Appalachignathus*? Bergström & others. While many of these species continue through much of the studied sections, they are most abundant low in the Coolibah Formation. Neither *Scandodus* sp. nov. A nor *Diaphorodus tortus* occurs in upper Coolibah Formation.

Middle strata frequently record first appearance of *Scolopodus* sp. aff. *S. filosus* Ethington & Clark, *Triangulodus* sp. cf. *T. brevibasis* (Sergeeva), *Ansella fengxiangensis* (An & others), *Protoprioniodus nyinti* Cooper, *Aurilobodus? leptosomatus* An, *Paroistodus originalis* (Sergeeva) and *Triangulodus larapintinensis* (Crespin). These last five species have not been found in basal Coolibah Formation.

Upper Coolibah Formation contains a few specimens of younger species (e.g. *Erraticodon tangshanensis* Yang & Xu). This is also the level of maximum abundance of *Triangulodus larapintinensis*.

Within this general scheme, there are exceptions. *Scolopodus multicostatus* may occur in sequences underlying the base of the Nora Formation (e.g. GEO 165) together with species more common to this stratigraphic level. *Triangulodus* sp. cf. *T. brevibasis*, commonly first found in mid Coolibah Formation, may occur in basal Coolibah Formation rocks. These, and similar perturbations in the

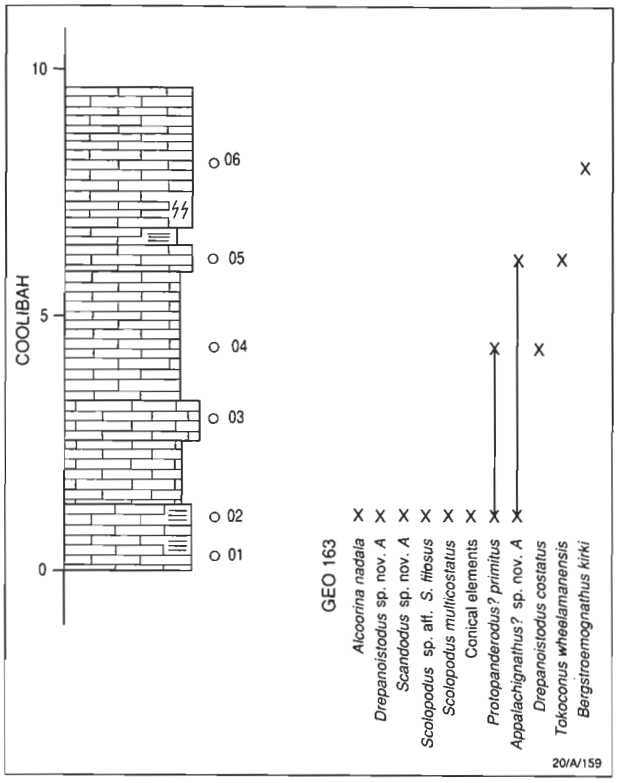

Figure 8. Stratigraphic section and associated conodont range chart, locality GEO 163, Alcoora Creek.
Stratigraphic thickness is measured in metres. Symbols and scale as in Figure 2.

succession of conodont species, suggest environmental control on conodont occurrence.

Possibly as a consequence, bases of both Coolibah and Nora formations appear to be diachronous (Fig. 11). While the upper conodont fauna of the Coolibah Formation is recorded below the base of the Nora Formation in GEO 156, and at localities spot sampled from the Toko Range, basal Nora Formation at GEO 165 contains the middle conodont fauna more typical of the Coolibah Formation. Conodonts from both underlying Kelly Creek Formation and overlying Nora Formation are similar to lower and upper faunas respectively of the Coolibah Formation. Study of these conodonts should reveal the extent of diachroneity of upper and lower boundaries of the Coolibah Formation.

Correlation with Australian successions

Correlation of Australian Ordovician sequences with the Coolibah Formation is shown in Table 1.

Oistodus multicorrugatus Harris, *Protoprioniodus nyinti* Cooper, *Triangulodus larapintinensis* (Crespin) and *Protopanderodus? primitus* Cooper are found in both Coolibah Formation and Horn Valley Siltstone. *Protoprioniodus nyinti* indicates lower Horn Valley Siltstone, while *Oistodus multicorrugatus* and *Triangulodus larapintinensis* are found throughout this formation. *Protopanderodus? primitus*, while restricted to upper Horn Valley Siltstone, may be excluded because of environmental differences. The uppermost Coolibah Formation conodont fauna most likely correlates with that of the lower Horn Valley Siltstone.

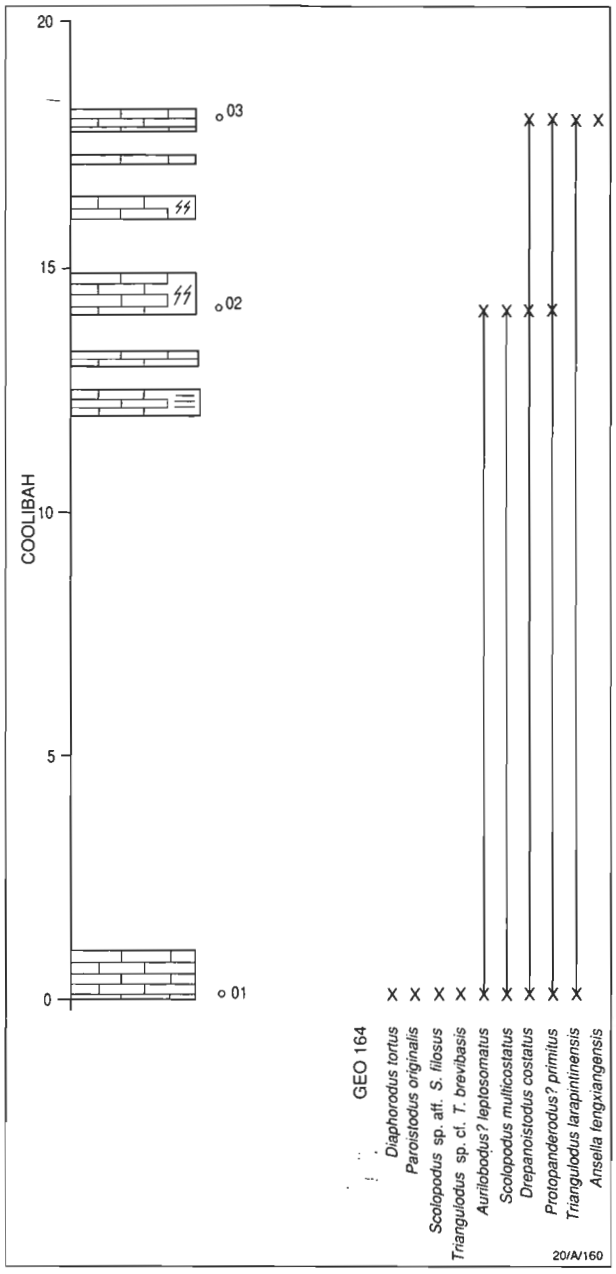

Figure 9. Stratigraphic section and associated conodont range chart, locality GEO 164, Halfway Dam.
Stratigraphic thickness is measured in metres. Symbols and scale as in Figure 2.

Conodont elements figured (Cooper, 1986) from interbeds within the Innamincka Red Beds of the Warburton Basin include one (Cooper, 1986, fig. 3) closely resembling the erectiform element of *Ansella fengxiangensis* (An & others). Some of Cooper's specimens (Cooper, 1986, figs 4, 5) are similar to elements of *Triangulodus* species from the Coolibah Formation. The Innamincka Red Beds and the Coolibah Formation are therefore likely to be approximately the same age.

Within the Canning Basin Ordovician sequence, *Diaphorodus tortus* is found in upper Emanuel Formation. This corresponds to zone OCC of McTavish & Legg (1976), which also contains species previously referred to the Chirognathacea. These are also found in the Coolibah Formation as part of *Bergstroemognathus* and *Appalachig-*

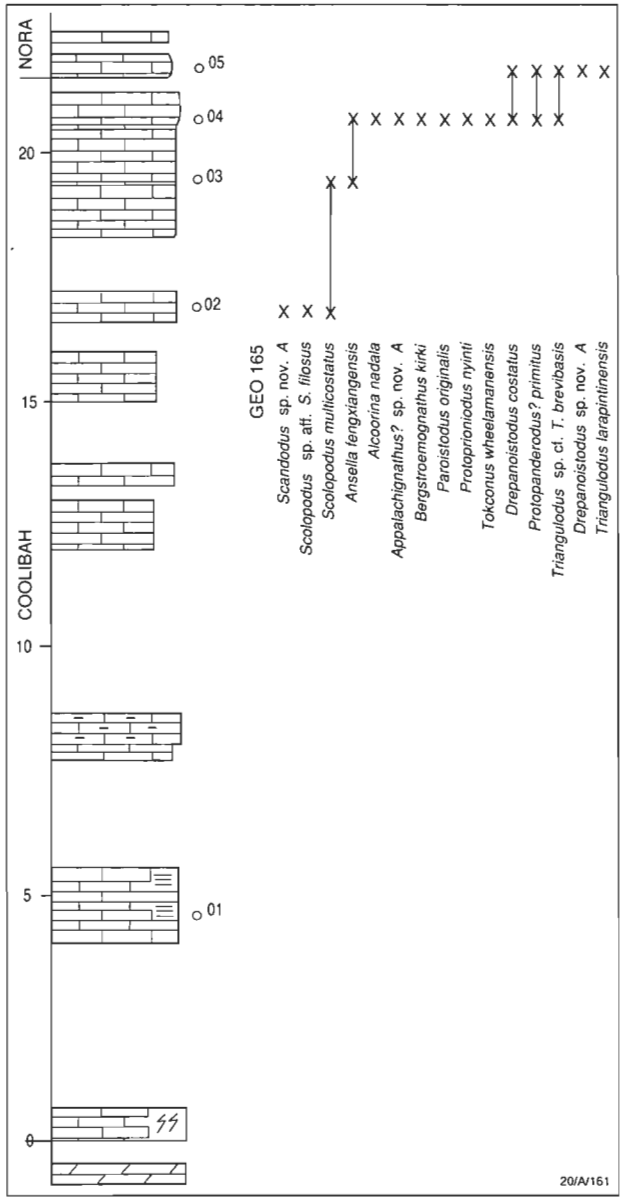

Figure 10. Stratigraphic section and associated conodont range chart, locality GEO 165, Bloodrock Creek near Marqua Tobermory boundary fence.
Stratigraphic thickness is measured in metres. Symbols and scale as in Figure 2.

nathus? apparatuses. *Protoprioniodus* species occur in overlying strata, which contains zone OCD conodonts, including *Paroistodus originalis*. It is concluded that the Coolibah Formation correlates with rocks containing faunas of upper zone OCC and zone OCD. This corresponds to the interval extending from upper Emanuel Formation to low in the Gap Creek Formation.

Conodonts from Mt Arrowsmith contain *Protoprioniodus nyinti*, and tentatively correlate with those from middle or upper Coolibah Formation (Kennedy, 1975).

The Victorian conodont fauna (Stewart, 1988) has no zonal fossils in common, and therefore cannot be directly correlated, with the Coolibah Formation.

International correlation

Coolibah Formation conodonts have strongest links with faunas of North China, and North and South Korea, supporting the prediction of 'close proximity (but not contiguity) of North China with ... Australia' during the early Ordovician (Burrett & Stait, 1987, 70). Appropriate correlations are detailed in Table 1.

The occurrence of *Drepanoistodus costatus, Tokoconus wheelamanensis, Triangulodus* sp. cf. *T. brevibasis, Aurilobodus? leptosomatus* and *'Oepikodus' maggolensis* Lee in lower Majiagou Formation rocks of northern China, and of *Protopanderodus? primitus* and *Oistodus multicorrugatus* within the Majiagou Formation indicates contemporaneity of lower and middle Coolibah Formation with lower Majiagou Formation.

On the basis of co-occurrence of *Ansella fengxiangensis*, Coolibah Formation conodonts probably correlate with those from part of the Dawan Formation of southern China (see An, 1987).

Protopanderodus? primitus is present in the Dumugol Formation of Kangweon-Do in South Korea (Lee, 1975a). The overlying Maggol Formation contains *'Oepikodus' maggolensis* and *Erraticodon tangshanensis* Yang & Xu (Lee, 1976). Coolibah Formation conodonts correlate with those from the Dumugol Formation and into the Maggol Formation.

Drepanoistodus costatus and *Scolopodus multicostatus* dominate faunas of the lower Coolibah Formation. These two species, together with *Oistodus multicorrugatus*, are found in strata of Ugorian to Kimaian age on the Siberian Platform (see Abaimova, 1975 and Moskalenko, 1984).

Presence and succession of *Scolopodus multicostatus, Oistodus multicorrugatus* and *Protoprioniodus nyinti* within both Coolibah Formation and Ordovician strata of the Ibex area indicate deposition of the Coolibah Formation during the time of Zone G2 to zone L conodont faunas (Ethington & Clark, 1981).

This corresponds, according to mutual presence of *Protopanderodus? primitus, Triangulodus* sp. cf. *T. brevibasis* and *Oistodus multicorrugatus*, with upper San Juan Formation of Argentina (Serpagli, 1974).

The presence of *Paroistodus originalis* indicates a tentative correlation of the Coolibah Formation conodonts with those of the Arenig or lower Llanvirn of northern Europe (see Löfgren, 1978).

Systematic palaeontology

Type and figured specimens are housed in the Commonwealth Palaeontological Collection at the Australian Geological Survey Organisation, Canberra, and have numbers prefixed by the letters CPC.

Only one association of elements remains unnamed because of small numbers of specimens. All other taxa described form part of multielement apparatuses.

Conodont apparatuses are described according to the nomenclatural system of Barnes & others (1979), together with the descriptive form terminology commonly used to designate general element shape. Apparatus positions of

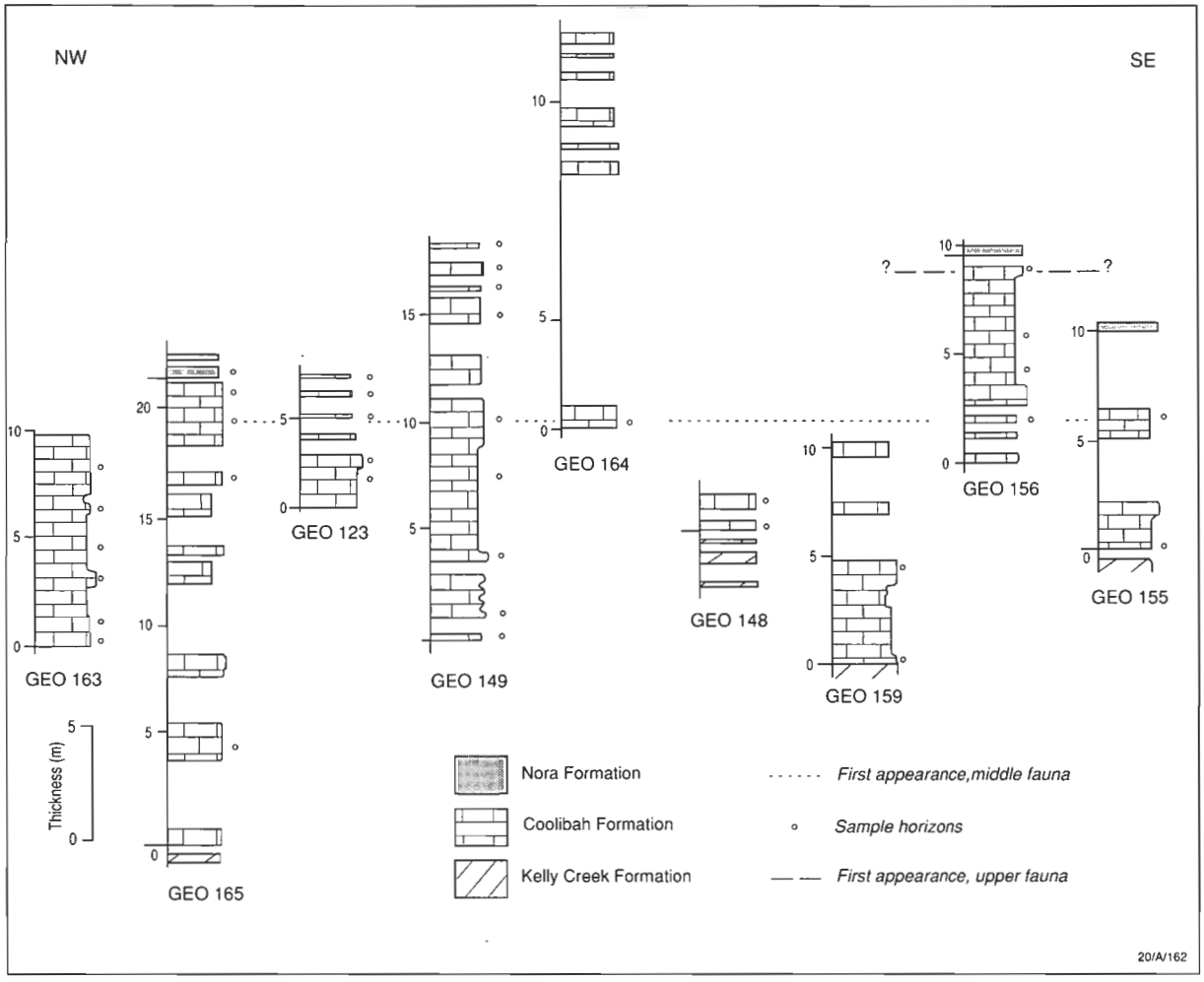

Figure 11. Correlation of Coolibah Formation measured sections.

Sweet (1981) are also indicated, where possible.

As a consequence of rapid evolution of Lower and Middle Ordovician conodonts, with a considerable variety of apparatuses, systematics of this group has not yet stabilised. Taxa considered herein are therefore listed alphabetically.

Conodont occurrence and abundance charts for all GEO localities are included in Table 2. Specimens were processed while in the field. No record of sample weight has been retained, and comparison of faunal abundance per kilogram of sample is not possible.

Genus *Alcoorina* gen. nov

Type species. *Alcoorina nadala* sp. nov.

Etymology. For Alcoora Creek, which passes one section from which specimens of this genus were collected.

Diagnosis. An apparatus of coniform elements with short base; cusp striate on inner or both lateral faces, with sharp edges, densely albid. Striae meet at acute angle at grooves. All elements have base flared to some extent.

Drepanodontiform (a, S_c), asymmetrical acontiodontiform (b, S_b), acontiodontiform (c, S_a), oistodontiform (e, M), scandodontiform (f, P_b) and suberectiform (g, P_a) elements are included within a Type IVB apparatus of Barnes & others (1979).

Remarks. Elements of this apparatus bear some similarity to co-occurring species of *Protopanderodus* Lindström, but are distinguished by their extremely short base and their cusp cross-section: lateral keels are poorly developed on b and c elements of *Alcoorina* when compared with those of *Protopanderodus*.

Alcoorina nadala sp. nov.
Figs 12A–D, 15A–J

Etymology. From the Old High German *nadal*, needle, alluding to the form of the diagnostic scandodontiform and suberectiform elements.

Type specimens. Holotype CPC 23312 (GEO 123/OO6), suberectiform element; paratypes CPC 23313 (GEO 123/003), suberectiform element; CPC 23314 (GEO 148/005) drepanodontiform element; CPC 23315 (GEO 149/005), asymmetrical acontiodontiform element; CPC 23316 (GEO 132/016), acontiodontiform element; CPC 23317 (TOK 9/6), oistodontiform element; CPC 23318 (GEO 123/005), scandodontiform element; CPC 23319 (GEO 123/005), scandodontiform element. All are figured specimens.

Table 1. Correlation of the Coolibah Formation with significant localities within Australia and internationally, on the basis of conodont faunas.

Only localities with conodonts showing faunal affinity with those of the Coolibah Formation are considered. Data for the Georgina Basin are from this study. Other sources include Cooper (1981) and Nicoll & others (1992) for the Amadeus Basin, McTavish (1973) and Cooper (1981) for the Canning Basin, An & others (1983) for North China, Lee (1975a, 1976) for South Korea, Serpagli (1974) for Precordilleran Argentina, and Ethington & Clark (1981) for the Ibex Area of Utah-Nevada in North America.

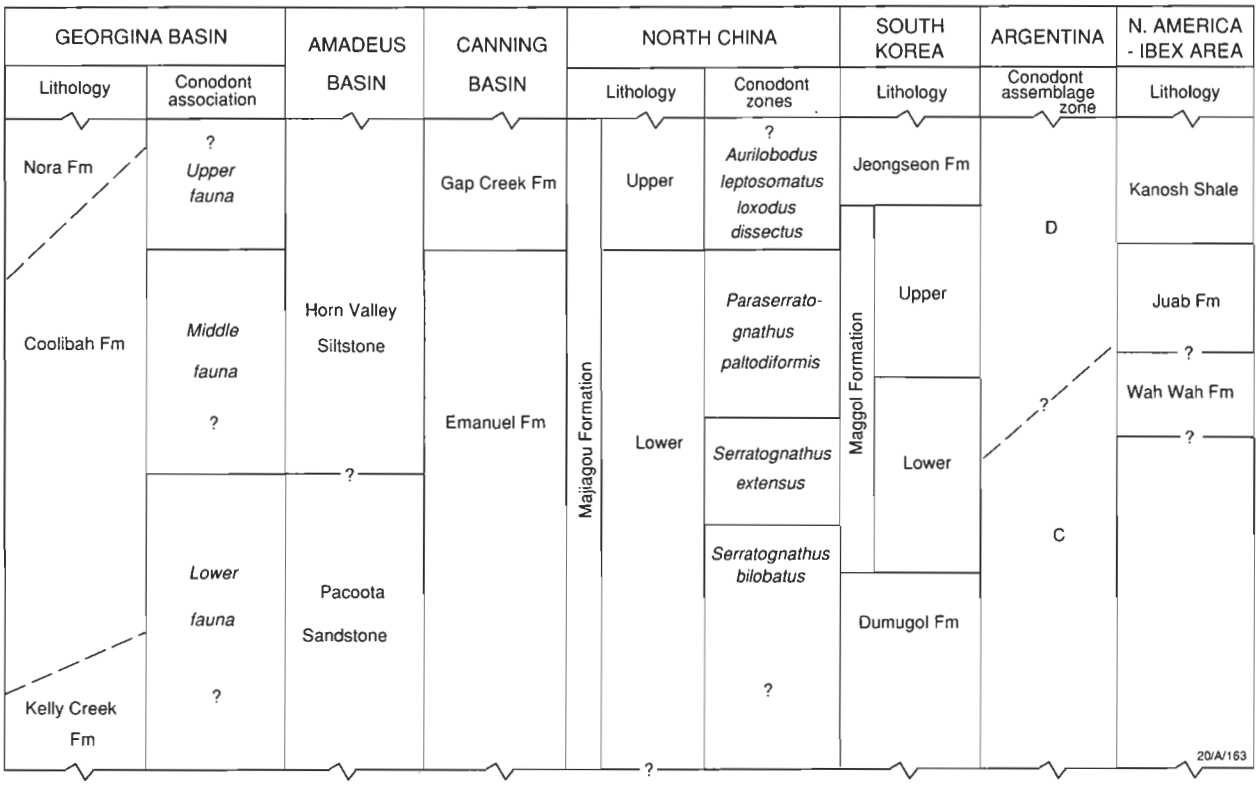

Type stratum. GEO 123/006, five m above base of Coolibah Formation exposed to side of Bloodwood Creek, (grid co-ordinates 596153, on Tobermory topographic 1:250 000 map SF 53–12, Edn 2, Series R 502).

Material studied. 67 specimens: 9 drepanodontiform, 11 asymmetrical acontiodontiform, 4 acontiodontiform, 8 oistodontiform, 20 scandodontiform and 15 suberectiform elements.

Diagnosis. As for genus.

Description. All elements with sharp edges to cusp, and short base; cusp striate on at least part of lateral faces, densely albid.

Drepanodontiform element with reclined to erect cusp; cusp edge, with or without narrow blocky keels; element has unequally biconvex cross-section. Intersection of posterior and oral margins is obtuse (approximately 130–150°); antero-aboral intersection is approximately perpendicular; aboral and oral margins form an acute to perpendicular intersection (70–90°). Oral margin is short; base occupies less than 1/6 length of element; aboral opening is teardrop to D-shaped, base may flare slightly inwards. Tip of shallow basal cavity is close to anterior margin of cusp; anterior edge of cavity convex towards cavity; posterior margin of cavity almost straight from oral–aboral intersection to tip.

Asymmetrical acontiodontiform element as above except that anterior margin has broad, blocky keel extending along cusp to base, and there is a shallow groove in posterior part of inner lateral face; cusp cross-section is triangular, but asymmetrical; intersection of aboral and oral margins is acute (approximately 60°). Inner lateral face of base flares inwards and up; aboral opening is teardrop-shaped; tip of basal cavity is situated at approximately 1/3 distance between anterior and posterior margins (at edge of anterior keel).

Acontiodontiform element has equidimensional cusp; lateral edges sharp and keeled only in region of greatest cusp curvature. Aboral opening has shape of gothic arch, with no projecting lateral flanges; oral margin short; postero-oral intersection obtuse (approximately 120°); each lateral edge intersects aboral opening approximately perpendicularly.

Oistodontiform element similar to asymmetrical acontiodontiform element except that postero-oral intersection is acute (30–40°); antero-aboral intersection approximates 130–150°; 30–40° is subtended by intersection of oral and aboral margins. Oral margin keeled, straight; a depression is formed on cusp anterior of postero-oral intersection. Base has inner lateral flare medially.

Scandodontiform element is similar to asymmetrical acontiodontiform element, but cusp is twisted, posterior groove may or may not be pronounced, and aboral opening is lenticular.

Suberectiform element as scandodontiform element, but cusp is more noticeably twisted, with more pronounced inner lateral flare to base, generally a pronounced posterior groove to inner lateral face and acontiodontiform cross-

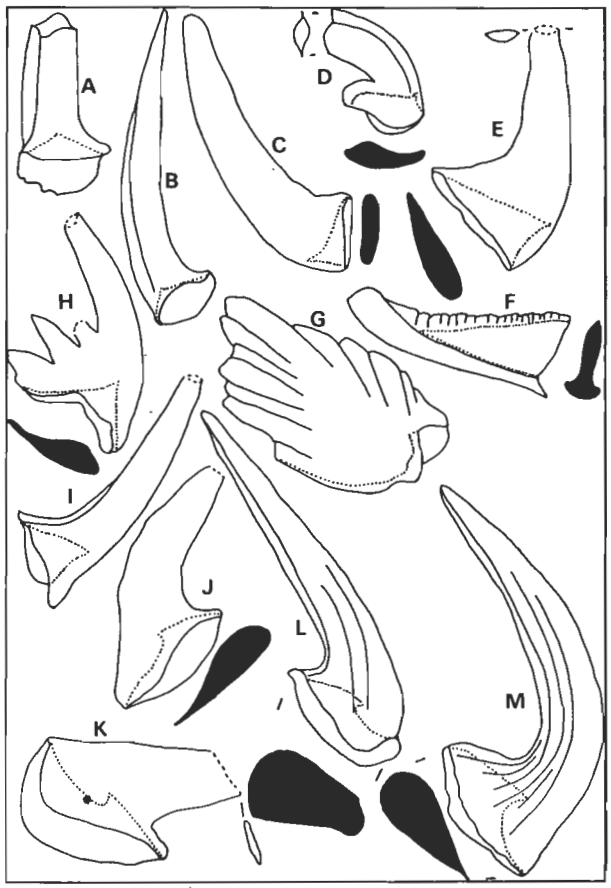

Figure 12. Selected conodont elements.
Basal cavity outline is indicated by dotted lines; cusp cross-section (unshaded) and shape of aboral opening (shaded) are included.
All specimens ×80 unless otherwise stated.
A-D, *Alcoorina nadala* gen. et sp. nov. A, suberectiform element, paratype, CPC 23313, posterior view, GEO 123/003. **B,** scandodontiform element, paratype, CPC 23319, inner lateral view, GEO 123/005. **C,** drepanodontiform element, paratype, CPC 23314, lateral view, GEO 148/005. **D,** oistodontiform element, paratype, CPC 23317, inner lateral view, TOK 9/6. **E, F *Ansella fengxiangensis*** (An & others). **E,** erectiform element, CPC 23324, lateral view, GEO 123/005. **F,** asymmetrical belodelliform element, CPC 23321, lateral view, GEO 123/006. **G, *Appalachignathus?* sp. nov.** Eoliginodiniform element, CPC 23326, inner view, GEO 123/005. **H, *Bergstroemognathus kirki* sp. nov.** ×70, cordylodontiform element, paratype, CPC 23334, inner lateral view, GEO 123/003. **I, *Diaphorodus tortus*** (McTavish) gothodontiform (b, s_b) element, CPC 23340, inner lateral view, GEO 132/022. **J, K, *Drepanoistodus* sp. nov. A,** ×70, from GEO 156/004. **J,** homocurvatiform element, CPC 23352, inner lateral view. **K,** oistodontiform element, CPC 23354, inner lateral view. **L, M, *Drepanoistodus costatus*** (Abaimova), ×40. **L,** oistodontiform element, CPC 23350, inner lateral view, GEO 148/005. **M,** scandodontiform element, CPC 23351, lateral view, GEO 132/016.

section to cusp; aboral opening is D-shaped to rectangular.

Remarks. Elements of *Alcoorina nadala* are superficially similar to *Scolopodus warendensis* Druce and Jones, *Scolopodus transitans* Druce and Jones and *Oneotodus erectus* Druce and Jones from the Ninmaroo Formation of the Georgina Basin. These may be congeneric with *A. nadala*, but differ in cusp cross-section and morphology of basal region.

Distribution. Throughout the Coolibah Formation within the study area.

Genus *Ansella* Fåhraeus and Hunter, 1985

Type species. *Belodella jemtlandica* Löfgren, 1978

Remarks. Apparatus of this genus, as reconstructed by Fåhraeus & Hunter (1985) and Watson (1988), include oepikodontiform, belodelliform, oistodontiform, and drepanodontiform elements. Symmetry transitions mentioned by Fåhraeus & Hunter allow for both asymmetrical and symmetrical forms of oepikodontiform, belodontiform and drepanodontiform elements in a Type IVB apparatus, as described by Watson (1988, 104). The following species was also found to follow this plan, with symmetrical oepikodontiform (a, Sc), asymmetrical oepikodontiform (b, Sb), symmetrical and asymmetrical belodelliform (c, Sa), oistodontiform (e, M), drepanodontiform (f, Pa) and erectiform elements (g, Pb). It is possible that asymmetrical belodelliform elements may occupy the d (Sd) position in this apparatus, in which case the apparatus is modified Type IVC.

Ansella fengxiangensis (An & others, 1981)
Figs 12E-F, 15K–N

Synonymy.
Multielement reconstructions
Belodella fengxiangensis An, Du, Gao, Chen & Lee. An & others, 1985, pp. 43–44, pl. 15, figs 16–19 only; An, 1987, pp. 129–130, pl. 21, figs 25–26, pl. 24, fig. 26, pl. 29, fig. 5 (synonymy).

Unfigured specimens. CPC 23322 (GEO 123/005), symmetrical belodelliform element; CPC 23325 (GEO 123/005), drepanodontiform element

Material studied. 36 specimens: 5 symmetrical oepikodontiform, 7 asymmetrical oepikodontiform, 2 symmetrical belodelliform, 3 asymmetrical belodelliform, 3 oistodontiform, 7 drepanodontiform and 9 erectiform elements.

Remarks. Intraspecific variation in denticle size and orientation, and strength of costae preclude use of these variables to distinguish between species of *Ansella* (Watson, 1988). However, depth and shape of basal cavity appear consistent within populations of *Ansella*. The relatively shallow and less convex anterior margin to basal cavity appears consistent throughout geographic occurrence of *A. fengxiangensis*. Additionally, cusp of belodelliform and oepikodontiform elements is consistently twisted. Symmetry of these elements is then determined by position of costae or lateral carinae on the base.

The oistodontiform element figured by An & others (1985, pl. 15, figs 13, 14) has a larger base than Coolibah Formation specimens, but is similarly twisted. Possibly this belongs to a related species.

Distribution. *Ansella fengxiangensis* is known from North and South China, and middle and upper Coolibah Formation of the Georgina Basin.

Genus *Appalachignathus* Bergström, Carnes, Ethington, Votaw & Wigley, 1974

Type species. *Appalachignathus delicatulus* Bergström, Carnes, Ethington, Votaw & Wigley, 1974.

Remarks. The apparatus reconstruction of Bergström & others (1974) is followed here. Eoliginodiniform (a, S_c), zygognathodontiform (b, S_b), trichonodelliform (c, S_a), spathognathodontiform (e, M) and ozarkodiniform (f, P_a) elements are recognised in a Type IVE apparatus.

Bergstroemognathus Serpagli and *Leptochirognathus* Branson & Mehl have similar apparatuses to that of *Appalachignathus*. All these genera have palmate elements and it is possible they are closely related. *Bergstroemognathus* is distinguished from *Appalachignathus* in having a cordylodontiform element in the a position and a prioniodontiform f element; *Leptochirognathus* also has a cordylodontiform a element, with similar f element to that of *Appalachignathus*.

Appalachignathus? sp. nov. A
Fig. 12G, 16A–C,E

Synonymy.
Ozarkodiniform? element
cf. *Loxodus dissectus* An. An & others, 1983, pp. 106–107, pl. 21, figs 12,13; An, 1990, pl. 8, figs 2-5.
cf. *Loxodus* aff. *dissectus* An. An, 1990, pl. 8, fig. 1.

Material studied. 15 specimens: 7 eoligonodiniform, 7 zygognathodontiform and 1 ozarkodiniform? elements. In addition, 7 blade-like fragments were located.

Description. All elements palmate, or curved blades, with cusp only slightly longer than denticles, but twice as broad; denticles thin, commonly eight times as high as broad, fused for most of length; basal region almost 1/3 height of element; basal cavity very shallow, consisting of narrow slit beneath processes, conical beneath cusp and flaring to posterior or posterolaterally. All elements may be completely hyaline, or with cone-in-cone growth axis in cusp and denticles, or with milky albid cusp and denticles.

Eoligonodiniform element with anterolaterally directed conical basal cavity which continues as a slit beneath one process; posterolateral region has up to six poorly developed denticles.

Zygognathodontiform element similar to eoliginodiniform element except that basal cavity is directed towards anterior margin; posterolateral process shorter than lateral process.

Ozarkodiniform? element blade-like, with proximal denticles isolate for half to quarter length, erect; distal denticles become progressively more reclined, fused for most of length; basal cavity conical and not flared, tip situated near anterior margin; first or second denticle on inner lateral face rather than within plane of blade.

Remarks. Only the three elements described above have been found in the Coolibah Formation. First symmetry transition (S) elements show the range of basal cavity morphology typical of *Appalachignathus delicatulus*, and are accompanied by a considerable number of fragmented blades. It is most likely that the apparatus is that of *Appalachignathus*, but ozarkodiniform? elements may be sufficiently distinct to separate these specimens into a previously undescribed genus.

Loxodus dissectus An has similar denticulation to specimens of P elements described above, and may belong to this apparatus, but no flexing, or misaligned denticles are reported within An's specimens.

Distribution. *Appalachignathus?* sp. nov. A is found through the Coolibah Formation, but is more common in lower parts of this formation.

Genus *Aurilobodus* Xaing & Zhang, 1983

Type species. *Tricladiodus? aurilobus* Lee, 1975.

Remarks. Apparatus of *A. aurilobodus* (Lee) consists of cordylodontiform (s), zygognathodontiform (t) and trichonodelliform, or acontiodontiform, where elements are not denticulate, (u) elements (Lee, 1975; An & others, 1983), which forms a Type IA apparatus.

Aurilobodus? leptosomatus An, 1983
Fig. 17A–C

Synonymy.
Aurilobodus leptosomatus An. An & others, 1983, pp. 72–73, pl. 21, figs 14–17, pl. 22, fig. 1.
Juanognathus leptosomatus (An). Watson, 1988, p. 116, pl. 1, figs 1–3, 6 (synonymy).

Material studied. 6 specimens: 2 zygognathodontiform, 3 acontiodontiform and 1 alate acontiodontiform elements.

Remarks. *Aurilobodus* is distinguished from *Juanognathus* by the shape of aboral opening, and alae on lateral flanges; the former genus generally has a basal ledge parallel to aboral opening, which is not present on most species of *Juanognathus*. *Aurilobodus leptosomatus* has a poorly developed basal ridge, and aboral opening with rounded rather than angulate posterior region, similar to Juanognathus. This species is clearly transitional between *Juanognathus* and *Aurilobodus*, and is tentatively assigned to *Aurilobodus* following An (*in* An & others, 1983).

Elements figured by Harris & others (1979, pl. 1, figs 3–5) and *Juanognathus serpaglii* Stouge may be congeneric with *A?. leptosomatus*, but the different angle in lateral outline on elements with alae and the more pronounced development of basal ledge preclude conspecificity.

Different lateral outlines distinguish Gen. nov. B of Cooper and Druce (1975) and *Aurilobodus simplex* Xiang & Zhang from *A?. leptosomatus*. In addition, Gen. nov. B has twisted cusp.

Distribution. *Aurilobodus? leptosomatus* is found in the lower Majiagou Formation of North China (An & others, 1983), lower and middle Goldweyer Formation of the Canning Basin in Western Australia (Watson, 1988) and lower to middle Coolibah Formation of the Georgina Basin.

Genus *Bergstroemognathus* Serpagli, 1974

Type species. *Oistodus extensus* Graves and Ellison, 1941.

Remarks. The apparatus of *Bergstroemognathus* has first symmetry transition of cordylodontiform, (a, S_c), zygognathodontiform (b, S_b) and trichonodelliform (c, S_a) elements accompanied by falodontiform (e, M) and prioniodontiform (f, P) elements in a Type IVE apparatus.

Serpagli's (1974, pp. 41–2) symmetry transition of prioniodontiform elements includes zygognathodontiforms, but no cordylodontiforms are reported from his material. These, however, occur together in material from the Appalachians of North America (Stait & Barnes, in press).

Bergstroemognathus kirki sp. nov.
Fig. 12H, 16D,F–H,J

Etymology. After R. and V. Kirk of Glenormiston Station,

Queensland, on which the type locality is situated.

Type specimens. Holotype CPC 23338 (GEO 123/ 003), prioniodontiform element; paratypes CPC 23334 (GEO 123/003), cordylodontiform element; CPC 23335 (GEO 132/016), zygognathodontiform element; CPC 23336 (GEO 149/007), trichonodelliform element; and CPC 23337 (GEO 149/001), falodontiform element.

Type stratum. GEO 123/003, 1.6 m above the base of outcropping Coolibah Formation to side of Bloodwood Creek. (Grid reference 596153 on Tobermory 1:250 000 topographic sheet SF 53–12, Edn 2, Series R 502.)

Material. 36 specimens: 2 cordylodontiform, 11 zygognathodontiform, 4 trichonodelliform, 11 falodontiform and 8 prioniodontiform elements.

Diagnosis. A species of *Bergstroemagnathus* with denticulate posterior processes on prioniodontiforms, minimal posterior process and cusp on falodontiforms, and first symmetr transition elements with pronounced aboral extension of anterior.

Description. All elements moderately robust to blocky; hyaline with cone-in-cone growth axis to cusp and denticles; cusp erect to reclined, with broad blocky keels; denticles free distally, fused proximally, laterally compressed with edges or narrow keels on anterior and posterior margins; antero-aboral extension marked in all elements; base has inner ridge parallel to aboral margin; basal cavity shallow, reduced to slit beneath processes, anteriorly directed, but does not reach anterior margin.

Cordylodontiform element has asymmetrically biconvex cusp; inner lateral carina extends onto base as flare of aboral margin. Zygognathodontiform element similar with anterior and posterior processes unequally developed. Trichonodelliform element without lateral flare to base. Falodontiform element with posterior process a round knob, denticles fused for half to two-thirds height, cusp reduced to size of denticles. Prioniodontiform element as zygognathodontiform, but element is not planar and processes may be considered posteriorly and anteriorly directed.

Remarks. Variation within elements includes degree of fusion of denticles, and development of aboral ridge on inner surface. From half to two thirds the length of adjacent denticles may be fused.

Bergstroemognathus kirki differs from previously described species in the poor development of posterior process on falodontiform element. It is distinguished from *B. extensus* (Graves and Ellison) by its aboral extension instead of sinuous aboral margin on other elements. It is similar to *B. pectiniformis* Yang and Zhang, which has adenticulate posterior process on prioniodontiform element (An & others, 1983, pl. 17, figs 14, 15).

Distribution. This species is found throughout the Coolibah Formation of the Georgina Basin.

Genus *Diaphorodus* Kennedy, 1980

Type species. *Acodus delicatus* Branson & Mehl, 1933.

Diaphorodus tortus (McTavish, 1973)
Fig. 12I, 17C–E,G-I

Synonymy.
Multielement reconstructions
Acodus deltatus tortus subsp. nov. McTavish, 1973, p. 40, pl. 1, fig. 18, text-figs 3a–d.

Figured specimens. CPC 23339, a, S_c element; CPC 23340, b, S_b element; CPC 23341, c, S_a element; CPC 23342, d, S_d element; CPC 23343, e, M element; CPC 23344, f, P element.

Remarks. Torsion of the cusp, shallower basal cavity and divergent cusp outlines distinguish *Diaphorodus tortus* from other species of *Diaphorodus*, including *D. deltatus* Lindström. We consider these differences significant at the species, rather than subspecies, level as was suggested by McTavish (1973).

Co-occurring specimens of *Triangulodus* sp. cf. *T. brevibasis* (Sergeeva) within the Coolibah Formation are superficially similar to those of *D. tortus*. First symmetry transition elements differ in depth of basal cavity, outline of element when viewed laterally, and cross-sectional symmetry of c and d elements. *Diaphorodus tortus* has shallower basal cavity, with tip further from anterior margin, generally more expanded basal region and more symmetrical arrangement of costae than *T.* sp. cf. *T. brevibasis*. Second symmetry transition elements are more easily distinguished, with oistodontiform (e) elements separated according to lesser development of oral region and broad cusp relative to base of *T.* sp. cf. *T. brevibasis*, and prioniodontiform f elements of *Diaphorodus* where *Triangulodus* has erect scandodontiform elements in the f position. These last are distinguished from gothodontiform (b) elements of *D. tortus* by biconvex cusp and aboral opening

Distribution. *Diaphorodus tortus* occurs in lower to middle Coolibah Formation of the Georgina Basin and uppermost Emanuel Formation of the Canning Basin, Western Australia.

Genus *Drepanoistodus* Lindström, 1971

Type species. *Oistodus forceps* Lindström, 1955

Remarks. *Drepanoistodus* differs from *Drepanodus* in the lack of pipaform and sculponeaform elements. Geniculate element of *Drepanoistodus* has postero-oral intersection which is commonly more acute than any (i.e. graciliform of Kennedy, 1980) which may be assigned to *Drepanodus*.

Elemental nomenclature of Barnes & others (1979) only is applied herein, since this apparatus as described does not yet comfortably fit the terminology of Sweet (1981). Arcuatiform elements (q') are herein considered to be modified homocurvatiform elements; scandodontiform elements are also regarded as modified drepanodontiform (q") elements.

Drepanoistodus costatus (Abaimova, 1971)
Fig. 12L–M, 17J–N

Synonymy.
Homocurvatiform (q) element
Drepanodus costatus. Abaimova, 1971, p. 490, pl. X, fig. 6, text-fig. 3; Abaimova, 1975, pp. 59–60, pl. III, figs 6–8,14, text-figs 6:25,28,29; Moskalenko, 1982, p. 109, pl. 27, figs1–3; Moskalenko, 1984, p. 123, pl. 13, figs 19,20.

Table 2. Occurrence and abundance of conodonts in conodont-bearing samples from sections 123, 132, 139, 147, 149, 152, 155, 156, 159, 163, 164 and 165. GEO 132 consists of spot samples of Coolibah Formation lithology collected from the Toko Range. Location of other sections is shown in Figure 1. Precise sample locations within each section are shown in Figures 2–10.

	GEO 123:					GEO 132:												139:
	3	4	5	6	7	2	5	7	11	12	13	14	15	16	22	23	26	1
ALCOORINA NADALA																		
drepanodontiform			1											2				
asym. acontiodontiform		1	2											1				
acontiodontiform														1				
oistodontiform	1				1									1				
scandodontiform	1	1	2		2						1			3				
suberectiform	4		1	1	1									2				
ANSELLA FENGXIANGENSIS																		
sym. oepikodontiform				1			1											
asym. oepikodontiform				2			1											
sym. belodelliform			1	1														
asym. belodelliform				1	1										1			
oistodontiform				1	1													
drepanodontiform			1	1										3				
erectiform			1	1										3				
APPALACHIGNATHUS? sp. nov. ***A***																		
eoliginodiniform	2		1	1										1				
zygognathodontiform	2			1										3				
?ozarkodiniform			1															
bladelike fragments	1		1												2			
AURILOBODUS? LEPTOSOMATUS																		
zygognathodontiform																		
acontiodontiform				1														
AURILOBODUS SERRATUS																		
trichonodelliform			1															
BERGSTROEMOGNATHUS KIRKI																		
cordylodontiform	2																	
zygognathodontiform	7										1			1				
trichonodelliform	1				1													
falodontiform	2				2									1				
prioniodontiform	5				1													
DIAPHORODUS TORTUS																		
drepanodontiform	1			1		1								4				2
gothodontiform	1		1			1								3	1			1
acontiodontiform	2		2	2										2	1	1		
distacodontiform	2													3				
oistodontiform	4		1	3		1								18	1			1
prioniodontiform	4					1								4				2
DREPANOISTODUS COSTATUS																		
suberectiform	3				1									1				2
arcuatiform	21			2										7			1	1
homocurvatiform	14			1		1		1		1			1	17				4
oistodontiform														1				
scandodontiform	8												2	2				
DREPANOISTODUS sp. nov. ***A***																		
suberectiform												1						
homocurvatiform				1			3					2	1		3			
oistodontiform				1								1			1			
scandodontiform																		
ERRATICODON TANGSHANENSIS																		
b element																		1
neoprioniodontiform															1			1
'OEPIKODUS' MAGGOLENSIS																		
symmetrical element							2											
alate element							1											
OISTODUS MULTICORRUGATUS																		
cordylodontiform																		
trichonodelliform											1	1						
d element												1						
oulodontiform												1						
PAROISTODUS ORIGINALIS																		
drepanodontiform			1	1	1		1					2						1
oistodontiform					2							1						
scandodontiform			1		2													2
PROTOPANDERODUS? PRIMITUS																		
unigrooved	3			2	3		1		1	1								
asym. acontiodontiform	4		4	3	3	1	3			1	1			2	1			2
acontiodontiform	2		2	3	4		3				1			3	5			
peltodontiform																		
scandodontiform	1		8	2	2		2		1					2	2			1
keeled scandodontiform	4		1	1	1							1		1	1			
PROTOPRIONIODUS NYINTI																		
cordylodontiform			1															
gothodontiform			1															
acontiodontiform																		
oistodontiform				1														
blade element			1															
SCANDODUS sp. nov. ***A***																		
drepanodontiform											1			1				
planoconvex								1			1			1				
acontiodontiform	1													1				
distacodontiform																		
oistodontiform			1								1			1				
scandodontiform	1								1					1				
SCOLOPODUS sp. aff. ***S. FILOSUS***																		
later. compr. peltodontiform																		
planoconvex		1										1					3	
acontiodontiform		1						1										
equidim. peltodontiform																		
scandodontiform		2			1			1							1		1	
keeled scandodontiform		1						1				1			1			
SCOLOPODUS MULTICOSTATUS																		
later. compr. peltodontiform	8													3			1	
planoconvex	22										1			10	1		2	
acontiodontiform	5					1								6				
equidim. peltodontiform	1			1										1				
scandodontiform	8													6			1	
keeled scandodontiform	11													3				
TOKOCONUS WHEELAMANENSIS																		
drepanodontiform	1				3									5				
gothodontiform	5			1	1									2				1
acontiodontiform	6													1				
distacodontiform	1				1									3				
acodontiform	4				1									3				
scandodontiform	4			1	1									4				
TRIANGULODUS sp. cf. ***T. BREVIBASIS***																		
drepanodontiform												1			2			1
acodontiform												2						1
roundyaform												1			1			1
paltodontiform												3			2			1
oistodontiform												7	1		1			5
erect scandodontiform		1										5			2			3
TRIANGULODUS LARAPINTINENSIS																		
drepanodontiform										1								2
acodontiform							2											3
acontiodontiform							1				1	1						4
paltodontiform							1											1
oistodontiform							3											3
erect scandodontiform							2											2
Conical elements																		
element I																		
element II																	1	
element III																	1	
element IV	1																	
element V					1													
element VI			1														2	
TOTAL:	181	8	39	39	38	7	27	5	3	4	10	33	5	145	31	1	13	49

GEO 147:					148:	GEO 149:					GEO 152:		GEO 155:		GEO 156:			GEO 159:		GEO 163:				GEO 164:			GEO 165:				TOTAL
2	3	4	5	6	5	1	5	6	7	9	4	6	4	5	1	3	4	8	9	2	4	5	6	1	2	3	2	3	4	5	
	1				3		1																						1		9
	1				4		1																						1		11
											1							1		1											4
					4		1																								8
	1			1	3		1													2									2		20
				1	3				1		1																				15
																												1	2		5
												1														1			2		7
																															2
																															3
												1																	1		3
											2	1																	1		7
						1															1										9
																						1									7
																				1											7
				1																1									1		7
							1																	1							2
							1																		1						3
																															1
																															2
											1							1													11
									1													1									4
					3	1			1																				1		11
									1									1													8
1					2													1													13
											1							1													10
1				1	5						2			1				1													21
					4						1																				10
1					7						1			1										1							40
					1						4																				16
						3							1											1						1	13
	1			2	5					1	2	1		1	2		1								1					2	51
	2		1		11		1				2	2	2		2			1			1				1	1			1	3	71
					3		1				1																				6
					7										1			1												2	23
																	2												1	4
																	1												2	13
																	1			1										5
																													1		1
																	1														1
																															3
																															2
																															1
				1																											1
																															2
																															1
																															1
				1											1	1								1					1		12
					2							1		1										1							8
					1																										6
			1		4																								2		18
		1	1	3	4		3		3						1			1		1	1			6	2				25		77
1	1			5	1		4		1		1				2			1		1					1	1			18	1	62
					1			1							1														1		4
1	1	1		2	2		2						1		1			1							1				17		51
				5			1				1													3	1				27		48
																	1														2
																															1
																													1		1
																													2		3
																															1
					1		1													1						1					4
																				1					1						7
																				1											4
																															3
1			1		1															4							1				11
																				4											7
1					1						1									8				1			1				27
					4						2	1			1			3	1	4							1				7
																		1		2							1				4
					7						1							2		2							1				19
					8													2		2							1				15
											1	1								2				1							17
				2		1					1	1								5				1	1		1				49
											1									3				1							17
						1					1													1							8
						1					1									7							2	1			27
																				9							1				24
		1			1		1																								12
1					3		2																						2		18
		1			2													1										1		12
					2																										7
					1		1															1									10
1							2				1																				15
					7						1	1					2													1	16
					3												1														7
			1		4						1				1														1		11
					5									1			3														15
			1		18						1			1		2	1												1	3	42
			1	1	5						2	2		1		2	1							1					1		28
															2	1	2							2						2	12
															2	2	2							1						2	14
																3	1							1		1				1	14
																2	1													1	6
															1	1	1							1						2	12
															1	2	2							1						4	14
																				1											1
					1																										1
					1														1	1											2
																															4
																															1
																															4
9	8	4	7	26	155	8	25	2	8	1	38	13	4	7	18	17	24	18	2	65	2	2	1	26	9	4	13	2	114	29	1296

20/A/164

Arcuatiform (g') element
Drepanodus sibiricus. Abaimova, 1975, p. 69, pl. VI, figs 4, 5, text–figs 7:3,9.
Multielement reconstructions
Scolopodus flexilis. An, 1981, p. 222 (incomplete), pl. 3, figs 1–2; An & others, 1983, pp. 142–3, pl. XIV, figs 13–18; An, 1990, pl. 5, figs 1–6.

Material. 163 specimens: 13 suberectiform, 71 homocurvatiform, 51 arcuatiform, 6 oistodontiform and 23 scandodontiform elements.

Description. Homocurvatiform, suberectiform and arcuatiform elements are well known (e.g. Abaimova, 1975; An, *in* An & others, 1981; Moskalenko, 1984). These are similar to oistodontiform and scandodontiform elements in their posteriorly costate cusp, commonly with one persistent costa extending entire length of cusp (An, *in* An & others, 1981). All are robust, with shallow basal cavity.

Oistodontiform and scandodontiform elements have sharp posterior and anterior edges on a laterally compressed cusp, are asymmetrically costate. Oistodontiform element has antero-aboral depression on inner lateral face; base short; aboral margin arcuate with antero-aboral intersection at approximately 80° and acute angle (30–45°) between oral and aboral margins; apex of basal cavity situated anterior of cusp midline. Scandodontiform element distinguished from other elements by slightly acute, instead of obtuse, postero-aboral intersection, posteriorly expanded base, and twisted cusp.

Remarks. No elements have the typically equidimensional cusp cross-section of *Scolopodus* Pander. Biconvex cusps, and elemental composition, are more characteristic of the genus *Drepanoistodus* (Lindström, 1971). *Drepanoistodus costatus* is distinguished from *D. pitjanti* Cooper by a more strongly costate cusp, shallower basal cavity and more slender cusp on most elements.

Distribution. *Drepanoistodus costatus* is known from upper Ugorian and Kimaian stages of the Siberian Platform (Abaimova 1971, 1975; Moskalenko 1982, 1984), and lower Majiagou Formation in the Tangshan area of North China (An, 1981). It occurs throughout the middle Coolibah Formation, Georgina Basin

Drepanoistodus sp. nov. A
Fig. 18A–C

Material studied. 23 specimens: 4 suberectiform, 13 homocurvatiform, 1 scandodontiform and 5 oistodontiform elements.

Description. All elements dominated by broad cusp, which tapers evenly, commonly without visible microstructure; basal cavity a shallow to moderately shallow 'phrygian cap' (Lindström, 1964), tip situated in posterior half of element, or close to midline; all elements are hyaline with central, dense, growth axis. Suberectiform elements with erect, asymmetrically biconvex, stout, evenly tapering cusp with sharp anterior and posterior margins, conical outline when viewed laterally, large specimens may have few fine costae close to posterior margin of inner lateral face; intersection of anterior and aboral margins approximately 70°, anterobasal area drawn out, postero-oral intersection obtuse (about 120°); base short, flares posteriorly and has teardrop shaped aboral opening, oral margin sharp.

Homocurvatiform element as above except aboral extension is more pronounced, with anterior and aboral margins intersecting at a more acute angle (60°); cusp plano-convex in cross-section, and reclined to recurved; inner lateral face has deep depression anterior of tip to basal cavity; base has plano-convex aboral opening.

Oistodontiform element differs from suberectiform element in angle of postero-oral intersection (around 60°) and subrectangular base, in which inner and outer lateral faces are unequally developed.

Remarks. This species is distinguished from previously described species of *Drepanoistodus* by subrectangular base of oistodontiform element, deeper basal cavity and unequal development of inner and outer lateral faces of oistodontiform elements.

Distribution. *Drepanoistodus* sp. nov. A occurs in middle and upper Coolibah Formation and is known from low in the overlying Nora Formation of the Georgina Basin.

Genus *Paroistodus* Lindström, 1971

Type species. *Oistodus parallelus* Pander, 1856.

Paroistodus originalis (Sergeeva, 1963)
Fig. 18F

Synonymy.
Paroistodus originalis Lindström. Löfgren, 1978, pp. 69–71, pl. 1, figs 22–25, text-fig. 28 (synonymy to 1976).

Material studied. 26 specimens: 12 drepanodontiform, 8 oistodontiform and 6 scandodontiform elements.

Remarks. While drepanodontiform, oistodontiform and scandodontiform elements are included, there are insufficient specimens to clarify the apparatus of this species.

Distribution. Löfgren lists occurrence of this species from middle Arenig to early Llanvirn: it is known from North America, Sweden, Norway, Estonia, the Leningrad area, Poland, and the Canning Basin of Western Australia. In the Georgina Basin, it occurs throughout the Coolibah Formation, usually in very low abundance.

Genus *Protopanderodus* Lindström, 1971

Type species. *Acontiodus rectus* Lindström, 1955.

Remarks. Specimens tentatively assigned to *Protopanderodus* from the Coolibah Formation, in common with those figured by recent authors (e.g. Serpagli, 1974; Löfgren, 1978; Olgun, 1987), vary not only with respect to cusp symmetry and twisting (McCracken, 1989), but also in degree of posterior extension of base. It is possible that elements without posteriorly extended base occupy different positions in the apparatus to those elements with similar cusp symmetry.

Reconstructions of the type species of *Protopanderodus* include asymmetrical and symmetrical acontiodontiform, and scandodontiform elements (Löfgren, 1978; Olgun, 1987; McCracken, 1989). Species described from North (e.g. Barnes & Poplawski, 1973; Ethington & Clark, 1981; McCracken, 1989; Stait & Barnes, in press) and South America (Serpagli, 1974) also have paltodontiform elements, with three grooves. Previously, these were consid-

ered to be modified asymmetrical acontiodontiform elements. They occur in such low abundance that this may be the case. However, the sequence of drepanodontiform–asymmetrical acontiodontiform–acontiodontiform–paltodontiform elements suggests a first symmetry transition (a, b, c and d elements respectively; i.e. S elements).

Protopanderodus? primitus Cooper, 1981
Fig. 13A–C,18D,E,G–K

Synonymy.

First symmetry transition (S) elements

Scolopodus sp. nov. A. Hill, Playford & Woods, 1969, p. O14, pl. O VII, fig. 13.

'Panderodus' sp. Serpagli, 1974, p. 43, pl. 24, figs 12, 13; pl. 30, figs 12, 13.

Panderodus striatus Lee. Lee, 1975a, p. 89, pl. 2, figs 11, 13; not Lee, 1975, p. 178, pl. 1, fig. 14; not Lee, 1977, p. 138, pl. 1, figs 11, 13; not Lee, 1979, p. 48, pl. 1, fig. 11.

Scolopodus euspinus Jiang & Zhang sp. nov. An & others, 1983, pp. 140–141, pl. 13, fig. 27, pl. 14, figs 1–8, text-fig. 12:3–4; An, 1990, pl. 11, figs 7–11, 13, 14, 16.

Second symmetry transition (P) elements

Scolopodus sp. nov. C. Hill, Playford & Woods, 1969, p. O14, pl. O VII, fig. 15.

Scolopodus nogamii Lee. Lee, 1975a, p. 89, pl. 2, figs 11, 14, text-fig. 4K; not Lee, 1975, p. 179, pl. 2, fig. 13, text-fig. 3L; not Lee, 1977, p. 141, pl. 2, fig. 12; not An & others, 1983, p. 144, pl. 13, figs 20–25; An, 1990, pl. 11, figs 15, 17, 20.

Multielement reconstructions

cf. *Scolopodus* cfr. *bassleri* (Furnish). Igo & Koike, 1967, p. 23, pl. III, figs 7,8, text-fig. 6-B.

Protopanderodus primitus Druce. Cooper, 1981, p. 174, pl. 27, figs 3,4.

Material studied. 260 specimens: 18 unigrooved, 77 asymmetrical acontiodontiform, 62 acontiodontiform, 4 paltodontiform, 51 scandodontiform, 48 laterally compressed acontiodontiform elements.

Description. Only a brief diagnosis of this species has previously been published (Cooper, 1981). Conical unigrooved, asymmmetrical and symmetrical acontiodontiform, and rare three-grooved paltodontiform elements, all expanding evenly from tip of cusp to aboral margin, are accompanied by laterally compressed, symmetrical acontiodontiform elements and scandodontiform elements, both with base rapidly expanding in lateral view. These last two have compressed morphology typical of second symmetry transition (P) elements, and are herein designated f (P_a) and g (P_b) respectively.

All elements are striate; striae parallel to posterior and lateral carinae and meeting at acute angle in lateral grooves, extending close to posterior margin, but anterior and lateral regions of rim of base are smooth; cusp is slender, smoothly tapering, arcuate, with region of greatest curvature at approximately one-third cusp length; antero-aboral intersection approximately perpendicular, acute intersection of posterior and aboral margins (70°–80°); aboral margin straight; basal cavity is shallow to moderate depth, triangular, with anterior margin close to anterior of cusp.

Remarks. Cooper (1981) illustrated and briefly described

Figure 13. Selected conodont elements.
Symbols as for Figure 12. Magnification approximately ×80.
A–C, *Protopanderodus? primitus* Cooper, GEO 123/006 **A,** element with symmetrical, laterally compressed cusp and expanded base, CPC 23364, lateral view. **B,** scandodontiform element, CPC 23363, inner lateral view. **C,** element with symmetrical cusp and unexpanded base, CPC 23360, lateral view. **D–F, *Scandodus* sp. nov. A,** GEO 132/016. **D,** oistodontiform element, CPC 23369, inner lateral view. **E,** drepanodontiform element, CPC 23366, lateral view. **F,** acontiodontiform element, CPC 23367, lateral view. **G, *Scolopodus* sp. aff. *S. filosus*** Ethington & Clark, keeled scandodontiform element, CPC 23377, posterolateral view, GEO 163/002. **H, I, *Scolopodus multicostatus*** Barnes & Tuke **H,** planoconvex element, CPC 23379, lateral view, GEO 123/003. **I,** keeled scandodontiform element, CPC 23384, posterolateral view, GEO 163/002. **J–L, *Tokoconus wheelamanensis* gen. et sp. nov. J,** acontiodontiform element, CPC 23391, posterolateral view, GEO 123/003. **K,** acodontiform element, CPC 23396, lateral view, GEO 132/016. **L,** distacodontiform element, CPC 23394, lateral view, GEO 123/003.

these forms as *Protopanderodus primitus* Druce. The name is therefore not a *nomen nudem,* but the species should be attributed to Cooper. No holotype was then designated. Examination of Cooper's types reveals that GSSA Co 71 & 72 (Cooper, 1981, 162) are both b elements: a further (unnumbered) specimen included in this collection is a c element of *Protopanderodus? primitus.*

As first revisers, we designate specimen number GSSA Co 72 as lectotype of *Protopanderodus primitus* sensu Cooper, and both GSSA Co 71 and the unnumbered specimen as paralectotypes. Type locality for this species is then Cooper's locality MC–13, within upper Horn Valley Siltstone (31 m above base of formation) of the Maloney Creek section, adjacent to the Stuart Highway Bridge, south of Alice Springs, Northern Territory, Australia.

Only the elements with unexpanded base were figured by

Cooper (1981). Consistency of microstructure, basal cavity morphology, preservational features and co-occurrence support the inclusion of forms with expanded base into the same apparatus as those figured by Cooper (1981, pl. 27, figs 3, 4; see also Watson, 1988, 124). This may be either in different position within the apparatus, or substituting within the position of elements with unexpanded base. Since these elements are found together throughout the Coolibah Formation, and since the morphology of one (unexpanded base with approximately equidimensional cusp cross-section) suggests first symmetry transition elements while elements with expanded base are laterally compressed in the style of second symmetry transition elements, it is likely that both types were incorporated within the one animal.

It is doubtful whether this species should then be assigned to *Protopanderodus*. *Protopanderodus primitus* Cooper has elements which are characteristic of *Protopanderodus* Lindström, but it is doubtful whether *P. rectus* has the same elemental composition.

Protopanderodus? primitus is similar to *Scolopodus gryphus* An and *Protopanderodus nogamii* (Lee). *Scolopodus gryphus* has a much longer base and reduced cusp when compared with Coolibah Formation specimens; *Protopanderodus nogamii* is considerably more anteroposteriorly compressed, and tip of basal cavity is posterior of anterior margin of base. Most likely, the apparatus of *P. nogamii* is the same as that of *P? primitus* (see Watson, 1988, 124–125), and the former is descended from the latter species.

Scolopodus cfr. *bassleri* of Igo & Koike (1967) is distinguished from *P? primitus* by the possession of basal alae.

Distribution. Within Australia, *P? primitus* is known from the Coolibah (this study) and Nora formations of the Georgina Basin (Hill & others, 1969), Horn Valley Formation of the Amadeus Basin (Cooper, 1981), and possibly from subsurface of the Warburton Basin in South Australia (Cooper, 1986). It is also found in the Majiagou Formation of North China (An & others, 1983), Dumugol Formation of Kangweon-Do in South Korea (Lee, 1975a), and uppermost San Juan Formation of Argentina (Serpagli, 1974).

Genus *Scandodus* Lindström, 1955

Type species. *Scandodus furnishi* Lindström, 1955.

Remarks. Lindström (1971, 39–40) redefined *Scandodus* with oistodontiform, drepanodontiform, acodontiform and distacodontiform elements with symmetry transition. Drepanodontiform elements include planoconvex and biconvex cusp cross-section. An acontiodontiform element present in the apparatus may have previously been considered part of symmetry transition between acodontiform and distacodontiform elements. The complete apparatus is Type IVD.

Scandodus sp. nov. A
Fig. 13D-F, 18L-Q

Unfigured specimen. CPC 23371 (GEO 132/016), planoconvex element.

Material studied. 30 specimens: 4 drepanodontiform (a, S_c), 7 planoconvex (b, S_b), 4 acontiodontiform (c, S_a), 1 distacodontiform (d, S_d), 3 oistodontiform (e, M) and 11 acodontiform (f, P) elements.

Description. All elements proclined to erect, striate with striae extending almost to aboral margin, slender, with moderately deep basal cavity. Striae parallel grooves on cusp, and meet in an acute angle at sharp edges.

Drepanodontiform element has unequally biconvex cusp, sharp anterior and posterior edges often with blocky keel on posterior margin of cusp, basal keel on anterior margin, narrow oral keel with arcuate outline in lateral view; base expanded to almost twice maximum cusp width; basal cavity extends to level of maximum cusp curvature, posterior margin almost straight, anterior margin sinuous, tip situated close to anterior margin; cone-in-cone growth axis.

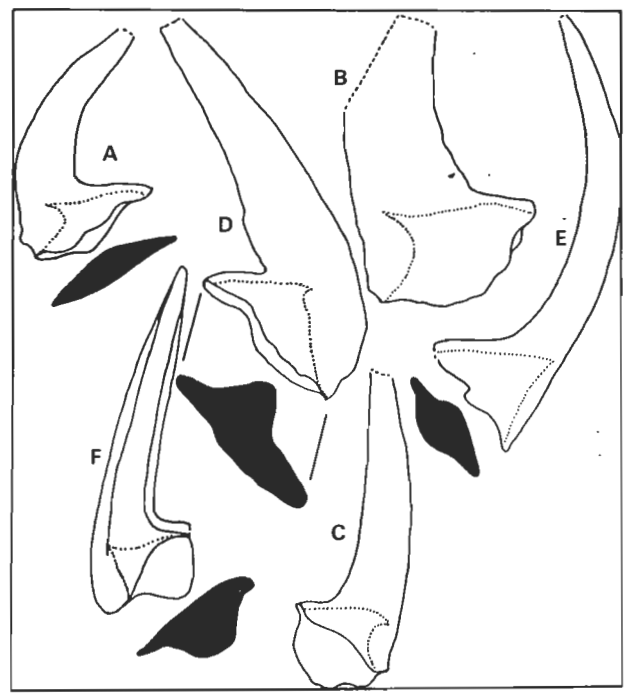

Figure 14. Elements of *Triangulodus* species.
Symbols as for Figure 12.
A–C, *Triangulodus larapintinensis* (Crespin), ×60 **A,** oistodontiform? element, CPC 23410, lateral view, GEO 165/005. **B,** drepanodontiform element, CPC 23406, lateral view, GEO 165/005. **C,** erect scandodontiform element, CPC 23411, posterolateral view, GEO 139/001. **D–F, *Triangulodus* sp. cf. *T. brevibasis*** (Sergeeva), ×80, from GEO 132/014. **D,** oistodontiform element, CPC 23403, inner lateral view.
E, drepanodontiform element, CPC 23399, lateral view. **F,** erect scandodontiform element, CPC 23405, posterolateral view.

Figure 15. Magnification ×120 unless otherwise stated.
A-J, *Alcoorina nadala* gen. et sp. nov. A, oistodontiform element, paratype, CPC 23317, inner lateral view, TOK 9/6. **B,** scandodontiform element, paratype, CPC 23319, detail of surface microstructure, ×600, GEO 132/016. **C,** drepanodontiform element, paratype, CPC 23314, lateral view, GEO 148/005. **D,** suberectiform element, paratype, CPC 23313, posterior view, GEO 123/003. **E,** acontiodontiform element, paratype, CPC 23316, posterior view, GEO 132/016. **F,** scandodontiform element, paratype, CPC 23318, inner lateral view, GEO 123/005. **G,** asymmetrical acontiodontiform element, paratype, CPC 23315, posterior view, GEO 149/005. **H,** same specimen as B, posterolateral view. **I,** suberectiform element, holotype, CPC 23312, posterolateral view, from GEO 123/006. **J,** same specimen, anterolateral view. **K-N, *Ansella fengxiangensis*** (An & others). **K,** erectiform element, CPC 23324, lateral view, GEO 123/005. **L,** asymmetrical belodelliform element, CPC 23321, lateral view, GEO 123/006. **M,** asymmetrical oepikodontiform element, CPC 23320, posterolateral view, ¥140, GEO 164/003. **N,** oistodontiform element, CPC 23323, inner lateral view, GEO 123/007.

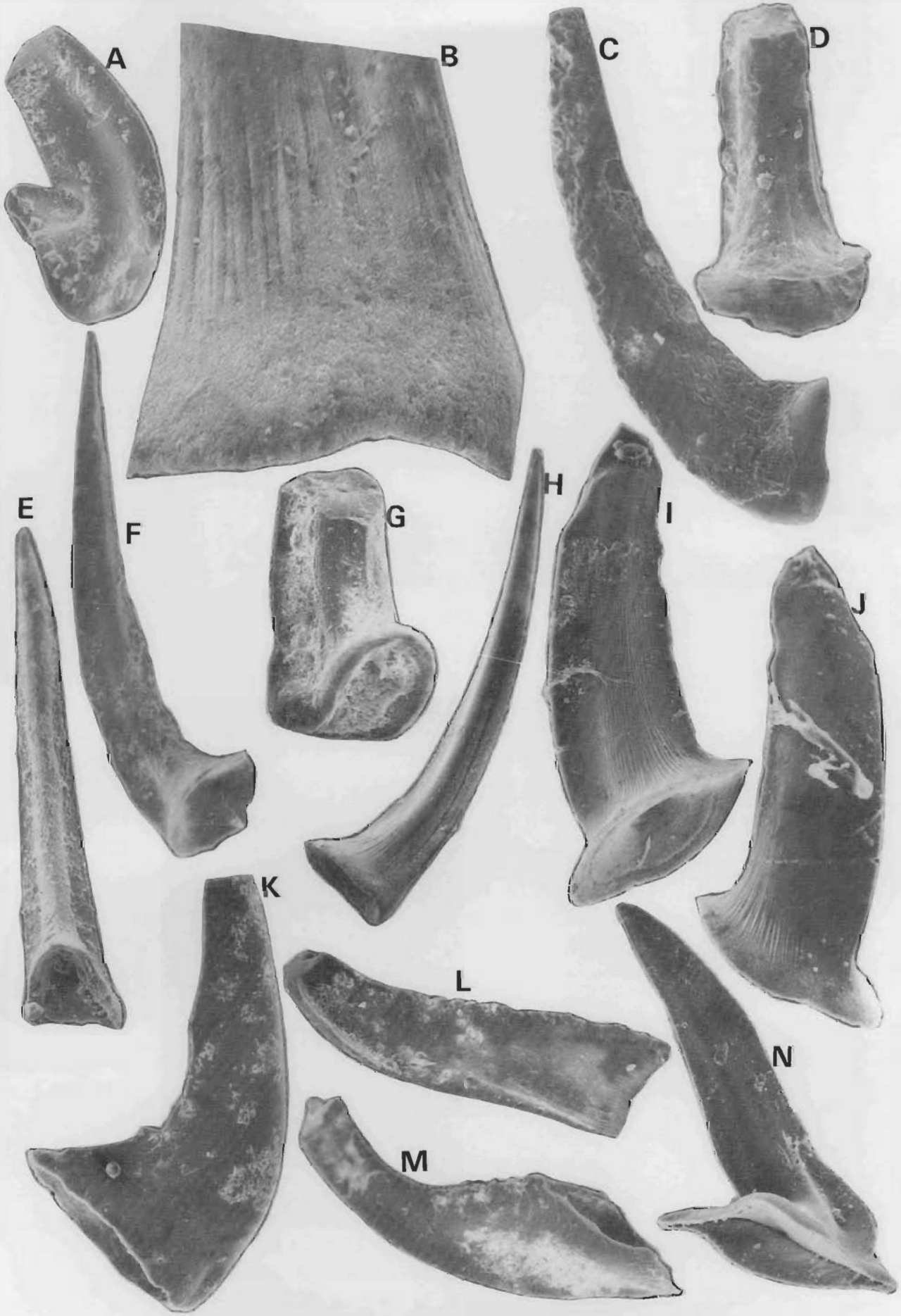
A
B
C
D
E
F
G
H
I
J
K
L
M
N

Planoconvex element differs in possession of anterolateral costa; expansion of base is less pronounced. Acontiodontiform and distacodontiform elements similarly, with narrow lateral and posterobasal keels.

Oistodontiform element twisted, cusp has carinate inner face, and posterior and anterior keels; base with inner lateral flare; cusp intersects base at approximately 80°; medium to wide keel on oral margin; intersection of posterior and oral keels notched; tip of basal cavity lies approximately one third distance from anterior to posterior of base and below level of intersection of cusp and base.

Acodontiform element differs from first symmetry transition elements in location of keels at anterolateral and posterolateral positions for distal two thirds of cusp; with posterolateral carina on inner cusp.

Remarks. Striate cusp distinguishes *Scandodus* sp. nov. A from previously known species of this genus. Development of costae and differentiation of base from cusp is reduced in *S. sinuosus* Mound. Elements of the latter are generally more robust than those of *Scandodus* sp. nov. A, which has slender elements. Some elements of *Scolopodus* sp. aff. *S. filosus* Ethington & Clark from the Coolibah Formation are similar to those of *Scandodus* sp. nov. A, but *Scolopodus* sp. aff. *S. filosus* has deeper basal cavity, and is more coarsely striate than *Scandodus* sp. nov. A.

Distribution. *Scandodus* sp. nov. A is found in low abundance throughout the Coolibah Formation of the Georgina Basin, although it is most common near the base of this formation.

Genus *Scolopodus* Pander, 1856

Type species. *Scolopodus sublaevis* Pander, 1856.

Remarks. Specimens to hand are congeneric with *Scolopodus rex* Lindström as reconstructed by Dzik (1976, 430). Accepting the current generic concept of *Scolopodus* Pander based on *S. rex* (Löfgren, 1978; Bergström, 1981; Ethington and Clark, 1981), the forms described below are referred to *Scolopodus* Pander, emended Dzik, 1976.

The current separation of hyaline elements of *Scolopodus* into asymmetrical and symmetrical forms (Löfgren, 1978; Bergström, 1981) is extended to the recognition of laterally compressed paltodontiform (a, S_c), planoconvex (b, S_b), acontiodontiform (c, S_a), equidimensional paltodontiform (d, S_d), scandodontiform (f, P_a) and posteriorly keeled scandodontiform (g, P_b) elements. The first four elements may be considered S elements (of Sweet, 1981), and the last two P elements.

Scolopodus sp. aff. *S. filosus* Ethington & Clark, 1964
Fig. 13G,19A–E,K

Synonymy.

?'Scolopodus' filosus Ethington & Clark. Ethington & Clark, 1981, p. 100, pl. 11, fig. 22 (synonymy to 1978).

Unfigured specimen. CPC 23372 (GEO 147/002), laterally compressed paltodontiform.

Material studied. 79 specimens: 7 laterally compressed paltodontiform, 27 planoconvex, 7 acontiodontiform, 4 equidimensional paltodontiform, 19 scandodontiform and 15 keeled scandodontiform elements.

Remarks. Specimens from the Coolibah Formation differ from *'Scolopodus' filosus* only in the presence of a fine lateral costa on all elements. General morphology, cusp cross-section, basal cavity and striae of drepanodontiform and equidimensional paltodontiform elements are those described by Ethington & Clark (1964). Additional specimens are required to determine whether this difference is significant at the specific level.

In all elements a fine anterolateral costa runs most of the length of the base and the entire length of the cusp on inner lateral face. This is almost in anterior position on laterally compressed paltodontiform, more lateral on planoconvex elements. The face bearing the costa is planar on this element. On acontiodontiform elements, two slightly asymmetrically disposed costae are modified into narrow keels: cusp compression is marked. Equidimensional paltodontiform elements still bear a reduced costa, but cusp cross-section and aboral opening are subcircular. On scandodontiform elements, the cusp is twisted so that anterior costa moves onto lateral face. This costa is keeled on keeled scandodontiform elements.

The markedly deeper basal cavity and finer striation of *Scolopodus* sp. aff. *S. filosus* distinguish this species from coeval *Scolopodus multicostatus* Barnes & Tuke.

Distribution. *Scolopodus* sp. aff. *S. filosus* is found throughout the Coolibah Formation, but is more abundant in upper parts of these strata.

Scolopodus multicostatus Barnes and Tuke, 1970
Fig. 13H-I, 19F–J,L

Synonymy.

?Scolopodus sp. Abaimova, 1975, pp. 106–107, pl. 9, figs 13, 18, text-fig. 8:32, 33.

Scolopodus multicostatus Barnes & Tuke. Ethington & Clark, 1981, pp. 101–102, pl. 11, figs 19–20 (synonymy).

Unfigured specimen. CPC 23385 (GEO 123/003), acontiodontiform element.

Material studied. 140 specimens: 17 laterally compressed paltodontiform, 49 planoconvex, 17 acontiodontiform, 6 equidimensional paltodontiform, 27 scandodontiform and 24 posteriorly keeled scandodontiform elements.

Description. All elements long, slender, finely costate to coarsely striate, proclined to erect drepanodontiforms. Base is only moderately expanded. Costae do not extend to aboral margin, and may not continue proximally beyond cusp mid-length. Basal cavity is deep, with tip reaching almost to level of maximum cusp curvature; anterior margin of basal cavity is slightly convex towards cavity, and lies close to cusp anterior margin. The laterally

Figure 16. Magnification ×100 unless otherwise stated.
A–C, E, ***Appalachignathus?*** **sp. nov. A. A,** eoliginodinaform element, CPC 23326, inner view, GEO 123/005. **B,** zygognathodontiform element, CPC 23327, inner view, GEO 132/016. **C,** same specimen as B, outer view. **E,** ozarkodinaform? element, CPC 23328, inner view, ×150, GEO 123/005. **D, F-H, J,** ***Bergstroemagnathus kirki*** **sp. nov. D,** trichonodelliform element, paratype, CPC 23336, posterior view, ×50, GEO 123/003. **F,** falodontiform element, paratype, CPC 23337, lateral view, ×60, GEO 149/001. **G,** zygognathodontiform element, paratype, CPC 23335, aboral view, ×80, GEO 132/016. **H,** cordylodontiform element, paratype, CPC 23334, inner lateral view, GEO 123/003. **J,** prioniodontiform element, holotype, CPC 23338, posterolateral view, ×75, GEO 123/003. **I,** ***Aurilobodus serratus*** Xiang & Zhang, ×200, trichonodelliform element, CPC 23333, posterior view, GEO 123/005.

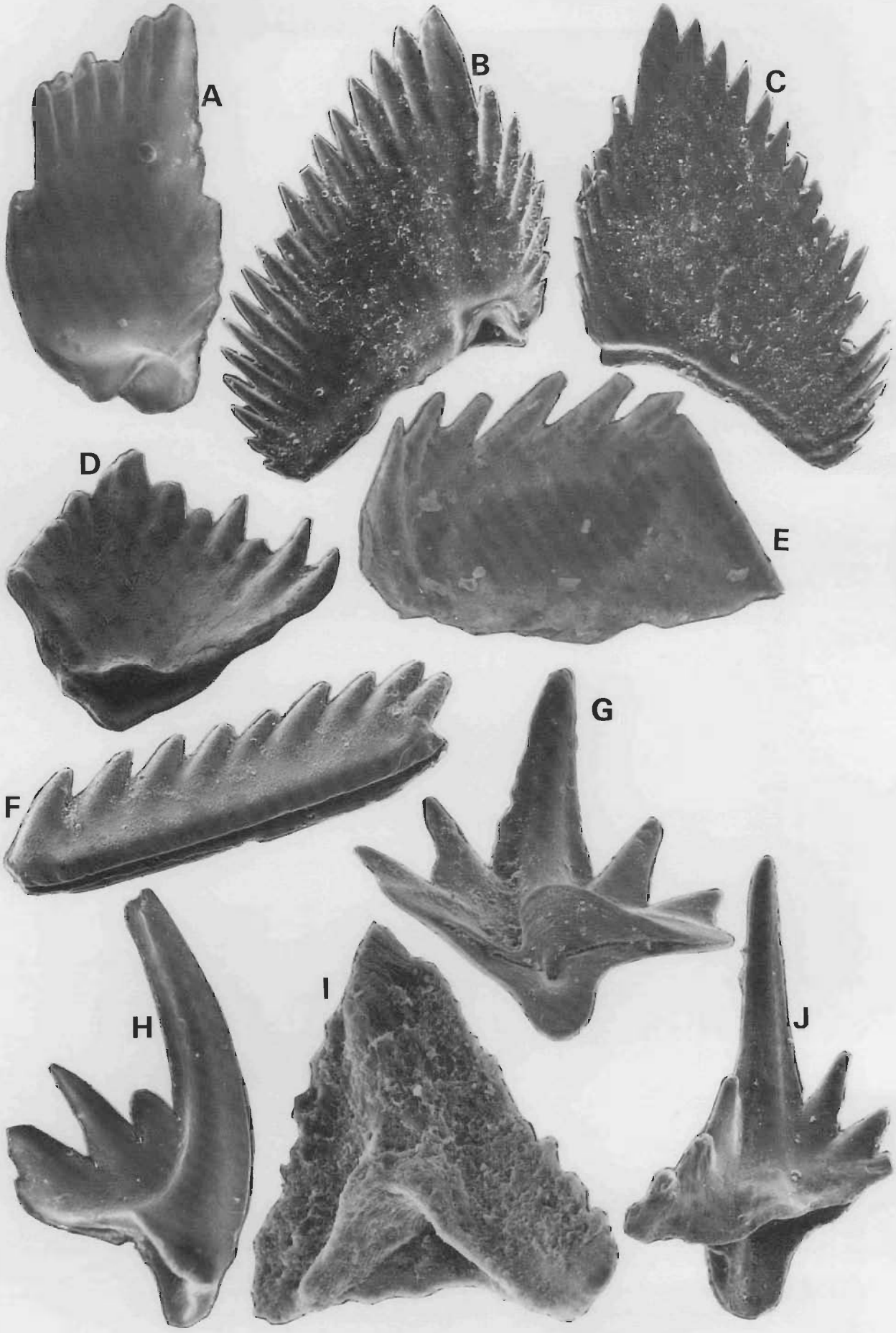
A
B
C
D
E
F
G
H
I
J

compressed paltodontiform element was described by Barnes & Tuke (1970, 92–3): it has asymmetrically biconvex cusp cross-section.

Planoconvex element has planoconvex cusp cross-section, and generally has fewer, less distinct costae on the convex (inner) face.

Acontiodontiform element has narrow anterolateral keels, highly convex posterior face, and rounded coarsely costate to acostate anterior face. Equidimensional paltodontiform element as acontiodontiform element except for absence of anterolateral keels on the former.

Scandodontiform element has a broad anterior edge, deep posterolateral groove on inner face becoming more lateral distally, and unequally biconvex cusp. The g element is similar to scandodontiform, but the anterior edge of the latter is replaced by a broad keel and the posterolateral groove is reduced; the g element is more highly laterally compressed than the f element.

Remarks. *S. multicostatus* is distinguished from most species of *Scolopodus* by a large number of fine costae on the cusp. It differs from *S. rex* in bearing costae close to the anterior margin of most elements, and lesser development of costae distally.*Scolopodus* sp. of Abaimova (1975) appears to be of similar morphology to Coolibah Formation specimens. *Scolopodus* rex illustrated from the Baltic region has costae extending further proximally up the cusp than is normal on specimens from the Coolibah Formation.

Distribution. *Scolopodus multicostatus* is found in the St George Group (upper Canadian) of western Newfoundland (Barnes & Tuke, 1970), Jefferson City Formation of central Missouri and middle Filmore Formation of the Ibex area (Ethington & Clark, 1981), and may occur in Kimaian strata near the River Lena, Siberian Platform (Abaimova, 1975). The range of this species covers the entire Coolibah Formation of the Georgina Basin, although lower strata contain more abundant faunas.

Genus *Tokoconus* gen. nov.

Type species. *Tokoconus wheelamanensis* sp. nov.

Etymology. For Toko Range, in which specimens of this genus are found.

Diagnosis. An assemblage of coniform elements consisting of drepanodontiform (a, S_c), gothodontiform (b, S_b), acontiodontiform (c, S_a), distacodontiform (d, S_d), acodontiform (f, P_b) and scandodontiform (g, P_a) elements in a Type IV apparatus. Cusp and base meet in continuous curve on all elements; posterior and anterior margins of cusp have sharp edges, which are not continued to the aboral margin.

Remarks. Elements of *Cornuodus* Fåhraeus, *Parapanderodus* Stouge and *Scalpellodus* Dzik are similar in general morphology to those of *Tokoconus*. All have a bi- or tri-membrate apparatus (Löfgren, 1978; Stouge, 1984; Watson, 1988; Stait & Barnes, in press). *Cornuodus* is not striate and has rounded anterior and posterior margins basally; *Scalpellodus* and *Parapanderodus* are striate, with sharp edges, but have short-based drepanodontiform elements which are not present in *Tokoconus*. Elements of *Tokoconus* are essentially graciliform (in the sense of *Scolopodus gracilis* Ethington & Clark s.f.) with apparatus position depending upon number and position of carinae and degree of torsion and compression of cusp.

Tokoconus wheelamanensis sp. nov.
Fig. 13J–L, 20A–I

Synonymy.
Cornuodus longibasis (Lindström). An & others, 1983, pp. 89–90, pl. 13, figs 1–7.

Etymology. From Wheelaman Creek, which transects outcrop of the Coolibah Formation.

Type stratum. GEO 123/007: 6 m above base of Coolibah Formation outcropping to side of Bloodwood Creek (grid reference 596153 on Tobermory 1:250 000 topographic map, sheet SF 53–12, Edn 2, Series R 502).

Material studied. 74 specimens: 12 drepanodontiform, 18 gothodontiform, 12 acontiodontiform, 7 distacodontiform, 10 acodontiform and 15 scandodontiform elements.

Diagnosis. A slender species of *Tokoconus* in which the base is relatively unexpanded, and anterior margin of the basal cavity lies close to cusp margin; cusp with broad shallow groove posterior of a posterior facing carina on all elements.

Description. Six elements of this apparatus have been identified. All are slender, with outline of posterior and anterior margins a continuous curve; tip of basal cavity at point of maximum curvature of cusp; striate with striae extending to aboral margin, striae strongest posteriorly and on base; dense white matter fills cusp from basal cavity to tip of element.

Drepanodontiform element has biconvex cusp with sharp anterior and posterior edges and broad, shallow, posterolateral depression; brief anterior keel at level of distal half of basal cavity. Gothodontiform element differs only in lateral position of shallow depression, with carina anterior to groove. Both lateral faces of acontiodontiform element have groove; cusp cross-section is triangular; anterior face round; distacodontiform element with asymmetrically positioned depressions, one to each lateral face.

Second symmetry transition elements differ from the above in possession of brief anterior keel for entire length of element, and oral keel; cusp cross-section is approximately plano-convex. Both elements have keel in anterolateral position basally, but anteriorly at distal end of cusp. Acodontiform and scandodontiform elements may be distinguished by degree of twisting of the cusp.

Figure 17. Magnification ×110 unless otherwise stated.
A, B, F, *Aurilobodus? leptosomatus* An. A, zygognathodontiform element, CPC 23329, posterior view, ×150, GEO 164/001. **B,** acontiodontiform element, CPC 23331, posterior view, ×100, GEO 123/006. **F,** ×150, alate acontiodontiform element, CPC 23332, posterior view, TOK 25/4. **C–E, G–I, *Diaphorodus tortus*** (McTavish). **C,** acontiodontiform element, CPC 23341, posterolateral view, GEO 159/008. **D,** distacodontiform element, CPC 23342, lateral view, GEO 148/005. **E,** drepanodontiform element, CPC 23339, lateral view, ×80, GEO 139/001. **G,** oistodontiform element, CPC 23343, inner lateral view, ×100, GEO 148/005. **H,** prioniodontiform element, CPC 23344, inner lateral view, GEO 148/005. **I,** gothodontiform element, CPC 23340, lateral view, GEO 132/022. **J–N, *Drepanoistodus costatus*** (Abaimova), GEO 132/016. **J,** oistodontiform element, CPC 23345, outer lateral view, ×60. **K,** suberectiform element, CPC 23349, lateral view, ×60. **L,** arcuatiform element, CPC 23348, lateral view, ×60. **M,** scandodontiform element, CPC 23346, lateral view, ×560. **N,** homocurvatiform element, CPC 23347, inner lateral view, ×60.

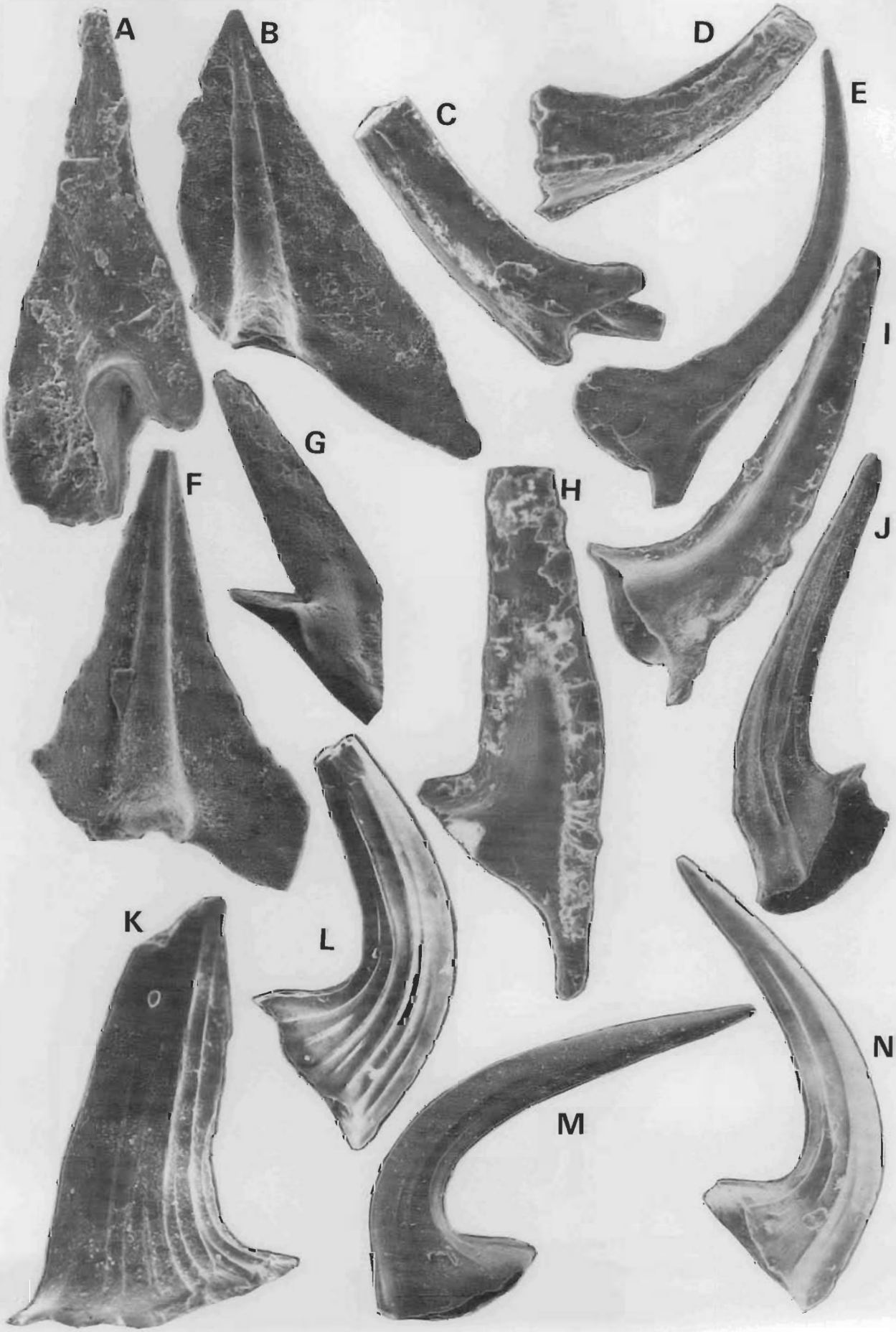
A
B
C
D
E
F
G
H
I
J
K
L
M
N

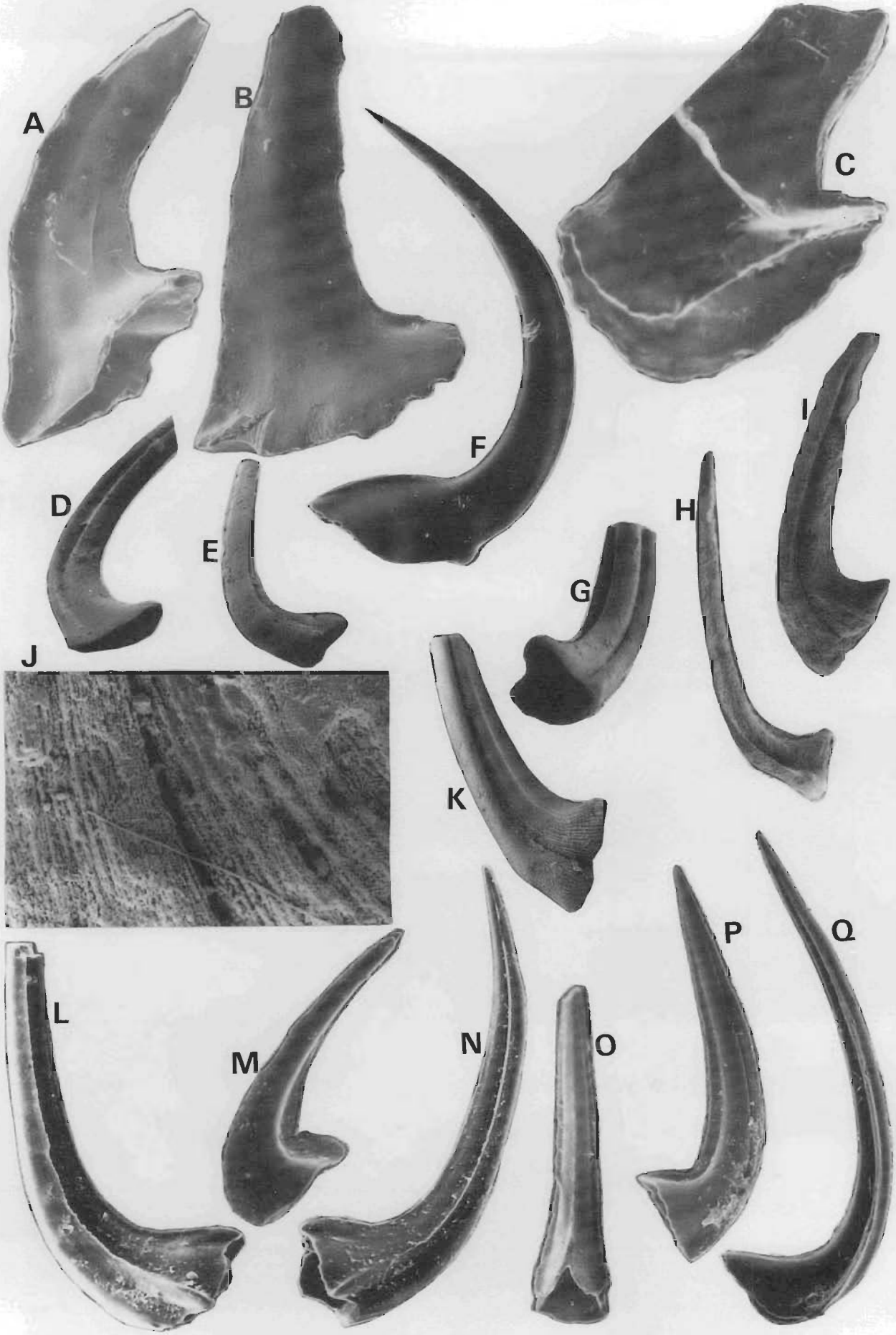
A
B
C
D
E
F
G
H
I
J
K
L
M
N
O
P
Q

Remarks. It is uncertain whether acodontiform and scandodontiform elements occupy (e) and (f) positions, or the apparatus lacks an (e) element and the second symmetry transition contains only (f) and (g). Similarity of these elements supports the second hypothesis.

Distribution. *Tokoconus wheelamanensis* occurs in the lower Majiagou Formation of North China and throughout the Coolibah Formation, Georgina Basin. It is most common in lower to middle strata of this formation.

Genus *Triangulodus* van Wamel, 1974

Type species. *Paltodus volchovensis* Sergeeva, 1963.

Remarks. All elements of this apparatus were described and figured by van Wamel (1974). His reconstruction of *T. brevibasis* (Sergeeva) is appropriate to specimens from the Coolibah Formation, whereas the *Scandodus brevibasis* apparatus of Lindström (1971) and Löfgren (1978) differ in the lack of erect scandodontiform elements. These latter are considered distinct from acodontiform elements.

Triangulodus consists of drepanodontiform (a, S_c), acodontiform (b, S_b), roundyaform (or acontiodontiform, c, S_a), paltodontiform (or distacodontiform, d, S_d), oistodontiform (e, M) and erect scandodontiform elements (f, P) in a Type IVC apparatus. The absence of dichognathodontiform elements within the apparatus, and of lobate processes on ramiform elements of *Triangulodus*, distinguish this genus from *Eoneoprioniodus* Mound.

Elements of *Triangulodus* have only rudimentary processes, consisting merely of costae continuing a short distance beyond the aboral margin, without widening or modification of free end of costae. In this regard, *Triangulodus* is similar to *Diaphorodus* Kennedy. The two latter genera differ in outline of ramiform elements: *Triangulodus* has essentially constant curvature from tip to aboral margin whereas the base of *Diaphorodus* elements is marked by a distinct flaring of the basal outline due to flaring of keels proximal to intersection of cusp and base. Additionally, first symmetry elements of *Triangulodus* have a twisted cusp, which is rare in *Diaphorodus*.

Cooper (1981) considered the apparatus of *'Trigonodus' larapintinensis* Crespin to be similar to that of *Triangulodus*, and suggested that these two taxa may be congeneric. Apparatus composition of both are identical in Coolibah Formation material, thereby supporting Cooper's contention. Since *Trigonodus* was pre-occupied when Crespin proposed the name (R.S. Nicoll, AGSO, pers. comm. to KS, 1989), the oldest available name for this conodont genus is *Triangulodus*.

Triangulodus sp. cf. *T. brevibasis* (Sergeeva, 1963)
Fig. 14D–F, 20J–L,N,O, 21K

Synonymy.
Multielement reconstructions
?Scandodus brevibasis (Sergeeva). Serpagli, 1974, pp. 82–83, pl. 18, figs 5a–7c, pl. 27, figs 10,11, pl. 30, figs 2a–3, text-fig. 21.
cf. *Triangulodus brevibasis* (Sergeeva). Van Wamel, 1974, pp. 96–97, pl. 5, figs 1–7.
Triangulodus cf. *brevibasis* (Sergeeva). Zhang *in* An & others, 1983, pp. 158–159, pl. 15, figs 15–20, text-fig. 11:12–15 (with synonymy to 1978).

Material studied. 119 specimens: 16 drepanodontiform, 7 acodontiform, 11 roundyaform, 15 paltodontiform, 42 oistodontiform and 28 erect scandodontiform elements.

Remarks. Specimens from the Coolibah Formation differ from those figured and described by van Wamel in slightly shallower basal cavity of all elements, more reclined cusp of ramiform elements, lessened asymmetry of cusp cross-section in drepanodontiform element, and fine, anticusp-like anterior extension to base of oistodontiform element.

In most respects Coolibah Formation specimens match *T.* cf. *brevibasis* described and figured in An & others (1983), but they differ from other rep[orted occurrences of *T. brevibasis* in the abbreviated oral zone of most oistodontiform elements, and diffuse white matter along keels and central growth axis of the former. Serpagli's (1974) specimens from the San Juan Formation are entirely hyaline. Determination of their relationship with *Triangulodus brevibasis* awaits study of more abundant material.

Distribution. This species occurs in the lower Majiagou Formation of North China (An others, 1983), possibly upper San Juan Formation of Precordilleran Argentina (Serpagli, 1974), and middle and upper Coolibah Formation of the Georgina Basin.

Triangulodus larapintinensis (Crespin, 1943 sensu Cooper, 1986)
Fig. 14A–C, 21D–F,H–J

Synonymy:
Multielement reconstructions
Trigonodus larapintinensis (Crespin). Cooper, 1981, p. 180, pl. 27, figs 5, 6, 11, 12, 16, 17 (synonymy to 1969).
?Trigonodus larapintinensis (Crespin). Watson, 1988, p. 129, pl. 2, figs 12–14, 18–20, 22, 23.

Material studied. 72 specimens: 12 drepanodontiform, 14 acodontiform, 14 acontiodontiform, 6 distacodontiform, 12 oistodontiform and 14 erect scandodontiform elements.

Remarks. The basal cavity of *T. larapintinensis* is distinctive. It is relatively deep, with tip anterior of cusp midline when viewed laterally. The tip is drawn into a fine, anteriorly-directed cone which almost parallels the aboral margin. Posterior margin of cavity is almost straight, while anterior margin of cavity is markedly convex towards cavity. The acontiodontiform figured (Fig. 21D; Cooper, 1981, pl. 27, fig. 16) also has this basal cavity, and is

Figure 18. Magnification ×100 unless otherwise stated.
A–C, *Drepanoistodus* sp. nov. A, GEO 156/004. **A,** homocurvatiform element, CPC 23352, inner lateral view. **B,** suberectiform element, CPC 23353, lateral view. **C,** oistodontiform element, CPC 23354, inner lateral view. **D, E, G-K, *Protopanderodus? primitus*** Cooper. **D,** ×70, unigrooved element, CPC 23362, inner lateral view, GEO 123/006. **E,** ×70, asymmetrical acontiodontiform element, CPC 23361, lateral view, GEO 123/006. **G,** ×70, acontiodontiform element, CPC 23360, oblique lateral view, GEO 123/006. **H,** ×50, scandodontiform element, CPC 23363, lateral view, GEO 123/006. **I,** ×70, laterally compressed acontiodontiform element, CPC 23364, lateral view, GEO 123/006. **J,** same specimen as G, ×700, surface microstructure near groove. **K,** ×70, paltodontiform element, CPC 23365, inner lateral view, GEO 149/006. **F, *Paroistodus originalis*** (Sergeeva), ×75, drepanodontiform element, CPC 23359, lateral view, GEO 123/007/12. **L-Q, *Scandodus* sp. nov. A. L,** acontiodontiform element, CPC 23330, lateral view, GEO 123/003. **M,** oistodontiform element, CPC 23369, inner lateral view, GEO 132/016. **N,** distacodontiform element, CPC 23368, lateral view, GEO 132/016. **O,** acontiodontiform element, CPC 23367, posterior view, GEO 132/016. **P,** drepanodontiform element, CPC 23366, lateral view, GEO 132/016. **Q,** ×80, acodontiform element, CPC 23370, inner lateral view GEO 163/002.


A
B
C
D
E
F
G
H
I
J
K
L
M
N
O

considered to be part of the apparatus of *T. larapintinensis*. Watson (1988, 129) considered Cooper's figured oistodontiform element to be a drepanodontiform with a more erect cusp than normal within this apparatus. Aboral opening and postero-oral intersection are more consistent with morphology of drepanodontiform than oistodontiform elements, but are not totally inconsistent with elements occupying e position in (for example) the *Drepanodus· concavus* apparatus (graciliform of Kennedy, 1980). It is, however, unusual within the *Triangulodus* apparatus, and the appropriate oistodontiform element may have been included within those assigned herein to *Triangulodus* sp. cf. *T. brevibasis*.

Distribution. *Triangulodus larapintinensis* is found throughout the Horn Valley Siltstone close to Alice Springs, Northern Territory, and upper Coolibah Formation of the Georgina Basin.

Conical elements, gen. et sp. indet.
Fig. 22A–G

Material studied. 13 specimens: 1 element I, 1 element II, 2 element III, 4 element IV, 1 element V and 4 element VI

Description. All specimens are conical, robust, with short, stout, coarsely striate cusp. A wide rim adjacent to aboral margin is not striate; striae parallel posterior margin, converge at lateral edges or in lateral region. All but scandodontiform element have compressed cusp, with greatest cusp thickness laterally. Oral and posterior margins are sharp-edged, anterior margin is smooth. Basal cavity conical with tip close to anterior margin, at top of base. Elements are hyaline, and may have a narrow growth axis subcentral to cusp.

Variation within these specimens includes cusp cross-section, shape and orientation of aboral opening, and extent of development of lateral edges.

A poorly defined transition may be represented by symmetry of basal opening. Elements with ovate aboral opening are generally more compressed than other elements. These former elements bear depressions on both posterolateral faces, but lateral edges are poorly developed. This is also true of elements with triangular aboral opening, but elements with subquadrate or circular aboral opening may have well developed, blocky but sharp-edged, lateral keels.

Scandodontiform elements similar, except an anterolateral edge is developed on base; this becomes more anteriorly situated distally. Cusp is biconvex, aboral opening ovate but long axis is in postero-anterior direction rather than lateral as in other elements.

Remarks. These elements are distinguished from conical elements of Landing & others (1986), and from *Oneotodus* sp. of Cooper (1981), by striate cusp, moderately deep basal cavity and hyaline nature. Scandodontiform elements are included in this association because of their similarity in surface micromorphology, basal cavity, robust nature, and hyaline elements.

It is possible that an almost complete apparatus is herein described. However, considerably more abundant material is required before evaluation of affinities is attempted. Some elements are similar to *Scolopodus warendensis* Druce and Jones, which has a considerably longer cusp and shallower basal cavity than those described above. Comparable, but considerably less robust, elements were described by Abaimova (1971) as *Oneotodus mitra* from southeastern Siberian Platform. These have a reduced cusp, and are probably not conspecific with Coolibah Formation specimens.

Distribution. These specimens were all located in lower to middle Coolibah Formation of the Georgina Basin.

Additional taxa. The following conodont species also occur in the Coolibah Formation, but were found in very low abundance. Their occurrence within studied sections is indicated on range charts (Figs 2–10). Selected elements are illustrated, as shown below in parentheses. All identified species correspond closely with original descriptions, and all taxa listed below are found in the Coolibah Formation only in upper part: *Aurilobodus serratus* Xiang & Zhang, 1983 (Fig. 16I), known from the Majiagou Formation of North China. Only one specimen was located. *Erraticodon tangshanensis* Yang & Xu, 1883 (Fig. 21B,C) ranges through much of the Majiagou Formation of North China (An & others, 1983). This species is also known from the Mandal Formation of North Korea (?Lower to Middle Ordovician; Lee, 1975b), and the Maggol (Arenig; Lee, 1976) and Yeongheung (Middle Ordovician, Lee, 1979) formations of South Korea. Only four specimens were located.

'Oepikodus' maggolensis Lee, 1976 (Fig. 20M), also occurring in the Maggol Formation of South Korea (Lee, 1976) and lower Majiagou Formation of North China (An & others, 1983). Three specimens found.

Oistodus multicorrugatus Harris, 1962 (Fig. 21A,G), present in many of the early Middle Ordovician carbonates of North America (Ethington & Clark, 1981), upper San Juan Formation of Argentina (Serpagli, 1974), Kimaian strata on the Siberian Platform (Moskalenko, 1982), Majiagou Formation of North China (An & others, 1983), and Horn Valley Siltstone of the Amadeus Basin, Australia (Cooper, 1981). Five specimens located.

Protoprioniodus nyinti Cooper, 1981 (Fig. 19M-O), known from the Juab Formation of western Utah, El Paso Group of west Texas, Eleanor River Formation of Arctic Canada, Horn Valley Siltstone of the Amadeus Basin, Australia (Cooper, 1981), found on Mt Arrowsmith in New South Wales, Australia, and in the Nora and upper Coolibah formations of the Georgina Basin (Cooper, 1981; this study). Eight specimens found.

Figure 19. Magnification ×70 unless otherwise stated.
A–E, K, *Scolopodus* sp. aff. *S. filosus* Ethington & Clark. **A,** ×250, planoconvex element, CPC 23373, surface microstructure, GEO 165/002. **B,** ×100, equidimensional paltodontiform element, CPC 23375, lateral view, GEO 163/002. **C,** keeled scandodontiform element, CPC 23377, lateral view, GEO 163/002. **D,** ×100, scandodontiform element, CPC 23376, posteroaboral view, GEO 163/002. **E,** ×80, acontiodontiform element, CPC 23374, posterolateral view, GEO 163/002. **K,** planoconvex element, same specimen as A, inner lateral view. **F–J, L, *Scolopodus multicostatus*** Barnes & Tuke. **F,** equidimensional paltodontiform element, CPC 23381, aboral view, GEO 132/016. **G,** ×60, laterally compressed paltodontiform element, CPC 23378, lateral view, GEO 123/003. **H,** keeled scandodontiform element, CPC 23383, posterolateral view, GEO 132/016. **I,** scandodontiform element, CPC 23382, inner lateral view, GEO 123/003. **J,** planoconvex element, CPC 23379, lateral view, GEO 123/003. **L,** acontiodontiform element, CPC 23380, lateral view, GEO 132/016. **M–O, *Protoprioniodus nyinti*** Cooper. **M,** ×150, cordylodontiform element, CPC 23386, lateral view, GEO 123/005. **N,** ×100, gothodontiform element, CPC 23387, inner lateral view, GEO 123/005. **O,** ×100, trichonodelliform element, CPC 23388, anterolateral view, GEO 165/004.

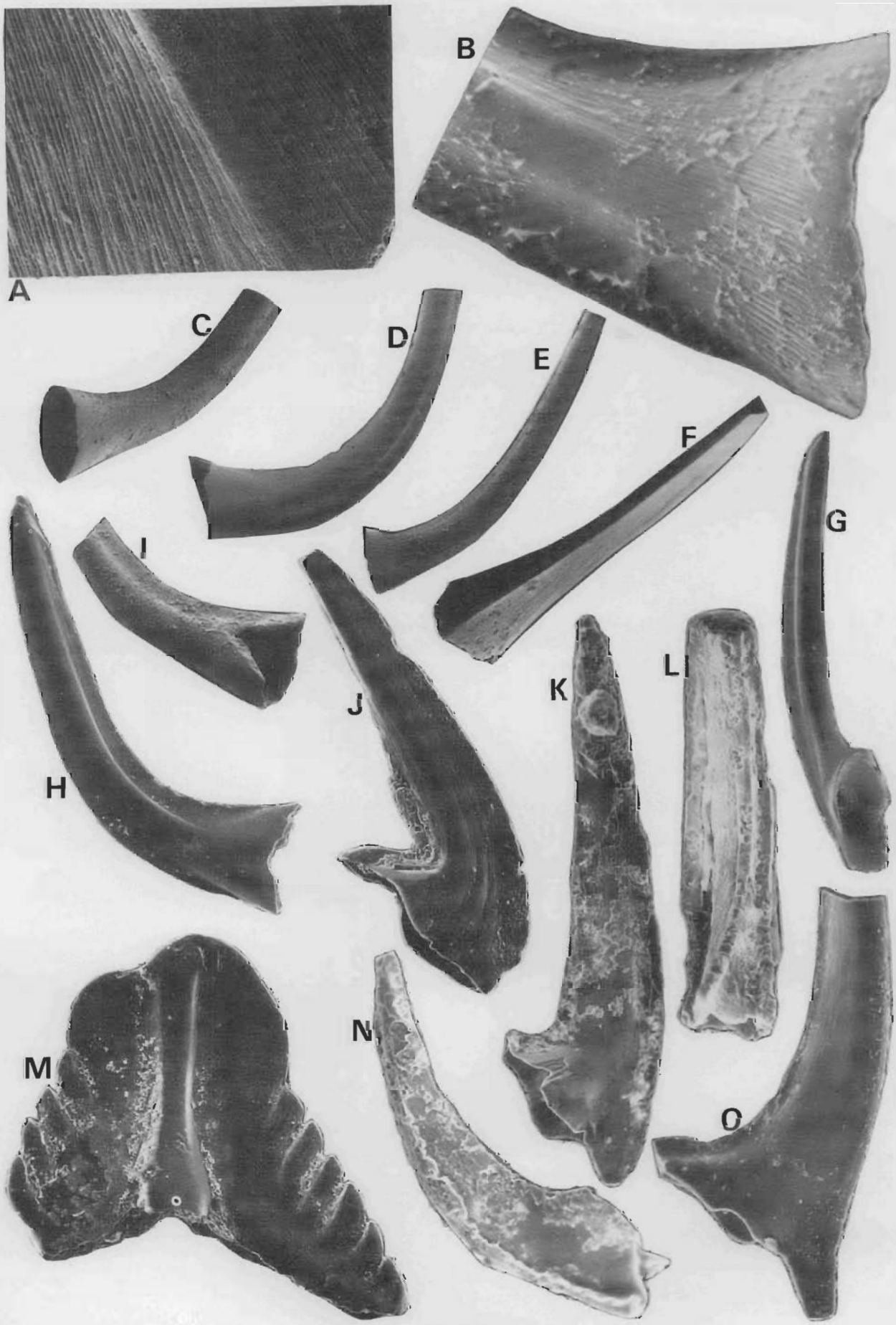
A
B
C
D
E
F
G
H
I
J
K
L
M
N
O

conodont-based correlations from the Tremadocian of Quebec. *Canadian Journal of Earth Sciences* 23, 1928–1949.

Lee, H.Y., 1975a — Conodonts from the Dumugol Formation (Lower Ordovician), South Korea. *Journal of the Geological Society of Korea* 11, 75–98.

Lee, H.Y., 1975b — Conodonten aus dem unteren und mittleren Ordovizium von Nordkorea. *Palaeontographica Abthandlungen, Series A* 150, 161–186.

Lee, H.Y., 1976 — Conodonts from the Maggol and Jeongseon Formation (Ordovician), Kangweon-Do, South Korea. *Journal of the Geological Society of Korea* 12, 151–181.

Lee, H.Y., 1977 — Conodonten aus den Jigunsan- und den Duwibong-Schichten (Mittelordovizium) von Kangweon-Do, Sudkorea. *Journal of the Geological Society of Korea* 13, 121–150.

Lee, H.Y., 1979 — A study on biostratigraphy and bioprovince of the Middle Ordovician conodonts from South Korea. *Journal of the Geological Society of Korea* 15, 37–60.

Lee, Y.N. & Lee, H.Y., 1986 — Conodont biostratigraphy of the Jigunsan Shale and Duwibong Limestone in the Nokjeon-Sangdong area, Yeongweol-Gun, Kangweondo, Korea. *Journal of the Palaeontological Society of Korea* 2, 114–136.

Lindström, M., 1964 — Conodonts. *Elsevier Publishing Company, Amsterdam.*

Lindström, M., 1971 — Lower Ordovician conodonts of Europe. *Geological Society of America Memoir* 127, 21–61.

Löfgren, A., 1978 — Arenigian and Llanvirnian conodonts from Jämtland, northern Sweden. *Fossils and Strata* 13, 1–129.

McCracken, A.D., 1989 — *Protopanderodus* (Conodontata) from the Ordovician Road River Group, northern Yukon Territory, and the evolution of the genus. *Geological Survey of Canada Bulletin* 388, 1–39.

McTavish, R.A., 1973 - Prioniodontacean conodonts from the Emanuel Formation (Lower Ordovician) of Western Australia. *Geologica et Palaeontologica Sonderdruck* 7, 27–58.

McTavish, R.A. & Legg, D.P., 1976 — The Ordovician of the Canning Basin, Western Australia. *In* Bassett, M.G. (editor), The Ordovician System: proceedings of a Palaeontological Association symposium, Birmingham, September 1974. *University of Wales Press and National Museum of Wales, Cardiff*, 447–478.

Moskalenko, T.A., 1982 — Konodonty [Conodonts]. *In* Sokolov, B.S. (editor), Ordovik Sibirskoi Platformy (Opornyi Razrez na R. Kulyumbe) [Ordovician of the Siberian Platform (Key Section on the Kulumbe River)]. *Akademiya Nauk SSSR, Sibirskoe Otdelenie, Institut Geologii i Geofiziki, Izdatel'stvo 'Nauka', Moskva*, 100–144 [Russian].

Moskalenko, T.A., 1984 — Gruppa Conodontophorida. *In* Moskalenko, T.A. (editor), Ordovik Sibirskoi Platformy. Paleontologicheskiy Atlas [Palaeontological atlas of the Ordovician of the Siberian Platform]. *Akademiya Nauk SSSR, Sibirskoe Otdelenie, Trudy Instituta Geologii i Geofiziki, Izdalet'stvo 'Nauka', Novosibirsk* 113–137 [Russian].

Nicoll, R.S., Nielsen, A.T., Laurie, J.R. & Shergold, J.H., 1992 — Preliminary correlation of latest Cambrian and Early Ordovician sea level events in Australia and Scandinavia. *In* Webby, B.D. & Laurie, J.R. (editors), Global perspectives on Ordovician geology. *A.A. Balkema, Rotterdam*, 381–394.

Olgun, O., 1987 — Komponenten-Analyse und Conodonten- Stratigraphie der Orthoceratenkalksteine im Gebeit Falbygden, Västergötland, Mittelschweden. *Sveriges Geologiska Undersökning* 70, 1–79.

Playford, G. & Wicander, R., 1988 — Acritarch palynoflora of the Coolibah Formation (Lower Ordovician), Georgina Basin, Queensland. *Memoir of the Association of Australasian Palaeontologists* 5, 5–40.

Serpagli, E., 1974 — Lower Ordovician conodonts from Precordilleran Argentina (Province of San Juan). *Bollettino della Società Paleontologica Italiana* 13, 17–98.

Shergold, J.H., 1985 — Notes to accompany the Hay River - Mt Whelan special 1:250 000 geological sheet, southern Georgina Basin. *Bureau of Mineral Resources, Australia, Report* 251, 1–47.

Shergold, J.H. & Druce, E.C., 1980 — Upper Proterozoic and Lower Palaeozoic rocks of the Georgina Basin. *In* Henderson, R.A. & Stephenson, P.J. (editors), The geology and geophysics of northeastern Australia. *Geological Society of Australia, Queensland Division, Brisbane*, 149–174.

Shergold, J.H., Druce, E.C., Radke, B.M. & Draper, J.J., 1986 — Cambrian and Ordovician stratigraphy of the eastern portion of the Georgina Basin, Queensland and eastern Northern Territory. *25th International Geological Congress, Australia, 1976. Field excursion guidebook 4C.*

Smith, K.G., 1972 — Stratigraphy of the Georgina Basin. *Bureau of Mineral Resources, Australia, Bulletin* 111, 1–156.

Stait, K., & Barnes, C.R., in press — Early Ordovician conodonts from Catoche and Aguathuna formations, western Newfoundland. *Geological Survey of Canada Bulletin.*

Stewart, I.R., 1988 — Conodonts. *In* Douglas, J.G. & Ferguson, J.A. (editors), Geology of Victoria. *Geological Society of Australia, Victorian Division, Melbourne*, 79–81.

Stouge, S.S., 1984 — Conodonts of the Middle Ordovician Table Head Formation, western Newfoundland. *Fossils and Strata* 16, 1–145.

Sweet, W.C., 1981 — Morphology and composition of elements. *In* Robison, R.A. (editor), Treatise on invertebrate paleontology, Part W, Miscellanea, Supplement 2, Conodonta. *The Geological Society of America, Inc, University of Kansas, Boulder, Colorado and Lawrence, Texas*, W5–W20.

van Wamel, W.A., 1974 — Conodont biostratigraphy of the Upper Cambrian and Lower Ordovician of north-western Oland, south-eastern Sweden. *Utrecht Micropaleontological Bulletins* 10, 1–126.

Watson, S.T., (1988) — Ordovician conodonts from the Canning Basin (Western Australia). *Palaeontographica Abthandlungen, Series A 203*, 91–147.

Figure 21. Magnification ×90 unless otherwise stated.

A, G, ***Oistodus multicorrugatus*** Harris, GEO 132/014. **A,** ×120, trichonodelliform element, CPC 23358, lateral view. **G,** ×80, d element, CPC 23357, lateral view. **B, C,** ***Erraticodon tangshanensis*** Yang & Xu. **B,** ×120, b element, CPC 23356, lateral view, GEO 139/001. **C,** ×180, neoprioniodontiform element, CPC 23355, inner lateral view, GEO 156/004. **D–F, H–J,** ***Triangulodus larapintinensis*** (Crespin). **D,** acontiodontiform element, CPC 23408, oblique lateral view GEO 139/001. **E,** erect scandodontiform element, CPC 23411, lateral view, GEO 139/001. **F,** acodontiform element, CPC 23407, inner lateral view, GEO 165/005. **H,** oistodontiform element, CPC 23410, lateral view, GEO 165/005. **I,** drepanodontiform element, CPC 23406, lateral view, GEO 165/005. **J,** distacodontiform element, CPC 23409, posterolateral view, GEO 165/005. **K,** ***Triangulodus* sp. cf. *T. brevibasis*** (Sergeeva), ×120, acodontiform element, CPC 23400, outer lateral view, GEO 148/005.

Acknowledgements

Thanks are due to AGSO personnel, particularly Bob Nicoll, John Shergold and Arthur Wilson, for enabling access to AGSO equipment and facilities. Technical assistance with SEM photography was provided by Arthur Wilson (AGSO) and Wys Jablonski (Central Science Laboratory, University of Tasmania). Tony Donaghy and Bryan Stait assisted with drafting of diagrams.

Early versions of this manuscript were improved by suggestions from Ray Ethington and Clive Burrett, and discussion with Bob Nicoll.

References

Abaimova, G.P., 1971 — New early Ordovician conodonts from the southeastern part of the Siberian Platform. *Paleontological Journal* 486–493.

Abaimova, G.P., 1975 — Ranneordovikskie konodonty srednego techeniya R. Leny [Early Ordovician conodonts of the middle flow of the Lena River]. Trudy SNIIGGIMS, 207, 1–129 [In Russian].

An, T., 1987 — The Lower Paleozoic conodonts of south China. Publishing House of Beijing University, Beijing [Chinese].

An, T., 1990 — Conodonts of the marginal areas around the Ordos Basin, North China. Geological Publishing House, Beijing.

An, T. & others, 1981 — Conodont biostratigraphy of the Ordovician System of Yichang, China. *In* Selected Papers on the First Convention of Micropalaeontology Society of China (1979). Science Press of China.

An, T., Du, G. & Gao, Q., 1985 — Ordovician conodonts from Hubei, China. *Geological Publishing House, Beijing.*

An, T., Zhang, F., Xiang W., Zhang, Y., Xu, W., Zhang, H., Jiang, D., Yang, C., Lin, L., Cui, Z. & Yang, X., 1983 — The conodonts of North China and the adjacent regions. *Science Press, Beijing.*

Barnes, C.R., Kennedy, D.J., McCracken, A.D., Nowlan, G.S. & Tarrant, G.A., 1979 — The structure and evolution of Ordovician conodont apparatuses. *Lethaia* 12, 125–151.

Barnes, C.R. & Poplawski, M.L.S., 1973 — Lower and Middle Ordovician conodonts from the Mystic Formation, Quebec, Canada. *Journal of Paleontology* 47, 760–790.

Barnes, C.R. & Tuke, M.F., 1970 — Conodonts from the St. George Formation (Ordovician), northern Newfoundland. *Geological Survey of Canada Bulletin* 187, 79–97.

Bergström, S.M., 1981 — Family Scolopodontidae. *In* Robison, R.A. (editor), Treatise on Invertebrate Paleontology, Part W, Miscellanea, Supplement 2, Conodonta. *Geological Society of America and University of Kansas Press, New York and Lawrence.*

Bergström, S.M., Carnes, J.B., Ethington, R.L., Votaw, R.B. & Wigley, P.B., 1974 — *Appalachignathus*, a new multielement conodont genus from the Middle Ordovician of North America. *Journal of Paleontology* 48, 227–235.

Burrett, C. & Stait, B., 1987 — China and southeast Asia as part of the Tethyan margin of Cambro-Ordovician Gondwanaland. *In* McKenzie, K. (editor), Shallow Tethys 2. *A.A. Balkema, Rotterdam,* 65–77.

Cooper, B.J., 1981 — Early Ordovician conodonts from the Horn Valley Siltstone, central Australia. Palaeontology, 24, 147–183.

Cooper, B.J., 1986 — A record of Ordovician conodonts from the Warburton Basin, South Australia. *Quarterly Geological Notes of the Geological Survey of South Australia* 100, 8–14.

Cooper, R.A. & Druce, E.C., 1975 — Lower Ordovician sequence and conodonts, Mount Patriarch, north-west Nelson, New Zealand. *New Zealand Journal of Geology and Geophysics* 18, 551–582.

Draper, J.J., 1980 — Ethabuka Sandstone, a new Ordovician unit in the Georgina Basin, and a redefinition of the Toko Group. *Queensland Government Mining Journal* 81, 469–475.

Dzik, J., 1976 — Remarks on the evolution of Ordovician conodonts. *Acta Palaeontologica Polonica* 21, 395–455.

Ethington, R.L. & Clark, D.L., 1964 — Conodonts from the El Paso Formation (Ordovician) of Texas and Arizona. *Journal of Paleontology* 38, 685–704.

Ethington, R.L. & Clark, D.L., 1981 — Lower and Middle Ordovician conodonts from the Ibex Area, western Millard County, Utah. *Brigham Young University Geology Studies* 28, 1–160.

Fåhraeus, L.E & Hunter, D.R., 1985 — Simple-cone conodont taxa from the Cobbs Arm Limestone (Middle Ordovician), New World Island, Newfoundland. *Canadian Journal of Earth Sciences* 22, 1171–1182.

Fortey, R.A. & Shergold, J.H., 1984 — Early Ordovician trilobites, Nora Formation, central Australia. *Palaeontology* 27, 315–366.

Harris, A.G., Bergström, S.M., Ethington, R.L. & Ross, R.J., 1979 — Aspects of Middle and Upper Ordovician conodont biostratigraphy of carbonate facies in Nevada and southeast California and comparison with some Appalachian successions. *Brigham Young Geology Studies* 26, 7–43.

Hill, D., Playford, G. & Woods, J.T., 1969 — Ordovician and Silurian fossils of Queensland. Queensland Palaeontographical Society, Brisbane.

Igo, H. & Koike, T., 1967 — Ordovician and Silurian conodonts from the Langkawi Islands, Malaya. *Geology and Palaeontology of Southeast Asia* III, 1–29.

Kennedy, D.J., 1975 — Conodonts from a Lower–Middle Ordovician formation, Mt. Arrowsmith, northwestern New South Wales, Australia. *Geological Society of America, Abstracts with Program,* 7, 796.

Kennedy, D.J., 1980 — A restudy of conodonts described by Branson and Mehl, 1933, from the Jefferson City Formation, Lower Ordovician, Missouri. *Geologica et Palaeontologica Sonderdruck* 14, 45–76.

Landing, E., Barnes, C.R. & Stevens, R.K., 1986 — Tempo of earliest Ordovician graptolite faunal succession:

Figure 20. Magnification ×50 unless otherwise stated.

A–I, *Tokoconus wheelamanensis* gen. et sp. nov. A, ×400, acontiodontiform element, paratype, CPC 23392, microstructure of cusp posterior region, GEO 123/003. **B,** ×250, scandodontiform element, paratype, CPC 23397, microstructure of cusp near basal opening, GEO 132/016. **C,** drepanodontiform element, paratype, CPC 23390, oblique lateral view, GEO 132/016. **D,** gothodontiform element, paratype, CPC 23391, inner lateral view, GEO 165/004. **E,** scandodontiform element, same specimen as in B, lateral view. **F,** acontiodontiform element, same specimen as in A, posterior view. **G,** distacodontiform element, holotype, CPC 23393, posteroaboral view, GEO 123/007. **H,** distacodontiform element, same specimen as in G, lateral view. **I,** acodontiform element, paratype, CPC 23395, lateral view, GEO 123/003. **J–L, N, O, *Triangulodus* sp. cf. *T. brevibasis*** (Sergeeva). **J,** ×90, oistodontiform element, CPC 23403, inner lateral view, GEO 132/014. **K,** ×90, erect scandodontiform elment, CPC 23404, lateral view, GEO 148/005. **L,** ×120, paltodontiform element, CPC 23402, posterior view, GEO 148/005. **N,** ×120, roundyaform element, CPC 23401, lateral view, GEO 148/005. **O,** ×120, drepanodontiform element, CPC 23398, lateral view, GEO 148/005. **M, *'Oepikodus' maggolensis*** Lee, symmetrical element, CPC 23389, posterior view, GEO 132/005.

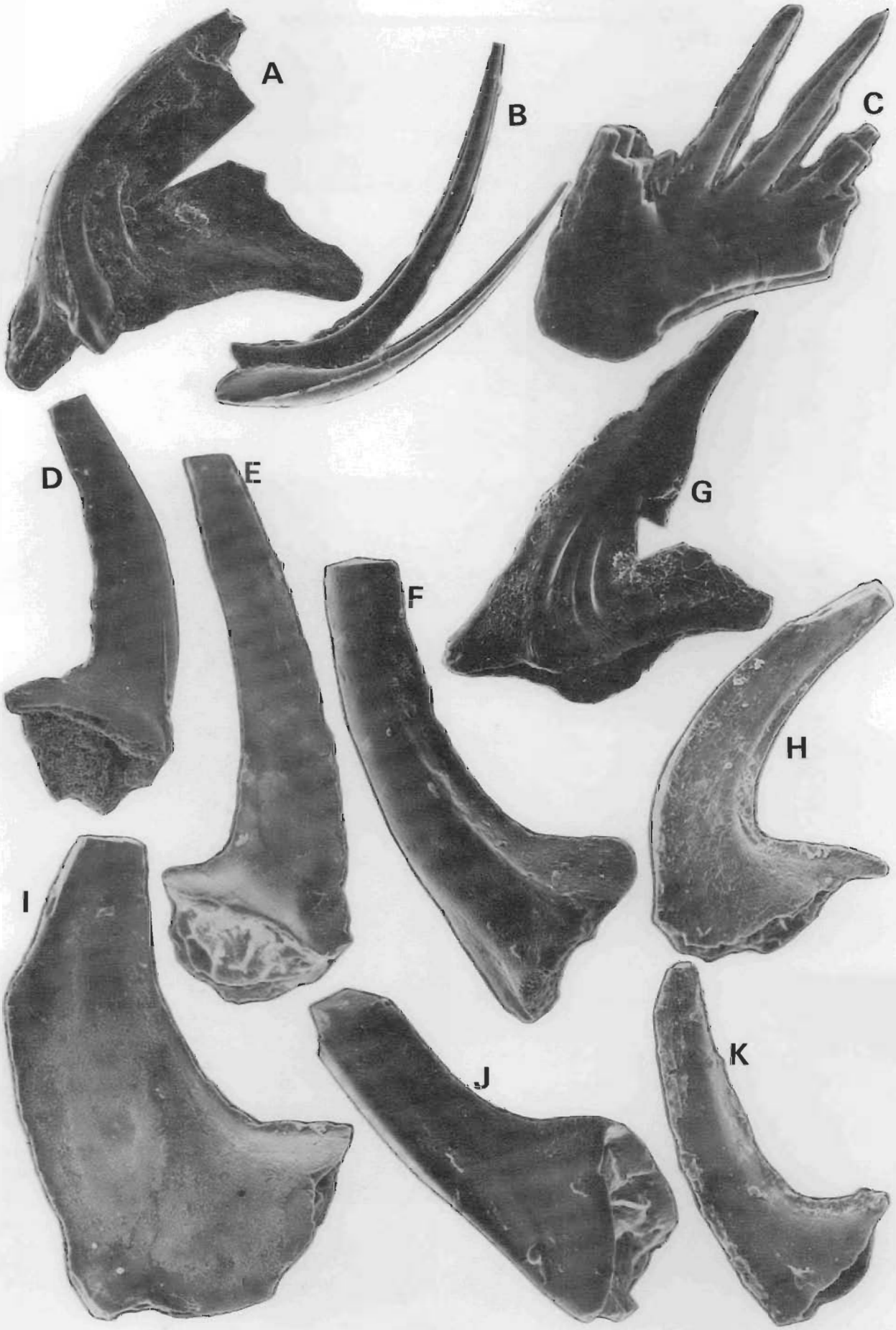
A
B
C
D
E
F
G
H
I
J
K

Webby, B.D., VandenBerg, A.H.M., Cooper, R.A., Banks, M.R., Burrett, C.F., Henderson, R.A., Clarkson, P.D., Hughes, C.P., Laurie, J., Stait, B., Thomson, M.R.A. & Webers, G.F., 1981 — The Ordovician System in Australia, New Zealand and Antarctica. *International Union of Geological Sciences, Publication No.* 6, 1–69.

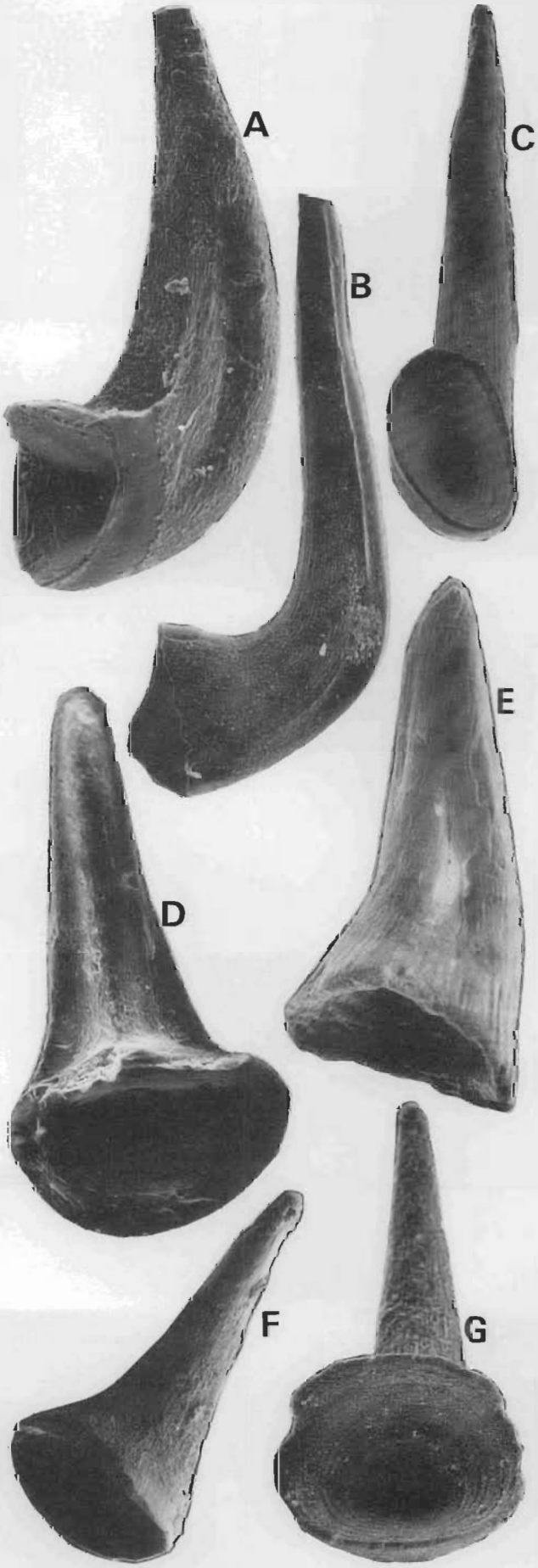

Figure 22. Conical elements.
Magnification ×100 unless otherwise stated.
A, ×120, element III, costate element with subrectangular aboral opening, CPC 23414, lateral view, GEO 148/005. **B,** ×90, same specimen, inner lateral view. **C,** ×90, element II, scandodontiform element, CPC 23413, aboral view, GEO 132/026. **D,** element V, costate element with ovate aboral opening, CPC 23416, posterior view, GEO 123/007. **E,** element IV, acostate element with triangular aboral opening, CPC 23415, posterolateral view, GEO 123/003. **F,** element VI, acostate element with ovate aboral opening, CPC 23417, posterior view, GEO 132/026. **G,** ×150, element I, acostate element with circular aboral opening, CPC 23412, aboral view, GEO 163/002.

BMR Journal of Australian Geology & Geophysics, 13, 323–331

A test of a global seismic system for monitoring earthquakes and underground nuclear explosions

J. Roger Bowman[1], Ken Muirhead[1], Spiro Spiliopoulos[1], David Jepsen[1] & Mark Leonard[1]

Australia is a member of the Group of Scientific Experts (GSE) to consider international cooperative measures to detect and identify seismic events, an *ad hoc* group of the United Nations Conference on Disarmament. The GSE conducted a large-scale technical test (GSETT-2) from 22 April to 9 June 1991 that focused on the exchange and analysis of seismic parameter and waveform data. Thirty-four countries participated in GSETT-2, and data were contributed from 60 stations on all continents. GSETT-2 demonstrated the feasibility of collecting and transmitting large volumes (around 1 gigabyte) of digital data around the world, and of producing a preliminary bulletin of global seismicity within 48 hours and a final bulletin within 7 days. However, the experiment also revealed the difficulty of keeping up with the flow of data and analysis with existing resources. The Final Event Bulletins listed 3715 events for the 42 recording days of the test, about twice the number reported routinely by another international agency 5 months later. The quality of the Final Event Bulletin was limited by the uneven spatial distribution of seismic stations that contributed to GSETT-2 and by the ambiguity of associating phases detected by widely separated stations to form seismic events. A monitoring system similar to that used in GSETT-2 could provide timely and accurate reporting of global seismicity. It would need an improved distribution of stations, application of more conservative event formation rules and further development of analysis software.

Introduction

Goals of the GSE

One approach to lowering the threat of nuclear war is to reduce or eliminate the testing of nuclear weapons. Seismic monitoring is an important method for verifying compliance with agreements on the testing of underground nuclear weapons. Since 1974 the United States and the former Soviet Union have observed a threshold test-ban treaty that limits the maximum size of underground tests to 150 kilotonnes (kt; the Treaty on the Limitation of Underground Nuclear-Weapons Tests, ratified in 1990). Underground explosions above this limit are equivalent in energy release to an earthquake of magnitude 5.5 or larger. It is therefore rather easy to detect and estimate the location and yield of tests that exceed the 150 kt threshold.

A number of countries including Australia are working toward a Comprehensive Test Ban Treaty that would prohibit all testing of nuclear weapons. Even if a Comprehensive Test Ban Treaty were to be accepted by all nuclear powers or nuclear-capable countries, the problem of verifying compliance would be much more demanding than it is for the threshold test-ban treaty. Not only are the signals from small underground explosions much weaker, which makes them more difficult to detect in the presence of noise, but also the number of naturally occurring events and quarry blasts increases markedly at smaller magnitudes. Therefore, it would be necessary to detect and determine source parameters for several orders of magnitude more events in order to identify possible clandestine nuclear tests. Moreover, seismic identification of possible treaty violations would need to be available within a few days so that other methods could then confirm or refute the seismic interpretation.

In this context, the United Nations Conference on Disarmament formed the *ad hoc* Group of Scientific Experts to Consider International Cooperative Measures to Detect and Identify Seismic Events (GSE). Australia has been a member of the GSE since its inception in 1976. The mandate of the GSE is to design and report on an international seismic system that could rapidly locate and report seismic events.

Goals of GSETT-2

In 1984 the GSE conducted a technical test of a preliminary global monitoring system, which is now referred to as GSETT-1. The Global Telecommunications System of the World Meteorological Organization was used to transmit parameter data measured from seismograms, and event bulletins were prepared from the reported phases. In the years following GSETT-1 it was recognised that seismic data would be most useful if entire seismograms, or waveforms, for events were exchanged in addition to parameter data. Furthermore, communication technology had evolved rapidly, providing the opportunity to increase the performance of the GSE monitoring system. The principal purpose of the second technical test (GSETT-2) was to test the methods and procedures developed by the GSE to extract and transmit data from stations to experimental data centres, to process the data and to transmit the results back to participants (GSE, 1991). In a broader sense, the purpose of GSETT-2 was to test the initial design concepts for a modern global seismic system.

GSE network and GSETT-2 system

The four critical elements of the GSE seismic monitoring system are the seismograph stations themselves, National Data Centres, Experimental International Data Centres and the communication links among the stations and centres. The seismic stations used in GSETT-2 (Fig. 1) are referred to here as the GSE network but, owing to their heterogeneous characteristics and uneven distribution, may be more appropriately called a collection of stations. Thirty-four countries participated in the main phase of GSETT-2, providing data from 60 stations from all continents. Twelve of the stations were seismic arrays consisting of a number of sensors arranged in a geometric pattern. Data from all the sensors in an array are recorded at a common site and are analysed jointly. The remaining 48 stations had one or more instruments at a single site. Most of these single-site stations recorded the ground motion digitally. About half used a three-component sensor, but the remainder had only a vertical-component sensor. Australia contributed data from the Warramunga (WRA) and Alice Springs (ASAR) arrays in Central Australia, from 3-component broadband

[1] Australian Seismological Centre, Australian Geological Survey Organisation, GPO Box 378, Canberra ACT 2601

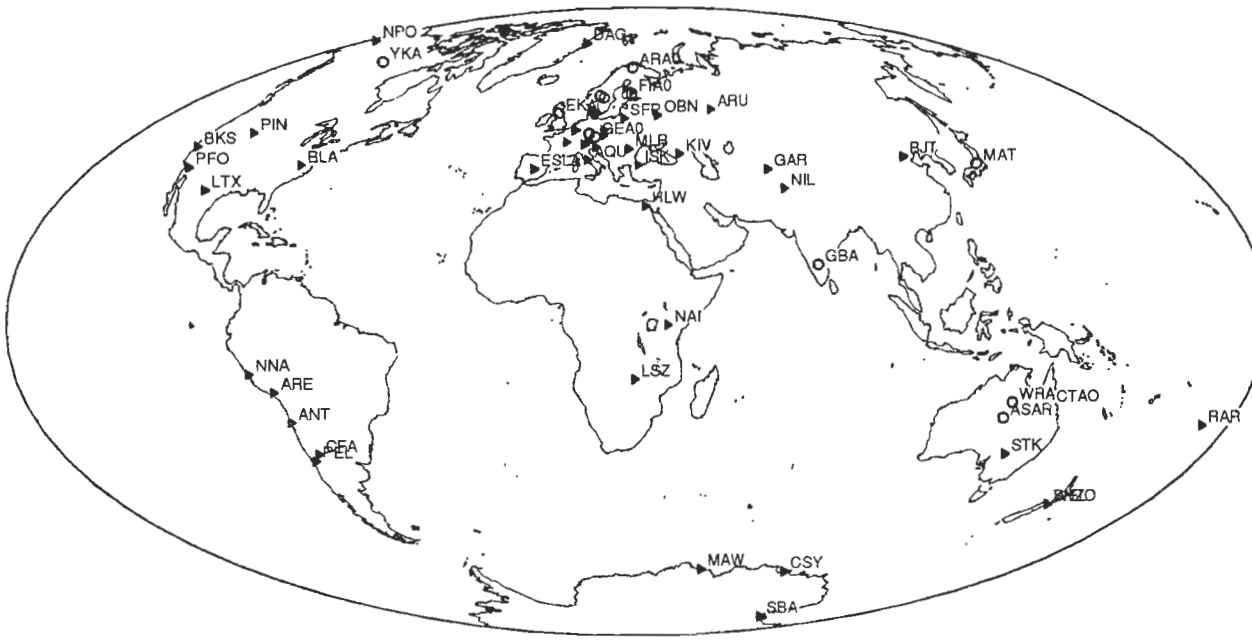

Figure 1a. Map of the 60 stations that contributed data during GSETT-2. Arrays are shown as open circles and other stations by triangles.

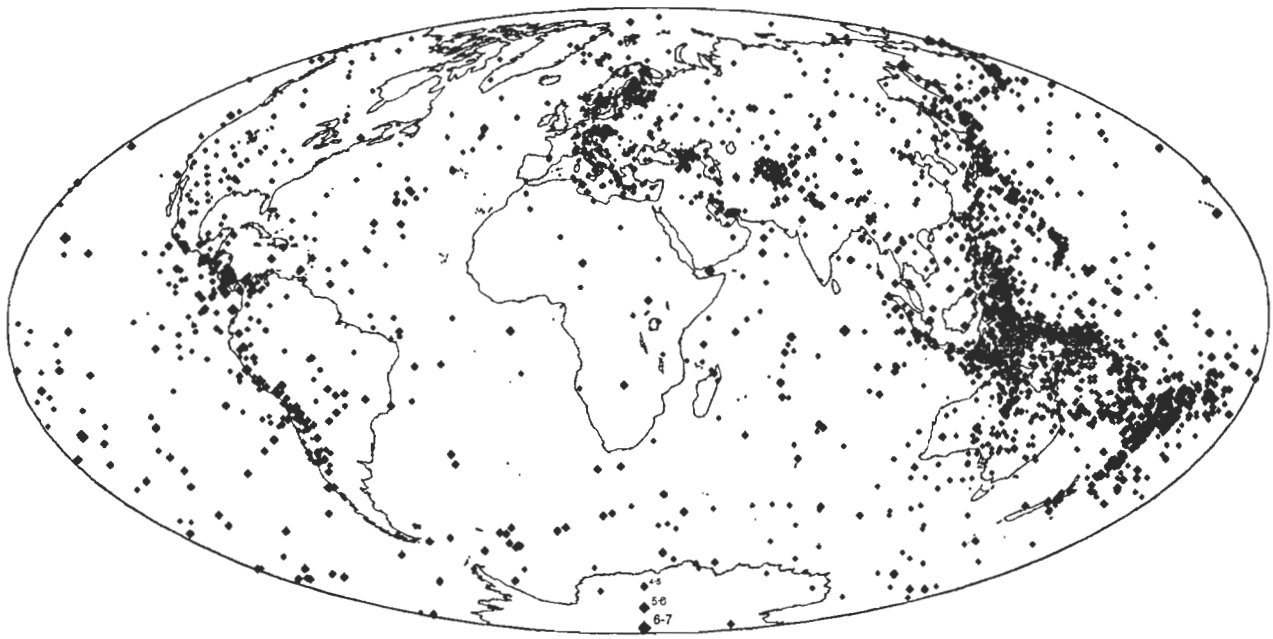

Figure 1b. Map of the 3715 events reported in the Final Event Bulletins during GSETT-2.

stations at Stephens Creek (STK), New South Wales, Charters Towers (CTA), Queensland and from its Antarctic bases at Mawson (MAW) and Casey (CSY) (Fig. 1a).

Each participating country operated a national data centre. The functions and procedures of the National Data Centres were based on the principle that parameter and waveform data would be reported for all seismic signals that were recorded digitally, so that the chance of defining new events at the Experimental International Data Centres would be greatest (GSE, 1992). The primary functions of the National Data Centres (GSE, 1992) were:

1. to collect data from stations;
2. to archive data for at least 15 days;
3. to detect seismic signals;
4. to extract parameter and waveform data;
5. to determine locations for local and regional seismic events;
6. to report data to Experimental International Data Centres; and
7. to respond to requests for retransmission of data or for extra data.

During GSETT-2, experimental international data centres were operated in Canberra, Moscow, Stockholm and Washington. Each of the four centres operated independently and exchanged data and processing results daily in order to prepare the final Experimental International Data Centre products. The agreed functions of each centre (GSE, 1992) were:

1. to collect parameter and waveform data from the National Data Centres;
2. to maintain a complete database;
3. to allow National Data Centres unrestricted access to all data and messages;
4. to respond to all National Data Centre requests for data and bulletins;
5. to exchange message transaction logs with other Experimental International Data Centres daily;
6. to request missing messages;
7. to prepare automatically initial event lists from parameter data and exchange these with other Experimental International Data Centres;
8. to update current event lists using information derived from waveform analysis;
9. on a rotating basis, to merge the most recent current event lists from each centre into one Final Event Bulletin and distribute this to all National Data Centres.

The communication system established for GSETT-2 consisted of high-capacity dedicated links between the four centres and connections between each of the National Data Centres and the GSE network (Fig. 2). Connections between data centres ranged from computer-to-computer file transfer on dedicated links to low-speed telex lines, according to availability, demands for capacity, technical experience at the National Data Centre and ability to pay. Testing of the communication links among stations and data centres was an important objective of GSETT-2 but is beyond the scope of this paper. In brief the communication links worked well where they had been tested before the main phase of the experiment.

GSETT-2 experiment

GSETT-2 was conducted in four distinct phases. Phase 1 began in 1988 and involved many technical and procedural developments. Phase 2 began with 8 days of data exchange and processing, one day a week, in early 1990. After revision of some of the procedures, Phase 2 continued with 4 days of data exchange and processing in mid-1990 and 19 days of data exchange in late 1990.

Phase 3 consisted of two parts. The first part involved 7 consecutive days of data exchange and processing in late 1990. The second and main part of Phase 3 was a full-scale test over 42 consecutive days from 22 April to 2 June 1991, with processing of the last day's data completed on 9 June. Phase 4 is the evaluation of the results of GSETT-2. This paper focuses only on the main part of Phase 3 and the subsequent evaluation.

Automation

It was ambitious to try to monitor global seismicity with a sparse seismic network and to generate preliminary and Final Event Bulletins in 2 and 7 days, respectively, so as many elements of the GSETT-2 system were automated as possible. For example, automatic detectors were used by many National Data Centres to detect arrivals from digital

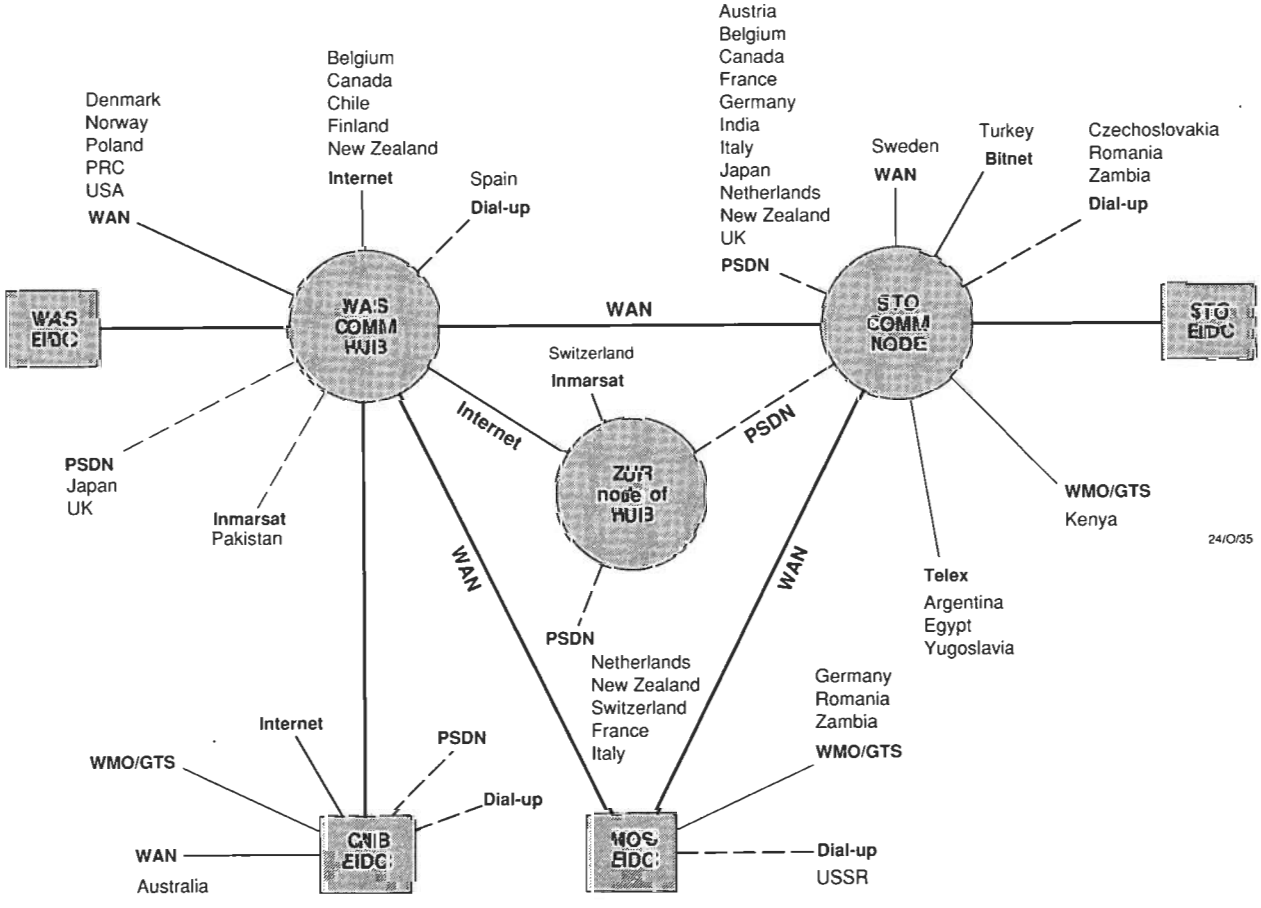

Figure 2. Some of the communications links used during GSETT-2.
Communication links included wide area networks (WAN), packet switched data networks (PSDN), the World Meteorological Organization's Global Telecommunications System (WMO/GTS) and a commercial satellite (Inmarsat).
EIDC Experimental International Data Centre

stations. Following review by an analyst, parameter files and waveform segments were transmitted automatically to the Experimental International Data Centres. Similarly, requests for retransmission of data or for supplementary data were often handled automatically at the National Data Centres. At the Experimental International Data Centres incoming data were incorporated automatically into a file structure or data base. The most critical task of the Experimental International Data Centres was to interpret the parameter and waveform data from all the stations in terms of discrete seismic events. In the first instance, events were formed from parameter data using an automatic phase association program or an expert system. The initial event list was then reviewed by an analyst, and waveform data were used to reject or confirm individual events and to further constrain locations.

Despite the high level of automation, GSETT-2 was very demanding for staff at the National Data Centres and Experimental International Data Centres. For example, at the Australian National Data Centre four temporary employees joined the three regular analysts during GSETT-2, but it was still difficult to review all detections from Australian stations and arrays on the schedule required for transmission to the Experimental International Data Centres. The Experimental International Data Centres were challenged by the requirement to prepare initial event lists within 48 hours and then to update the current event list as additional data arrived over the next 5 days. The Experimental International Data Centres had insufficient time to analyse difficult event sequences completely or to refine their systems.

Results of GSETT-2

The primary product of GSETT-2 is the set of Final Event Bulletins for the 42 data days of the experiment, which list for every event the hypocentral solutions from each reporting Experimental International Data Centre as well as the associated parameter data. Responsibility for compiling the Final Event Bulletins from the last current event list available from each of the four centres was rotated among the International Data Centres, one each fourth day. Epicentres of all 3715 events given in the bulletins are shown in Figure 1b. The major seismic zones at collisional plate boundaries, such as Indonesia, Fiji and South America can be seen, but the distribution of events is a blurred image of the familiar pattern of global seismicity.

The National Earthquake Information Center of the U.S. Geological Survey routinely prepares a bulletin of global seismicity, the Earthquake Data Report, with a lag of about 5 months. Epicentres of the 1953 events from the Earthquake Data Report for the period of GSETT-2 form a substantially clearer image of the active seismic zones (Fig. 3b) than do the GSETT-2 epicentres. However, the number and distribution of stations used in preparing the bulletins must be considered. GSETT-2 used stations at only 60 sites, concentrated in the northern hemisphere and Europe in particular (Fig. 1a), whereas the National Earthquake Information Center used data from 1456 stations, which had superior global coverage (Fig. 3a).

Other factors that contributed to the scatter of GSETT-2 epicentres relative to the Earthquake Data Report were the size of the events and the criteria for defining events. The GSETT-2 identified 3715 events, or an average of 88 a day compared with 1953, or 47 a day, in the Earthquake Data Report. The additional events in the GSE bulletins are mostly small, and have less well constrained hypocentres. A key operational principle of the Experimental International Data Centres was to form as many events as possible, and rules on the minimum number of observations were prescribed in Conference Room Paper/190 (GSE, 1991, appendix B). These rules proved insufficiently restrictive to assure reliable epicentres for all events formed. Some events were grossly mislocated because of poor resolution capability or because of errors introduced by misassociated phases. Other events were spurious, that is, formed by phase associations that are allowable under Conference Room Paper/190 rules, but that do not represent legitimate seismic events. For example, an event could be erroneously formed by association of a teleseismic P phase reported by one of the Australian arrays with a local or regional P phase from a European station. Because of the high seismicity in the island arcs north and east of Australia, the ASAR and WRA arrays each detected an average of 190 events a day, so it was not uncommon for automatic association programs to mismatch one of these phases with a phase observed at one or a few other distant stations from a different event. The result was a fictitious event.

The quality or reliability of the Final Event Bulletins and various subsets can be assessed by the method described in Australian Delegation (1992) using the Hypocenter Data File for 1963–1987 as a reference catalogue. This method formalises seismological judgement by calculating the mean probability of occurrence for a set of epicentres in a subject catalogue, which is a measure of correlation with the reference catalogue. Under the assumption that the spatial distribution of seismicity is stationary with time, the mean probability is interpreted to be a measure of reliability of a subject catalogue. By this measure, the Final Event Bulletins (Fig. 1) have a relative reliability of 6.2, the Earthquake Data Report for the period of GSETT-2 has a reliability of 15, and a random distribution of events has a score of 1.1. This measure of reliability cannot be applied to regions such as Fennoscandia where the capability of the GSE network exceeds that of the global network used for the reference catalogue.

The rules used to form events determined the number of events formed as well as the reliability of the epicentres. Figure 4 shows the trade-off between the number of events and the reliability. The reliability increases dramatically with an increase of the minimum number of defining observations (Fig. 4a) or defining stations (Fig. 4b). These trade-off curves demonstrate that it is easy to improve the quality of a bulletin, but at the expense of the number of events reported. Figure 5 shows all 1839 bulletin locations based on nine or more observations (either travel time, slowness or azimuth) or based on four or more independent stations. The seismicity pattern is more consistent with actual global seismicity than are the Final Event Bulletins as a whole (Fig. 1b), which is reflected by the increase from 6.2 to 7.1 in the measure of reliability. The number of events remaining in the catalogue is similar to those reported in the Earthquake Data Report; but the Earthquake Data Report is based on 1456 stations compared to only 60 used in compiling the Final Event Bulletins, and was issued 5 months in arrears compared with only 7 days for the Bulletins. This demonstrates that a system similar to that used in GSETT-2, but with improved station distribution and more conservative event formation rules, could provide timely and accurate monitoring of global seismicity.

In addition to reliability of hypocentre solutions, the

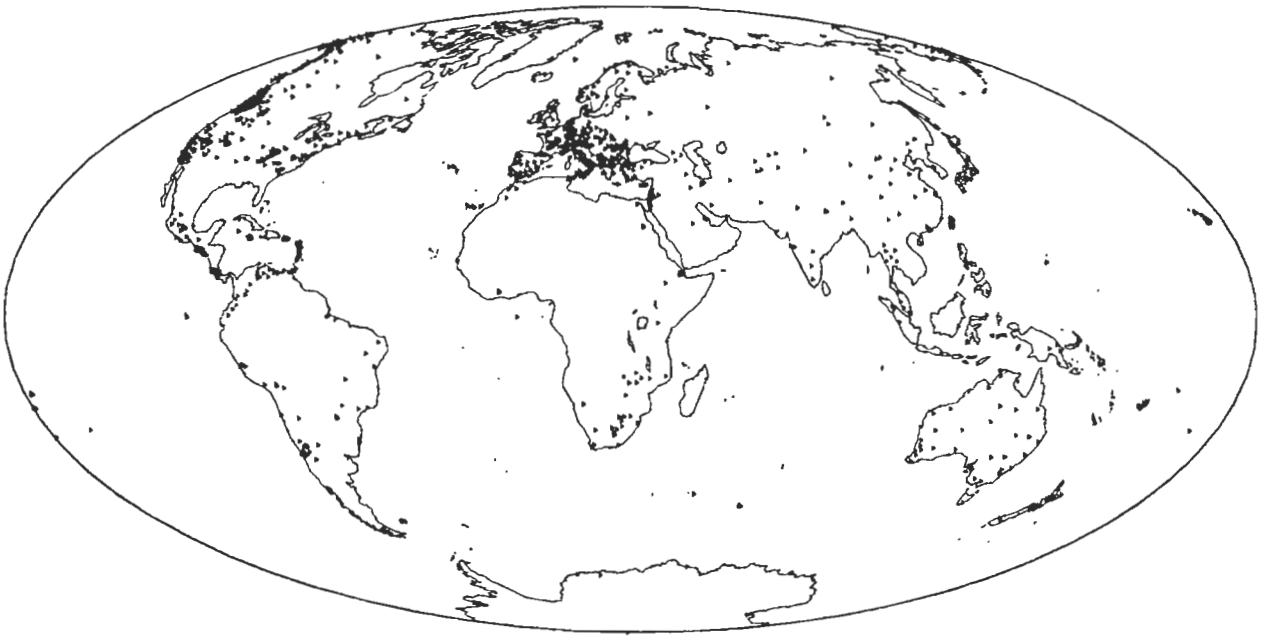

Figure 3a. Map showing 1289 of the 1456 stations that contributed to locations in the Earthquake Data Report for the period of GSETT-2, April-June 1991.
The coordinates of the remaining 168 stations were unavailable.

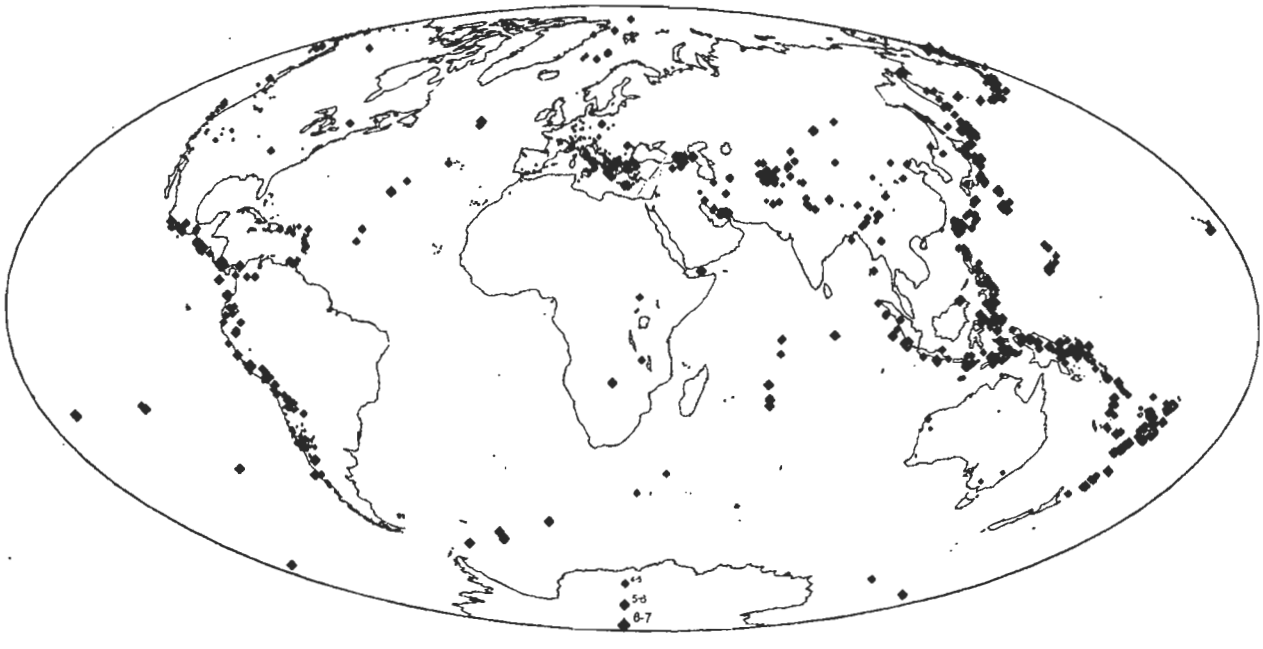

Figure 3b. Map of 1953 epicentres listed in the Earthquake Data Report for the period of GSETT-2, April-June 1991.

detection threshold and level of catalogue completeness are important measures of the performance of GSETT-2. The probability of detection for GSETT-2 can be estimated by comparing the distribution as a function of magnitude of events reported in the bulletins with those in the National Earthquake Information Center's monthly Preliminary Determination of Epicenters using the method of Ringdahl (1975). The histograms in Figures 6 and 7 show all events in the Preliminary Determination of Epicenters as open bars, and those bulletin events that occurred within 3° and 60 s of a Preliminary Determination of Epicenters event, as shaded bars. Many small Final Event Bulletin events that were not included in the Preliminary Determination of Epicenters are not shown in Figures 6 and 7. Open bars extending above the filled bars indicate events that were omitted from the bulletins, and analysis of the percentage of Preliminary Determination of Epicenters events reported in the bulletins indicates the capability of the GSE system. In the northern hemisphere (Fig. 6) there is a 50% chance of locating an event of m_b 3.4 and 90% chance for an event of m_b 4.4. Because there are fewer stations in the southern hemisphere, the location thresholds are higher (Fig. 7), with 50% and 90% probability of location for m_b 4.1 and 5.1 events, respectively.

For Scandinavia, analogous detection capability comparisons were made between the Final Event Bulletins and bulletins of the Universities of Bergen and Helsinki

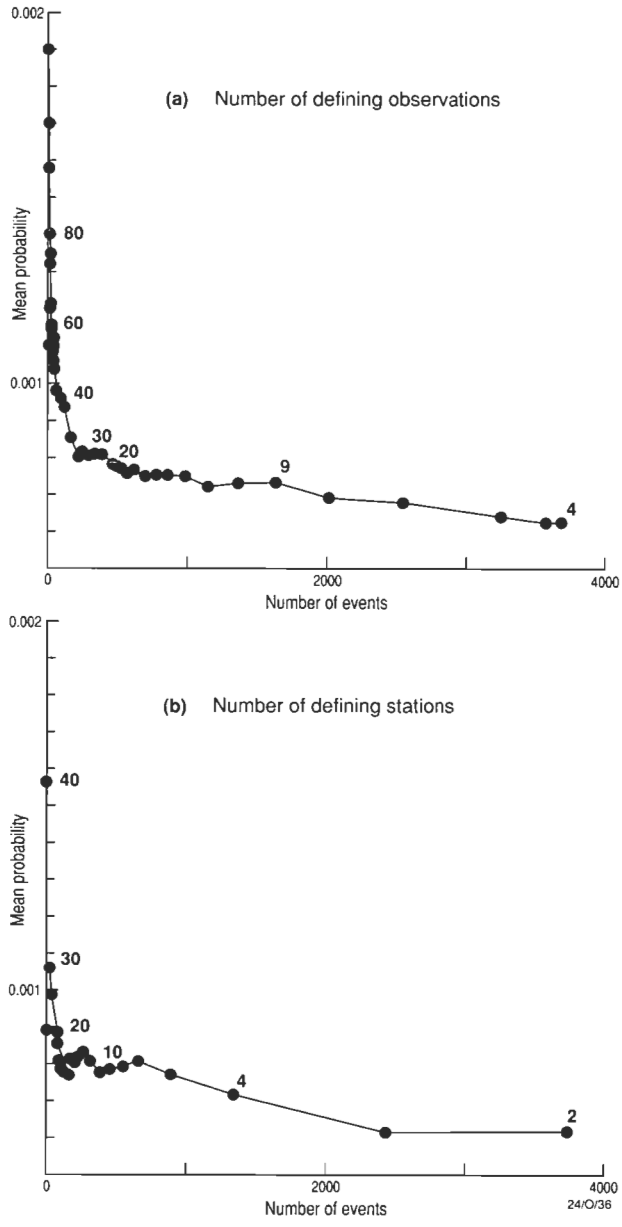

Figure 4. Trade-off curves between the number of events in the Final Event Bulletins and the mean probability of occurrence relative to the Hypocenter Data File from 1963 to 1987 as a function of a) minimum number of defining observations and b) minimum number of defining stations.

(Norwegian and Finnish Delegations, 1992). Owing to the presence of four seismic arrays as well as numerous independent stations in Scandinavia, the detection thresholds for that region are very low. For western Norway, there is a 50% (90%) probability that an M_L 2.2 (2.5) event was reported by an National Data Centre, and for northwest Russia a 50% (90%) probability that an M_L 2.2 (2.5) was included in the Final Event Bulletins. Thus, the detection capability during GSETT-2 varied by 3 orders of magnitude between the Scandinavian region and the southern hemisphere as a whole. The uneven capability of the existing network will need to be addressed in order to verify a Comprehensive Test Ban Treaty effectively.

Regional variations of detection capability and location resolution of the GSE network have been simulated numerically (Bratt & others, 1992). The station geometry, instrument response and characteristic noise spectra measured during GSETT-2, typical earthquake source spectra, and reported rates of station failure were used to calibrate the simulations to actual conditions. The predicted detection and location threshold (Fig. 8) is a function both of the local density of stations and of the broader station geometry (Bratt & others, 1992). The simulations overestimate the capability of the GSETT-2 network compared to an empirical approach (Fig. 5), probably because the simulations did not account for variability in reporting practices such as choice of detection threshold, poor phase association, possible errors in software or blunders by analysts. As a consequence, some events of up to m_b 5 that occurred in areas with detection and location capability estimated at m_b 4 were omitted from the Final Event Bulletins. Several of the largest events omitted from the bulletins were from the Indonesian and Tongan arcs and occurred during a failure of one or both of the Australian arrays. The lack of sufficient redundancy (numerous stations recording each event) within the sparse GSE network made it vulnerable to serious degradation of detection capability.

The correct association of seismic phases to form seismic events is a complex process. For each station, detectors or analysts at National Data Centres produce a list of phases with preliminary identifications and attributes, such as amplitude and period. Phases used for event formation during GSETT-2 were local and regional phases (Pg, P*, Pn, Sg, S*, and Lg), teleseismic P and S, and the core phase PKP. Surface reflections pP and sP were also allowed to aid in constraining focal depths. Other phases that were not used for purposes of location, such as PP, ScP and PKKP, were of course still detected and reported to the Experimental International Data Centres. Altogether, 65 000 phases were reported by the centres, and additional phases were gleaned from the waveform data. Largely because of the high seismicity to the north and east of Australia, phases from the ASAR and WRA arrays in central Australia were reported at a rate of one every 8 minutes.

The Canberra, Moscow and Stockholm Experimental International Data Centres used automatic phase association programs, whereas the Washington centre used an expert system. The abundant phases reported during GSETT-2 and the tight timetable for preparing bulletins revealed shortcomings in both the automatic association programs and the expert system. Here we discuss recent and potential improvements to the automatic association program used at the Canberra centre as a result of experience gained from GSETT-2.

The automatic phase association consists of four main stages. In the first stage, a group of starting solutions for an event location is selected. One type of starting solution is based on an array measurement of arrival time, azimuth and horizontal slowness. Together with a global velocity model, an array measurement implies a location and origin time. Another type of starting solution may be available from an S-P time at a local or regional station, which gives estimates of the distance from that station and of the origin time. A third type of starting solution comes from differential travel times at several observing stations. In the second stage, theoretical arrival times at each GSE station are calculated for each starting solution. Reported phases that occurred within some error allowance of the theoretical time are then 'associated' with that starting solution.

The third stage is a linearised, least-squares inversion for

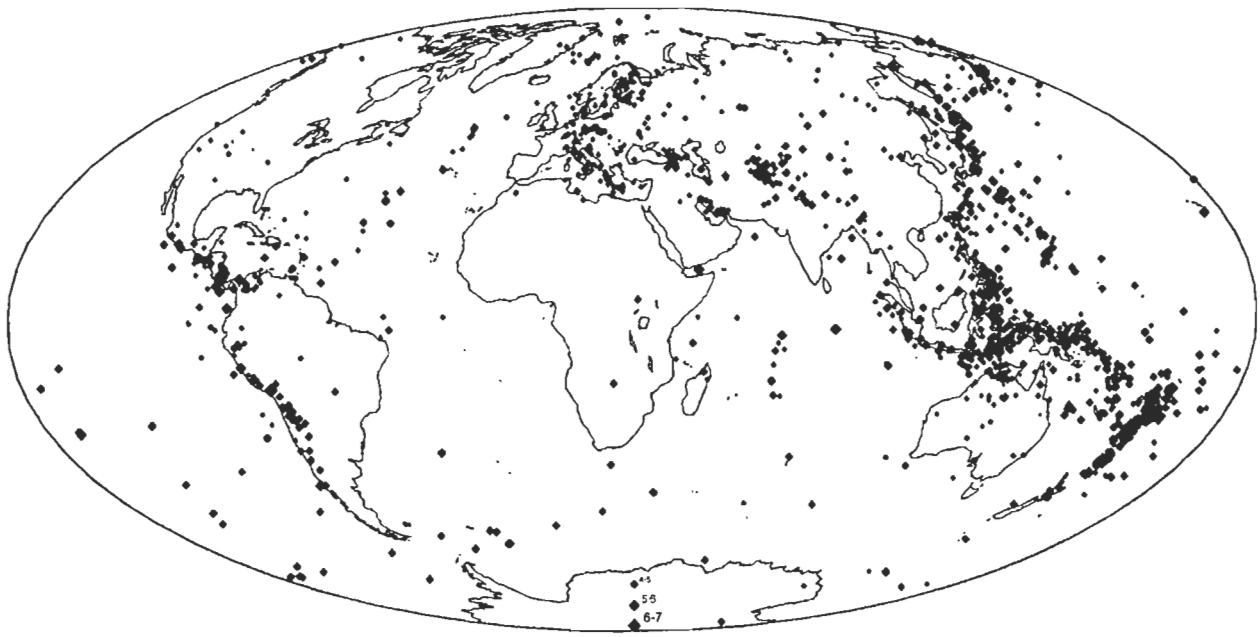

Figure 5. Map of 1839 events from the Final Event Bulletins with 4 or more defining stations or 9 or more defining observations.

the best solution that corresponds to the data associated with each starting solution. The problem of earthquake location is highly non-linear, and as a result linearised inversions are susceptible to finding a local rather than a global minimum in the error space. The automatic association program attempts to overcome this limitation by generating multiple starting solutions, but the strategy is not always successful. In the fourth stage, the final solutions are compared, initially automatically but later by an analyst, to select the best overall solution. For well constrained events, the solutions generally converge toward a single location. On the other hand, for events with

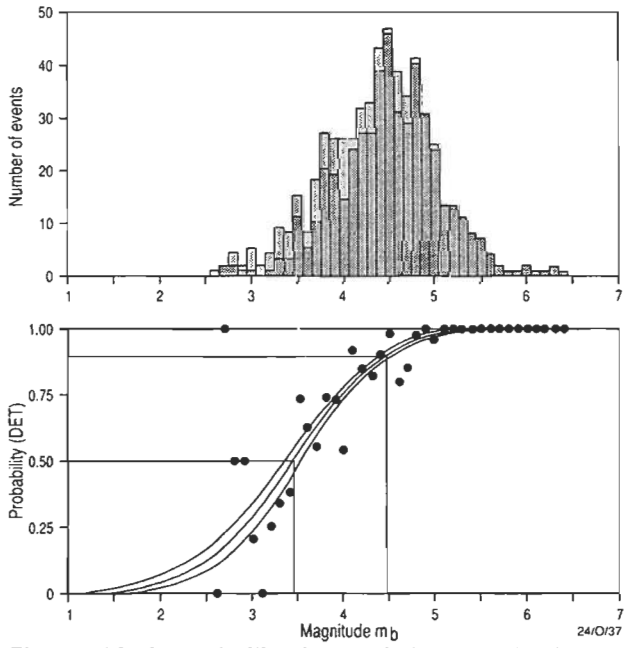

Figure 6. Maximum likelihood detectability estimation for the northern hemisphere using the monthly Preliminary Determination of Epicenters as a reference catalogue.
From Ringdahl & others, 1992.
The upper panel shows the reference event set from the Preliminary Determination of Epicenters bulletin (open bars) and the number of events actually reported by the GSE (shaded bars) for each magnitude interval. The lower panel shows the maximum likelihood detectability curve and its confidence limits. The actual percentage of detected events is also shown.

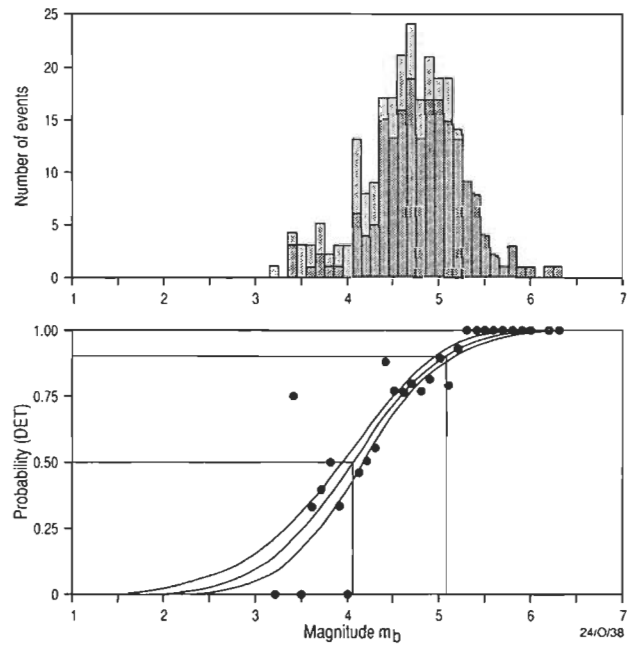

Figure 7. Maximum likelihood detectability estimation for the southern hemisphere using the monthly Preliminary Determination of Epicenters as a reference catalogue.
From Ringdahl & others, 1992.
The upper panel shows the reference event set from the Preliminary Determination of Epicenters bulletin (open bars) and the number of events actually reported by the GSE (shaded bars) for each magnitude interval. The lower panel shows the maximum likelihood detectability curve and its confidence limits. The actual percentage of detected events is also shown.

few data or conflicting observations, the best solution may be ambiguous.

A new strategy has recently been implemented at the Canberra Experimental International Data Centre for generating starting solutions and associating phases. Rather than using the three types of starting solutions, which may be widely spread, and generous error allowances for matching theoretical and observed times, we concentrate on a larger group of starting solutions in the neighbourhood of an array location and use a narrower error allowance. This strategy is illustrated for an event near Japan (Fig. 9). Although the resolution of a single array location of a teleseismic event is rather poor, starting solutions can be distributed at about 2° intervals throughout the region consistent with array observations. Because these starting solutions are closely spaced, tighter error bounds can be required for phases to be initially associated with each starting solution, which reduces substantially the chance that a misassociated phase will corrupt the location of a legitimate event. The 'capture area' of allowable associations has been reduced from 10° to 1.5° using this strategy.

The revised phase association algorithm has been successfully applied to two data days from GSETT-2 that were reanalysed by all Experimental International Data Centres. The reprocessed Final Event Bulletins are the union of event lists prepared by the four centres, so the proportion of Final Event Bulletin events that can be automatically defined by a phase association algorithm is an indicator of its performance. The revised algorithm at the CNB centre defined 66 of the 68 events in the reprocessed Final Event Bulletin for 2 June 1991, compared with 45–57 for other algorithms including an expert system. The locations of the remaining two events were based on slowness vectors from two arrays, and were automatically rejected because the slowness-vector residuals were larger than allowed by CRP/190. The performance of the algorithm was also encouraging for 29 April 1991. This was a difficult data day because a large earthquake in the West Caucasus region and its aftershock sequence produced many primary and later phases that were intermingled with phases from other earthquakes worldwide. The revised algorithm defined 70 out of the 76 aftershocks for which there were sufficient phase data available to provide a solution. Further refinements to the algorithm will be required to identify the remaining events that were contributed by other Experimental International Data Centres.

Discussion and conclusions

GSETT-2 was ambitious in many ways. The GSE tried to prepare a 'final' global seismicity bulletin in 7 days,

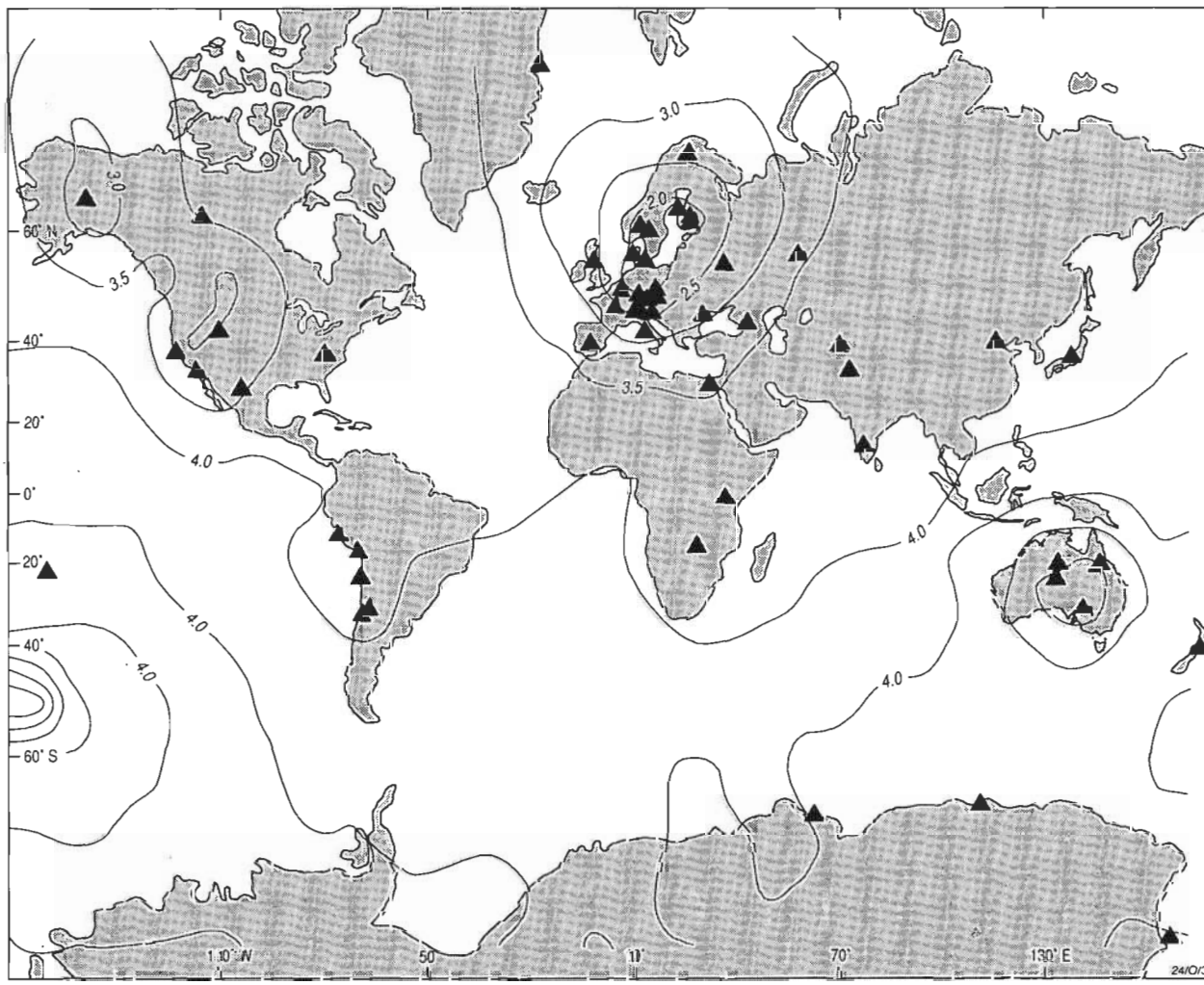

Figure 8. Theoretical detection and location threshold for the GSETT-2 station configuration based on the average noise level at each station.
From Bratt & others, 1992. Contour interval is 0.5 m_b units.

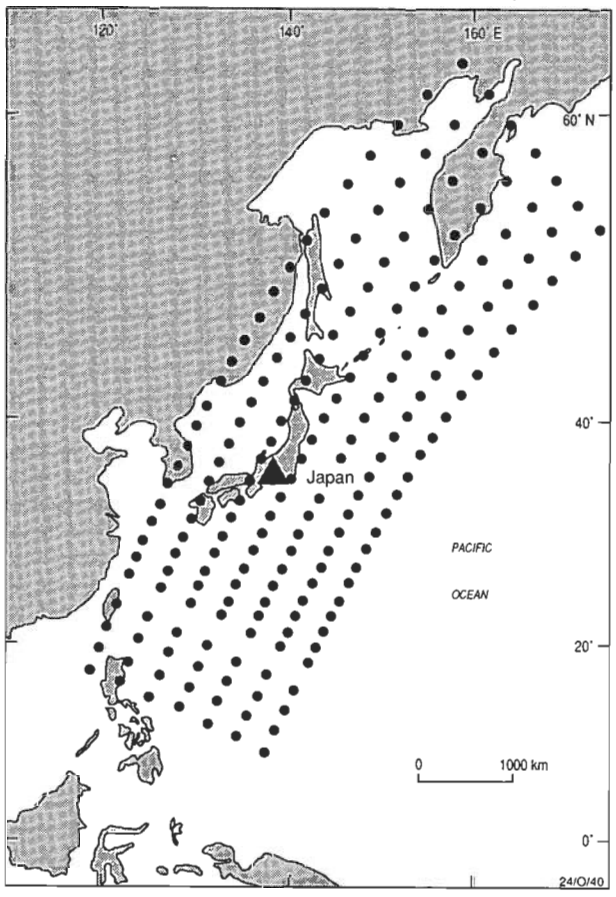

Figure 9. Distribution of starting solutions (filled circles) used in the revised phase association program at the Canberra Experimental International Data Centre for an event near Japan.
The final location given by the phase association and linearised inversion is shown by the star.

whereas the U.S. National Earthquake Information Center publishes the Earthquake Data Report 5 months in arrears, and the International Seismological Centre (ISC) publishes a bulletin that is more complete than the Earthquake Data Report after 2 years. Moreover, the GSE depended on voluntary contribution of data from those countries that were participating officially, so all detections and locations in the Final Event Bulletins were based on stations at only 60 sites. Nevertheless, GSETT-2 demonstrated that it is feasible to exchange rapidly a large quantity of seismic waveform and parameter data, as well as interim and final results of Experimental International Data Centre processing. Furthermore, GSETT-2 revealed some of the weaknesses of the GSE monitoring system and therefore provided an impetus to improve the methodology, hardware and software that will be required for the effective verification of a Comprehensive Test Ban Treaty.

A number of improvements to the GSE system were proposed at an international GSE workshop held in Canberra in April 1992. For example, in order to improve the reliability of event locations, event formation rules can be made more restrictive. Checking the consistency of amplitudes and periods of phases associated with an event can be used to identify unlikely associations and thus reduce the number of spurious events. Use of travel-time curves appropriate for specific regions and a more accurate global travel time model such as IASP91 (Kennett & Engdahl, 1991) will improve the accuracy of locations. Standardisation of analysis techniques for 3 component seismograms will help improve the reliability of locations based on data from only a few stations.

Participation of more stations in the southern hemisphere will improve the detection capability. The Australian Seismological Centre is working to install satellite telemetry links to increase the number of Australian stations for which data are available in real time, and is investigating sites for a possible third seismic array. Both initiatives will improve detection and location capability in Southeast Asia and the South Pacific. The United States is installing four stations in Africa, four in South America and one in Antarctica that will contribute data to the GSE and improve the system capability throughout the southern hemisphere.

Future installation of open stations will improve the capability of the GSE monitoring system. Open stations record and store data locally and make the data available to any person or institution who solicits the data by computer. Open stations will supplement the core stations of the GSE network and will allow confirmation of a detection or refinement of a location made using the core GSE network. Through these and other developments, the performance of the GSE monitoring system will be enhanced in the coming years.

Acknowledgements

The Australian Geological Survey Organisation's participation in the GSE is sponsored by the Department of Foreign Affairs. We thank S. Bratt and S. Mykkeltveit for allowing reproduction of their figures and S. Bratt, D. Denham and two anonymous referees for their comments on the manuscript.

References

Australian Delegation, 1992 — An objective measure of the reliability of a seismic bulletin, GSE/AUS/49. *Conference on Disarmament, Geneva, Switzerland.*

Bratt, S., Grant, L. & Corley, D., 1992 — Simulated and actual monitoring capability of the GSETT-2 system. *Proceedings of Workshop on Seismological Evaluation, 27 April–1 May, 1992, Canberra, Australia.*

Group of Scientific Experts (GSE), 1991 — Instructions for the conduct of Phase 3 of GSETT-2, Conference Room Paper/190/Rev. 4. *Conference on Disarmament, Geneva, Switzerland.*

GSE, 1992 — Report on the Group of Scientific Experts' Second Technical Test, CD/1144. *Conference on Disarmament, Geneva, Switzerland.*

Kennett, B.L.N. & Engdahl, E.R.,1991 — Travel-times for global earthquake location and phase identification. *Geophysical Journal Int.ernational* 105, 429–465.

Norwegian and Finnish Delegations, 1992 — Regional detection and location performance during GSETT-2: Initial result for the Fennoscandian array network, GSE/NOR, FIN/1. *Conference on Disarmament, Geneva, Switzerland.*

Ringdahl, F., 1975 — On the estimation of seismic detection thresholds, *Bulletin of the Seismological Society of America* 65, 1631–1642.

Ringdahl, F., S. Mykkeltveit and U. Baadshaug, 1992 — Global event detection performance during GSETT-2, in Semiannual Technical Summary, 1 October 1991–31 March 1992, NORSAR Scientific Report 2–91/92. *NORSAR, Kjeller, Norway.*

BMR Journal of Australian Geology & Geophysics, 13, 333–343

Structure of the southern New South Wales continental margin, southeastern Australia

J.B. Colwell[1], M.F. Coffin[1,2] & R.A. Spencer[3]

High-quality, regional seismic data collected on the continental margin of southern New South Wales indicate that the margin lacks major basin development, consistent with its interpretation as an 'upper plate' margin. The most striking structural feature is a mid-slope graben or half graben which is bounded on its eastern (seaward) side by a westerly-dipping fault system and a basement ridge. The half-graben contains up to 2.2 seconds TWT (~2500 m) of sediment, including syn-rift deposits possibly as old as Late Jurassic. A seaward-thickening wedge of sediment overlies a generally flat basement surface beneath the shelf. This contrasts with large areas of the lower continental slope which are essentially free of sediment. Sediment thicknesses beneath the Tasman Sea abyssal plain reflect basement structure. The greatest thickness occurs next to the foot of the slope where sediment loading has produced flexuring in either oceanic or thinned-continental crust. Overall, the petroleum potential of the margin (excluding the pre-rift Sydney Basin rocks) appears to be low.

Introduction

The continental margin of southern New South Wales (southeast Australia) is a typical 'passive' margin developed by rifting and breakup between Australia and the Lord Howe Rise/Dampier Ridge in the Late Cretaceous and Paleogene (Fig. 1; Hayes & Ringis, 1973; Weissel & Hayes, 1977; Shaw, 1978, 1979). The margin has a narrow continental shelf (generally less than 50 km wide) and steep continental slope (up to 20°). It is backed by a range of mountains forming a continental divide and shows little evidence, at least in the upper part of the section, of the presence of widespread rift development (Jones & others, 1975; Davies, 1979). Two models have been proposed to account for these features:

(i) non-axial (asymmetric) breaching of a rift valley (Jongsma & Mutter, 1978; Mutter & Jongsma, 1978), where the entire pre-breakup rift valley remained attached to Lord Howe Rise when seafloor spreading began; and

(ii) separation along a detachment fault (modified simple-shear) (Etheridge & others, 1989; Lister & Etheridge, 1989; Lister & others, 1991), where the New South Wales margin is interpreted as an 'upper-plate' margin with relatively minor rift structure development and an uplifted hinterland. Uplift of the hinterland to produce the eastern Australian highlands may have occurred during continental extension, before and during continental breakup (e.g. Ollier, 1982; Bishop, 1989; Lister & Etheridge, 1989). The Lord Howe Rise is interpreted to be the conjugate 'lower-plate' margin on the other side of the Tasman Basin, characterised by widespread rift structures on its western side.

In 1987, the Bureau of Mineral Resources (now the Australian Geological Survey Organisation, AGSO) collected 3100 km of 48-channel (24-fold) seismic reflection data on the southern New South Wales and adjacent Victorian continental margins to assist in testing models of the margins' development and assess the margins' petroleum potential (Colwell & others, 1987). Data (BMR Survey 68) were collected using the Research Vessel *Rig Seismic* and comprise the first, modern, regional, multichannel seismic data set on this part of the Australian margin. Lines were run in a zig-zag pattern south from Wollongong extending onto the abyssal plain of the Tasman Basin and into the eastern part of the Gippsland Basin (Fig. 1). This paper discusses the New South Wales margin lines (Lines 1-8, Fig. 1). which were all shot with a 26.2 litre 10-element airgun array and recorded using a 2400 m streamer. Gravity, magnetic and bathymetric data were recorded concurrently with the seismic.

1 Australian Geological Survey Organisation, GPO Box 378, Canberra ACT 2601
2 Now at: Institute for Geophysics, University of Texas at Austin, 8701 Mopac Blvd, Austin TX 78759-8397 USA
3 New South Wales Geological Survey, PO Box 536, St Leonards NSW 2065

Pattern of seafloor spreading

The pattern of breakup and seafloor spreading in the Tasman Basin adjacent to the southern New South Wales margin is still somewhat uncertain because of the difficulty in precisely defining spreading azimuths with the current data set. Several sets of fracture zones with slightly differing strikes have been proposed (Hayes & Ringis, 1973; Weissel & Hayes, 1977; Shaw, 1978, 1979). In each, spreading is portrayed as having been oblique to the margin and orientated broadly northeast-southwest separating the Dampier Ridge and western Lord Howe Rise from southern New South Wales (Fig. 1). Magnetic anomalies 33 to 24 have been identified with varying degrees of certainty (Hayes & Ringis, 1973; Weissel & Hayes, 1977; Shaw, 1978, 1979; Fig. 1). These suggest that seafloor spreading occurred from approximately 80 Ma to 55 Ma ago, based upon the timescale of Kent & Gradstein (1985) and Berggren & others (1985).

According to Shaw (1978, 1979), evolution of the Tasman Basin before C32 can be best described by rotations around a relatively remote stage pole (producing a largely left-lateral strike-slip component), whereas evolution since C32 can be attributed to rotations around a sequence of initially nearby but rapidly retreating stage poles producing typical rifted margin characteristics in the south, and pull-apart margins in the north. For the southern New South Wales margin, opening appears to have been principally in a northeast—southwest direction i.e. oblique to the present-day shelf and slope. Willcox & others (1992) have recently suggested that early rifting along Australia's eastern margin was connected through a series of largely transtensional basins in Bass Strait to rifting along the southern margin of Australia. Rifting in both areas may have begun at broadly the same time, in the Late Jurassic.

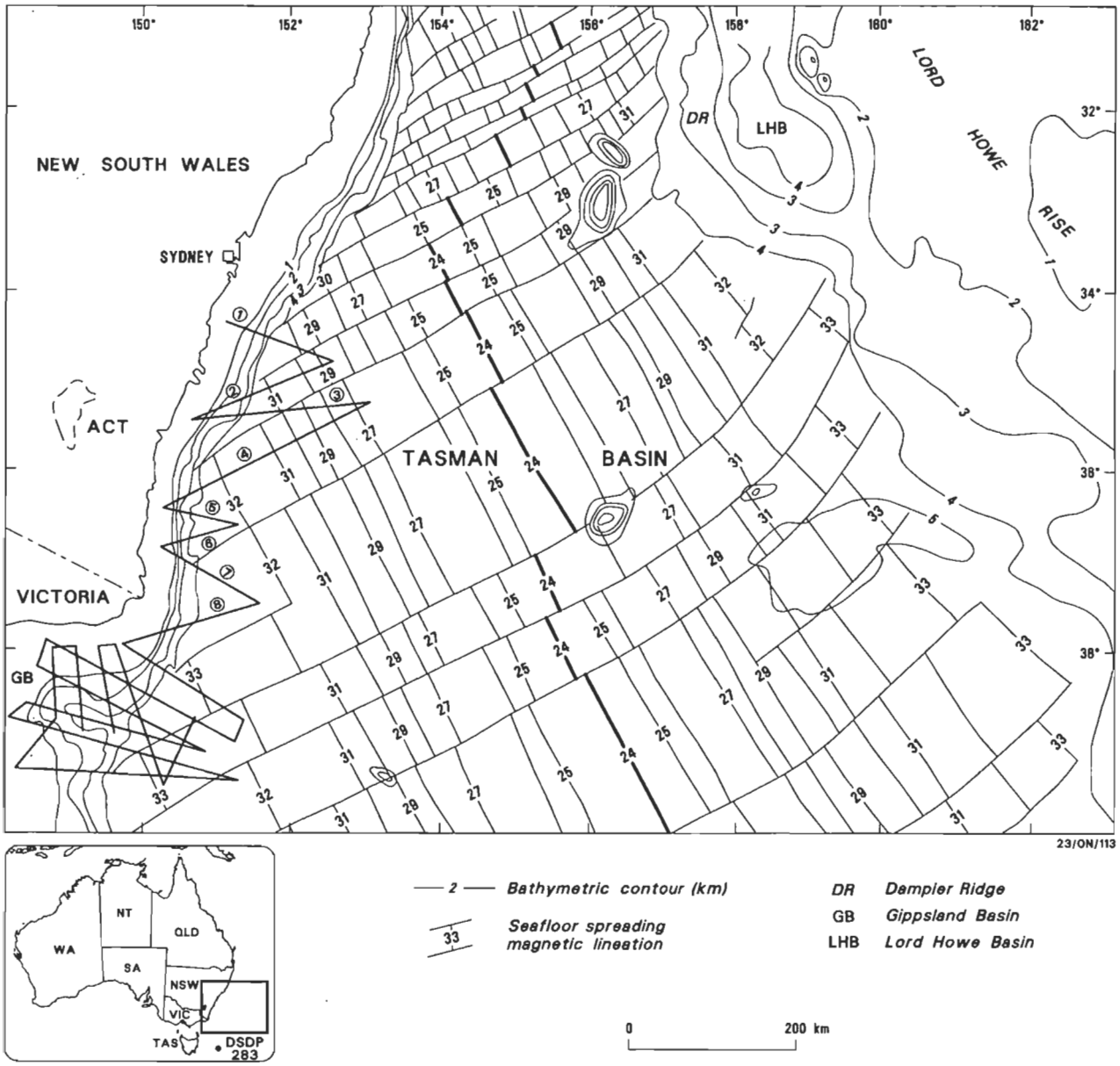

Figure 1. General location of BMR 1987 (Survey 68) seismic lines.
Seafloor spreading lineations and fracture zones after Shaw (1978, 1979).

Geology

Onshore, southeastern New South Wales consists of Palaeozoic rocks of the Lachlan Fold Belt overlain between latitudes 32° and 36°S by Permo-Triassic sediments of the Sydney Basin (Packham, 1969; Fig. 2) and younger surficial deposits. Offshore, the continental shelf is less than 40 km wide and is backed by a rugged, embayed coastline, closely controlled by local geology. The shelf break varies in water depth from 130 to 170 m and is largely controlled by basement structure (Jones & others, 1975; Davies, 1979; BMR Continental Margins Survey, unpublished data). The margin is highly sediment starved. Only a thin sediment wedge overlies basement on the shelf and parts of the slope (Fig. 3; Davies, 1979; Shaw, 1979).

The nature and age of basement rocks on the margin are largely unknown; only a minor amount of coring and dredging has been undertaken (Packham, 1983; Hubble & Jenkins, 1984; Hubble & others, 1992). Sydney Basin sediments appear to extend out under the shelf in the region between 32° and 35°S and may be exposed in canyon systems (Kamerling, 1966; Mayne & others, 1972). Elsewhere, correlatives of the Palaeozoic rocks of the Lachlan Fold Belt almost certainly comprise most of the basement beneath the shelf and slope. Rocks recovered in the few dredge hauls from the slope include metabasic volcanics and serpentinites of Palaeozoic age, and dacites, limestones, mudstones, granodiorites, and monzodiorites of post-Ordovician age (Hubble & others, 1992).

Studies of the southern New South Wales margin using GLORIA long-range sidescan, Seabeam bathymetric swath mapping, seismic and sub-bottom profiling techniques have documented numerous slumps and slides resulting from slope failure (Jenkins & Lawrence, 1990; Jenkins & Keene, 1992). Areas at the seaward edge of the shelf sediment wedge appear to have been the most susceptible

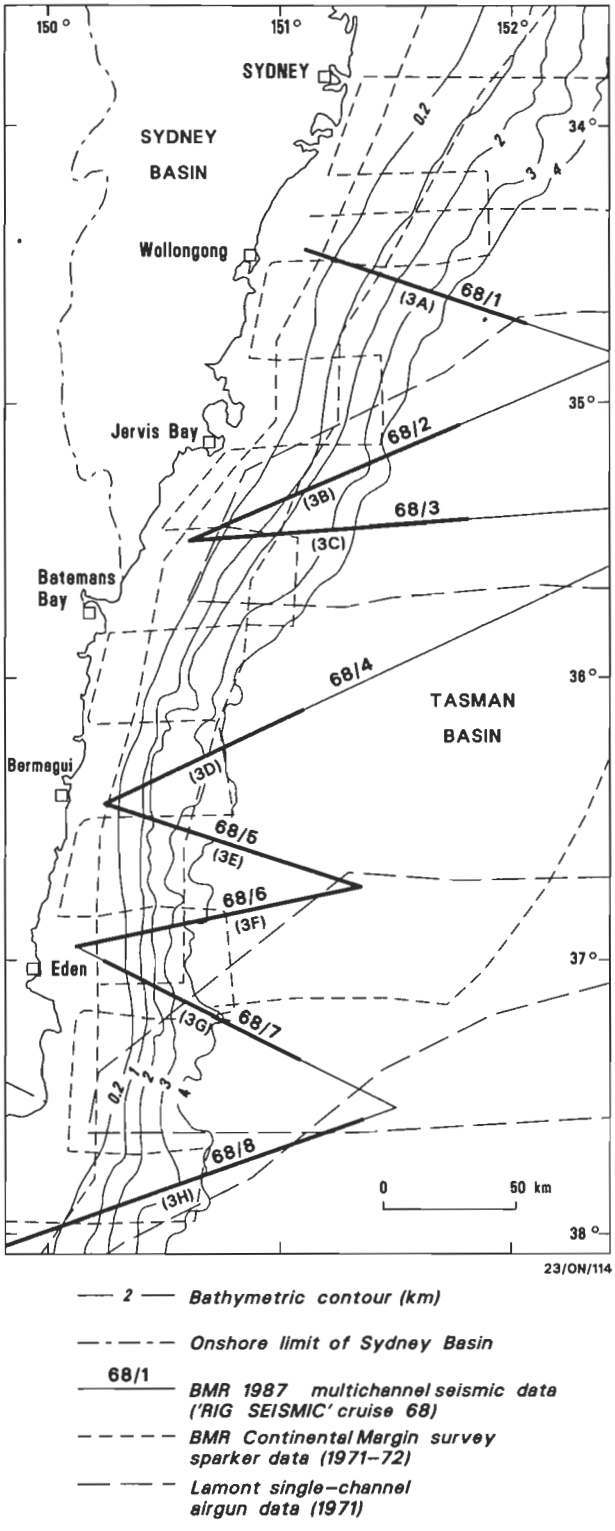

Figure 2. Seismic coverage and bathymetry along the southern New South Wales margin.
BMR shelf, high-resolution sparker lines and localised Sydney University single/dual-channel airgun lines not shown. Highlighted line segments shown in Figure 3.

to failure (Jenkins & Keene, 1992).

Structure of the margin

In this study, we map the gross structure of the southern New South Wales margin south from Sydney (Fig. 2) using 1300 km of BMR's 1987 Survey 68 multichannel seismic data combined with 1850 km of BMR's 1971-72 Continental Margins Survey sparker data. The sparker data provide reasonable resolution on the shelf, but the modern, multichannel data are needed to image basement surface and structures on the slope and adjacent abyssal plain. Line drawings of the BMR 1987 seismic lines are shown in Figure 3; maps of total sediment thickness over basement and basement structure in seconds two-way-time (TWT) are displayed in Figures 4 and 5, respectively.

Continental shelf

The most pronounced feature on the continental shelf is the major sediment wedge which overlies a generally flat, eroded basement surface dipping seawards at 2° to 5°; minor faulting of the basement surface occurs in places (Fig. 3). As noted by Davies (1979), Shaw (1979) and Packham (1983), the wedge generally thickens to the shelf break. Thicknesses at the shelf break range from 0.3 secs TWT (approximately 270 m) off Wollongong to 1.0 secs TWT (900 m) off Eden (Figs 3A,G and 4). Commonly, the wedge shows evidence of slope failure on its outer edge (Jenkins & Keene, 1992).

The wedge is composed of broadly progradational sequences which are separated by erosional unconformities, possibly associated with low stands of sea level or current activity (Fig. 6). Its base is generally transgressive on (i.e. onlaps) basement. Coring and dredging at localities intersected by BMR Line 68/6 recovered Pleistocene, Pliocene and middle Miocene muds, suggesting that most, if not all, of the wedge at this site consists of Neogene deposits (Fig. 6 lower; Packham, 1983; Hubble & Jenkins, 1984). As noted by Jones & others (1975), the position of the shelf break reflects the extent of upward and outward building of the wedge (e.g. Fig. 6 upper), and morphology of the basement (e.g. Fig. 6 lower). Assuming a middle Miocene maximum age for the wedge, average sedimentation rates along this sediment-starved margin are low (less than 6 cm/1000 years), resulting from low sediment input, possibly sediment bypassing, redistribution of sediments by longshore currents and slumping.

Little seismic energy succeeded in penetrating basement below the sediment wedge. Only in a few places can unequivocal events be seen within rocks of the Lachlan Fold Belt or Sydney Basin, which almost everywhere effectively form acoustic basement.

Short-wavelength magnetic anomalies of up to several hundred nT amplitude are present on the shelf (Colwell & others, 1987). These indicate that magnetised basement (probably including Tertiary extrusives and/or older intrusives) lies close to the surface. This is confirmed by aeromagnetic data from the southern and central parts of the coast which show a complex magnetic field on the shelf (NSW Dept. Minerals & Energy, 1990; Bureau of Mineral Resources, 1978a,b).

Continental slope

The morphology of the modern continental slope is dominated by basement structure and reflects the distribution of syn-rift and post breakup sediments, and basement grabens, half-grabens and ridges. The slope is generally broadly concave, particularly in the south. Its gradient varies from less than 1° on the mid-slope where sediments

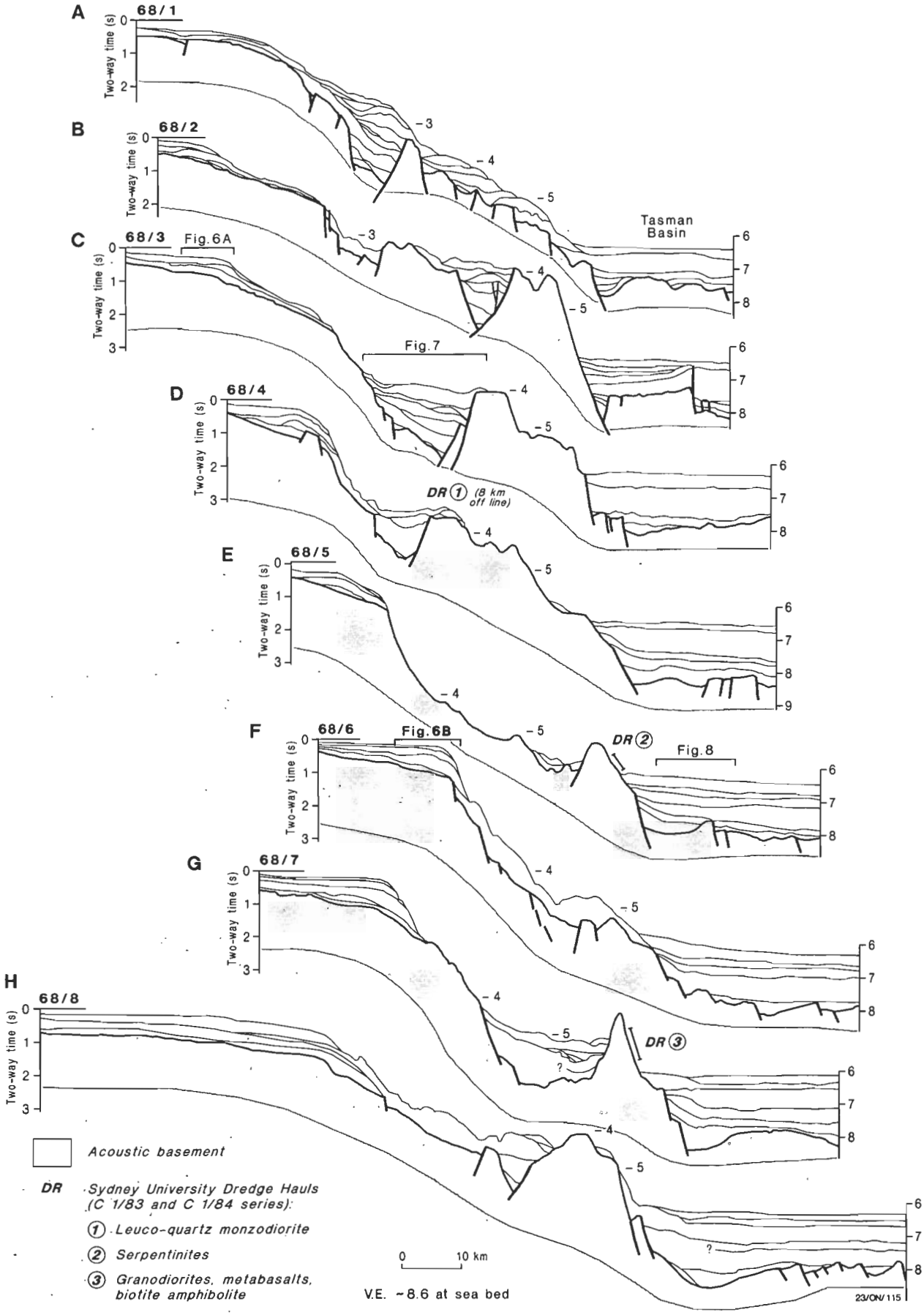

Figure 3. Line drawings of BMR's 1987 (Survey 68) data on the southern NSW margin.
Line locations shown in Figure 2.

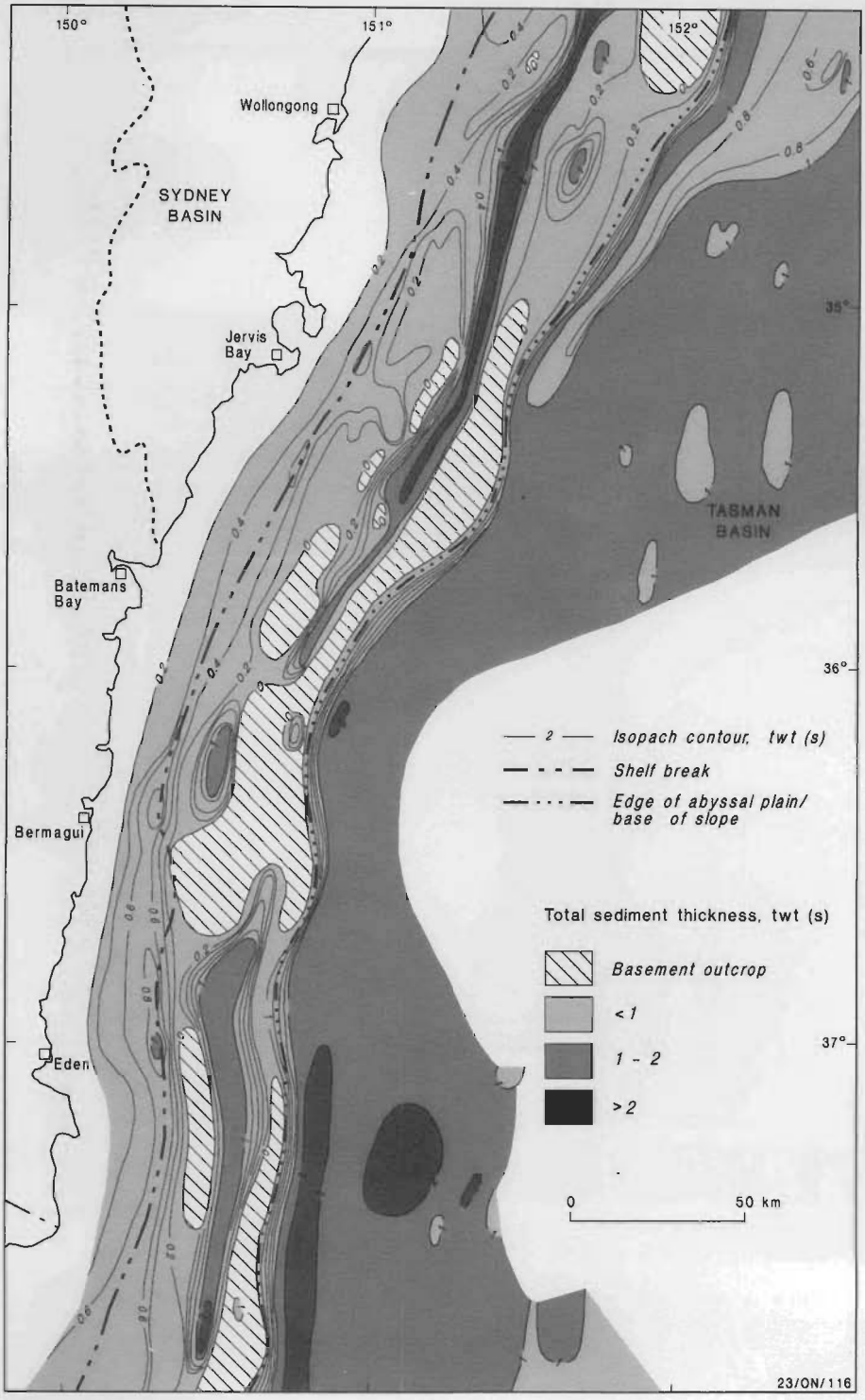

Figure 4. Generalised map of total sediment thickness over basement (seconds TWT).
The seismic lines which were used to construct the map are shown in Figure 2.

are trapped behind basement ridges (e.g. Fig. 3C,D) to 20° where basement is exposed at the seafloor (e.g. Fig. 3B,G). In general, its gradient is greatest on the lower slope reflecting the widespread exposure of basement (Fig. 4). Canyon systems are common on the slope; Davies (1979) identified ten canyons or canyon-like features on the upper slope in the area between Jervis Bay and Bermagui with major canyon systems extending down the slope southeast of Batemans Bay, southeast of Bermagui, and east of Eden.

The BMR seismic data show that the basement underlying the continental slope forms a mid-slope graben and half-graben (Figs 3, 5). The mid-slope half-graben (or graben) is generally bounded on its eastern side by a prominent westerly (landward)-dipping fault; relatively minor, easterly-dipping faults commonly occur on its

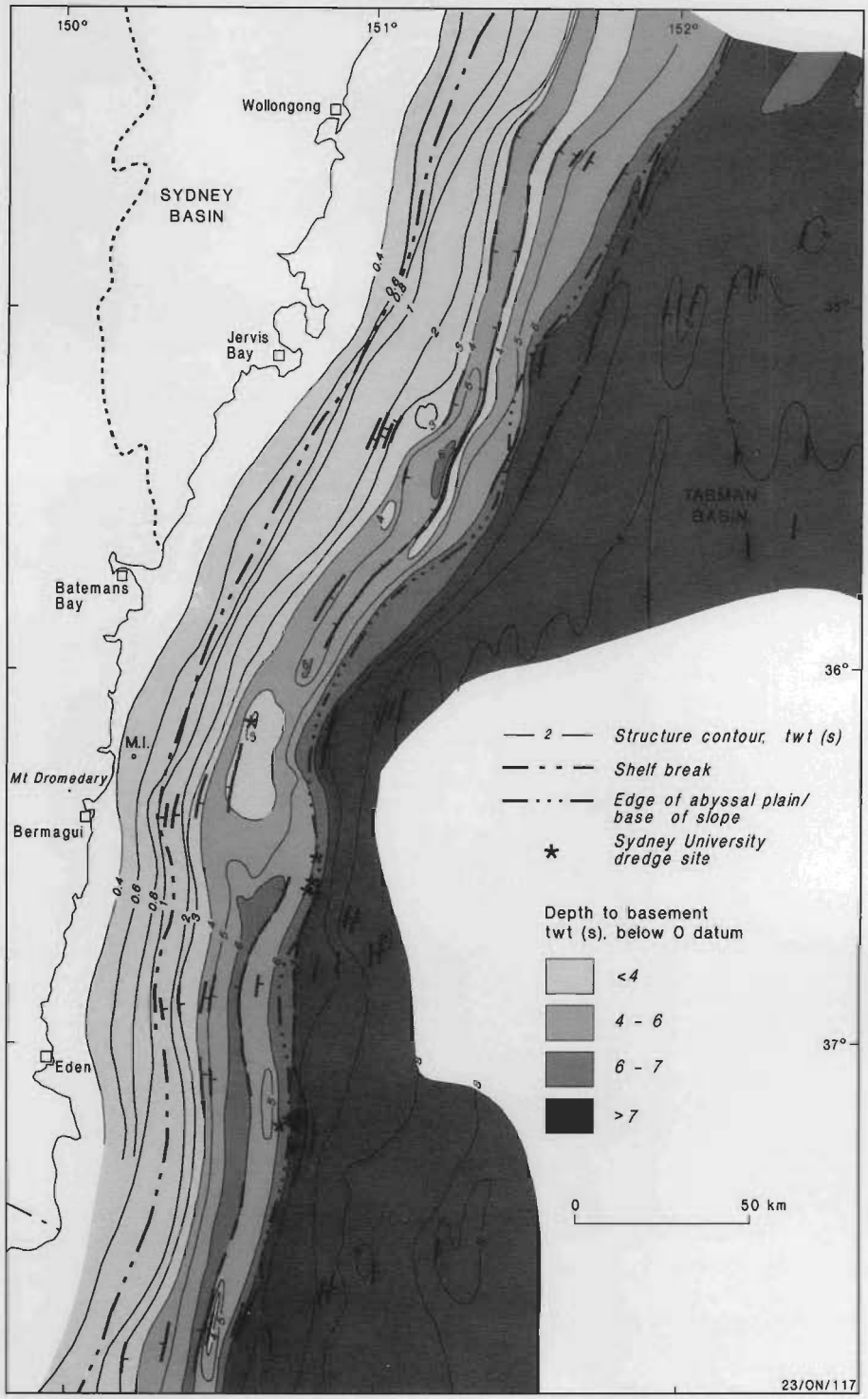

Figure 5. Generalised map of basement structure contoured in seconds TWT.
The seismic lines which were used to construct the map are shown in Figure 2. M.I. Montague Island.

western flank (Fig. 3). The eastern margin of the half-graben is marked by a faulted basement ridge which generally controls seafloor morphology on the lower slope. In general, the half-graben is better developed in the north (Lines 1-3) than in the south where it is disrupted by a basement high (possibly a continuation of the Mt Dromedary–Montague Island igneous complex) northeast of Bermagui (Figs 3, 5).

Up to 2.2 secs TWT (~2500 m) of sediment is present in the mid-slope half-graben (Figs 3, 4), and several sequences can be recognised. Commonly (e.g. on Lines 3 and 4) the lower sequences show evidence of syn-rift deposition with the sequences thickening into the major westerly-dipping faults on the graben's eastern side (Figs 3, 7). The syn-rift sediments are up to 1.4 secs TWT (~1800 m) thick. In general, these sediments pass upwards into rift-fill units

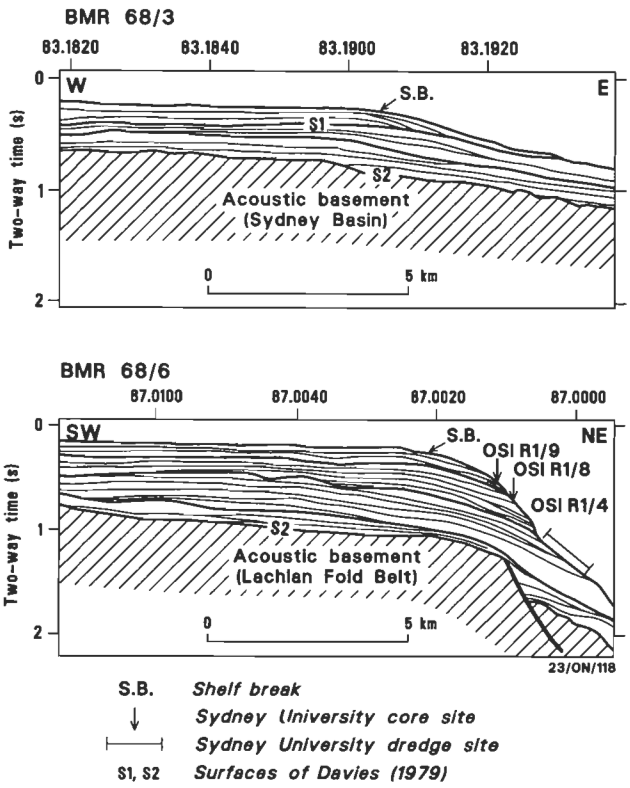

Figure 6. Line drawing of sections of BMR lines 68/3 (upper) and 68/6 (lower) showing the prograding sediment wedge overlying acoustic basement on the shelf and the location of Sydney University sampling sites.
Location of sections shown on Figure 3. Cores and dredges contained a Pleistocene (early N22) foraminifera fauna in OSI R1/9, Pliocene in R1/8 and middle Miocene in R1/4 (Packham, 1983; Hubble & Jenkins, 1984).

which are overlain in places by slump deposits trapped behind the lower-slope basement ridge. Current scouring and redeposition are common, particularly adjacent to basement highs (see, for example, Fig. 7). The seismic character of sequences in the half-graben varies considerably. In places (e.g. Fig. 7), the syn-rift section is seismically transparent, possibly indicating monotonous shale or sand deposits; elsewhere it is stratiform. High amplitude, low-frequency events adjacent to basement may represent volcanic flows or sills.

The sediments in the half graben have not been directly dated. However, assuming that they are of similar age to the sediments in the Bass Strait rift basins, they could be as old as Late Jurassic. Most of the section above the syn-rift sediments is probably Tertiary in age with an increasing marine component following Tasman Basin breakup at about 80 Ma. Lithologically, the sediments probably range from non-marine sands and muds (possibly including lacustrine deposits) at the base of the half-graben, to hemipelagic, sandy muds at the top.

On the lower slope, sediment thicknesses are usually less than 0.5 secs TWT (500 m). Basement crops out over large areas (Fig. 3). Dredging of lower-slope exposed basement has revealed a complex geology including serpentinites, metabasalts, and biotite amphibolite of probable Palaeozoic age, and a mid-Devonian granodiorite (Hubble & others, 1992; Figs 3, 5). Elsewhere, an Early Cretaceous leuco-quartz monzodiorite has been dredged from a large seamount 50 km northeast of Bermagui (Fig. 5). This rock appears on the basis of age and geochemistry to be comagmatic with the Mount Dromedary–Montague Island igneous complex located nearby (Hubble & others, 1992).

Basement structure is represented by magnetic and gravity signatures in data recorded along the BMR seismic lines. Free-air gravity anomalies with amplitudes of up to 2000 $\mu m.s^{-2}$ characterise the shelf—slope–Tasman Basin transition, presumably related to the continental margin edge effect and basement structure (Colwell & others, 1987). Magnetic and gravity anomalies are commonly associated with the major basement ridge, implying a largely igneous nature.

A continental rise is virtually non-existent off southern New South Wales (Fig. 3). This reflects a low level of sediment input probably caused by sediment trapping on the shelf or slope (e.g. in the mid-slope half-graben), the sediment-starved nature of the margin (low terrigenous input and carbonate productivity) and sediment bypassing in canyon systems.

Abyssal plain

The Tasman Sea abyssal plain extends seaward from the lower continental slope at water depths of 4600–4850 m (Fig. 3; GEBCO, 1984). Its upper surface is typically smooth, although in places at the base of the slope, current scour has produced a small channel or moat.

Sediment thickness beneath the abyssal plain varies considerably, reflecting variations in basement structure. In general, between 1 and 2 secs TWT (~1000–2000 m) of sediment overlie acoustic basement which may be either highly-extended continental, or oceanic crust; evidence from the few *Rig Seismic* lines which extend well out onto the Tasman Basin abyssal plain suggests that thinned, highly-rotated blocks of continental crust may be isolated within oceanic crust along the edge of the Tasman Basin. Preliminary analysis of our magnetic data suggests several identifiable seafloor spreading anomalies along Lines 2 and 4.

Sediment thicknesses are generally greatest (up to 2.2 secs TWT, or about 2200 m) next to the foot of the slope and decrease gradually away from the margin (Figs 3, 4). This suggests that most sediment has bypassed the shelf and slope for much of the margin's history; loading of the oceanic or thinned continental crust at the foot of the slope probably augmented thermal subsidence of the basement.

Structure beneath the abyssal plain consists of mainly easterly-dipping, normal faults offsetting acoustic basement. Syn-rift sediments appear to be absent (e.g. Fig. 8), suggesting that the crust post-dates the main phase of rifting on the margin, i.e. it is probably largely of oceanic origin, and that the sediments are essentially basin fill. On Line 68/2 (Fig. 3B) a fault was apparently active through much of the Tertiary based on rotation of the overlying sediments. Much of the sedimentary fill beneath the abyssal plain has undergone minor faulting, possibly related to compaction.

Several seismic sequences of unknown age are separated by regional unconformities which were probably formed by changes in ocean circulation (Fig. 8; Kennett & others, 1974a). Results from the nearest DSDP drill hole (Site 283), 800 km away in the southern Tasman Basin (Fig. 1),

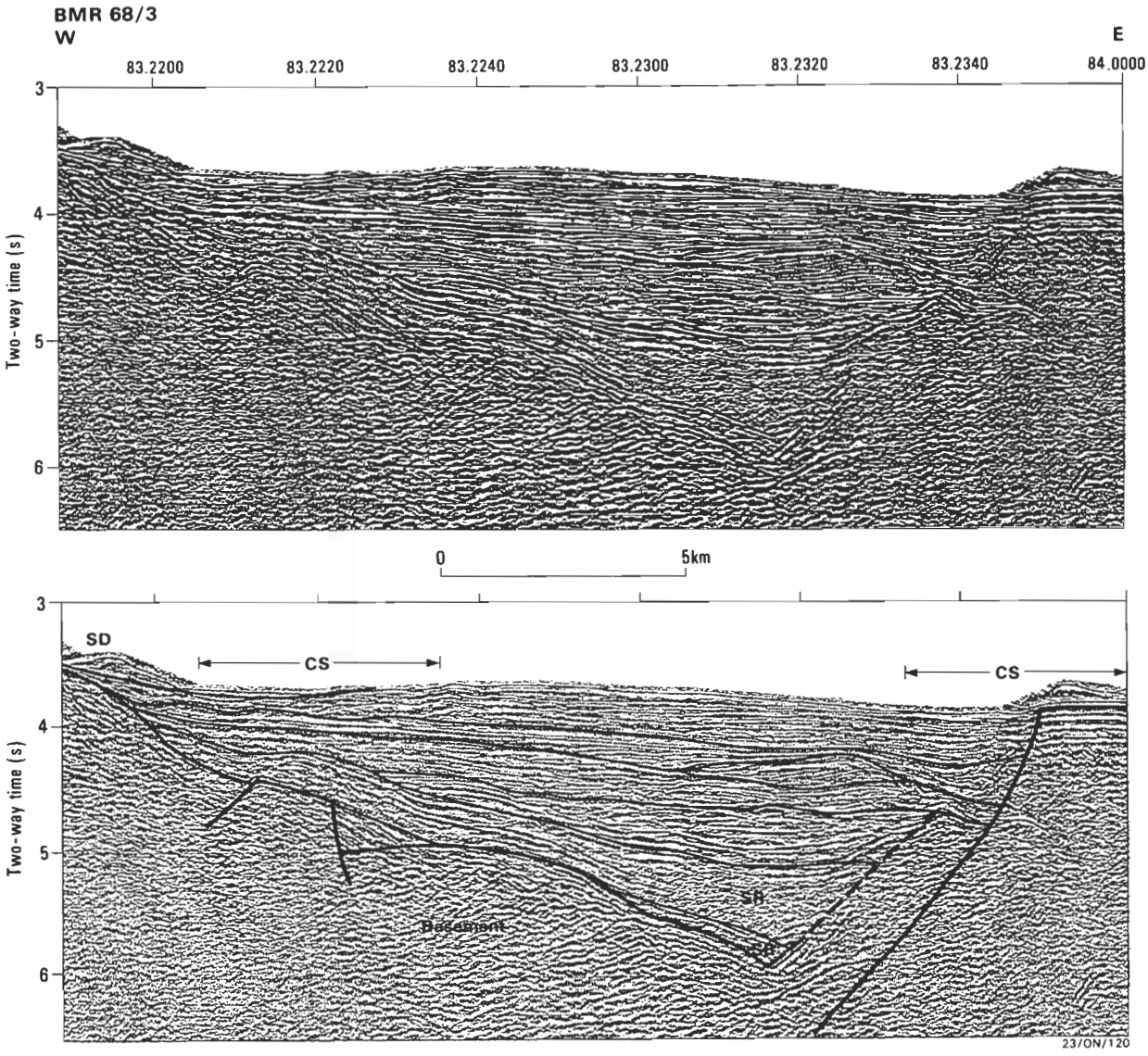

Figure 7. Segment of BMR line 68/3 showing the mid-slope half graben.
Location shown on Figure 3C. SR syn-rift deposits, SD slump deposits, CS current scour and redeposition.

suggest that much of the fill is probably Eocene and older with only a thin Neogene cover (Kennett & others, 1974b). The highly-continuous, high-amplitude and high-frequency nature of much of the section suggests that it consists mainly of pelagic and/or hemipelagic deposits. Turbidites may make up a significant part of these deposits.

Discussion

As first noted by Jongsma & Mutter (1978), the narrow, steep, and relatively unstructured southern New South Wales margin differs markedly from its conjugate, the western side of Lord Howe Rise and adjacent Dampier Ridge (Fig. 1). On the Lord Howe Rise a major zone of horst and graben structures up to 200 km wide and containing up to 4500 m of sediment is present on its western flank (Fig. 9; Willcox & others, 1980; Roeser & others, 1985). Dredging on the Dampier Ridge yielded fragments of continental rocks, including granite and feldspathic sandstone (Symonds & others, 1988), proving its continental origin.

The principal differences between the New South Wales and Lord Howe Rise margins can be accounted for by either the asymmetric rifting model (Jongsma & Mutter, 1978) or the detachment model (Lister & others, 1986). However, the latter model provides a better explanation of features such as landward-dipping faults observed on the southern NSW margin seismic lines and the presence of the Eastern Highlands along Australia's eastern seaboard. In the detachment model, the NSW margin is an 'upper plate' margin characterised by few rift structures and by uplift resulting in passive-margin mountains (the Eastern Highlands) related to thermal buoyancy caused by rise of the asthenosphere as well as igneous underplating of mantle-derived melts (Etheridge & others, 1989; Lister & Etheridge, 1989; Lister & others, 1991). The Lord Howe Rise forms a 'lower-plate' margin characterised by extensive rift development on its western side. The major landward-dipping fault system which commonly bounds the mid-slope grabens and half-grabens may form part of a series of faults dipping beneath the Australian margin linked to a major upper mantle/lower crust detachment beneath eastern Australia (see Scheibner, 1991).

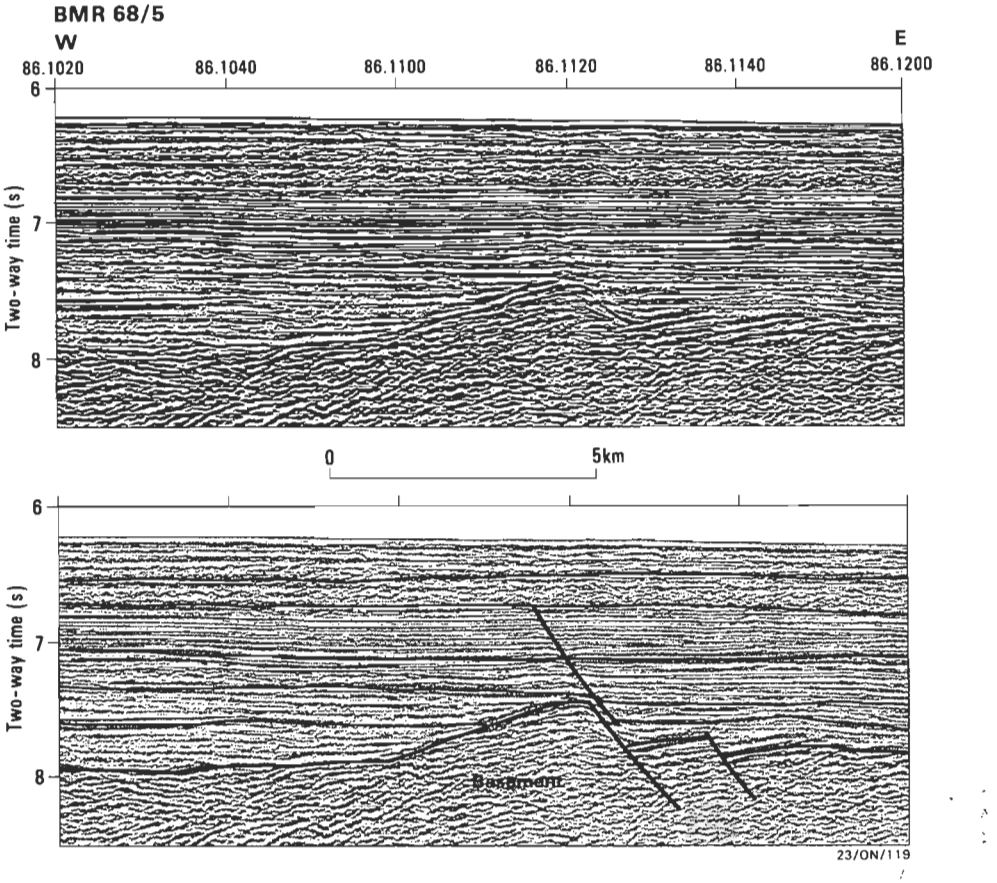

Figure 8. Segment of BMR line 68/5 showing seismic sequences and basement faults beneath the abyssal plain. Location of Figure shown in Figure 3E.

The large basement ridge which lies on the mid-slope northeast of Bermagui (Fig. 5) disrupts the mid-slope graben zone and lies broadly on strike with the Mt Dromedary–Montague Island igneous complex. A monzodiorite dredged from the northern part of this ridge (Fig. 5) yielded a mid Cretaceous age of 101 Ma (Hubble & others, 1992). This is similar to the 98 Ma age recorded for Mt Dromedary onshore (Smith & others, 1988). Both of these complexes were probably emplaced along a line of crustal weakness as suggested by Ringis (1975) for a number of southeastern Australian igneous bodies. The fact that the ridge disrupts the mid-slope graben suggests that the main phase of graben formation (although not necessarily growth) occurred before about 100 Ma, suggesting that rifting preceded seafloor spreading in the Tasman Basin by at least 20 million years.

An offset and change in the orientation of the continental slope at about 36°S (Figs 4, 5) may mark the position of a former transfer fault. This transfer fault may, if present, have been the precursor to the transform fault located in the Tasman Basin crossed by BMR line 3 (Fig. 1). It may also have been a zone of weakness along which the Mt Dromedary–Montague Island–offshore igneous complexes were emplaced.

The nature of the continent–ocean transition off New South Wales is somewhat enigmatic. Crust between the oldest identifiable magnetic anomalies and the base of the continental slope (Fig. 1) displays varying seismic characters, and may contain islolated blocks of highly-thinned continental material surrounded by predominantly oceanic crust. The absence of syn-rift sediment, however, suggests that most of the Tasman Basin's basement formed after the rift phase which formed the conjugate southeast Australia—Lord Howe Rise margins, and is thus oceanic.

From a petroleum perspective, the southern New South Wales margin appears to have little resource potential except within the Permo-Triassic Sydney Basin rocks. The thickest (up to 2500 m) post-Sydney Basin sediments lie in grabens and half-grabens on the slope in water depths of 1500–3800 m, well below the limit of normal oil exploration around Australia. A greater long-term petroleum potential probably lies in the extensive horst and graben province on the other side of the Tasman Basin, on the Lord Howe Rise 'lower plate'. That area is poorly known, even at a reconnaissance level.

Acknowledgements

The authors gratefully acknowledge the valuable contribution made to the success of BMR Survey 68 by the technical and scientific staff aboard *Rig Seismic*. Barry Willcox, John Marshall, Chris Jenkins and an anonymous referee are thanked for their comments on the manscript. Figures were drafted by Ms M. Huber.

References

Berggren, W.A., Kent, D.V., Flynn, J.J. & van Couvering, J.A., 1985 — Cenozoic geochronology. *Geological Society of America Bulletin* 96, 1407–1418.

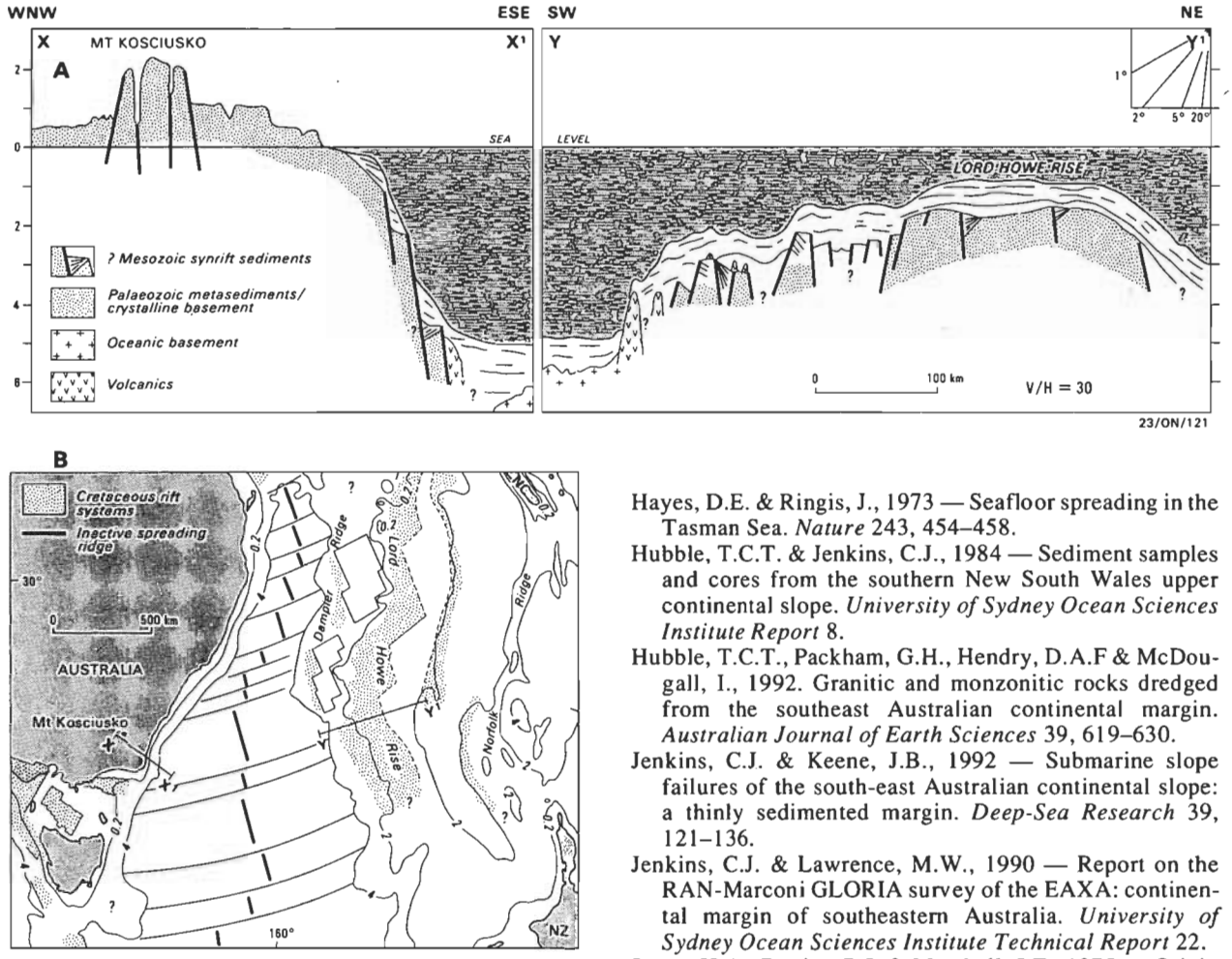

Figure 9A. Reconstructed schematic section across the Tasman Basin with about 800 km of oceanic crust removed (from Etheridge & others, 1989). B. Location of section.

Bishop, P., 1989 — Geomorphology and evolution of the eastern highlands. *In* Johnson, R.W. (editor), Intraplate volcanism in eastern Australia and New Zealand. *Cambridge University Press, Cambridge*, 21–26.

Bureau of Mineral Resources, Australia, 1978a — Bega 1:250 000 magnetic contour map. *Bureau of Mineral Resources, Canberra.*

Bureau of Mineral Resources, Australia, 1978b. Ulladulla 1:250 000 magnetic contour map. *Bureau of Mineral Resources, Canberra.*

Colwell, J.B., Coffin, M.F. & Shipboard Party, 1987 — *Rig Seismic* research cruise 13: structure and stratigraphy of the northeast Gippsland Basin and southern New South Wales margin — initial report. *Bureau of Mineral Resources, Australia, Report* 283.

Davies, P.J., 1979 — Marine geology of the continental shelf off southeast Australia. *Bureau of Mineral Resources, Australia, Bulletin* 195.

Etheridge, M.A., Symonds, P.A. & Lister, G.S., 1989 — Application of the detachment model to reconstruction of passive continental margins. *In* Tankard, A.J. & Balkwill, H.R. (editors) Extensional tectonics and stratigraphy of the North Atlantic margins. *American Association of Petroleum Geologists Memoir* 46, 23–40.

Gebco, 1984 — General bathymetric chart of the oceans, Sheets 413 and 443. *International Hydrographic Bureau, Monaco.*

Hayes, D.E. & Ringis, J., 1973 — Seafloor spreading in the Tasman Sea. *Nature* 243, 454–458.

Hubble, T.C.T. & Jenkins, C.J., 1984 — Sediment samples and cores from the southern New South Wales upper continental slope. *University of Sydney Ocean Sciences Institute Report* 8.

Hubble, T.C.T., Packham, G.H., Hendry, D.A.F & McDougall, I., 1992. Granitic and monzonitic rocks dredged from the southeast Australian continental margin. *Australian Journal of Earth Sciences* 39, 619–630.

Jenkins, C.J. & Keene, J.B., 1992 — Submarine slope failures of the south-east Australian continental slope: a thinly sedimented margin. *Deep-Sea Research* 39, 121–136.

Jenkins, C.J. & Lawrence, M.W., 1990 — Report on the RAN-Marconi GLORIA survey of the EAXA: continental margin of southeastern Australia. *University of Sydney Ocean Sciences Institute Technical Report* 22.

Jones, H.A., Davies, P.J. & Marshall, J.F., 1975 — Origin of the shelf break off southeast Australia. *Journal of the Geological Society of Australia* 22, 71–78.

Jongsma, D. & Mutter, J.C., 1978 — Non-axial breaching of a rift valley: evidence from the Lord Howe Rise and the southeastern Australian margin. *Earth and Planetary Science Letters* 39, 226–234.

Kamerling, P., 1966 — The Sydney Basin offshore. *The APEA Journal* 6, 76–80.

Kennett, J.P. & others, 1974a — Cenozoic paleoceanography in the southwest Pacific Ocean, Antarctic glaciation, and the development of the Circum-Antarctic Current. *In* Kennett, J.P., Houtz, R.E. & others, Initial reports of the Deep Sea Drilling Project, 29. *U.S. Government Printing Office, Washington* 1155–1169.

Kennett, J.P. & others, 1974b — Site 283 — *In* Kennett, J.P., Houtz, R.E. & others, Initial reports of the Deep Sea Drilling Project, 29. *U.S. Government Printing Office, Washington* 365–377.

Kent, D.V. & Gradstein, F.M., 1985 — A Cretaceous and Jurassic geochronology. *Geological Society of America Bulletin* 96, 1419–1427.

Lister, G.S. & Etheridge, M.A., 1989 — Detachment models for uplift and volcanism in the Eastern Highlands, and their application to the origin of passive margin mountains. *In* Johnson, R.W. (editor), Intraplate volcanism in eastern Australia and New Zealand. *Cambridge University Press, Cambridge*, 297–313.

Lister, G.S., Etheridge, M.A. & Symonds, P.A., 1986 — Detachment faulting and the evolution of passive continental margins. *Geology* 14, 246–250.

Lister, G.S., Etheridge, M.A. & Symonds, P.A., 1991 —

Detachment models for the formation of passive continental margins. *Tectonics* 10, 1038–1064.

Mayne, S.J., Nicholas, E. & Bigg-Wither, R, A.L., 1972 — Geology of the Sydney Basin — a review. *Bureau of Mineral Resources, Australia, Record* 1972/76.

Mutter, J.C. & Jongsma, D., 1978 — The pattern of the pre-Tasman Sea rift system and the geometry of the breakup. *Bulletin of the Australian Society of Exploration Geophysicists* 9, 70–75.

New South Wales Department of Minerals & Energy, 1990 — Sydney 1:250 000 magnetic contour map.

Ollier, C.D., 1982 — The great escarpment of eastern Australia: tectonic significance. *Journal of the Geological Society of Australia* 29, 12–23.

Packham, G.H., 1969 (editor) — The geology of New South Wales. *Geological Society of Australia, Sydney.*

Packham, G.H., 1983 — Morphology and acoustic properties of the N.S.W. slope with special reference to the Coffs Harbour–Point Plommer and Montague Island–Green Cape areas. *University of Sydney Ocean Sciences Institute Report* 1.

Ringis, J., 1975 — The relationship between structures on the southeast Australian margin and in the Tasman Sea. *Bulletin of the Australian Society of Exploration Geophysicists* 6, 39–41.

Roeser, H.A., Fritsch, J., Gorling, L. & others, 1985 — Report on SonneCruise SO-36, Part 1: geophysical, geological and geochemical investigations of the Lord Howe Rise, 1985. Bundesanstalt für Geowissenschaften und Rohstoffe, Hannover, Cruise Report.

Scheibner, E., 1991 — Broken Hill–Sydney–Tasman Sea Geoscience Transect. *American Geophysical Union, Global Geoscience Transect Project.*

Shaw, R.D., 1978 — Sea floor spreading in the Tasman Sea: a Lord Howe Rise-eastern Australian reconstruction. *Bulletin of the Australian Society of Exploration Geophysicists* 9, 75–81.

Shaw, R.D., 1979 — On the evolution of the Tasman sea and adjacent continental margins. *Ph.D. thesis, University of Sydney.*

Smith, I.E.M., White, A.J.R., Chappell, B.W. & Eggleton, R.A., 1988 — Fractionation in a zoned monzonite pluton: Mt Dromedary, southeastern Australia. *Geological Magazine* 125, 273–284.

Symonds, P.A., Willcox, J.B. & Kudrass, H.R., 1988 — Dampier Ridge in the Tasman Sea — a continental fragment. *Abstracts 9th Australian Geological Convention, Brisbane, February 1988,* 393–394.

Weissel, J.K. & Hayes, D.E., 1977 — Evolution of the Tasman Sea reappraised. *Earth and Planetary Science Letters* 36, 77–84.

Willcox, J.B., Colwell, J.B. & Constantine, A.E., 1992 — New ideas on Gippsland Basin regional tectonics. *Proceedings of the Joint AusIMM/PESA Gippsland Basin Symposium, Melbourne, Australia, June 1992* 93–110.

Willcox, J.B., Symonds, P.A., Hinz, K. & Bennett, D., 1980 — Lord Howe Rise, Tasman Sea — preliminary geophysical results and petroleum prospects. *BMR Journal of Australian Geology & Geophysics* 5, 225–236.

BMR Journal of Australian Geology & Geophysics, 13, 345–358

The Iverian, a proposed Late Cambrian Stage, and its subdivision in the Burke River Structural Belt, western Queensland

J. H. Shergold[1]

The Iverian Stage is proposed for the concept of a post-Idamean/pre-Payntonian, Late Cambrian, interval in the eastern Georgina Basin, western Queensland. Designation and definition of this stage completes the local stadial biochronological scheme for the Upper Cambrian platform sequences of Australia and conterminous regions. Lithostratigraphic and biostratigraphic material diagnostic of this stage in its type area is integrated and correlated within Australia and globally. In the interests of simplification and clarification, it is suggested that a generic zone concept be overlaid on the current assemblage-zone biostratigraphic scheme for the Iverian Stage.

Introduction

The Iverian Stage is proposed as a local stage of Late Cambrian age, named from the Parish of Iver in the County of Windsor, western Queensland, for the undifferentiated biostratigraphic interval originally designated as pre-Payntonian A and pre-Payntonian B (Jones & others, 1971), but currently informally known as post-Idamean/pre-Payntonian (Shergold, 1989, p. 13). Jones & others (1971) did not formally name this interval because of uncertainty about the temporal relationship of the lower Chatsworth Limestone, defined by Casey (1959) at Lily Creek, 3.5 km south of Chatsworth Homestead, and 'Chatsworth Limestone' occurring in the core of the periclinal structure at Black Mountain, 50 km to the south. It has since been demonstrated that the Lily Creek and Black Mountain sections overlap biostratigraphically (Shergold, 1980; and below). In 1971 it would not have been possible to satisfactorily define a base for any stage proposed for this interval since the relationships of faunas at the top of the Pomegranate Limestone, the *Irvingella tropica/Agnostotes inconstans* Zone of Öpik (1963), to those of the lowest Chatsworth Limestone, which was then undescribed, were not known.

Because *Agnostotes inconstans* does not occur at the type section for the Idamean Stage, at Browns Creek, south of Glenormiston and some 150 km west of Boulia, Henderson (1976b) considered a revised *Irvingella tropica* Zone as the youngest zone of the Idamean Stage. Subsequently, for essentially practical reasons, Shergold (1982) restricted the Idamean Stage by excluding the *Irvingella tropica* Zone, regarding it as the initial biostratigraphic division of a then un-nominated post-Idamean stage. This was an important step, as *Irvingella* has a cosmopolitan distribution which facilitates international correlation. Equally important, the redefinition of the Payntonian and Datsonian Stages at the top of the Cambrian on the basis of new and realigned conodont assemblages (Nicoll & Shergold, 1991; Shergold, Nicoll & others, 1991; Shergold & Nicoll, 1992) has clarified the concept of the Iverian/Payntonian boundary.

The need now to formally name the post-Idamean/pre-Payntonian interval and integrate all previous observations on it, is to complete the sequence of Australian Late Cambrian stages commenced by Öpik in 1963; to promote the use of an Australian timescale for the Cambrian in basin studies and sequence stratigraphic analyses (Shergold, 1989); and to provide an appropriate framework for palaeogeographic reconstructions, map legends, and similar literature.

Concepts

Although the Iverian Stage is introduced and documented in accordance with the requirements of the Stratigraphic Nomenclature Committee of the Geological Society of Australia, its conceptualisation differs from definitions of stages published in the International Stratigraphic Guide (Hedberg, 1976) adopted by that Society. This is because the idea of a stage as a global chronostratigraphic unit (Hedberg, 1976) is unsustainable (e.g. Ludvigsen & Westrop, 1985). As acknowledged aggregates of zones (e.g. Jones & others, 1971; Hancock, 1977; Ludvigsen & Westrop, 1985), stages are clearly biostratigraphic units. Their dependence on zonal distribution patterns guarantees the local nature of stages. Tied to biofacies distributions influenced by sedimentary environment controls, both zones and stages are undeniably bound to rock sequences thus assuming stratigraphic and time contexts by virtue of succession. Accordingly, they inherit biochronological attributes to complement their biostratigraphic utility. Therefore, stages are regarded here as principally biochronological units, in general, facilitators of correlation at the most convenient level of resolution.

Definitions

The base of the Iverian Stage is defined by the first appearance of elements of the *Irvingella tropica* Zone in the top of the Pomegranate Limestone at Mount Murray (Fig. 2), where it occurs in measured sections 301 and 302, as documented by Shergold (1982). This datum also occurs at locality D120b (Öpik, 1963, figs 2–3; Shergold, 1982, fig. 1; herein Fig. 2), the type locality for *Irvingella tropica* Öpik, and where it is associated with *Agnostotes (A.) inconstans* Öpik. Section 302 at Mount Murray (Radke *in* Shergold, 1982, fig. 4), at 21°47.7'S, 139°59'E, is regarded here as the type section for the definition of the base of the stage. *Irvingella tropica* occurs in collection 302/3, 37 m above the base of the section and 3 m above 302/2, which contains elements of the late Idamean *Stigmatoa diloma* Zone. The contact between the Idamean and Iverian Stages is considered to be conformable, within a sedimentary continuum, although on Figure 4 non-outcropping intervals are shown on Section 302.

The top of the Iverian Stage is defined by the appearance of the *Sinosaukia impages* trilobite assemblage-zone and the *Hispidodontus resimus* conodont zone. These mark the base of the Payntonian Stage as redefined by Shergold, Nicoll & others (1991) and Shergold & Nicoll (1992) at

[1] Onshore Sedimentary and Petroleum Geology, Australian Geological Survey Organisation, GPO Box 378, Canberra ACT 2601

Black Mountain, some 90 km south-southeast of Mount Murray, at 22°32.17'S, 140°17.01'E. The Iverian/Payntonian contact lies between the *Rhaptagnostus clarki maximus/R. papilio* and *Sinosaukia impages* Assemblage-Zones. Lithostratigraphically, the boundary lies approximately at the base of Chatsworth Limestone Unit E (Shergold, *in* Druce & others, 1982, figs 4, 5), a massive cliff-forming sandy limestone at which the conodont *Hispidodontus resimus* Nicoll & Shergold first appears. Though lithostratigraphically abrupt, the stadial contact is thought to be conformable. No sedimentological studies have been undertaken to prove otherwise.

Between Mount Murray in the north and Black Mountain in the south, rocks assigned an Iverian age, representing the lower Chatsworth Limestone, crop out intermittently (Fig. 1). They are documented in the black soil plains near Chatsworth Homestead; in shallow stratigraphic coreholes, BMR Duchess #13 (Kennard & Draper, 1977), BMR Boulia #6 (Kennard & Draper, 1977) and its extension (Shergold & Walter, 1979); and in the measured type section of the Chatsworth Limestone at Lily Creek, south of Chatsworth Homestead (Shergold, 1980) and at Black Mountain (Shergold, 1975). Besides occurring in the core of the Black Mountain pericline, Iverian rocks also crop out in the Momedah anticline at Momedah Creek, 19 km east-northeast of Black Mountain (Fig. 3). From disparate measured sections, they appear to be at least 725 m thick.

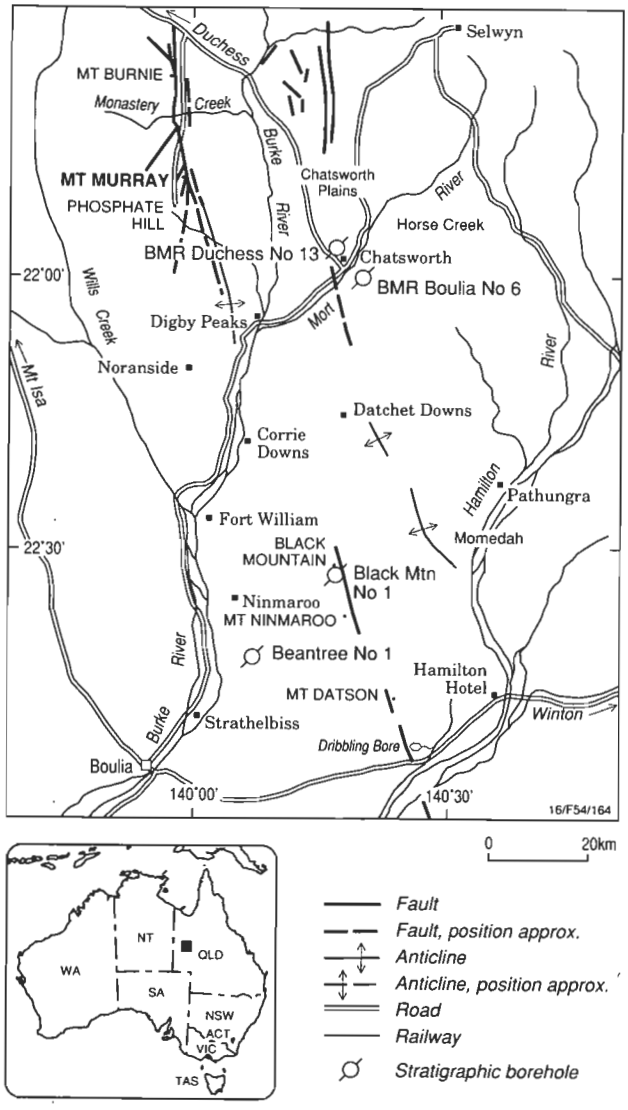

Figure 1. Distribution of the main Iverian sections and localities in the Burke River Structural Belt.

Lithostratigraphy

With the exception of the Momedah Anticline, Iverian rocks in each of the areas noted above — Mount Murray, the Chatsworth district, and Black Mountain — are represented by a series of upward-shallowing sequences. At Momedah, only superficial sedimentological observations have been made and not enough rock crops out for a detailed reference section.

At Mount Murray (Sections 301, 302), the earliest Iverian is represented on the type section (302) in the interval 37–107 m by mottled micritic carbonate pelletal wackestone and laminated pelletal skeletal grainstone, whose upper surfaces often bear silicified veneers. These rocks, referred to the uppermost Pomegranate Limestone, crop out as discrete layers, or groups of layers, separated by non-outcropping presumed clastic intervals. They pass upwards into a thick (255 m) sequence of interbedded muddy carbonate, intraclastic grainstone and dolostone referred to the basal Chatsworth Limestone (Shergold, 1982, *in* Druce & others, 1982).

Younger Iverian sequences are seen among scattered outcrops in the black soil plains north and northwest of Chatsworth Homestead and in the BMR stratigraphic coreholes noted above. The subsurface sequence found in BMR Duchess #13 is an alternation of pelletal grainstone, occasionally skeletal, and packstone, 70 m thick (Kennard & Draper, 1977; Druce & others, 1982). In BMR Boulia #6 (*ibid*) and its extension, Kennard (*in* Shergold & Walter, 1979) recognised three broad groups of rocks, 178 m thick in total, comprising an uppermost shelly grainstone and mudstone intercalation with intraclastic grainstone; a middle calcareous siltstone and shaly limestone; and a basal mudstone and micritic carbonate alternation (*in* Druce & others, 1982). Both upper and lower units have been recognised among the scattered outcrops on the black soil plains around Chatsworth. None of the coreholes penetrated recognisable Pomegranate Limestone, so the exact relationship between the basal Chatsworth Limestone at Mount Murray and that at the bottom of BMR Boulia #6 extension remains unclear.

BMR Boulia #6 and BMR Duchess #13 can be biostratigraphically correlated directly to the type section of the Chatsworth Limestone at Lily Creek (Shergold, 1980) where Radke (*in* Shergold & others, 1976; *in* Shergold, 1980) measured a 300 m section of peloidal, skeletal and intraclastic grainstone with interbedded calcareous siltstone and mudstone. This sequence is capped by a massive (12 m) calcareous sandstone unit, which has been separated as the Lily Creek Sandstone Member of the Chatsworth Limestone (Druce & others, 1981).

Biostratigraphically, it has been demonstrated (Fig. 4; Shergold, 1980) that the top of the sequence at Lily Creek overlaps the base of the Chatsworth Limestone sequence at Black Mountain, although the Lily Creek Sandstone Member is younger there. Late Iverian rocks in the basal 248 m of section at Black Mountain have been divided into four lithostratigraphic units (A–D; Shergold *in* Druce & others, 1982; Shergold, Nicoll & others, 1991), essentially the earlier units 1–4 of Shergold (1975).

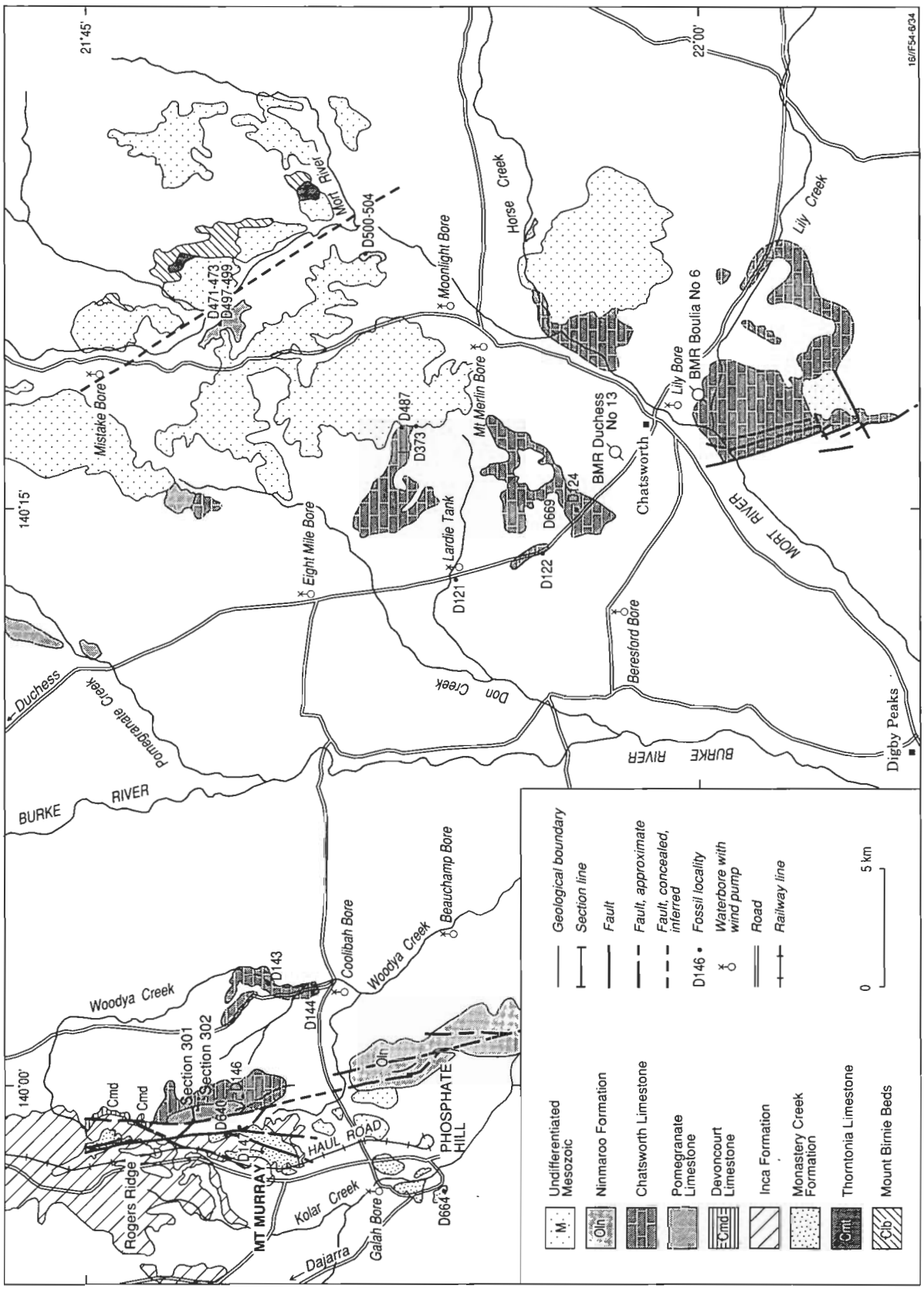

Figure 2. Location of the type section for the base of the Iverian Stage (section 302) at Mount Murray; Iverian sections and localities at Lily Creek, Horse Creek and on Chatsworth Plains; and locations of BMR stratigraphic coreholes.

Unit A (40 m) contains intercalated skeletal grainstone, intraclastic grainstone, silty micrite and calcareous siltstone; Unit B (40–128 m) comprises intercalated mottled micrite, skeletal wackestone and grainstone, and calcareous siltstone; Unit C (128–158 m) is a predominantly calcareous siltstone with layers of skeletal grainstone and packstone, laminated micrite, and brown chert; and Unit D (158–248 m) contains rapid alternations of thin-bedded micrite, siltstone, skeletal grainstone, wackestone and packstone. Iverian sedimentation at Black Mountain is terminated by thick-bedded, cross-laminated micritic limestone and sandy limestone heralding typical Payntonian

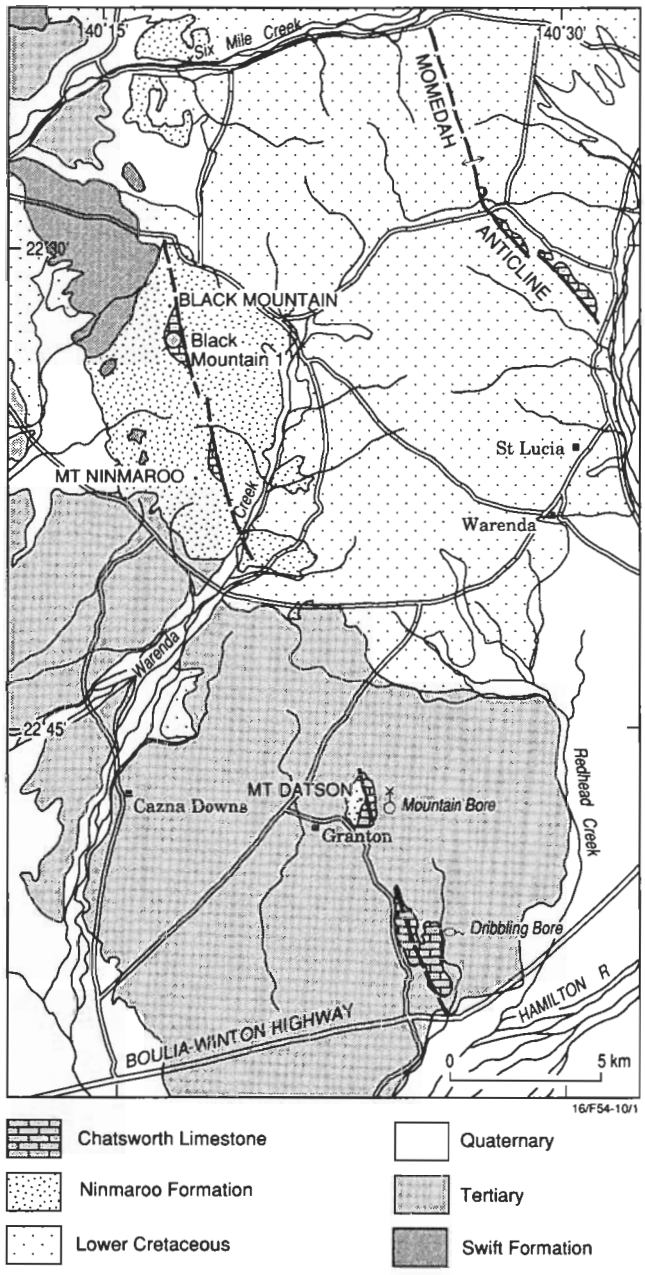

Figure 3. Location of Iverian sections at Black Mountain and Momedah Creek, southern Burke River Structural Belt.

lithofacies, as most recently reinterpreted by Shergold & Nicoll (1992).

Lateral equivalents of Unit D have been called Gola beds at Momedah Creek. The dominant and autochthonous lithology of these beds is fine to medium-grained, medium-dark grey sandy limestone with allochthonous pale, coarse-grained, intraclastic shelly grainstone interbeds, having a minimum thickness of 97 m (Shergold, 1972).

Throughout their extensive outcrop area in the southern Burke River Structural Belt, Iverian rocks show subtly distinctive lithofacies distributions within shallow subtidal to peritidal carbonate environments. These environments influence the faunal distributions.

Biostratigraphy

The Iverian Stage is palaeontologically clearly distinguishable from the preceding Idamean and following Payntonian Stages. With regard to trilobites, it is characterised by:

- the occurrence of the cosmopolitan genus *Irvingella* at its inception in Australia;
- the diversification of the agnostoid subfamily Pseudagnostinae (Diplagnostidae) during which *Pseudagnostus, Rhaptagnostus* and *Neoagnostus* separate and become biostratigraphically important;
- diversification of the Leiostegioidea, particularly the family Kaolishaniidae, and the first occurrence of the subsequently important Missisquoiidae;
- the first occurrence of the Dikelocephaloidea, Remopleuridoidea and Shumardiidae;
- the separation of the true asaphids from ceratopygids.

Among non-trilobite faunas, the Iverian is further characterised by the occurrence of the first isorophid edrioasteroids, an early eocrinoid, and a primitive edrioblastoid (Jell & others, 1985; Smith & Jell, 1990). While Iverian conodonts are well known, particularly at Black Mountain (Druce & Jones, 1971), they appear not to be especially diagnostic biostratigraphically (Müller & Hinz, 1991).

In total, the Iverian Stage currently embraces ten trilobite assemblage-zones, of which the youngest two at Lily Creek *(Peichiashania tertia/P. quarta and Hapsidocare lilyensis)* and the oldest two at Black Mountain *(Rhaptagnostus clarki patulus/Caznaia squamosa* and *R. c. prolatus/C. sectatrix)* overlap (see cluster analyses in Shergold, 1980, and further discussion below). The separate status of the post-*Irvingella tropica* assemblage (designated by Shergold, 1982) is here reconsidered. Its fauna bridges the interval between the *Irvingella tropica* Assemblage-Zone, which precedes it, and the *Wentsuia iota/Rhaptagnostus apsis* Assemblage-Zone, which follows, and is not as readily distinguishable as previously thought (Shergold, 1982). Accordingly, it is here amalgamated with the fauna of the *Irvingella tropica* Zone.

The enumerated faunal assemblages succeed each other in regular chronological fashion. They represent recognisable biofacies of sedimentary environments, which have not been thoroughly sedimentologically investigated, within or near a carbonate shoal complex. Present knowledge is based on observations mostly incorporated into locality appendices and descriptions of sections (e.g. Radke *in* Shergold, 1975, 1980; *in* Shergold & others, 1976; *in* Druce & others, 1982; Kennard *in* Shergold, 1982); accounts of stratigraphic drilling (Kennard & Draper, 1977; Shergold & Walter, 1979); and a preliminary review of the sedimentology of the Chatsworth Limestone by Kennard (*in* Shergold & Walter, 1979).

The early Iverian faunas at Mount Murray effectively continue previously established Idamean lineages based mainly on cosmopolitan olenoidean trilobites because similar deep or cool water environments span the Idamean/Iverian boundary there. Near Chatsworth Homestead, faunas are from predominantly shallow subtidal environments and the assemblages represent more provincialised biofacies based on leiostegioidean, asaphoidean and ceratopygoidean genera. Similar but demonstrably younger environments at Black Mountain are also characterised by leiostegioideans and asaphoideans, but now in association with saukiid dikelocephaloideans, remopleuridoideans and ptychoparioideans. Lateral equivalents, in presumed deeper water at Momedah Creek, are characterised by kaolishaniids and kainelloid remopleuridoideans.

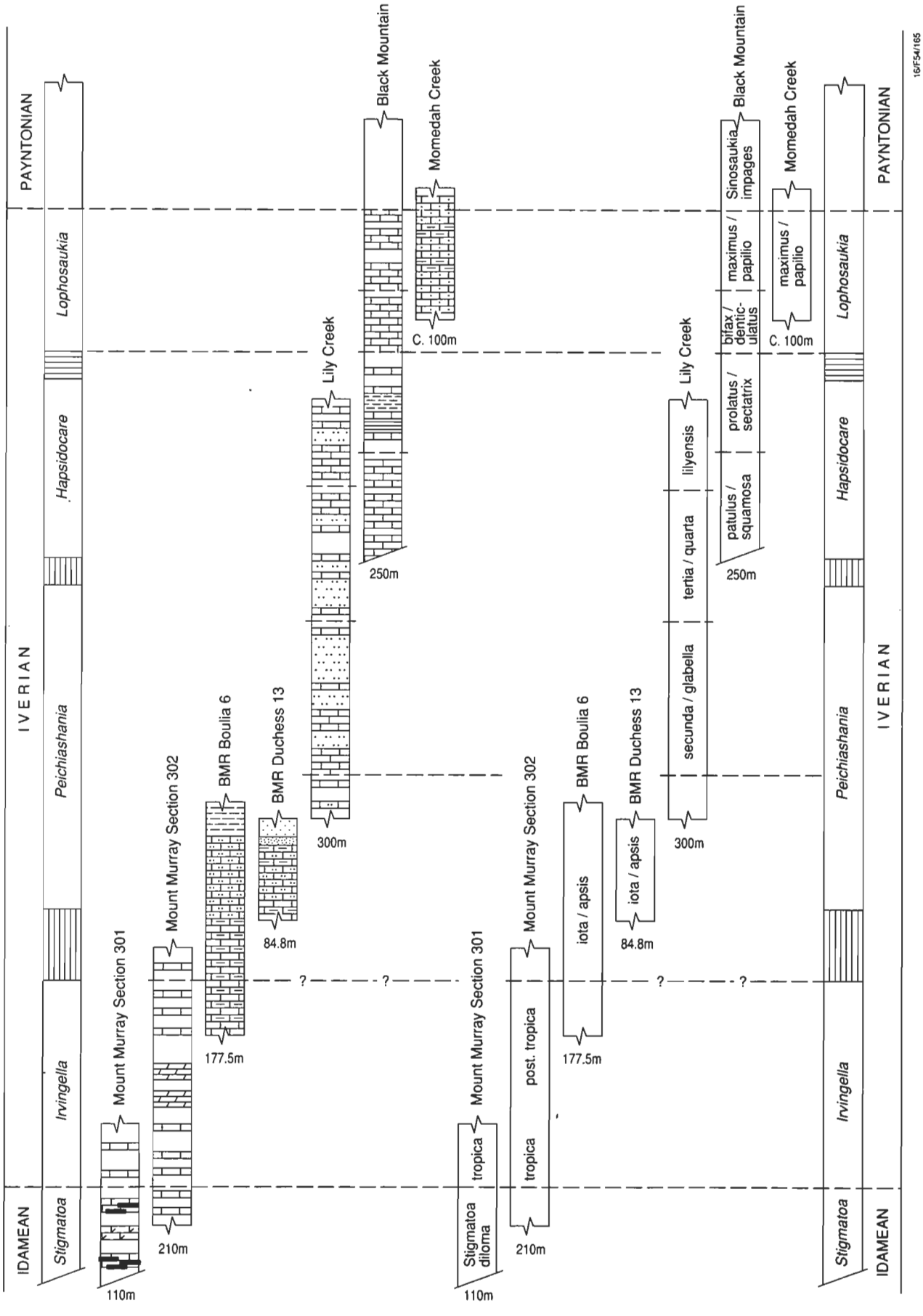

Figure 4. Spatial distribution of sections and zonal correlations.

1. *Irvingella tropica* Zone

The Iverian Stage commences with the Zone of *Irvingella tropica* in the sense of Henderson (1976a, b), substituted for the *I. tropica* with *Agnostotes inconstans* Zone of Öpik (1963). The zone was formerly included by both Öpik and Henderson in the Idamean Stage because of the continuing occurrence of similar biofacies. Shergold (1982) justified the *I. tropica* Zone as post-Idamean on the documented co-occurrence of the taxa listed below, particularly *Irvingella tropica* and *Agostotes (A.) inconstans* which have both biostratigraphic and international correlation potential. At the type section for the base of the Iverian Stage, the *I. tropica* Zone, as indicated above, is succeeded by what Shergold (1982) considered as an un-named post-*tropica* assemblage, confined in Australia to the Georgina Basin. Here, it is regarded as a continuation of the *I. tropica* assemblage because it contains species of *Stigmatoa* and *Mecophrys* related to those of the *I. tropica* assemblage. However, it also contains *Parakoldinioidia* cf. *typicalis* and asaphasoideans and ceratopygoideans related more closely to forms occurring later in the *Wentsuia iota/Rhaptagnostus apsis* Assemblage-Zone. Thus this fauna bridges the interval between the *I. tropica* Zone at Mount Murray and the *Wentsuia iota/Rhaptagnostus apsis* Assemblage-Zone, penetrated by stratigraphic coreholes on the Chatsworth Plains and seen in outcrop in the basal 24 m of the Chatsworth Limestone type section at Lily Creek, south of Chatsworth Homestead.

Fauna recorded to date, combined from the Burke River Structural Belt and the Glenormiston area, 160 km to the west-southwest (Öpik, 1963; Henderson, 1976a; Shergold, 1982), and combining both zonal intervals, includes: *Agnostotes (Agnostotes) inconstans, Aphelaspis?* sp. B, asaphoidean gen. et sp. undet. B, ceratopygid gen. et sp. nov. C, *Chalfontia alta,* elviniid gen. et sp. undet. D, *Eugonocare tessellatum, Hercantyx rudis, Irvingella tropica, Mecophrys mecophrys, M. selenis?, Olenus* sp., *Oncagnostus (Oncagnostus)* sp. 1, *Oncagnostus (O.)?* sp., *Pagodia (Idamea) baccata, Parakoldinioidia* sp. aff. *P. typicalis, Proceratopyge (Proceratopyge) lata, "Proceratopyge"* sp. cf. *"P." chuhsiensis, Prochuangia* sp. undet., *Protemnites burkensis, Pseudagnostus (Pseudagnostus) vastulus, Pseudagnostus (Pseudagnostus)* sp. IX, pterocephaliid gen. et sp. undet. A, *Stigmatoa sidonia* and *Stigmatoa?* sp. undet. These taxa are listed in the Appendix which gives revised taxonomic determinations after the original descriptions.

2. *Wentsuia iota/Rhaptagnostus apsis* Assemblage-Zone

This zone contains 35 trilobite taxa described by Shergold (1980), as well as undescribed bradoriid ostracodes, inarticulate brachiopods, a species of *Billingsella,* pelmatozoan debris, poriferan spicules, dendroid graptolite fragments, and molluscs (Shergold, 1980). Trilobites include *Acmarhachis hybrida, Atopasaphus* sp. cf. *A. stenocanthus, Atopasaphus* sp. undet., asaphoidean undet., *Cermatops vieta, Cermatops* sp. indet., *Eugonocare?* sp. undet., *Guizhoucephalina?* sp. undet., *Haniwa varia, Innitagnostus medius, Leptoplastus?* sp. nov., *Lorrettina (Lorrettina) depressa, Lotosoides bathyora, Maladioidella doylei, Neoagnostus (Neoagnostus) felix, N. (N.) greeni, Norinia?* sp. undet., *Oncagnostus (Oncagnostus) aversus, Oncagnostus (O.)* sp. indet., *Onchonotellus* sp. undet., *Peichiashania prima, Peratagnostus* sp. cf. *P. nobilis, Plicatolina* sp. cf. *P. yakutica, Prochuangia glabella, Pseudagnostus (P.) aulax, P. (P.) mortensis, P. (P.) parvus, P. (P.) tricanthus, Pseudagnostus (P.)* sp. VII, *Rhaptagnostus apsis, Rhaptagnostus* sp. cf. *R. impressus, Taenicephalites plerus, Wentsuia iota* and gen. et sp. undet. A. Some 40 per cent of these trilobites range into younger assemblage-zones.

3. *Peichiashania secunda/Prochuangia glabella* Assemblage-Zone

This zone is so far confined to the Lily Creek section, where it ranges over a 120 m interval. Twenty-three trilobite taxa occur: *Atopasaphus* sp. cf. *A. stenocanthus, Cermatops vieta, Cermatops* sp. undet., *Haniwoides varia, Iveria iverensis, Lorrettina (L.) depressa, Lotosoides bathyora, Maladioidella doylei, Neoagnostus (N.) felix, Oncagnostus (O.) aversus, Oncagnostus (O.)* sp. undet., *Parakoldinioidia* sp. cf. *P. bigranulosa, Peichiashania prima, P. secunda, P. tertia, Prochuangia glabella, Pseudagnostus (P.) aulax, P. (P.) parvus, P. (P.) tricanthus, Pseudagnostus (P.)* sp. VI, *Taenicephalites plerus, Wentsuia iota* and *Wuhuia silex.*

With the trilobites are undescribed inarticulate brachiopods, a gastropod, a monoplacophoran aff. *Proplina* sp., sponge spicules, calcispheres, conodonts and a range of echinoderms. Among the last, Jell, Burrett & Banks (1985) have described the oldest isorophid edrioasteroids *Chatsworthia spinosa* and *Hadrodiscus parma* associated with a primitive edrioblastoid — *Cambroblastus enubilatus.* These echinoderms originate from locality K204, which is 69 m above the base of the measured section.

4. *Peichiashania tertia/Peichiashania quarta* Assemblage-Zone

Six trilobite species persist into the overlying assemblage-zone of *Peichiashania tertia* with *P. quarta.* The index species *P. tertia* links assemblages characterised below by *P. secunda* and above by *P. quarta.* The *P. tertia/P. quarta* Assemblage-Zone is also confined to the Lily Creek section, where it ranges over an interval of 101 m. Twelve trilobite taxa occur: *Atopasaphus stenocanthus, Iveria iverensis, Lorrettina (L.) depressa, Lyriamnica antyx, Neoagnostus (N.)* sp. I, *Parakoldinioidia* sp. cf. *P. bigranulosa, Peichiashania tertia, P. quarta, Pseudagnostus (P.) parvus, Rhaptagnostus auctor, Taishania platyfrons* and *Wuhuia silex.*

The fauna also contains undetermined inarticulate brachiopods, a gastropod, a hyolith and echinoderm fragments.

5. *Hapsidocare lilyensis* Assemblage-Zone

Only two trilobite taxa continue into the *Hapsidocare lilyensis* Assemblage-Zone, the youngest assemblage to occur at Lily Creek, in the uppermost 55 m of section. Nine trilobites characterise this assemblage: *Atopasaphus stenocanthus, Hapsidocare lilyensis, Lorrettina (L.) licina, Lotosoides* sp. aff. *L. calcarata, Lyriamnica antyx, Neoagnostus (N.)* sp. II, *Oncagnostus (O.) conspectus, Plecteuloma strix, Prosaukia* sp. cf. *Prosaukia* sp. A. Non-trilobite components include *Billingsella* sp. and pelmatozoan debris.

The *H. lilyensis* Assemblage-Zone provides the correlation between the top of the Lily Creek section and the base of the measured section at Black Mountain, 34 km to the south, because it contains species occurring in both sections, or closely related species, e.g. *Atopasaphus stenocanthus, Plecteuloma strix, Lotosoides calcarata,* a

similar species of *Prosaukia*, and related species of *Hapsidocare* and *Lorrettina*. R-mode cluster analysis presented by Shergold (1980, fig. 6) shows the *lilyensis* assemblage to relate both to the *Rhaptagnostus clarki patulus/Caznaia squamosa* and *R. c. prolatus/C. sectatrix* Assemblage-Zones at Black Mountain.

Late Iverian rocks crop out in the core of the periclinal structure known as Black Mountain and in the Momedah Anticline at Momedah Creek, 19 km east-northeast of Black Mountain. A section measured at Black Mountain, initially for the collection of conodonts (Druce & Jones, 1971) and trilobites (Shergold, 1975), has been redocumented (Radke *in* Shergold, Nicoll & others, 1991) for the purpose of magneto-stratigraphic sampling (Ripperdan & Kirschvink, 1992). At the same time, its biochronology has been re-evaluated (Nicoll & Shergold, 1991; Shergold & Nicoll, 1992). Partly contemporaneous Chatsworth Limestone at Momedah Creek was originally investigated for conodonts by Druce & Jones (1971) and for trilobites by Shergold (1972).

Rocks of late Iverian age constitute the initial 240 m of Section 305 (=Section GEO202 of Radke *in* Shergold & others, 1976; *in* Shergold, Nicoll & others, 1991) at Black Mountain (collections K103-128 of Shergold, 1975). They embrace four further trilobite assemblages, characterised by rapidly evolving agnostoid trilobites of the subfamily Pseudagnostinae. These assemblages represent a more cosmopolitan ocean-facing biofacies than that seen at Lily Creek, which is restricted to taxa composing the Australo-Sinian shelf biofacies.

6. *Rhaptagnostus clarki patulus/Caznaia squamosa* Assemblage-Zone

This zone ranges over the initial 68 m of section. It contains 15 trilobite species including five agnostoids, a species of *Hapsidocare*, and *Plecteuloma strix*, which also occurs at the top of the Lily Creek section. The trilobite assemblage comprises *Caznaia squamosa, Ceronocare* sp., *Hapsidocare chydaeum*, indeterminate idahoiid, *Koldinioidia* sp. cf. *K. cylindrica, Mendosina* sp., *Neoagnostus (N.) coronatus, Neoagnostus (N.)* spp. A, B, *Pagodia (Pagodia)* sp., *Plecteuloma strix, Rhaptagnostus clarki patulus, R. elix, Sigmakainella primaeva* and *Wuhuia* sp. cf. *W. dryope*.

Associated conodonts (Druce & Jones, 1971, revised by Nicoll *in* Shergold, Nicoll & others, 1991, fig. 4, Appendix) include *Furnishina furnishi* Müller, *F. primitiva* (Müller), *Proconodontus tenuiserratus* Miller, *Prooneotodus rotundatus* (Druce & Jones), *Rossodus tenuis* (Müller) and *Westergaardodina bicuspidata* Müller.

7. *Rhaptagnostus clarki prolatus/Caznaia sectatrix* Assemblage-Zone

The *R. c. prolatus/C. sectatrix* Assemblage-Zone has been identified in samples K107-115 (Shergold, 1975), ranging over section between 68.3 m and 140 m. It contains 21 trilobite species, four ranging from the previous assemblage: *Atopasaphus stenocanthus, Atratebia nexosa, Caznaia sectatrix, C. squamosa, Ceronocare pandum, Duplora clara, Hapsidocare grossum, Koldinioidia* sp. cf. *K. cylindrica, Lophosaukia torquata, Lorrettina (L.) macrops, Lotosoides calcarata, L. turbinata, Neoagnostus (N.) coronatus, Neoagnostus (N.)* sp. C, *Oreadella* sp. cf. *O. buda, Prosaukia* sp. A, *Rhaptagnostus bifax, R. clarki patulus, R. c. prolatus, Richardsonella?* sp. and *Sigmakainella translira*.

All listed conodonts of the previous assemblage, with the exception of *Furnishina furnishi*, continue and become associated with *Proconodontus posterocostatus* Miller, *Prooneotodus gallatini* (Müller), *Teridontus nakamurai* (Nogami) and *Westergaardodina amplicava* Müller.

8. *Rhaptagnostus bifax/Neoagnostus (N.) denticulatus* Assemblage-Zone

This is the penultimate Iverian assemblage-zone at Black Mountain. It characterises the section between 140 m and 172 m, having been identified in collections K116-120. Twenty-three trilobite species occur, of which 11 extend their ranges from earlier assemblages. Included are *Atopasaphus stenocanthus, Atratebia nexosa, Ceronocare pandum, Duplora clara, Golasaphus simus, G. triquetrus, Hapsidocare grossum, Lorrettina (L.) macrops, Lotagnostus (Distagnostus) irretitus, Lotosoides calcarata, L. turbinata, Lophosaukia acuta, L. torquata,* mansuyiinid undet., *Neoagnostus (N.) clavus, N. (N.) denticulatus, Oncagnostus (O.) conspectus, Oncagnostus (Strictagnostus) chronius, Parakoldinioidia* sp. cf. *P. bigranulosa, Rhaptagnostus bifax, Sigmakainella translira* and *S? trispinosa*.

Nine conodont species have also been determined (Nicoll *in* Shergold, Nicoll & others, 1991): *Furnishina primitiva, Nogamiconus tricarinatus* (Nogami), *Proconodontus posterocostatus, P. tenuiserratus, Prooneotodus gallatini, P. rotundatus, Rossodus tenuis, Teridontus nakamurai* and *Westergaardodina amplicava*.

9. *Rhaptagnostus clarki maximus/Rhaptagnostus papilio* Assemblage-Zone

The youngest Iverian assemblage-zone is that of *Rhaptagnostus clarki maximus* with *R. papilio*, which occurs in samples K121-128, between 172 m and 240 m. At Black Mountain, the assemblage contains 16 trilobite and 14 conodont taxa, including species potentially valuable for international correlation. The trilobite association includes *Atratebia nexosa?, Golasaphus simus, G. triquetrus, Lophosaukia* sp. A, *Lotagnostus (Distagnostus) irretitus, Maladioidella* sp. cf. *M. chinchiaensis, Mansuyites?* sp. indet., *Neoagnostus (N.) clavus, Oncagnostus (Strictagnostus) chronius, Palacorona* sp. indet., *Prosaukia* sp. indet., *Protopeltura?* sp., *Rhaptagnostus clarki maximus, R. papilio, Sigmakainella longilira* and *S? trispinosa*. A previous reference to the occurrence of *Sinosaukia impages* at the top of the assemblage-zone (Shergold, 1975) cannot be sustained as the material is too fragmentary to determine.

The conodont assemblage comprises coniform genus A (Nicoll, 1991), *Furnishina primitiva, Nogamiconus tricarinatus, Proconodontus muelleri* Miller, *P. posterocostatus, P. tenuiserratus, Prooneotodus gallatini, P. rotundatus, P. terashimai* (Nogami), *Prosagittodontus dahlmani* (Müller), *Rossodus tenuis, Teridontus nakamurai*, and *Westergaardodina amplicava, W. mossebergensis* Müller.

The *maximus/papilio* Assemblage-Zone is also identified in the Gola Beds at Momedah Creek, but relationships to the biostratigraphic units immediately above and below are not established there. Twenty-five species of trilobites have been described (Shergold, 1972), associated with 12 conodont taxa, and inarticulate and articulate brachiopods. The trilobite assemblage contains eight agnostoid species. Four of these, including the two index species, occur in the *maximus/papilio* A.-Z. at Black Mountain, as do seven of

the 17 non-agnostoid taxa. Other taxa are represented by closely related species. However, the autochthonous sediments at Momedah Creek are particularly characterised by kainelloid trilobites which may indicate deeper water environments than at Black Mountain. Ten of the 14 conodont species also occur at Black Mountain, but the Gola Beds are notable for their lack of westergaardodinids.

The recorded trilobite assemblage at Momedah Creek includes *Atopasaphus petasatus, Crucicephalus ocellatus, Dellea? laevis, Duplora clara, Golasaphus momedahensis, Kaolishania australis, Koldinioidia cylindrica, Lophosaukia torquata, Lorrettina (L.) macrops, Lotagnostus (Distagnostus) ergodes, Mansuyites futilliformis, Mendosina laciniosa, Neoagnostus (N.) clavus, Oncagnostus (O.) acrolebes, O. (O.) junior, Palacorona bacculata, Rhaptagnostus clarki maximus, R. papilio, Rhaptagnostus sp., Richardsonella? kainelliformis, Richardsonella* sp., *Sigmakainella longilira, S. translira, 'Tostonia'* sp., and *Trilobagnostus avius*.

The associated conodonts are *Furnishina furnishi, F. primitiva, Nogamiconus tricarinatus, ?Proacontiodus tortus* An [=*Sagittodontus eureka* Müller], *Proconodontus muelleri, P. posterocostatus, P. serratus* Miller, *P. tenuiserratus, Prooneotodus gallatini, P. rotundatus, Prosagittodontus dahlmani* and *Teridontus nakamurai*.

At Black Mountain, Iverian rocks are conformably overlain by the Chatsworth Limestone lithostratigraphic Unit E, with an apparent marked shift to a shallower sedimentary environment (Druce & others, 1982). This unit contains the *Sinosaukia impages* Assemblage-Zone, containing an impoverished fauna of six trilobites. Eight conodonts define the contemporaneous *Hispidodontus resimus* Zone (Nicoll & Shergold, 1991; Shergold, Nicoll & others, 1991; Shergold & Nicoll, 1992). These biostratigraphic units are now regarded as defining the base of the Payntonian Stage.

Correlation

Relationships of correlatable components of the Iverian faunas noted above have previously been explored by Shergold (1972, 1975, 1980, 1982) in analyses of the faunas of the uppermost Pomegranate Limestone, Chatsworth Limestone and Gola Beds. Some of those previous comments are collated here, revised and supplemented.

1. Australia

Rocks of Iverian age are undoubtedly best developed (approx. 725 m thick) and biostratigraphically documented in the Burke River Structural Belt, western Queensland. Elsewhere in the Georgina Basin, west of the Burke River area, only rocks of earliest Iverian age (*Irvingella tropica* Zone) have been identified with certainty. These occur in the top 30 m of the Georgina Limestone, at Browns Creek (Henderson, 1976b), south of Glenormiston Homestead (115 km west of Boulia), and at a depth of 22.9 m in GSQ Mount Whelan #1 stratigraphic corehole, approximately 45 km south of Glenormiston (Green & Balfe, 1980). In this general area, and in correlative rocks along the southern margin of the Georgina Basin to the west (e.g. Arrinthrunga Formation), according to seismic stratigraphic interpretations of Harrison (1979), the top of the Georgina Limestone is a truncation surface. A significant hiatus occurs between this and the overlying Ninmaroo Formation and correlatives elsewhere, of latest Cambrian and early Ordovician age (i.e. late Payntonian and younger) (Shergold & Druce, 1980).

In the Amadeus Basin, this hiatus is partly filled by the upper Goyder Formation, an enigmatic dolomitic and kaolinitic sequence of equivocal age, currently thought to overlie disconformably the carbonate sequences of the lower Goyder Formation and correlatives which have a Mindyallan (*Glyptagnostus stolidotus* Zone) age (Kennard & Lindsay, 1991; Shergold, 1991a). In turn, the upper Goyder Formation is disconformably, or unconformably, overlain by the Pacoota Sandstone having a Payntonian (*Neoagnostus quasibilobus/Shergoldia nomas* A.-Z.) age (Shergold, 1991b; Shergold, Gorter & others, 1991). Thus, the age of the upper Goyder Formation is post-Mindyallan and pre-Payntonian, and may be either Idamean or Iverian. It contains a low diversity fauna characterised by 'parabolinoidid' trilobites, which differ from any known Idamean assemblages in the Georgina Basin. It may represent an as yet unrecognised lateral Idamean biofacies. However, the assemblage has some affinity with 'faunal sequence VII' (Öpik, 1969) in the Bonaparte Basin, which has parabolinoidid trilobites in a biostratigraphically similar position. Typical Idamean trilobite assemblages are also restricted in the Bonaparte Basin. According to Öpik (1969), aphelaspine trilobites occur 'but are inconclusive as regards their position within the stage'. As noted by Shergold (1991a), the upper Goyder trilobites also resemble some taxa occurring in northern Victoria Land, Antarctica, which have a suggested post-Idamean, hence Iverian, age (Shergold & Cooper, 1985).

The Iverian Stage is clearly present in the Bonaparte Basin. Apart from 'faunal sequence VII', based on parabolinoidid trilobites, likely to have some affinity with elements of the *Wentsuia iota/Rhaptagnostus apsis* A.-Z., the quoted occurrence of *Paramansuyella* in 'faunal sequence VIII' probably represents a taxon similar to *Peichiashania* as documented in the Chatsworth Limestone at Lily Creek (see Öpik, 1963, p. 22, locality D124; Shergold, 1980, p. 101). 'Faunal sequence IX', containing a kaolishaniid trilobite, may suggest correlation with late Iverian faunas such as those represented by Kaolishaniidae in the Gola Beds at Momedah Creek and Chatsworth Limestone at Black Mountain. Since the kaolishaniid faunal sequence in the Bonaparte Basin is overlain by younger sequences containing saukiid and tsinaniid trilobites which suggest a Payntonian age, an almost complete Iverian Stage may be represented there. To date, only the *Irvingella tropica* Zone is unrecognised.

Iverian rocks of the Bonaparte Basin are dominantly sandstone deposited in shallow inner shelf environments, and their equivalents in the Georgina Basin are predominantly carbonate deposited in mid to outer shelf environments. Outer shelf and shelf margin correlatives apparently occur in Tasmania. In the Dundas Trough of northwest Tasmania, between biostratigraphically documented Idamean (Jago, 1974, Jago & Brown, in press) and Payntonian rocks (Jago & Corbett, 1990), are faunas assigned a post-Idamean age. These include the material from the Climie Formation at Dundas (Jago, 1978) and the Upper Huskisson Group — the Higgins Creek fauna — described by Jell & others (1991). The last authors also make a case for correlating the trilobite faunas of the Singing Creek Formation, a submarine clastic fan sequence in the Denison Range, southwest Tasmania (Adamsfield Trough: Jago, 1987). Jago & Brown (1989) further suggest a post-Idamean age for poorly preserved material from the Newton

Creek Sandstone of the Tyndall Range (Corbett, 1975).

A possibly contemporaneous basinal late Iverian biofacies has been reported from western New South Wales — Watties Bore faunas — by Webby & others (1988), but it is difficult to apply the shelf carbonate biochronology developed mainly in the Georgina Basin to them since there is little taxonomic correlation between the two areas. The upper faunas at Watties Bore, containing *Hysterolenus*, would seem to post-date the Iverian, but the lower one, dominated by ceratopygoideans and agnostoids, may be significantly older. The ranges of the associated taxa appear to be long and their relationships to shelf taxa not known in detail. They do, however, permit correlation with similar environments in China (western Zhejiang, northwest Hunan, Tianshan).

Earlier shelf margin or slope deposits have been identified in the Wagonga Beds on the New South Wales coast, at Burrewarra Point (Bischoff & Prendergast, 1987). Neither of the trilobites described, aff. *Innitagnostus*, aff. *Onchonotellus*, is age diagnostic, and the fauna, which also contains westergaardodinid conodonts, could be early Iverian, Idamean, or perhaps older.

2. Elsewhere

Outside Australia, the early Iverian is widely correlated by the occurrence of the cosmopolitan genus *Irvingella*. This, for example, permits correlation to northern Victoria Land, Antarctica, where a possible species of *Irvingella*, associated with species of *Olentella*, *Apheloides?* and *Notoaphelaspis*, inter alia, has been reported by Shergold & others (1976). These record a shelf edge (?) biofacies classifiable only with difficulty in terms of Georgina Basin biochronology.

Correlation with the Sino-Korean Platform, particularly sections in Liaoning, Hebei, Shandong and South Korea, and with western Nei Monggol and Tianshan belt of Xinjiang and southern Kazakhstan, is less difficult. However, as in central Australia, there are stratigraphic hiatuses in several places. In the Taitzuho valley of Liaoning, on the Jehol Block (Shakuotun), and in the Ordos Basin (northern Shaanxi), zones between the Gushanian (Mindyallan) and Fengshanian (Payntonian) are missing. In north Shanxi (Datong), Fengshanian is unconformable on Middle Cambrian, and in the Alashan (SW Nei Monggol) and western Tianshan, Upper Cambrian rocks are missing altogether (Kobayashi, 1967).

The most complete sequences seem to be in the Yokusen Geosyncline (Machari and Tsuibon facies) of South Korea (Kobayashi, 1935, 1960, 1962, 1966, 1967, 1971) where the many faunal elements in common with early Iverian assemblages of western Queensland have been documented at length by Shergold (1980, 1982). Relationships between the Korean *Eochuangia* Zone and the Australian *Irvingella tropica* through *Peichiashania tertia*/*P. quarta* interval are extremely close when synonymies and revised taxonomic concepts are considered. Other areas of the Sino-Korean Platform with relatively complete sequences containing common faunal elements with the Georgina Basin are in the Liaoning Peninsula (Kobayashi, 1931, 1933; Endo, 1937, 1939, 1944; Resser & Endo, 1937) and in Shandong and Hebei Provinces (Sun, 1924, 1935). The early Changshanian of these regions (Lu & Qian, 1983), like the Iverian, is recognised by the initial appearance of *Irvingella*, followed by species of *Maladioidella*, *Wentsuia* and *Peichiashania* (Shergold, 1980). Late Iverian assemblages also have quite close relationships with the late Changshanian of the Siberian Platform. These have been discussed in depth by Shergold (1972, 1975; *in* Druce & others, 1982, fig. 5). Little consequential new information has been published to significantly alter the statements made in these papers.

Elsewhere in China, an apparently complete sequence occurs in the northwest of Nei Monggol at Ejin Qi (Lu & others, 1986). This sequence is remarkably correlatable with the late Iverian of the Georgina Basin, containing 13 genera in common with the Momedah anticline section. Among the agnostoid trilobites are three species referred to *Rhaptagnostus*, including *R. papilio* (Shergold); five species of *Neoagnostus*, including one quite similar to *N. (N.) clavus* (Shergold); two of *Oncagnostus*, listed as *Geragnostus (Micragnostus)*; and one species of *Lotagnostus (Distagnostus)*, resembling *L. (D.) irretitus* (Shergold). Among other taxa are species of *Onchonotellus*, *Atopasaphus*, *Golasaphus*, *Sigmakainella*, *Crucicephalus*, *Plecteuloma*, *Koldinioidia*, *Lorrettina* and *Richardsonella*. Furthermore, from conformably older strata, not described by Lu & others (1986), are quoted occurrences of species of *Mansuyia*, *Peichiashania*, *Irvingella* and *Pseudagnostus* which must be of early Iverian age. Thus, the whole of Iverian time is likely to be represented there.

Another complete Iverian section containing correlatable trilobites has been described from the western part of the northern Tianshan (Borohoro Shan), in Xinjiang (Xiang & Zhang, 1984). There, early Iverian is represented in the Gouzigou Formation by the *Agnostotes tianshanicus* Zone which contains common or similar species of *Agnostotes*, *Innitagnostus*, *Rhaptagnostus*, *Haniwoides* and the genus *Sayramaspis*, a composite of what in Australia has been referred to *Maladioidella*, *Cermatops* and *Norinia?* This zone is succeeded by that of *Lotagnostus (L.) punctatus*, containing a faunal assemblage remarkably similar to that described from northwest Tasmania by Jell & others (1991), and considered to have a biostratigraphic range from post-*Irvingella* to Payntonian. Essentially similar biofacies are also found in Anhui (Lu, 1956; Lu & Zhu, 1980), northwest Hunan (Peng, 1983, 1984), Jiangxi (Lin, 1986) and western Zhejiang (Lu & Lin, 1980, 1983, 1984).

Rocks of Iverian age certainly occur in neighbouring Kazakhstan and Kirghizia, as indicated by the occurrence of *Irvingella* and strikingly similar agnostoid faunas. However, in Maly Karatau particularly, non-agnostoid trilobites occurring through the interval between the assemblage-zones of *Ivshinagnostus ivshini-Lotagnostus scrobicularis* (Ergaliev, 1980) are predominantly of Siberian Platform provenance.

Irvingella also forms the basis for correlation with Yakutia where, in the Karaulakh Mountains and on the Olenek Uplift, Lazarenko (1966, 1972) has illustrated trilobites remarkably similar to *Maladioidella [Cedarellus felix]*, *Taenicephalites [Amorphella modesta]* and *Peratagnostus [Cyclopagnostus orientalis]* overlying sequences containing *Irvingella*. This Yakutian fauna also contains *Rhaptagnostus impressus* (Lermontova) also recorded in western Queensland and, in an immediately succeeding assemblage *Plicatolina perlata* Lazarenko, cranidially similar to *P. yakutica* Pokrovskaya, which is also recorded in Queensland.

Apart from the occurrence of the cosmopolitan *Irvingella*,

which permits almost global correlation of the base of the Iverian Stage, there is little faunal relationship with the Siberian Platform, northern Europe or North America. Faunas containing Iverian elements, e.g. *Maladioidella*, do extend westwards from the Tianshan, and have been recorded in central Turkey (Shergold & Sdzuy, 1984) and the Sierra de la Demanda, Logroño Province, Spain (Shergold & others, 1983).

Discussion

The Iverian Stage currently embraces two kinds of biostratigraphical zone: the range-zone of *Irvingella tropica* as its initial zone, followed by a succession of assemblage-zones. The first type of zone is based on the range of a single taxon, whereas those that follow are characterised by the overlapping ranges of associations of species, and are essentially Oppel-zones.

Historically, these zones were established during the time that the post-Idamean Late Cambrian was being pioneered by the Bureau of Mineral Resources Georgina Basin Project (1974–1980), and the local biostratigraphy was in the process of development and regarded as preliminary. The zonation developed then provided the first essential steps in the biostratigraphic synthesis of the Iverian interval. Mainly named by two associated or concurrently ranging index species, these assemblage-zones lack elegance and are often awkward to present graphically. Some of them have since been used elsewhere, and it is becoming clear that a simpler, more direct, zonal scheme should be explored, particularly with the recent promotion of a cohesive Australian Cambrian timescale (Shergold, 1989). As explained below, this does not necessarily entail the abandonment of the present scheme, which in practice serves its purpose in high resolution correlation.

Theoretically, it is possible to continue with the application of the single taxon zonal scheme adopted for the Mindyallan and Idamean Stages by Öpik (1963, 1967), since the Iverian Stage contains at least 93 trilobite taxa (see Appendix). In practice, in the Burke River Structural Belt, this is not so easy to attain, particularly at specific level, mainly because the assemblage-zone sequence has been established from three environmentally displaced sections, which makes difficult the precise resolution of the true ranges of potential index taxa. However, it is possible to work at generic level, as demonstrated below.

Post-dating the *Irvingella tropica* Zone (including here the taxa previously included in the post-*Irvingella* assemblage), early Iverian rocks in the vicinity of Chatsworth contain the mansuyiinid genera *Peichiashania* and *Hapsidocare*. The latter permits correlation with concurrent species at Black Mountain, where the latest Iverian is discriminated by successive species of *Lophosaukia*.

However, the first appearances (FADs) of *Hapsidocare*, *Peichiashania* and *Lophosaukia*, although documented from current information, are likely to change with more intensive research. For example, the FAD of *Peichiashania prima* occurs near the base of BMR Duchess #13 corehole (at 82.80 m) and its range in this hole is limited to this occurrence. In BMR Boulia #6 it first appears at 43.85 m and has a similarly constrained range. In this latter hole, a further 100 m of strata bearing other elements of the *Wentsuia iota/Rhaptagnostus apsis* Assemblage-Zone were penetrated, so the actual first appearance of *P. prima* might well be expected at a significantly lower level in that corehole.

Similarly, there is uncertainty about the total range of the youngest species of the *Peichiashania* lineage, *P. quarta*, in respect to the FAD of *Hapsidocare lilyensis* at Lily Creek. In fact, the latter appears some 64 m above the former. Furthermore, the exact amount of overlap suggested by the R-mode cluster analysis performed by Shergold (1980, fig. 6), which shows the *H. lilyensis* Assemblage-Zone sandwiched between assemblages containing *H. chydaeum* below and *H. grossum* above, is unknown. Unfortunately, adverse environmental conditions, represented by the early onset of the Lily Creek Sandstone Member of the Chatsworth Limestone, prevent the occurrence of associated taxa (like species of *Rhaptagnostus*) which would permit correlation of the Lily Creek and Black Mountain sections

There is, however, good correlation between the last appearance of *Hapsidocare* and the FAD of *Lophosaukia* at Black Mountain, where these genera overlap over 10 m of section.

Peichiashania and *Hapsidocare*, together with many of their associated taxa, are useful for correlation only within the Australo-Sinian biofacies. *Lophosaukia* offers a little extra correlation potential since it has a wider geographical distribution, being recorded around the margins of the Siberian Platform in southern Kazakhstan and the Irkutsk Amphitheatre. For the wider international correlation of zones based on these genera it is necessary to identify the more cosmopolitan elements of the assemblages. *Irvingella* is such a genus, permitting the initial Iverian Stage to be widely correlated with Korean, Chinese, Kazakhstanian, Siberian, north European, and North and South American biostratigraphic units. This is not possible with the proposed index taxa which follow *Irvingella*, which are more constrained by biofacies. However, they may be indirectly correlated by their stratigraphic sequences of agnostoid trilobites and the often close taxonomic relationships of these species elsewhere.

Key agnostoid taxa are species of *Agnostotes* and its subgenera, which are frequently associated with *Irvingella*, and the Pseudagnostinae. Among the latter, species of *Pseudagnostus*, rampant in the earlier Idamean, last appear at the top of the *Peichiashania secunda/Prochuangia glabella* Assemblage-Zone (Shergold, 1977, 1981). *P. (P.) parvus* has a long range, extending from a depth of 142.7 m in BMR Boulia #6 extension through to the last appearance datum of the genus, and has potential biostratigraphic use. Five species of *Neoagnostus* occur during the Iverian, but all have very limited stratigraphic ranges. Similarly, there are eight species of *Rhaptagnostus* having good correlation potential, but again with limited biostratigraphical ranges. The pseudagnosti that have previously given their names to assemblage-zones have been used because of their ready determination. Used in combination, their ranges have more stratigraphic significance than if used individually.

Summary

Undoubtedly, the assemblage-zone scheme used originally has the highest resolution for correlation. The alternative generic zone scheme suggested above is intended to simplify the terminology, involving the genera *Irvingella*, *Peichiashania*, *Hapsidocare* and *Lophosaukia* in stratigraphically ascending order. In this scheme:

- The *Irvingella tropica* Zone and post-*I. tropica* Assemblage-Zone, as documented above, are integrated into an *Irvingella* Zone.

- The lineage of the species *Peichiashania prima–P. secunda–P. tertia–P. quarta* forms the basis of the *Peichiashania* Zone. This lineage unites the *Wentsuia iota/Rhaptagnostus apsis, Peichiashania secunda/Prochuangia glabella* and *Peichiashania tertia/P. quarta* Assemblage-Zones. In the Burke River Structural Belt, there is an interzone of uncertain thickness between the *Peichiashania* Zone and that of *Irvingella*.

- The *Peichiashania* Zone is superseded by another, based on the concurrent ranges of species of *Hapsidocare: H. lilyensis* at the top of the Lily Creek section, and *H. chydaeum* followed by *H. grossum* in the lower part of the Black Mountain section. Thus the *Hapsidocare* Zone binds the *H. lilyensis, Rhaptagnostus clarki patulus/Caznaia squamosa* and *R. c. prolatus/C. sectatrix* Assemblage-Zones. An interzone amounting to 64 m of the Lily Creek section is interposed between the *Peichiashania* and *Hapsidocare* Zones.

- Immediately following the *Hapsidocare* Zone is the initial part of the range of *Lophosaukia*, whose species form the lineage *L. torquata–L. acuta–Lophosaukia* sp. A (younger species occur in the Payntonian). These unite the *Rhaptagnostus bifax/Neoagnostus denticulatus* and *R. clarki maximus/R. papilio* Assemblage-Zones at the top of the Iverian Stage. The FAD of *L. torquata* overlaps the last appearance of *Hapsidocare* between 128 and 138 m in the Black Mountain section.

References

An Taixiang, 1983 — *See* An Taixiang & others, 1983.

An Taixiang, Zhang Fang, Xiang Weida, Zhang Youqiu, Xu Wenhao, Zhang Huijuan, Jiang Dedbiao, Yang Changsheng, Lin Liandi Cui Zhantang & Yang Xinchang, 1983 — The conodonts of North China and the adjacent regions. *Science Press, Beijing,* 223 pp., 33 pls.

Bassett, M.G. & Dean, W.T. (editors), 1982 — The Cambrian-Ordovician Boundary: sections, fossil distributions, and correlations, 193–209. *National Museum of Wales, Geological Series* 3, 277 pp

Bischoff, G.C.O. & Prendergast, Elaine I., 1987 — Newly-discovered Middle and Late Cambrian fossils from the Wagonga Beds of New South Wales, Australia. *Neues Jahrbuch für Geologie und Paläontologie, Abhandlung* 175(1), 39–64.

Burrett, C.F. & Martin, E.L. (editors), 1989 — Geology and Mineral Resources of Tasmania. *Geological Society of Australia., Special Publication* 15, 574 pp.

Casey, J.N., 1959 — New names in Queensland stratigraphy (part 5). *Australian Oil and Gas Journal* 5, 31–35.

Corbett, K.D., 1975 — Preliminary report on the geology of The Red Hills-Newton Creek area, West Coast Range, Tasmania. *Tasmanian Department of Mines Technical Report* 19, 11–25.

Druce, E.C. & Jones, P.J., 1971 — Cambro-Ordovician conodonts from the Burke River Structural Belt, Queensland. *Bureau of Mineral Resources, Australia, Bulletin* 110, 158 pp., 20 pls.

Druce, E.C., Radke, B.M. & Shergold, J.H., 1981 — Appendix IV: Proposed stratigraphic members of the Chatsworth Limestone and Ninmaroo Formation, Georgina Basin. *In* Radke, B.M., 137–141, *q.v.*

Druce, E.C., Shergold, J.H. & Radke, B.M., 1982 — A reassessment of the Cambrian-Ordovician boundary section at Black Mountain, western Queensland, Australia. *In* Bassett, M.G. & Dean, W.T. (editors), 193–209, *q.v.*

Endo, R., 1937 — See Endo, R & Resser, C.E., 1937.

Endo, R., 1939 — Cambrian fossils from Shantung. Jubilee Publication Commemorating Professor Yabe's 60th Birthday, 1–18, pls 1–2.

Endo, R., 1944 — Restudies on the Cambrian formations and fossils of southern Manchukuo. *Central National Museum of Manchukuo* 7, 1–100, pls 1–10.

Endo, R. & Resser, C.E., 1937 — The Sinian and Cambrian formations and fossils of southern Manchukuo. *Manchukuo Science Museum Bulletin* 1, 1–474, pls 14–73.

Ergaliev, G.K., 1980 — Middle and Upper Cambrian trilobites of Lesser Karatau. *Kazakhstan SSR Academy of Sciences, K.I.Satpaev Institute of Geological Sciences* 1–211, 20 pls, Science Press, Alma–Ata (in Russian).

Green, P.M. & Balfe, P.E., 1980 — Stratigraphic drilling report -GSQ Mt Whelan 1 and 2. *Queensland Government Mining Journal* 81 (941), 162–178.

Hancock, J.M., 1977 — The historic development of concepts of biostratigraphic correlation. *In* Kauffman, E.G. & Hazel, J.E. (editors), 3–22, *q.v.*

Harrison, P.L., 1979 — Recent seismic studies upgrade the petroleum prospects of the Toko Syncline, Georgina Basin. *The APEA Journal* 19 (1), 30–42.

Hedberg, H.D. (editor), 1976 — International Stratigraphic Guide. *John Wiley Interscience, New York,* 200 pp.

Henderson. R.A., 1976a — Upper Cambrian (Idamean) trilobites from western Queensland, Australia. *Palaeontology* 19(2), 325–364, pls 47–51.

Henderson, R.A., 1976b — Stratigraphy of the Georgina Limestone and a revised zonation for the early Upper Cambrian Idamean Stage. *Journal of the Geological Society of Australia* 23(4), 423–433.

Henderson, R.A. & Stephenson, P.J. (editors), 1980 — The Geology and Geophysics of Northeastern Australia. *Geological Society of Australia, Queensland Division,* 468 pp.

Jago, J.B., 1974 — *Glyptagnostus reticulatus* from the Huskisson River, Tasmania. *Papers and Proceedings of the Royal Society of Tasmania* 107, 117–127, pl. 1.

Jago, J.B., 1978 — Late Cambrian fossils from the Climie Formation, western Tasmania. *Papers and Proceedings of the Royal Society of Tasmania* 112, 137–153, pls 1–3.

Jago, J.B., 1987 — Idamean (Late Cambrian) trilobites from the Denison Range, south-west Tasmania. *Palaeontology* 30(2), 207–231, pls 24–27.

Jago, J.B. & Brown, A.V., 1989 — Middle to Upper Cambrian fossiliferous sedimentary rocks. *In* Burrett, C.F. & Martin, E.L. (editors), 1989, 74–82, *q.v.*

Jago, J.B. & Brown, A.V., (in press) — Early Idamean (Late Cambrian) agnostoid trilobites from the Huskisson River, Tasmania. *Papers and Proceedings of the Royal Society of Tasmania.*

Jago, J.B. & Corbett, K.D., 1990 — Latest Cambrian trilobites from Misery Hill, western Tasmania. *Alcheringa* 14, 233–246.

Jell, P.A., Burrett, C.F. & Banks, M.R., 1985 — Cambrian and Ordovician echinoderms from eastern Australia. *Alcheringa* 9, 183–208.

Jell, P.A., Hughes, N.C. & Brown, A.V., 1991 — Late Cambrian (post-Idamean) trilobites from the Higgins Creek area, western Tasmania. *Memoirs of the Queensland Museum* 30(3), 455–485.

Jones, P.J., Shergold, J.H. & Druce, E.C., 1971 — Late

Cambrian and Early Ordovician Stages in western Queensland. *Journal of the Geological Society of Australia* 18(1), 1–32.

Kauffman, E.G. & Hazel, J.E. (editors), 1977 — Concepts and methods of biostratigraphy. *Dowden, Hutchinson & Ross Inc., Stroudsburg, Pennsylvania,* 658 pp.

Kennard, J.M. & Draper, J.D., 1977 — BMR stratigraphic drilling in the Burke River Structural Belt, southeast Georgina Basin, 1974. *Bureau of Mineral Resources, Australia, Record* 1977/19, 7 pp.

Kennard, J.M. & Lindsay, J.F., 1991 — Sequence stratigraphy of the latest Proterozoic-Cambrian Pertaoorta Group, northern Amadeus Basin, central Australia. *Bureau of Mineral Resources, Australia, Bulletin* 236, 171–194.

Kobayashi, T., 1931 — Studies on the stratigraphy and palaeontology of the Cambro-Ordovician formations of Hualienchai and Niuhsintai, south Manchuria. *Japanese Journal of Geology and Geography* 8(3), 131–189, pls 16–22.

Kobayashi, T., 1933 — Upper Cambrian of the Wuhutsui Basin, Liaotung, with special reference to the limit of the Chaumitien (or Upper Cambrian) of eastern Asia, and its subdivision. *Japanese Journal of Geology and Geography* 11(1–2), 55–155, pls 9–15.

Kobayashi, T., 1935 — The Cambro-Ordovician formations and faunas of South Chosen. Palaeontology, Pt 3. Cambrian faunas of South Chosen with special study on the Cambrian trilobite genera and families. *Journal of the Faculty of Science of the Imperial University of Tokyo* [2], 4(2), 49–344, pls 1–24.

Kobayashi, T., 1960 — The Cambro-Ordovician formations and faunas of South Korea, Part 7. Palaeontology 6. *Journal of the Faculty of Science of the University of Tokyo* [2], 12(2), 329–420, pls 19–21.

Kobayashi, T., 1962 — The Cambro-Ordovician formations and faunas of South Korea, Part 9. Palaeontology 8. The Machari fauna. *Journal of the Faculty of Science of the University of Tokyo* [2], 14(1), 1–152, pls 1–12.

Kobayashi, T., 1966 — The Cambro-Ordovician formations and faunas of South Korea, Part 10. Stratigraphy of the Chosen Group in Korea and south Manchuria, and its relation to the Cambro-Ordovician formations of other areas. Section A. The Chosen Group of South Korea. *Journal of the Faculty of Science of the University of Tokyo* [2], 16(1), 1–84.

Kobayashi, T., 1967 — The Cambro-Ordovician formations and faunas of South Korea, Part 10, Section C. The Cambrian of eastern Asia and other parts of the continent. *Journal of the Faculty of Science of the University of Tokyo* [2], 16(3), 381–534.

Kobayashi, T., 1971 — The Cambro-Ordovician formations and faunas of South Korea, Part 10, Section E. The Cambro-Ordovician faunal provinces and the interprovincial correlation. *Journal of the Faculty of Science of the University of Tokyo* [2], 18(1), 129–299.

Lazarenko, N.P., 1966 — Biostratigraphy and some new trilobites from the Upper Cambrian of the Olenek Uplift and Karaulakh Mountains. Learned *Papers of the All-Union Institute of Arctic Geology, Palaeontology and Biostratigraphy* 11, 33–78, pls 1–8 (in Russian).

Lazarenko, N.P. & Nikiforov, N.I., 1972 — Middle and Upper Cambrian of the northern Siberian Platform and adjoining mountain regions. *Learned Papers of the All-Union Institute of Arctic Geology* 4–9 (in Russian).

Lermontova, E.V., 1940 — Arthropoda. *In* Vologdin, A.G. (editor), 1940, 112–157, pls 35–49.

Lin Tianrui, 1986 — A late Upper Cambrian trilobite fauna from northwestern Jiangxi. *Journal of Nanjing University (Natural Sciences Edition)* 22(1), 129–146, 3 pls (in Chinese).

Lu Yen-hao, 1956 — An Upper Cambrian faunule from eastern Kueichou. *Acta palaeontologia sinica* 4, 365–372 (in Chinese).

Lu Yan-hao & Lin Huan-ling, 1980 — Cambro-Ordovician boundary on western Zhejiang and the trilobites contained therein. *Acta palaeontologia sinica* 19(2), 118–131 (Chinese), 131–134 (English), pls 1–3.

Lu Yanhao & Lin Huanling, 1983 — Zonation and correlation of Cambrian faunas in W. Zhejiang. *Acta geologica sinica* 1983(4), 317-325 (Chinese), 325–327 (English), pls 1–2.

Lu Yan-hao & Lin Huan-ling, 1984 — Late Late Cambrian and earliest Ordovician trilobites of Jiangshan-Changshan area, Zhejiang. *In* Nanjing Institute of Geology and Palaeontology (Compilers), Stratigraphy and Palaeontology of Systemic boundaries in China. Cambrian-Ordovician Boundary, 1, 45–143, pls 1–19. *Anhui Science and Technology Publishing House, Beijing.*

Lu Yan-hao & Qian Yi-yuan, 1983 — New zonation and correlation of the Upper Cambrian Changshanian Stage in North China. *Acta palaeontologia sinica* 22(3), 235–247 (Chinese), 247–253 (English), pls 1–3.

Lu Yan-hao, Zhou Zhi-qiang & Zhou Zhi-yi, 1986 — New materials of Onychopyge faunas, with a discussion on the evolution of Onychopyge (Trilobita). *Bulletin of the Nanjing Institute of Geology and Palaeontology, Academia Sinica* 7, 69–114 (Chinese), 114–122 (English), pls 1–12.

Lu Yanhao & Zhu Zhaoling, 1980 — Cambrian trilobites from Chuxian-Quanjiao region, Anhui. *Memoir of the Nanjing Institute of Geology and Palaeontology, Academia Sinica* 16, 1–25, (Chinese), 25–30 (English), pls 1–6.

Ludvigsen, R. & Westrop, S.R., 1985 — Three new Upper Cambrian stages for North America. *Geology* 13, 139–143.

Miller, J.F., 1969 — Conodont fauna of the Notch Peak Limestone (Cambro-Ordovician), House Range, Utah. *Journal of Paleontology* 43(2), 413–439, pls 63–66.

Miller, J.F., 1980 — Taxonomic revisions of some Upper Cambrian and Lower Ordovician conodonts with comments on their evolution. *University of Kansas Paleontological Contributions, Paper* 99, 1–39, pls 1–2.

Müller, K.J., 1959 — Kambrische Conodonten. *Zeitschrift der Deutschen Geologischen Gesellschaft* 111, 434–485, pls 11–15.

Müller, K.J. & Hinz, Ingelore, 1991 — Upper Cambrian conodonts from Sweden. *Fossils and Strata* 28, 1–152, pls 1–45.

Nicoll, R.S., 1991 — Differentiation of Late Cambrian-Early Ordovician species of *Cordylodus* (Conodonta) with biapical basal cavities. *BMR Journal of Australian Geology & Geophysics* 12(3), 223–244.

Nicoll, R.S. & Shergold, J.H., 1991 — Revised Late Cambrian (pre-Payntonian to Datsonian) conodont biostratigraphy at Black Mountain, Georgina Basin, western Queensland, Australia. *BMR Journal of Australian Geology & Geophysics* 12(1), 93–118.

Nogami, Y., 1967 — Kambrische Conodonten von China. Teil 2, Conodonten aus den hoch oberkambrischen Yencho-Schichten. *Memoirs of the College of Science, University of Kyoto, Series* B33, 211–218.

Öpik, A.A., 1963 — Early Upper Cambrian fossils from Queensland. *Bureau of Mineral Resources, Australia, Bulletin* 64, 5–133, pls 1–9.

Öpik, A.A., 1967 — The Mindyallan fauna of northwestern Queensland. *Bureau of Mineral Resources, Australia,*

Bulletin 74, vol. 1, 1–404; vol. 2, 1–166, pls 1–67.

Öpik, A.A., 1969 — Appendix 3. The Cambrian and Ordovician sequence, Cambridge Gulf area. pp 74–77 *In* Kaulbach, J.A. & Veevers, J.J., Cambrian and Ordovician geology of the southern part of the Bonaparte Gulf Basin, Western Australia. *Bureau of Mineral Resources, Australia, Report* 109, 1–80, pls 1–12.

Peng Shan-chi, 1983 — Cambrian-Ordovician boundary in the Cili-Taoyuan border area, northwestern Hunan. *In* Nanjing Institute of Geology and Palaeontology (Compilers), Papers for the Symposium on the Cambrian-Ordovician and Ordovicia-Silurian boundaries, Nanjing, China, October 1983, 44–49, pls 1–2. *Academia Sinica, Nanjing.*

Peng Shan-chi, 1984 — Cambrian-Ordovician boundary in the Cili-Taoyuan border area, northwestern Hunan, with descriptions of relative trilobites. *In* Nanjing Institute of Geology and Palaeontology (Compilers), Stratigraphy and Palaeontology of Systemic Boundaries in China. Cambrian-Ordovician Boundary, 1, 285–405, pls 1–17. *Anhui Science and Technology Publishing House, Beijing.*

Pokrovskaya, N.V., 1966 — Trilobites of the Family Olenidae from the Upper Cambrian of Yakutia. *Paleontologicheskiy Zhurnal* 1966 (2), 67–80, pl. 10 (in Russian).

Radke, B.M., 1981 — Lithostratigraphy of the Ninmaroo Formation (Upper Cambrian-Lower Ordovician), Georgina Basin, Queensland and Northern Territory. *Bureau of Mineral Resources, Australia, Report* 181, BMR Microform MF153.

Resser, C. E. & Endo, R., 1933 — *See* Kobayashi, T., 1933.

Resser, C. E. & Endo, R., 1937 — See Endo, R. & Resser, C. E., 1937.

Ripperdan, R.L. & Kirschvink, J.L., 1992 — Paleomagnetic results from the Cambrian-Ordovician boundary section at Black Mountain, Georgina Basin, western Queensland, Australia. *In* Webby, B.D. & Laurie, J.R. (editors), 1992, 93–104.

Shergold, J.H., 1972 — Late Upper Cambrian trilobites from the Gola Beds, western Queensland. *Bureau of Mineral Resources, Australia, Bulletin* 112, 1–126, pls 1–19.

Shergold, J.H., 1975 — Late Cambrian and Early Ordovician trilobites from the Burke River Structural Belt, western Queensland, Australia. *Bureau of Mineral Resources, Australia, Bulletin* 153, vol. 1, 1–251; vol. 2, pls 1–58.

Shergold, J.H., 1977 — Classification of the trilobite *Pseudagnostus*. *Palaeontology* 20(1), 69–100, pls 15–16.

Shergold, J.H., 1980 — Late Cambrian trilobites from the Chatsworth Limestone, western Queensland. *Bureau of Mineral Resources, Australia, Bulletin* 186, 1–111, pls 1–35.

Shergold, J.H., 1981 — Towards a global Late Cambrian agnostid biochronology. *In* Taylor, M.E. (editor), 1981, 208–214.

Shergold, J.H., 1982 — Idamean (Late Cambrian) trilobites, Burke River Structural Belt, western Queensland. *Bureau of Mineral Resources, Australia, Bulletin* 187, 1–69, pls 1–17.

Shergold, J.H., 1989 (compiler) — Australian Phanerozoic Timescales, 1: Cambrian. *Bureau of Mineral Resources, Australia, Record* 1989/31, 25 pp.

Shergold, J.H., 1991a (coordinator) — Late Proterozoic and Early Palaeozoic palaeontology and biostratigraphy of the Amadeus Basin. *Bureau of Mineral Resources, Australia, Bulletin* 236, 97–111.

Shergold, J.H., 1991b — Late Cambrian and Early Ordovician trilobite faunas of the Pacoota Sandstone, Amadeus Basin, central Australia. *Bureau of Mineral Resources, Australia, Bulletin* 237, 15–75, pls 1–9.

Shergold, J.H. & Cooper, R.A., 1985 — Late Cambrian trilobites from the Mariner Group, northern Victoria Land, Antarctica. *BMR Journal of Australian Geology & Geophysics* 9(2), 91–106.

Shergold, J.H. & Druce, E.C., 1980 — Upper Proterozoic and Lower Palaeozoic rocks of the Georgina Basin. *In* Henderson, R. A. & Stephenson, P.J. (editors), 149–174.

Shergold, J.H. & Nicoll, R.S., 1992 — Revised Cambrian-Ordovician boundary biostratigraphy, Black Mountain, western Queensland. *In* Webby, B.D. & Laurie, J.R. (editors), 81–92.

Shergold, J.H. & Sdzuy, K., 1984 — Cambrian and early Tremadoc trilobites from Sultan Dag, central Turkey. *Senckenbergiana lethaea* 65(1/3), 51–135, pls 1–8.

Shergold, J.H. & Walter, M.R., 1979 — BMR stratigraphic drilling in the Georgina Basin, 1977 and 1978. *Bureau of Mineral Resources, Australia, Record* 1979/36, 34 pp.

Shergold, J.H., Cooper, R.A., MacKinnon, D.I. & Yochelson, E.L., 1976 — Late Cambrian Brachiopoda, Mollusca and Trilobita from northern Victoria Land, Antarctica. *Palaeontology* 19(2), 247–291, pls 38–42.

Shergold, J.H., Druce, E.C., Radke, B.M. & Draper, J.J., 1976 — Cambrian and Ordovician stratigraphy of the eastern portion of the Georgina Basin, Queensland and eastern Northern Territory. *25th Session International Geological Congress, Field Excursion 4C Guidebook,* 1–54.

Shergold, J.H., Gorter, J.D., Nicoll, R.S. & Haines, P.W., 1991 — Stratigraphy of the Pacoota Sandstone (Cambrian- Ordovician), Amadeus Basin, N.T. *Bureau of Mineral Resources, Australia, Bulletin* 237, 1–14.

Shergold, J.H., Liñán, E. & Palacios, T., 1983 — Late Cambrian trilobites from the Najerilla Formation, north-eastern Spain. *Palaeontology* 26 (1), 71–92, pls 11–12.

Shergold, J.H., Nicoll, R.S., Laurie, J.R. & Radke, B.M., 1991 — The Cambrian-Ordovician boundary at Black Mountain, western Queensland. 6th International Symposium on the Ordovician System, Guidebook for Field Excursion 1, 1–50. *Bureau of Mineral Resources, Australia, Record* 1991/48.

Smith, A. B. & Jell, P. A., 1990 — Cambrian edrioasteroids from Australia and the origin of the starfishes. *Memoirs of the Queensland Museum* 28 (2), 715–778.

Sun, Yun-chu, 1924 — Contribution to the Cambrian faunas of China. *Palaeontologia sinica* [B] 1, Fascicule 4, 1–109, pls 1–5.

Sun, Yun-chu, 1935 — The Upper Cambrian trilobite faunas of north China. *Palaeontologia sinica* [B] 2, Fascicule 2, 1–69, pls 1–6.

Taylor, M.E. (editor), 1981 — Short papers for the Second International Symposium on the Cambrian System 1981. *U.S. Department of the Interior, Geological Survey, Open-File Report* 81–743, 1–252.

Vologdin, A.G. (editor), 1940 — Atlas of the leading forms of fossil faunas in the USSR. Volume 1, Cambrian, 1–194, pls 1–49. *State Editorial Office for Geological Literature, Moscow, Leningrad.*

Walcott, C.D., 1905 — Cambrian faunas of China. *Proceedings of the U.S. National Museum* 29, 1–106.

Webby, B.D. & Laurie, J.R. (editors), 1992 — Global perspectives on Ordovician geology, 1-513. *A.A. Balkema, Rotterdam.*

Webby, B.D., Wang Qizheng & Mills, K.J., 1988 — Upper Cambrian and basal Ordovician trilobites from western New South Wales. *Palaeontology* 31(4), 905–938, pls 83–86.

Whitehouse, F.W., 1936 — The Cambrian faunas of northeastern Australia. Part 1, Stratigraphical outline. Part 2, Trilobita (Miomera). *Memoirs of the Queensland Museum* 11, 59–112, pls 8–10.

Whitehouse, F.W., 1939 — The Cambrian faunas of northeastern Australia. Part 3, The polymerid trilobites. *Memoirs of the Queensland Museum* 21(3), 179–282, pls 19–25.

Xiang Li-wen & Zhang Tai-rong, 1984 — Tremadocian trilobites from the western part of the northern Tianshan, Xinjiang. *Acta palaeontologica sinica* 23(4), 399–407 (Chinese), 407–409 (English), pls 1–3.

Appendix 1. Formal documentation of determined Iverian taxa

Trilobita

Acmarhachis hybrida Shergold, 1980
Agnostotes (Agnostotes) inconstans Öpik, 1963
Atopasaphus petasatus Shergold, 1972
Atopasaphus stenocanthus Shergold, 1975
Caznaia sectatrix Shergold, 1975
Caznaia squamosa Shergold, 1975
Cermatops vieta Shergold, 1980
Ceronocare pandum Shergold, 1975
Chalfontia alta (Henderson, 1976)
Crucicephallus ocellatus Shergold, 1972
Dellea? laevis Shergold, 1972
Duplora clara Shergold, 1972
Eugonocare tessellatum Whitehouse, 1939
Golasaphus momedahensis Shergold, 1972
Golasaphus simus Shergold, 1975
Golasaphus triquetrus Shergold, 1975
Haniwa varia Shergold, 1980
Hapsidocare chydaeum Shergold, 1975
Hapsidocare grossum Shergold, 1975
Hapsidocare lilyensis Shergold, 1980
Hercantyx rudis Öpik, 1963
Innitagnostus medius Shergold, 1980
Irvingella tropica Öpik, 1963
Iveria iverensis Shergold, 1980
Kaolishania australis Shergold, 1972
Koldinioidia sp. cf. *K. cylindrica* (Shergold, 1972)
Lophosaukia acuta Shergold, 1975
Lophosaukia torquata Shergold, 1972
Lorrettina (Lorrettina) depressa Shergold, 1980
Lorrettina (Lorrettina) licina Shergold, 1980
Lorrettina (Lorrettina) macrops Shergold, 1972
Lotagnostus (Distagnostus) ergodes (Shergold, 1972)
Lotagnostus (Distagnostus) irretitus (Shergold, 1975)
Lotosoides bathyora Shergold, 1980
Lotosoides calcarata Shergold, 1975
Lotosoides turbinata Shergold, 1975
Lyriamnica antyx Shergold, 1980
Maladioidella doylei Shergold, 1980
Maladioidella sp. cf. *M. chinchiaensis* (Endo, 1937)
Mansuyites futilliformis Shergold, 1972
Mecophrys mecophrys Shergold, 1982
Mecophrys selenis Shergold, 1982
Mendosina laciniosa (Shergold, 1972)
Neoagnostus (Neoagnostus) clavus (Shergold, 1972)
Neoagnostus (Neoagnostus) coronatus (Shergold, 1975)
Neoagnostus (Neoagnostus) denticulatus (Shergold, 1975)
Neoagnostus (Neoagnostus) felixi Shergold, 1980
Neoagnostus (Neoagnostus) greeni Shergold, 1980
Oncagnostus (Oncagnostus) aversus (Shergold, 1980)
Oncagnostus (Oncagnostus) conspectus (Shergold, 1975)
Oncagnostus (Oncagnostus) junior (Shergold, 1972)
Oncagnostus (Strictagnostus) chronius (Shergold, 1975)
Oreadella sp. cf. *O. buda* (Resser & Endo, 1933)
Pagodia (Idamea) baccata Öpik, 1967
Palacorona bacculata Shergold, 1972
Parakoldinioidia bigranulosa Shergold, 1975
Parakoldinioidia sp. cf. *P. typicalis* Endo, 1937
Peichiashania prima Shergold, 1980
Peichiashania secunda Shergold, 1980
Peichiashania quarta Shergold, 1980
Peichiashania tertia Shergold, 1980
Peratagnostus sp. cf. *P. nobilis* Öpik, 1967
Plecteuloma strix Shergold, 1975
Plicatolina sp. cf. *P. yakutica* Pokrovskaya, 1966
Proceratopyge (Proceratopyge) lata Whitehouse, 1939
"Proceratopyge" sp. cf. *"P." chuhsiensis* Lu, 1956
Prochuangia glabella Shergold, 1980
Protemnites burkensis Shergold, 1982
Pseudagnostus (Pseudagnostus) aulax Shergold, 1980
Pseudagnostus (Pseudagnostus) mortensis Shergold, 1980
Pseudagnostus (Pseudagnostus) parvus Shergold, 1980
Pseudagnostus (Pseudagnostus) tricanthus Shergold, 1980
Pseudagnostus (Pseudagnostus) vastulus Whitehouse, 1936
Rhaptagnostus apsis Shergold, 1980
Rhaptagnostus auctor Shergold, 1980
Rhaptagnostus bifax (Shergold, 1975)
Rhaptagnostus clarki maximus (Shergold, 1975)
Rhaptagnostus clarki patulus (Shergold, 1975)
Rhaptagnostus clarki prolatus (Shergold, 1975)
Rhaptagnostus elix (Shergold, 1975)
Rhaptagnostus sp. cf. *R. impressus* (Lermontova, 1940)
Rhaptagnostus papilio (Shergold, 1972)
Richardsonella? kainelliformis (Shergold, 1972)
Sigmakainella longilira Shergold, 1972
Sigmakainella primaeva Shergold, 1975
Sigmakainella translira Shergold, 1972
Sigmakainella? trispinosa Shergold, 1975
Taenicephalites plerus Shergold, 1980
Taishania platyfrons Shergold, 1980
Trilobagnostus avius (Shergold, 1972)
Wentsuia iota Shergold, 1980
Wuhuia sp. cf. *W. dryope* (Walcott, 1905)
Wuhuia silex Shergold, 1980

Conodonta

Furnishina furnishi Müller, 1959
Furnishina primitiva Müller, 1959
Nogamiconus tricarinatus (Nogami, 1967)
?Proacontiodus tortus An, 1983
Proconodontus muelleri Miller, 1969
Proconodontus posterocostatus Miller, 1980
Proconodontus serratus Miller, 1969
Proconodontus tenuiserratus Miller, 1980
Prooneotodus gallatini (Müller, 1959)
Prooneotodus rotundatus (Druce & Jones, 1971)
Prooneotodus terashimai (Nogami, 1967)
Prosagittodontus dahlmani (Müller, 1959)
Rossodus tenuis (Müller, 1959)
Teridontus nakamurai (Nogami, 1967)
Westergaardodina amplicava Müller, 1959
Westergaardodina bicuspidata Müller, 1959
Westergaardodina mossebergensis Müller, 1959

Echinodermata

Cambroblastus enubilatus Smith & Jell, 1990
Chatsworthia spinosa Smith & Jell, 1990
Hadrodiscus parma Smith & Jell, 1990
Ridersia watsonae Jell, Burrett & Banks, 1985

BMR Journal of Australian Geology & Geophysics, 13, 359–368

Seismic structure and continuity of the Redbank Thrust Zone, central Australia

C. Wright[1], B.R. Goleby[2], R.D. Shaw[2], C.D.N. Collins[2], B.L.N. Kennett[3] & K. Lambeck[3]

The Redbank Thrust Zone in central Australia is a major Proterozoic Province boundary that was reactivated during the compressional Alice Springs Orogeny (300–400 Ma). To investigate its three-dimensional structure, three deep seismic reflection profiles were recorded over this boundary in 1985. This paper presents new seismic results that provide clear supporting evidence that the Redbank Thrust Zone has a similar geometry in two crustal sections spaced 70 km apart. In both seismic dip-sections the Redbank Thrust Zone is a planar, sub-parallel band of reflections that dip to the north at 35-40° and extends to depths in excess of 20 km. This similarity indicates a definite three-dimensional geometry, and, in-conjunction with existing structural data, gravity and teleseismic data suggests that the Redbank Thrust Zone is a major boundary, of considerable lateral magnitude, separating crustal blocks with different geological composition and structure and reinforces earlier interpretations that the Redbank Thrust Zone represents a crust-cutting 'thick-skinned' feature.

Introduction

In 1985, the Australian Bureau of Mineral Resources (BMR) recorded about 200 km of deep seismic reflection data within the Proterozoic Arunta Block of central Australia. This work consisted of three profiles: L1, the main regional seismic profile whose results have previously been described (e.g. Goleby & others, 1989); L2, a short parallel profile, and L3, a short profile perpendicular to L1. The main objective of the deep seismic profiling was to image the crustal structural of the Arunta Block and so discriminate between models for the tectonic evolution and structural style of the region.

Existing seismic results

The most important result emerging from the analysis of the main seismic profile (L1, Fig. 1) has been the confirmation of the 'thick-skinned' or crust-penetrating deformation associated with the Redbank Thrust Zone, proposed and developed by earlier workers (Forman & Shaw, 1973; Shaw, 1987; Lambeck & others, 1988).

The existing seismic data for L1 imaged the Redbank Thrust Zone as a fault zone displacing the Moho over a vertical depth range of at least 15 km with mantle rocks on the northern hanging wall at relatively shallow depths to approximately 25 km (Goleby & others, 1989). This interpretation is supported by gravity and teleseismic travel-time residual models.

New seismic results

This paper presents the results from the two shorter seismic profiles, L2 & L3. L2, a north-south profile, is 40 km long, parallel to, but about 70 km east of L1, and crosses the Redbank Thrust Zone. L3 is a 14 km long east-west profile located over the Redbank Thrust Zone and perpendicular to L1.

We compare the deep seismic images of the Redbank Thrust Zone in widely separated localities that have significant differences in surface geology. The north-south profiles show that there is a significant along-strike continuity of the Redbank Zone, and confirm our earlier interpretation that the Redbank Zone represents a 'thick-skinned' crustal penetrating fault. In addition, the new seismic section provides supporting evidence that the Redbank Thrust Zone is the dominant structure, and other faults like the Ormiston Nappe Thrust Zone are secondary faults.

The new deep seismic data also remove any suspicion that artifacts of processing or any other seismological phenomenon could satisfactorily explain the bands of seismic energy previously interpreted as steeply-dipping reflections on L1.

Geology of the Arunta Block

The Arunta Block is a region of exposed Proterozoic crust that has been interpreted as a major ensialic mobile belt (Shaw & others, 1984; Stewart & others, 1984). It has been divided into three tectonic provinces, the Northern and Central Provinces, to the North of the Redbank Thrust Zone, and the Southern Province, to the south (Fig. 1). Each has undergone a separate history of deformation and metamorphism.

A pervasive north-dipping fabric extends into the Central and Northern Provinces, where planar north-dipping structures have been imaged. These structures correlate with inferred faults and can be traced to depths of 30 to 35 km, at which point they appear to sole at the crust-mantle boundary (Goleby & others, 1989).

Near profile L1, the Southern Province comprises amphibolite facies quartzofeldspathic and migmatitic gneiss and minor potassic anatectic granitoid, whereas the Central Province consist mainly of hypersthene-bearing augen gneiss, migmatitic and quartzofeldspathic gneiss and felsic granulite (Fig. 2; Shaw, 1987; Glikson, 1987).

Near profile L2, migmatitic and quartzofeldspathic gneiss occurs in the Southern Province, while the rocks of the Central Province are predominantly mafic and minor felsic granulite (Fig. 3; Shaw, 1987; Glikson, 1987).

The Redbank Thrust Zone

The Redbank Thrust Zone itself is an east-west trending zone 7–10 km wide, of anastomosing mylonites, outcrops of which dip north at about 45° (Shaw, 1987). It forms the boundary between the Central and Southern Provinces. The

[1] Present address: Centre for Earth Resources Research, Department of Earth Sciences, Memorial University of Newfoundland, St. John's, Newfoundland A1B 3X5, Canada
[2] Australian Geological Survey Organisation, GPO Box 378, Canberra ACT 2601
[3] Research School of Earth Sciences, Australian National University, GPO Box 4, Canberra ACT 2601

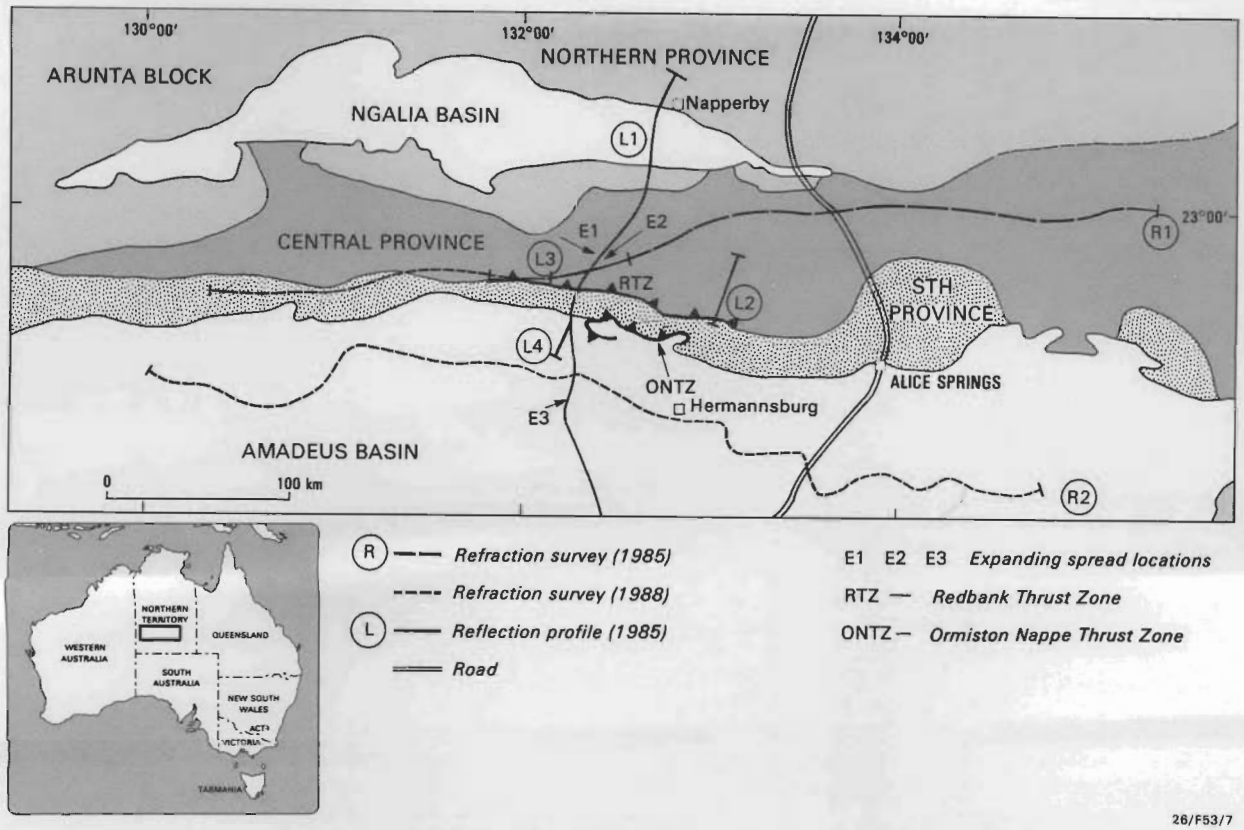

Figure 1. Location of seismic reflection (L1, L2, L3 and L4), refraction profiles (R1, 1985, and R2, 1988), expanding spreads (E1, E2 and E3), Redbank Thrust Zone and Ormiston Nappe Thrust Zone.

structure of the Zone near L1 is particularly complicated (Fig. 2), with the strike of the thrust structures deviating locally from the regional west-northwesterly strike evident on maps of the surface geology (Fig. 2; Glikson, 1987, fig. 2; Shaw & Black, 1990, figs 3, 5). Near L2, the structure of the Zone is much simpler (Fig. 3), with the main thrust mapped as a single structure separating gneissic material of the Southern Province from the granulites of the Central Province.

Shaw (1987), Shaw & Black (1991) and Shaw & others (in press) have suggested that, based on Rb-Sr and $^{40}Ar/^{39}Ar$ isotopic data and metamorphic history, the crustal blocks north and south of the Redbank Thrust Zone evolved independently until 1450 Ma and possibly until 1100 Ma. They interpret the Redbank Thrust Zone as a major Proterozoic crustal province boundary (but not necessarily a boundary between ancient microcontinents separated by oceanic crust) which has been reactivated during the Alice Springs Orogeny (300–400 Ma). More recent geochemical and U-Pb geochronological data support the notion of a major province boundary at the Redbank Thrust Zone (Black & Shaw, 1992).

Seismic data acquisition and processing

Seismic acquisition

The deep seismic reflection data for all profiles were collected using the common mid-point (CMP) seismic technique. Data were recorded on a 48-channel system to 20 s two-way time at a 2 ms sample rate from buried explosive sources (Goleby & others, 1988; 1990).

To maximise the chance of imaging all structures within the Arunta Block crust, L1 was recorded using a conventional approach, involving a symmetric split and moderate (2 km) shot-to receiver offsets.

Recording parameters for L1 were chosen to focus energy on the Redbank Thrust Zone, and designed, using the information obtained from L1, to record energy from the northerly dipping structures known to dominate the surface geology. Therefore, the recording geometry was an asymmetric split spread with the shot closer to the northern end of the spread. This spread did not preclude imaging sub-horizontal reflectors but was not optimal for imaging deeper south-dipping structures; though shallow south-dipping structures would be imaged. Although the resulting section shows a predominance of northerly dipping structures in the Central Province, the asymmetrical recording configuration showed no dramatic improvement in reflector clarity over the section obtained for L1 by the conventional symmetric split spread.

The same processing sequences were used for L1 and L2. For both profiles, it was important to compute accurate refraction statics, using first break times because of the marked variations in weathering and overburden thicknesses. The refraction statics technique used was based on a modification of the reciprocal method (Hawkins, 1961) in the manner described by Taylor (1988). Other stages in the processing of final seismic sections have been described by Goleby & others (1988; 1990), noting that the median stack gave a clear section for L2, just as it had for L1.

All sections were migrated; however because of the short reflector lengths, the results were difficult to reproduce as figures. Instead, line drawing representations of the seismic section were generated and line-migrated for interpretation and display purposes.

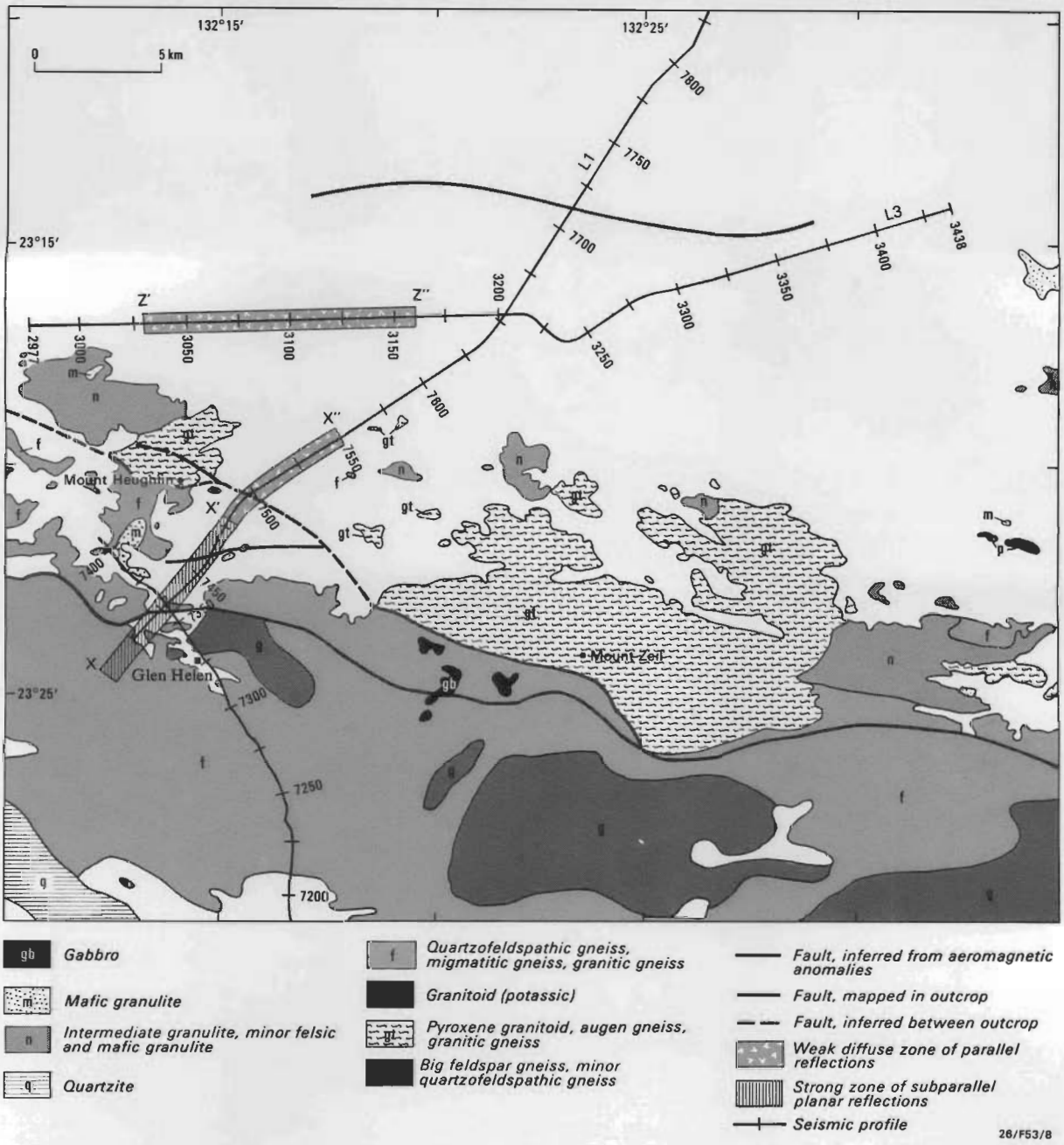

Figure 2. Simplified geology (after Shaw 1987) in the vicinity of L1 and L3
Expanding reflection spreads E1 and E2 extended from stations 7421 to 7882 and from 2977 to 3438, respectively.

Reflection character of the Redbank Thrust Zone and related faults

L1 data revisited

The strongest band of sub-parallel planar reflections has an apparent dip of 35°–40° and projects to the surface between station 7478 and the southern end of L1 (Fig. 4, X-X'), a width of 8 km. These points are displaced slightly to the south of two major fault traces of the Redbank Thrust Zone inferred from geological mapping of surface outcrop (Fig. 2, X-X'). The southernmost part of this band of reflectivity may therefore be associated with splays off the Redbank Thrust Zone, which have been mapped south of the main thrust zone in this region.

A more diffuse band of parallel reflections (Fig. 4, X'-X") defines a similar zone which projects to the surface about 6 km north of the stronger band of reflectivity (Fig. 2, X'-X"), making a total surface width of the Redbank Thrust Zone along the seismic section of about 14 km.

The westward equivalent of Ormiston Nappe Thrust Zone is imaged as a diffuse band of reflections dipping at about 15° (Fig. 4; Goleby & others 1989). This band starts at about 2.5 s at the southern end of the section and merges with the Redbank Thrust Zone at 4–5 s (12–15 km depth, Fig. 4).

The L1 section shows a zone of increased reflectivity below the Ormiston Thrust Nappe Zone from about 6.2 s to 10.0 s

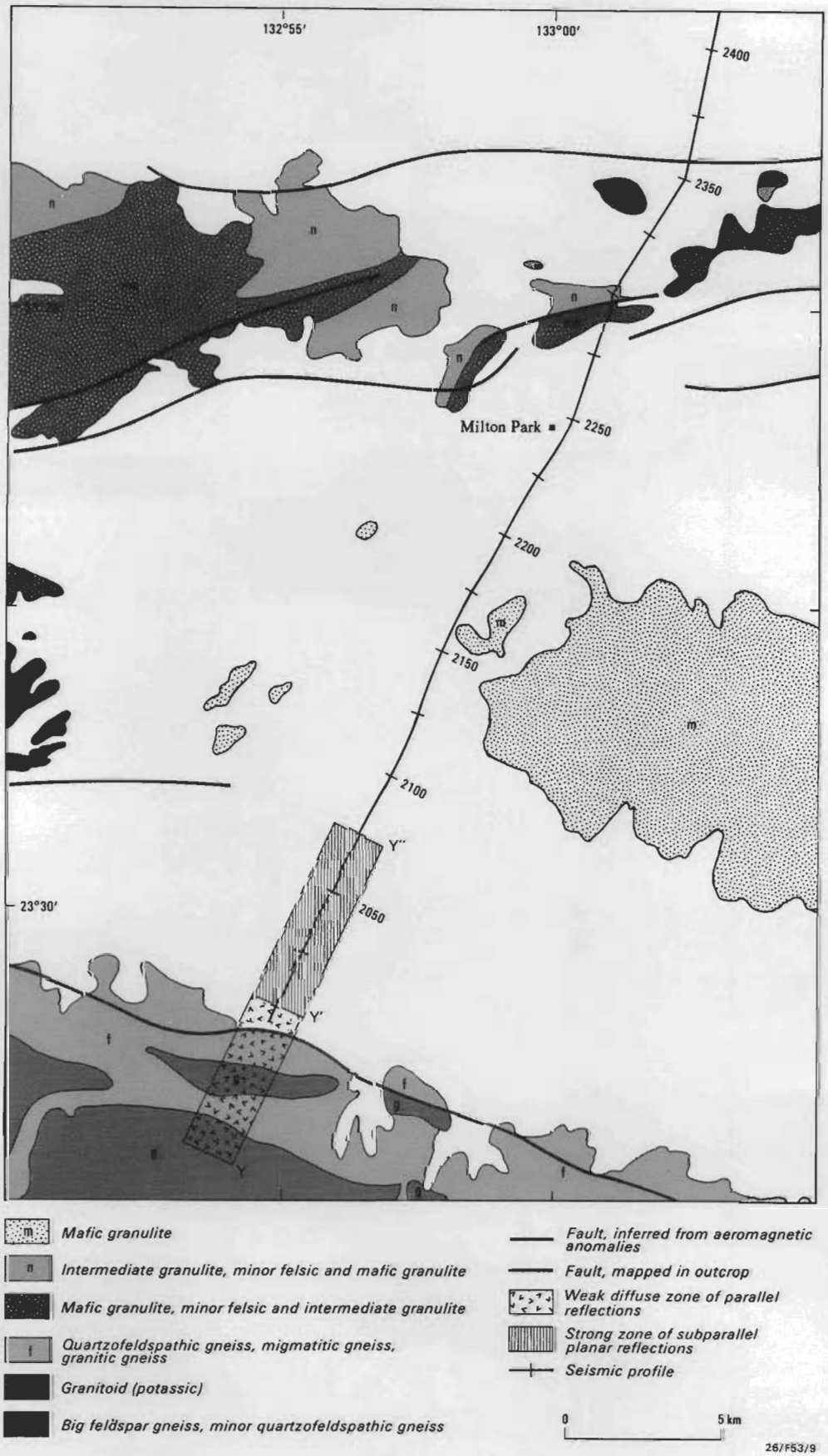

Figure 3. Simplified geology (after Shaw, 1987) in the vicinity of L2.

(Figs 4, 5a) with a small apparent dip to the north. This reflection band continues northwards to station 7550, where reflections from the Redbank Thrust Zone merge.

Although particularly strong between 7 and 10 s in the southern region, crustal reflectivity continues to about 16.5 s (50 km depth; Figs 4, 5a). This region of strong, high density, short sub-horizontal reflectors is limited to the Southern Province and extends northwards to the Redbank Thrust Zone. These sub-horizontal reflections are truncated against the downwards extension of the Redbank Thrust Zone to well below 35 km which, with the depth of these reflection further south, suggests the Redbank Thrust Zone extends down to 50 km, the base of the crust. The fault mapped in outcrop as the main trace of the Redbank Thrust Zone (Fig. 3, Y'). More diffuse reflections can be traced south of and sub-parallel to the main region of strong reflectivity. These disappear south of a band of reflections that projects to the surface for about 4.5 km south of the end of L2, giving a total surface projection nearly 11 km wide, associated with the upward continuation of reflectivity (Fig. 6).

Splays off the Redbank Thrust Zone have been mapped south of the Zone in this region. L2 runs almost parallel to the local dip of the Redbank Thrust Zone which, at this point (Fig. 3), has a much simpler outcrop geometry than near L1. However, the similarity of the two seismic profiles

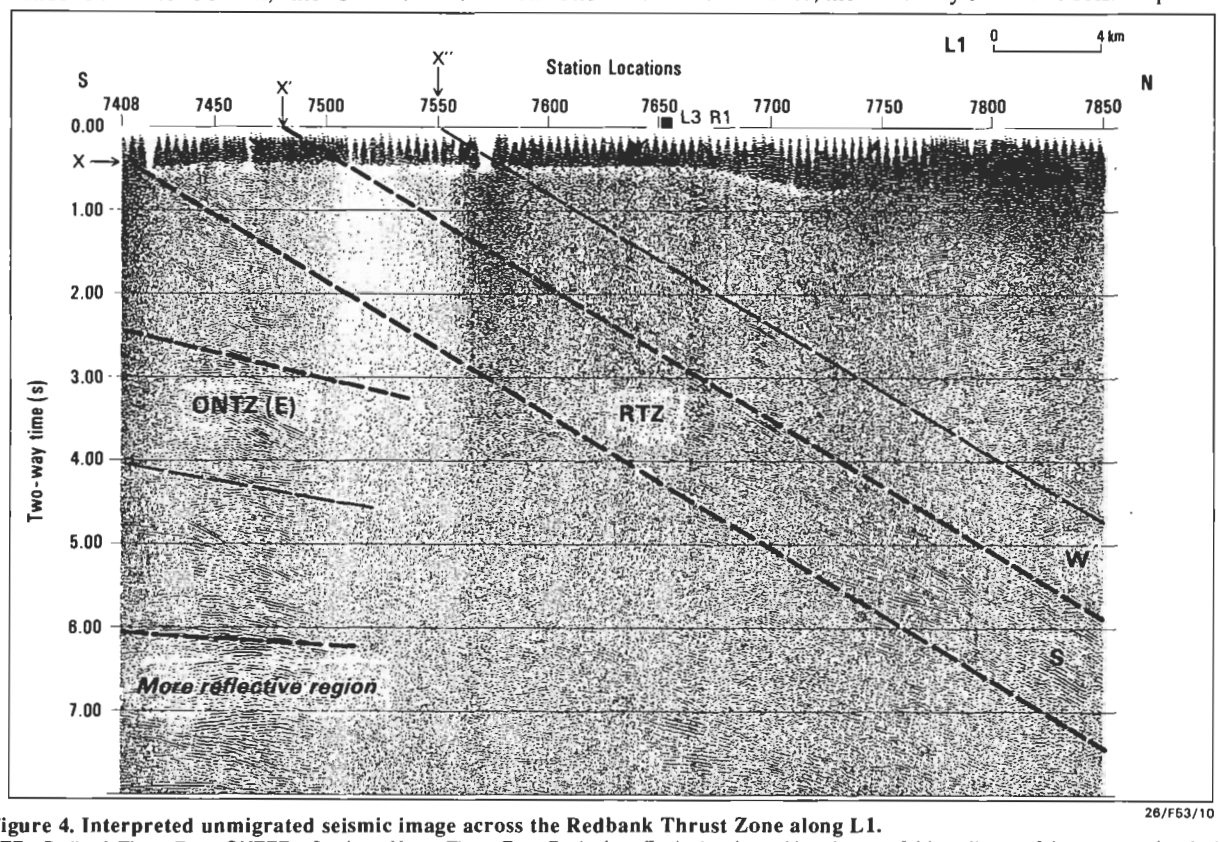

Figure 4. Interpreted unmigrated seismic image across the Redbank Thrust Zone along L1.
RTZ = Redbank Thrust Zone; ONTZE = Ormiston Nappe Thrust Zone Equivalent. Equivalent is used here because L1 is well west of the area associated with the ONTZ (see Fig. 1). The stronger dashed lines enclose the region of moderate to strong reflectivity (S) with weak to moderate reflectivity (W) above.

interpretation that the base of the reflective region is the crust-mantle boundary is in reasonable agreement with the results of the 1985 long-range seismic refraction survey (Figs 1, 2) which indicates an average crustal thickness of at least 50 km (Wright & others 1990b).

No reflections have been recorded from an inferred fault located north of station 7700 (Fig. 2), whose presence has been determined from aeromagnetic anomalies (Shaw, 1987).

L2 data

The reflection data from L2 (Fig. 6), although some 70 km east of L1, are remarkably similar to those on L1. In L2, the reflections associated with the Redbank Thrust Zone have an apparent dip of 35°–40°, and are imaged to depths of about 20 km at the northern end of the profile. The region of strong reflectivity projects to the surface over about 6 km (Fig. 6, Y'-Y''); its northern boundary (Fig. 3, Y'') corresponds closely to a fault buried beneath overburden, whose presence is inferred from aeromagnetic anomalies, and its southern boundary corresponds closely to a major gives no indication of differences in deep structure, suggesting that the near-surface complexities near L1 may be a relatively localised shallow phenomenon.

The band of strong sub-horizontal reflectivity on L2 associated with rocks of the Southern Province (Figs 5b, 6) starts at about 5.8 s, which is rather shallower than on L1, and also has a small northerly component of dip. The particularly strong band of reflectivity between 8 and 10 s can be traced to station 2300 (Fig. 5b). Reflectivity can be traced to about 16 s at the southern limit of the line (48 km) and to about 16.5 s (50 km) at station 2170 (Fig. 5b). There is also a band of dipping reflections starting at about 3 s below the southern end of L2 which is associated with the Ormiston Nappe Thrust Zone (ONTZ in Fig. 1).

L3 data

The short east-west seismic line L3 intersects L1 at station 7652 (3208 on L3; Fig. 2). On L3 there is a strong band of easterly-dipping reflections (Reflective Zone, Fig. 7) that start at about 0.7 s and extends to at least 4 s at the eastern end of the profile. The top of this band projects to the

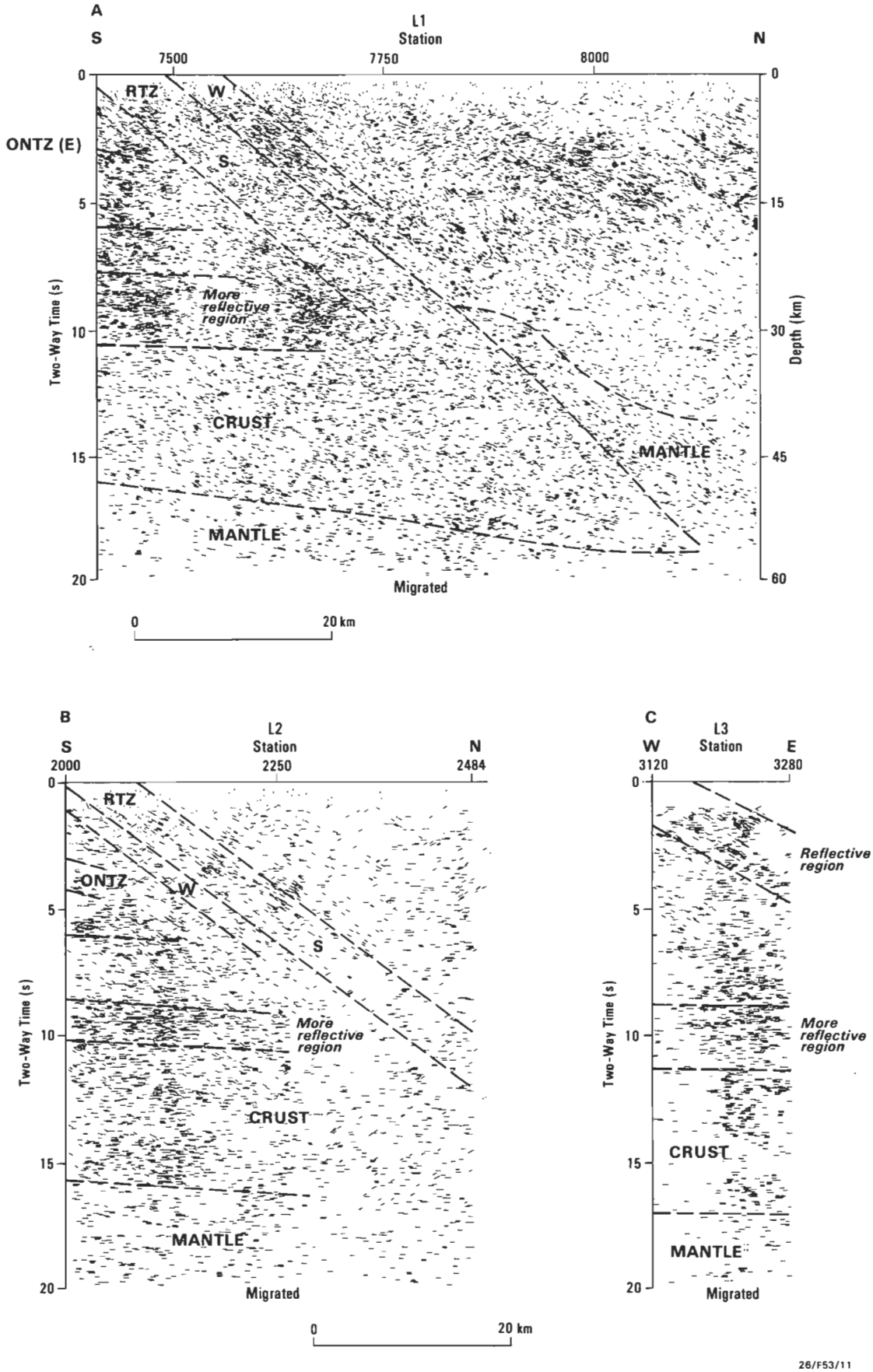

Figure 5. Migrated computer-generated line diagrams for the seismic sections: A - L1, B - L2, C - L3
RTZ = Redbank Thrust Zone; ONTZ = Ormiston Nappe Thrust Zone; ONTZE = Ormiston Nappe Thrust Zone Equivalent. S = moderate to strong reflectivity; W = weak to moderate reflectivity.

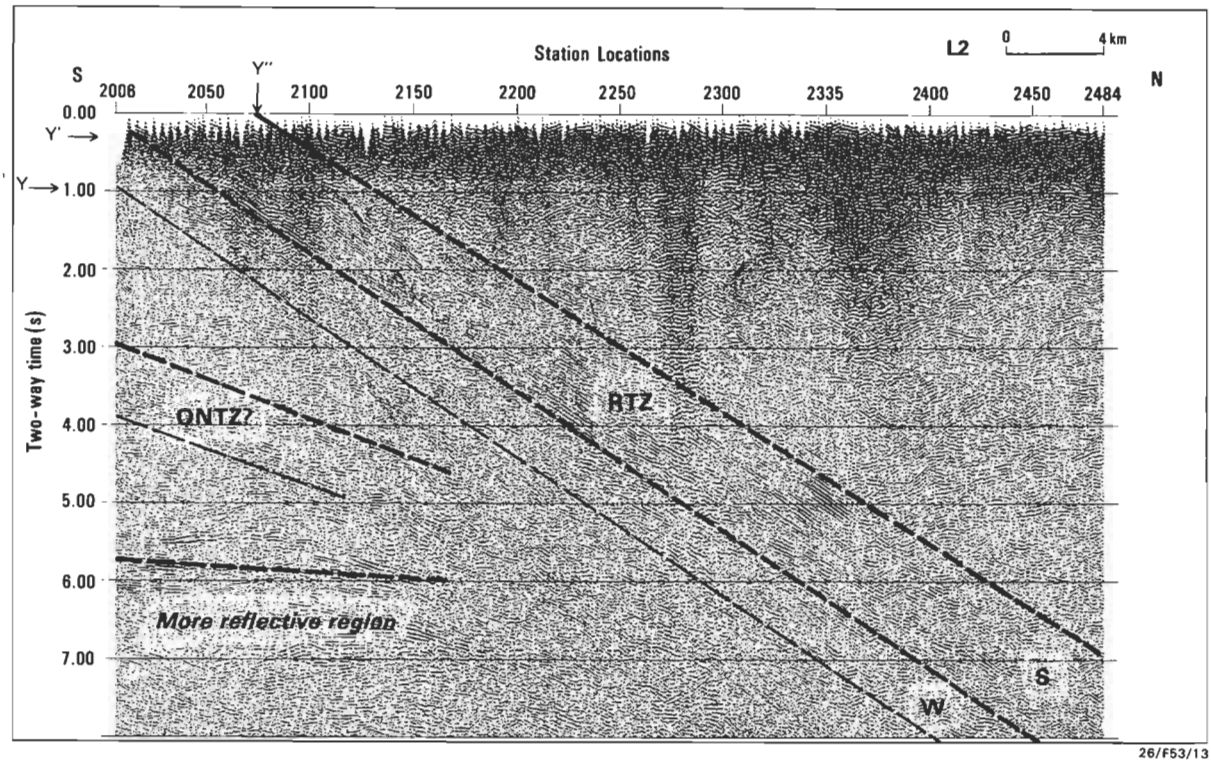

Figure 6. Interpreted unmigrated seismic reflection image near the Redbank Thrust Zone along L2
RTZ = Redbank Thrust Zone; ONTZ = Ormiston Nappe Thrust Zone. The stronger dashed lines enclose the region of moderate to strong reflectivity (S) with weak to moderate reflectivity (W) below.

surface at station 3160 (Fig. 7, Z''). These reflections cannot be correlated with those of L1, but define structures which are covered by alluvium and aeolian sand well north of the Redbank Thrust Zone. This alluvium is seen on L1 as a zone of the dark zone of reflections from the surface to between 0.4 and 1.0 s (Fig. 4).

The band of particularly strong reflectivity seen on L1 and L2, occurs on L3 as a horizontal zone between 8 and 12 s (Fig. 5c). Redbank Thrust Zone reflections are obscured by the dipping reflections from the alluvium, but can be seen as disjoint sub-horizontal reflections between 1.5–4 s (Fig. 7).

Causes of Arunta Block reflectivity

It has been shown that major fault zones can produce significant reflectivity. For example, Fountain & others (1984) and Jones & Nur (1984) used synthetic seismograms computed from models based on the physical properties of mylonites to show that mylonites, which tend to be more anisotropic than the protolith, can explain reflectivity from fault zones.

The data from both L1 and L2 clearly image major faults and shear zones. But what are the causes of the higher reflectivity at depth? It may be related to structures in the source region of doleritic dykes seen in the surface geology of the Southern Province, the Stuart Dyke Swarms (south of L2 of Fig. 1). The thermal event which produced these dykes, at about 900 Ma (Black & others, 1980), could also have produced deeper crustal sills.

Mafic intrusions may also have accompanied the Ormiston Tectonothermal Event (Black & Shaw, 1992; Shaw & others, in press), which affected the Southern Province at about 1100–1200 Ma. This event is characterised by high temperature, low pressure metamorphism (Shaw & Black, 1991). The Mordor Igneous Complex (~1150 Ma) was possibly generated by remelting of the lower crust during the Ormiston Event (Shaw & others, 1984; Shaw & Black, 1990; Langworthy and Black, 1978). The Sm-Nd systematics of the Mordor Complex indicate that the magmas were derived from a crustal source formed at about 2000 Ma, 850 million years earlier (Nelson & others, 1989).

Another possibility is that this highly reflective zone, with interval velocities as high as 7.8 km/s, may represent a layered mafic igneous complex like the Giles Complex in the Musgrave Block. Mafic sills have generated similar bands of reflections in other parts of the world (e.g. Litak & Hauser, 1992). Mafic intrusions therefore provide our preferred explanation of the increased reflectivity that is associated with higher seismic velocities and reflectivity at depths greater than 20 km south of the Redbank Thrust Zone.

We suggest that one or both of these tectonic events at 900 Ma and 1100–1200 Ma resulted in the emplacement of prominent sills between about 24 and 30 km depth, and are now the cause of the sub-horizontal reflectivity seen only in the Southern Province.

Evidence from other seismic profiling

Supporting evidence for the unique seismic character of this region is provided by expanding spread refraction analysis and long-range seismic refraction profiling.

The two expanding spreads E1 and E2 (Fig. 1) on lines L1 and L3 respectively were recorded using the shot-receiver configuration of Musgrave (1962) to maximum offsets of 36 km, and show regions of increased reflectivity corresponding to vertical reflection times between 8.7 and 10.7 s. E1 and E2 have a common mid-point at the intersection of L1 and L3.

The reflectivity imaged is associated with the deeper parts of the Southern Province beneath the Redbank Thrust

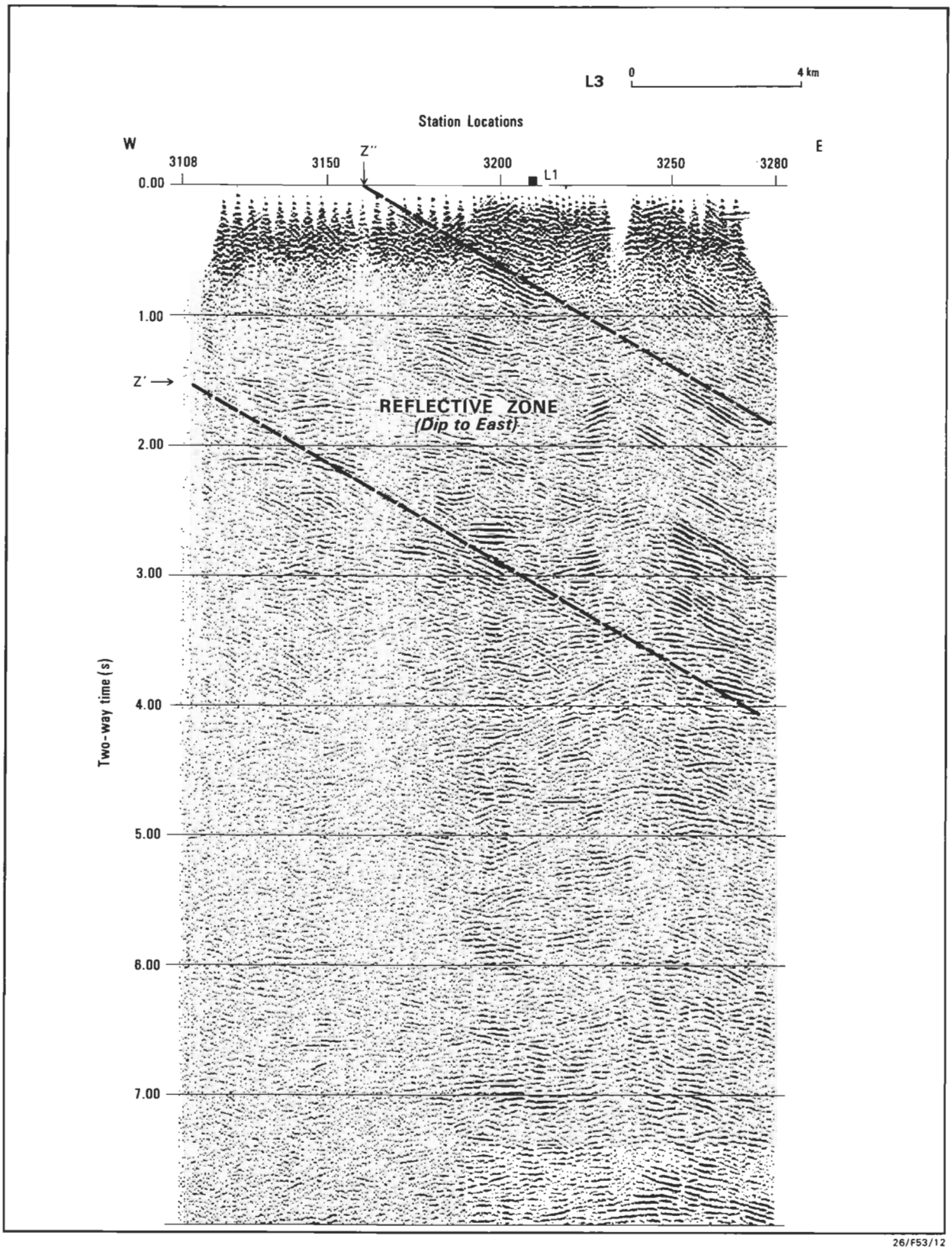

Figure 7. Interpreted unmigrated seismic reflection image near the Redbank Thrust Zone along L3.
L1 = intersection with L1.

Zone, even though the shots and receivers are located on the Central Province. The interval velocity for this more reflective region is 7.8 km/s (depths 27.5–34.3 km), implying the presence of ultramafic material, although this velocity is not tightly constrained given the methodology. The expanding-spread analysis for the overlying crustal section has a velocity close to 6 km/s (Wright & others, 1990a). The coincident long-range seismic refraction profile indicates an increase in seismic velocity to about 7.2 km/s at about 30 km depth for a broad region in the

general vicinity of L1 and L3 (Wright & others, 1990b), in satisfactory agreement with the expanding spread results.

The region of increased reflectivity observed on the expanding spreads is evident in the coincident near-vertical incidence reflection profiles of L1 and L3 (Figs 4, 7), but becomes more clearly defined farther south. The reason for the fading of the more reflective region is probably the greater thickness of Tertiary and Quaternary sands and gravels that occurs just north of the surface exposure of the Redbank Thrust Zone, making seismic energy generation and propagation less efficient. However, the region of increased reflectivity detected on the expanding spreads is readily associated with the increase in reflectivity between 8 and 10 s (about 2 km shallower) observed at the southern end of L2 (Fig. 2).

Gravity constraints and crustal models

In the region where L1 crosses the Redbank Thrust Zone, the Zone shows marked local variations from its prevailing west-northwesterly strike. While the surface geology shows granulite-facies gneiss to the north of the thrust zone, the observed and computed gravity anomalies indicate that high-density rocks can be linked to rocks exposed at the surface (Lambeck & others, 1988; Goleby & others, 1989). This suggests that mafic granulite with relatively high seismic velocity (~6.8 km/s; Shaw, 1987), seen in outcrop both northeast of L1 and north of L2, also occurs on the hanging wall of the main part of the thrust zone immediately below both L1 and L2, and gives rise to the strongest band of reflections seen on L1 and L2 (Figs 4–6).

The deep seismic data favour a tectonic model in which the major deformation within the Arunta Block occurred along faults and shear zones that extend from the surface to the crust mantle boundary, with the Redbank Thrust Zone acting as a major crustal shear and upthrusting lower crustal material to the surface. This model is supported by geological, gravity and teleseismic models (Forman & Shaw, 1973; Shaw, 1987; Lambeck & others, 1988). The data from L2 provide supporting evidence that the Redbank Zone is the major structural feature in the region and that it persists as a planar structure to depths well below 20 km.

L2 is very close to the 'Redbank' line of seismic recorders of Lambeck & others (1988), which produced a similar teleseismic travel-time anomaly to that recorded along the 'Arunta' line (Lambeck & others 1988) close to L1. Thus the planar geometry of the thrust zone along L2 can also be associated with an offset in the Moho of about 20 km, similar to that inferred along L1 (Lambeck & others, 1988; Goleby & others, 1989).

Crustal blocks of different geological composition and structure may be deduced from the pronounced change in reflection character. For example, the reflection character changes from relatively steeply-dipping reflections (apparent dips ~30–35°) north of the Redbank Thrust Zone to sub-horizontal, gently-dipping bands of reflections within the Southern Province.

Teleseismic modelling in progress at the Research School of Earth Sciences, Australian National University, also supports a major horizontal velocity inhomogeneity corresponding to the Redbank Zone. This velocity boundary extends to mantle depths and possible much deeper (H. McQueen, RSES, ANU, personal communication, 1992).

Shaw & others (in press) have used $^{40}Ar/^{39}Ar$ isotopic data to restore the section to its configuration before initiation of the Amadeus Basin. Crustal mass balancing based on this restored section is consistent with a 'thick-skinned' model and 20–30% shortening across the region of the Arunta Block between the Ngalia and Amadeus Basins (Fig. 1), including the Redbank Thrust Zone and Ormiston Nappe Thrust Zone.

In contrast, Teyssier (1985) interprets the crustal section, using surface geology, to be dominated by relatively shallow-dipping thrusts linked to a duplex complex at the surface and flattening to become sub-horizontal at the crust-mantle boundary. He estimates crustal shortening of ~50 per cent, on the basis of partial balanced sections. Our interpretation of the deep seismic results highlight several geological problems associated with Teyssier's interpretation. Firstly, because the Redbank Zone represents a major province boundary (Black & Shaw, 1992), section balancing is not possible to mantle depths. Secondly, Teyssier's model does not account for synorogenic erosion during the Alice Springs Orogeny. Thirdly, Shaw & others (1992a) have emphasised that the near-surface structure is not a simple duplex, but is an imbricate thrust fan dominated by the Ormiston Nappe Thrust Zone (Fig. 1) that splays at depth southwards from the Redbank Thrust Zone. Fourthly, recent detailed mapping indicates that the thrusts making up this fan are not simply linked along strike, as they have en-echelon segments.

Teyssier's (1985) gravity model, assuming a thrust complex whose master sole thrust flattens at depth and merges with the crust-mantle boundary, is incomplete as only half the gravity anomaly is modelled. More importantly, this model assumes that the Redbank Thrust Zone is one of several splay faults off a master sole thrust corresponding to the Ormiston Nappe Thrust Zone and, as such, is of no particular significance. The seismic data from both L1 and L2 do not support this model and indicate the Redbank Thrust Zone, not the Ormiston Nappe Thrust Zone, is the dominate structure.

Conclusions

The two north-south seismic profiles, L1 and L2, show a very similar reflection character for the Redbank Thrust Zone. In both, planar bands of reflections have an apparent northerly dip of 35–40°. Along L1 the bands are obvious to more than 20 km deep and, on the more detailed sections, they persist to at least 35 km depth. Along L2 they persist to the northern limit of the line corresponding to a depth close to 20 km (Figs 5a,b). The region of high-density, short, sub-horizontal reflectors associated with Southern Province is truncated against the Redbank Thrust Zone at depths well below 35 km, further evidence that the Redbank Zone persists as a planar structure below 35 km.

L1 and L2 indicate the Redbank Thrust Zone has remarkable lateral extension. The similarity between the two profiles and the coincidence of the surface projection of the events interpreted as reflections with the mapped exposure of the Redbank Thrust Zone strengthen the earlier interpretation of the events observed on L1 as reflections from a major Proterozoic province boundary characterised by mylonites produced by thrusting. The new results for L2, like the earlier results for L1, provide no evidence for listric geometry of the Redbank Thrust Zone deep in the crust; but strengthen the earlier interpretations for 'thick-skinned' models of tectonic evolution of the Arunta Block (Shaw, 1987; Lambeck & others 1988; Goleby & others 1989), and cast doubt on the 'thin-skinned' types of model.

Acknowledgements

We thank Barry Drummond and Alastair Stewart for critically reading earlier drafts of the manuscript and offering many suggestions for its improvement. We also thank Dr Herb McQueen and Mr Derecke Palmer for reviewing this manuscript. We also thank Lindell Emerton and Ken Barrett for drafting the figures.

References

Black, L.P. & Shaw, R.D., 1992 — U-Pb zircon chronology of prograde Proterozoic events in the Central and Southern Provinces of the Arunta Block, central Australia. *Australian Journal of Earth Sciences* 39, 153–171.

Black, L.P., Shaw, R.D. & Offe, L.A., 1980 — The age of the Stuart Dyke Swarm and its bearing on the onset of late Precambrian sedimentation in central Australia. *Journal of the Geological Society of Australia* 27, 151–155.

Forman, D.J. & Shaw, R.D., 1973 — Deformation of the crust and mantle in central Australia. *Bureau of Mineral Resources, Australia, Bulletin* 144, 20 pp.

Fountain, D.M., Hurich, C.A. & Smithson, S.B., 1984 — Seismic reflectivity of mylonite zones in the crust. *Geology* 2, 195–198.

Glikson, A.Y., 1987 — Regional structure and evolution of the Redbank-Mount Zeil thrust zone: a major lineament in the Arunta Inlier, central Australia. *BMR Journal of Australian Geology & Geophysics* 10, 89–107.

Goleby, B.R., Kennett, B.L.N., Wright, C., Shaw, R.D. & Lambeck, K., 1990 — Seismic reflection profiling in the Proterozoic Arunta Block, central Australia: processing for testing models of tectonic evolution. *Tectonophysics* 173, 257–268.

Goleby, B.R., Shaw, R.D., Wright, C., Kennett, B.L.N. & Lambeck, K., 1989 — Geophysical evidence for 'thick-skinned' crustal deformation in central Australia. *Nature* 337, 325–330.

Goleby, B.R., Wright, C., Collins, C.D.N. & Kennett, B.L.N., 1988 — Seismic reflection and refraction profiling across the Arunta Block and Ngalia and Amadeus Basins. *Australian Journal of Earth Sciences* 35, 275–294.

Hawkins, L.R., 1961 — The reciprocal method of routine shallow refraction investigations. *Geophysics* 26, 806–819.

Jones, T. & Nur, A., 1984 — The nature of seismic reflections from deep fault zones. *Journal of Geophysical Research* 89, 3153–3171.

Lambeck, K., Burgess, G. & Shaw, R.D., 1988 — Teleseismic travel-time anomalies and deep crustal structure in central Australia. Geophysical *Journal of the Royal Astronomical Society* 94, 105–124.

Langworthy, A.P. & Black, L.P., 1978 — The Mordor Complex: a highly differentiated potassic intrusion with kimberlitic affinities in central Australia. *Contributions to Mineralogy and Petrology* 67, 51–62.

Litak, R.K. & Hauser, E.C., The Bagdad Reflection Sequence as tabular mafic intrusions: Evidence from seismic modelling of mapped exposures. *Geological Society of America Bulletin* 104, 1315–1325.

Musgrave, A.W., 1962 — Applications of the expanding reflection spread. *Geophysics* 27, 981–993.

Nelson, D.R., Black, L.P. & McCulloch, M.T., 1989 — Nd-Pb isotopic characteristics of the Mordor Complex, Northern Territory: Mid-Proterozoic potassic magmatism from an enriched mantle source. *Australian Journal of Earth Sciences* 36, 541–551.

Shaw, R.D., 1987 — Basement uplift and basin subsidence in central Australia. *Ph.D. thesis, Australian National University, Canberra* (unpublished).

Shaw, R.D. & Black, L.P., 1990 — The history and tectonic implications of the Redbank Thrust Zone, central Australia, based on structural, metamorphic and Rb-Sr isotopic evidence. *Australian Journal of Earth Sciences* 38, 307–332.

Shaw, R.D., Goleby, B.R., Korsch, R.J. & Wright, C., 1992a — Basement and cover thrust tectonics in central Australia based on the Arunta-Amadeus Seismic-Reflection Profile. *In* Rickard, M.J. (editor) Basement Tectonics 9. *Klewer Academic Publishers, The Netherlands*, 55–84.

Shaw, R.D., Stewart, A.J. & Black, L.P., 1984 — The Arunta Inlier: a complex ensialic mobile belt in central Australia, part 2: tectonic history. *Australian Journal of Earth Sciences* 31, 457–484.

Shaw, R.D., Zeitler, P.K., McDougall, I. & Tingate, P.R., 1992b — The Palaeozoic history of an unusual intracratonic thrust belt in central Australia based on ^{40}Ar-^{39}Ar, K-Ar and fission track dating. *Journal of the Geological Society, London* 149, (in press).

Stewart, A.J., Shaw, R.D. & Black, L.P., 1984 — The Arunta Inlier: a complex ensialic mobile belt in central Australia, part 1: stratigraphy, correlations and origin. *Australian Journal of Earth Sciences* 31, 445–455.

Taylor, F.J., 1988 — Static corrections for land seismic processing. *Bureau of Mineral Resources, Australia, Record* 1988/49, 13p.

Teyssier, C., 1985 — A crustal thrust system in an intracratonic tectonic environment. *Journal of Structural Geology* 7, 689–700.

Wright, C., Barton, T., Goleby, B.R., Spence, A.G. & Pfister, D., 1990a — The interpretation of expanding spread reflection profiles: examples from central and eastern Australia. *Tectonophysics* 173, 73–82.

Wright, C., Goleby, B.R., Collins, C.D.N., Korsch, R.J., Barton, T., Greenhalgh, S.A. & Sugiharto, S., 1990b — Deep seismic profiling in central Australia. *Tectonophysics* 173, 247–256.

BMR Journal of Australian Geology & Geophysics, 13, 369–372

The West Tasman Sea (Flinders Island) earthquake of 14 September 1946

Marion Michael-Leiba[1] & Vagn Jensen[2]

The largest southeastern Australian earthquake this century occurred in the West Tasman Sea, 100 km east of Flinders Island, at 1948 UTC on 14 September 1946. Its epicentre was at 39.97°S, 149.35°E and its Richter magnitude ML 6.0. It was felt strongly throughout Tasmania and Gippsland, Victoria, and caused minor damage in Launceston. The isoseismal map of the earthquake is consistent with lower strong ground motion attenuation in Tasmania than in mainland southeastern Australia, and the macroseismic effects suggest amplification of seismic shaking by Tertiary lake sediments in Hobart and Launceston.

Introduction

On 14 September 1946 at 1948 UTC (Co-ordinated Universal Time) (5.48 am local time on 15 September) a large earthquake occurred in the West Tasman Sea, northeast of Tasmania, which was felt strongly and caused some minor damage. The event, which also woke people in Victoria, is the largest this century in the West Tasman Sea Zone (Michael-Leiba & Gaull, 1989). Around 2000 events in the zone were felt in northeastern Tasmania or the islands off the coast from 1883 to 1892 (Ripper, 1963). Several had magnitudes exceeding ML 6.0, were felt in Victoria and did damage in Launceston (Michael-Leiba, 1989a). This century, activity in the zone has declined and only four events have had magnitudes of ML 5.0 or greater (Michael-Leiba & Gaull, 1989). The earthquake of 14 September 1946 is not only the largest in the Zone since 26 January 1892, but also appears to be the highest magnitude event in southeastern Australia this century.

Epicentral parameters

In the International Seismological Summary for 1946 (British Association Seismological Committee, IUGG, 1955), the epicentre is given as 40.2°S, 149.0°E. This location was based on readings from 43 stations of which 29 had P and/or S residuals of 5 s or less. The maximum gap in azimuth of seismographs relative to the epicentre was 139°. The closest station used in the location was Riverview (Sydney, NSW) at an epicentral distance of 6.6°. The event was very widely recorded, and P and/or S residuals of 5 s or less were obtained from stations as far away as Riverside (California, USA), Moscow (Russia), Rome (Italy), Paris (France) and Toledo (Spain), the most distant seismograph with an epicentral distance of 159°. The P residuals were 3 s or less at the four nearest stations: Riverview, Brisbane, Christchurch and Wellington, as were the S residuals at Riverview, Christchurch, Wellington and Auckland. The origin time was 19 hr 48 min 42 s.

The earthquake was also recorded on the Milne-Shaw E-W component seismograph at Melbourne (Victoria), the closest station, at an epicentral distance of 4.0°, so a relocation was done using program EQLOCL written by staff of the Seismology Research Centre, Royal Melbourne Institute of Technology, with a southeastern NSW crustal model out to 600 km with a spline fit to the Jeffreys-Bullen tables. The program uses P and S waves only for distances beyond about 1000 km and up to 101°. The P and S arrival times from Melbourne, Riverview, Christchurch and Wellington, the Brisbane P, and the Auckland and New Delhi S were used in the location. The Brisbane S, Auckland P and Suva P and S were deferred because their residuals were greater than 10 s. The epicentral coordinates obtained were 40.07°S, 149.30°E, and the residuals of the readings used were 4 s or less. The origin time was 19 hr 48 min 49 s with an uncertainty of 13 s.

The two epicentres are very close, ours being 29 km ENE of the International Seismological Summary's. However, the maximum gap in azimuth relative to the epicentre is 193° for the seven stations used in the EQLOCL location. The International Seismological Summary's epicentre lies within the error ellipse of this solution for which the uncertainty in easting is 30 km, in northing 56 km and in origin time 13 s.

A relocation was also done with the Melbourne arrival times and ISS data having residuals of 5 s or less. The program was written by Ken Muirhead (AGSO) and uses Jeffreys-Bullen tables. The epicentre, based on 25 stations with a gap of 169 and maximum residual 5.3 s, is (39.97±0.21)°S, (149.35±0.15)°E and the origin time is 19 hr 48 min (50.1±0.6) s. The Muirhead epicentre is 39 km northeast of the International Seismological Summary epicentre. All three epicentres are shown in Figure 1 but we prefer the Muirhead solution.

Magnitude

The Riverview College Observatory (RIV) Seismological Bulletin recorded a maximum vertical ground amplitude for SN of 16 μm at a period of 2.5 s. This gives a magnitude ML 5.5 using Michael-Leiba & Malafant's (1992) southeastern Australian attenuation.

The Milne-Shaw seismograph at Melbourne (MEL) recorded a maximum trace amplitude of 70.8 mm (zero-to-peak) at a period of 1.5 s. The magnification of the instrument at this period is 250, giving a ground motion amplitude of 283 μm and a magnitude ML 6.4 using Michael-Leiba & Malafant's (1992) attenuation.

The duration of the vibrations on the Milne-Shaw measured from the onset to when the oscillations on the record decay to double the background level is 2914 s, which gives a duration magnitude MD 6.2, using the formula $MD = 2.1 \log\tau + 0.0009\Delta - 1.52$, where τ(s) is duration and Δ(km) is distance. This formula is used routinely by the Australian Seismological Centre.

From the isoseismal map (Fig. 1). the intensity-based magnitudes measured from the MM III (McCue, 1980) and IV (Michael-Leiba, 1989b) isoseismals are ML(I) 6.1 and ML(IV) 6.4. The MM III and IV isoseismals are close together. This may be because the former is poorly

[1] Australian Seismological Centre, Bureau of Mineral Resources, GPO Box 378, Canberra ACT 2601
[2] Geology Department, University of Tasmania, GPO Box 252C, Hobart TAS 7001

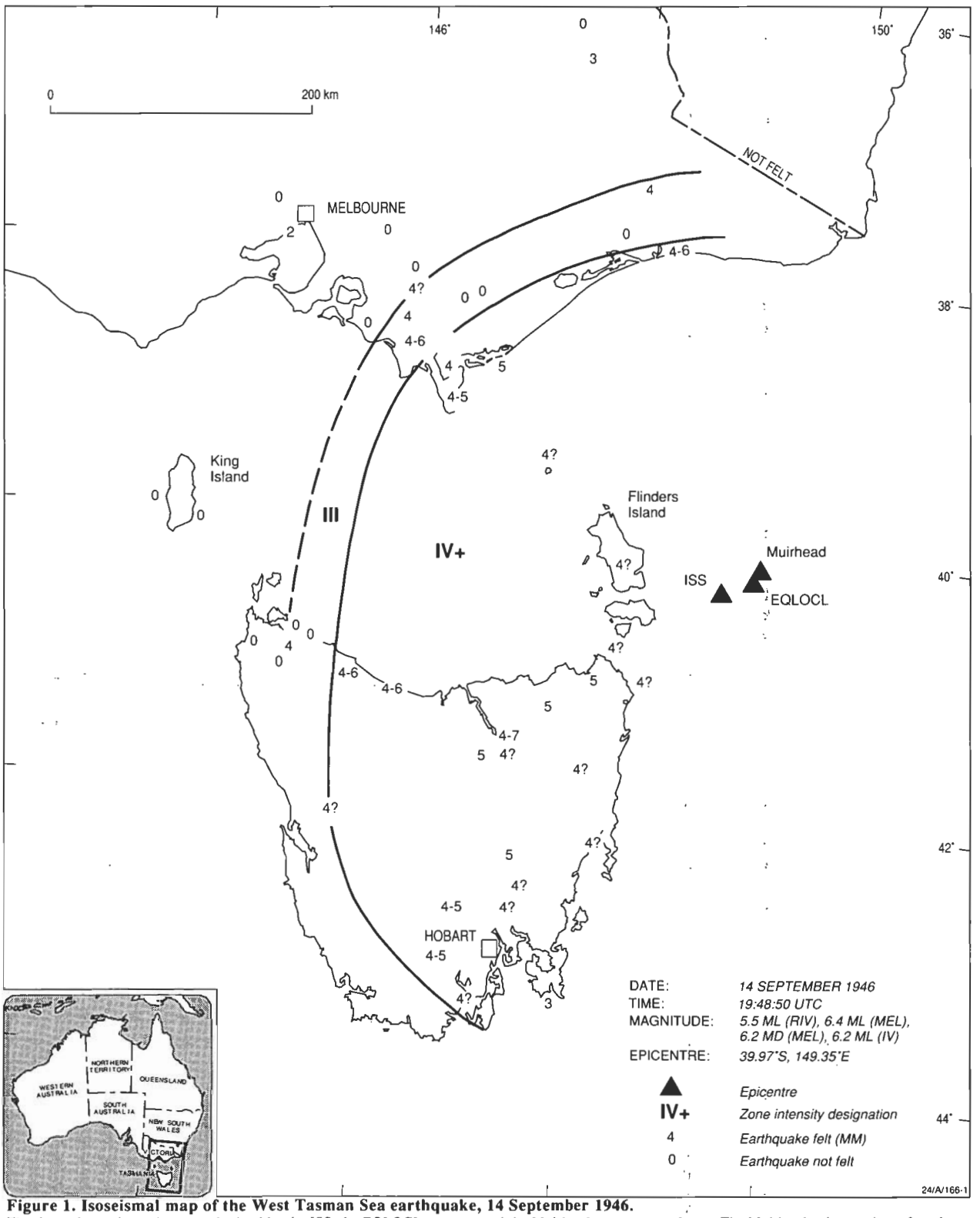

Figure 1. Isoseismal map of the West Tasman Sea earthquake, 14 September 1946.
The three alternative epicentres obtained by the ISS, the EQLOCL program and the Muirhead program are shown. The Muirhead epicentre is preferred.

constrained due to the early hour of the earthquake and the absence of felt reports from Bass Strait and the Southern Ocean, and the Tasmanian part of the latter is uncertain because of the lack of detail in some of the felt reports in newspapers. In the Discussion, we propose that ground motion attenuation may be lower in Tasmania than in mainland southeastern Australia. This could mean that the magnitude was overestimated, so separate measurements were made using only the Victorian part of the isoseismals. These gave magnitudes of ML(I) 6.1 and ML(IV) 6.2. As the MM IV isoseismal is better constrained in Victoria, ML(IV) 6.2 is the preferred intensity-based magnitude. The

figure of 6.1 obtained for ML(I) is probably a minimum value.

The preferred estimates of the local magnitude are ML 5.5 (RIV), ML 6.4 (MEL), MD 6.2 (MEL) and ML(IV) 6.2. Their mean is (6.1±0.4) but, as the first three were rounded up, we assign a magnitude ML 6.0 to the earthquake. This makes it the largest event recorded in southeastern Australia this century. The second largest ones were of magnitude ML 5.6 and included the 1989 Newcastle earthquake. The other three were in the West Tasman Sea (1929), Dalton-Gunning, NSW (1934) and Robertson-Bowral, NSW (1961).

Macroseismic effects

The isoseismal map (Fig. 1) and the description of the effects of the earthquake are based on contemporary newspaper reports and lighthouse logs. The sources are The Mercury (Hobart), The Examiner (Launceston), The Advocate (Burnie), The Circular Head Chronicle, The King Island News, North Eastern Advertiser (northeast Tasmania), Foster Mirror, Omeo Standard, Morwell Advertiser, Leongatha Echo, The Star (Moe), Upper Murray & Mitta Herald, The Powlett Express (Wonthaggi), The Warburton Mail, The Warragul Guardian, The Sydney Morning Herald, The Age (Melbourne), The Argus (Melbourne), and lighthouse logs from Swan Island, Maatsuyker Island, Low Head, Eddystone, Cape Sorell, and Tasman Island.

The earthquake was felt strongly throughout Tasmania and in Gippsland, Victoria. It was accompanied by a low rumbling sound. The shaking was variously estimated to have lasted between 20 and 50 seconds.

Where intensities have been marked with a question mark in Figure 1, the newspaper reports were not specific about the felt effects.

As with other large events in the West Tasman Sea (Michael-Leiba, 1989a), the highest intensities and most damage were recorded in Launceston, where the earthquake broke windows and crockery and cracked plaster in some buildings. Two hotels were affected. Wireless poles swayed and buildings were seen to rock.

The Mercury of 17 September 1946 said of the Rosevears Hotel in Launceston that

> It would be necessary to plaster walls split by the shock, but foundations were not seriously affected ... The front entrance was damaged, part of the staircase torn away, and the bannister broken from the wall. Four rooms were damaged and some crystal goblets broken.

The Examiner of 16 September 1946 stated that:

> The only injury reported in Launceston was suffered by John Tipping, whose left leg was bruised when plaster from the ceiling above his bed in the Court House Hotel, Paterson Street, fell on him during the tremor. The fallen plaster left a bare patch on the ceiling 5ft. long and 18in. wide. The piece which struck Tipping was 18in. long and a foot wide and weighed about 40 lb. He said yesterday that he owed his escape from serious injury to the fact that he was awake when the tremor began and saw the plaster falling. He jumped from the bed and the plaster struck him only a glancing blow. Mr. E. Lee, who occupies the next room to Tipping, said 'If the plaster had struck Tipping a direct blow, it would certainly have broken his leg. I carried the piece which hit him down from the bed to the hotel yard. It weighed about 40lb. The weight falling from the 9ft. high ceiling would be sufficient to kill a man if it hit him on the head'. A woman living at 96 York St. was thrown out of bed but was uninjured by the fall.
>
> The tremor caused one of the relay bells at the Launceston fire station to ring. Fireman A. Neville, one of the four men on duty at the time, said the station shook so violently he thought it was 'falling to bits.' He said the trestle beds in the dormitory at the station were shot back and forth by the force of the tremor.

In Hobart, there were reports of four distinct rocking motions from north to south, gradually increasing in intensity. Although many parents said that children were terrified when the houses shook, there was no damage reported.

In the North West Coast district of Tasmania, household crockery and fragile ornaments which fell during the earthquake were broken.

In northeastern Tasmania, the North Eastern Advertiser of 17 September 1946 noted that the tremor 'was probably the most severe disturbance recorded in the district, but only slight damage to property has been reported'. There was mention of houses rocking and the earthquake sounding like loud rumbling.

The event is said to have woken thousands of people in Gippsland, Victoria, where it was felt from Orbost to Leongatha. In Foster, the earthquake had caused crockery to fall off shelves in some houses and had made the police station grandfather clock, which was not going, chime. A few ornaments and crockery items in houses were damaged in Orbost where the tremor was accompanied by a roaring sound. No building damage was reported in Gippsland.

The earthquake was also felt slightly at Mitta Mitta in northeastern Victoria and at the breakwater pier off Williamstown, and the 18 m high Harbour Trust observation tower at the entrance to Victoria Dock, just southwest of Melbourne city, shook violently twice as though a large ship had bumped the wharf heavily. There were no other Melbourne reports. These are the northernmost and westernmost locations in Victoria which reported that the earthquake was felt.

Discussion

Figure 1 and the above reports show that the most damage was experienced in Launceston, 210 km from the epicentre. Launceston has been damaged also by earthquakes in the West Tasman Sea on 13 July 1884, 12 May 1885, 26 January 1892 (Michael-Leiba, 1989) and 28 December 1929 (UTC dates). Michael-Leiba & Gaull (1989) attribute the relatively high level of earthquake damage there to local site effects due to ground motion amplification by Tertiary lake sediments up to 200 m thick. A similar situation appears to exist in Hobart. The Advocate of 16 September 1946 reported that 'in Hobart the tremor was most marked in the Sandy Bay area and least of all at North Hobart and New Town'. It is significant that Sandy Bay is predominantly underlain by Tertiary lake sediments whereas at North Hobart and New Town the foundation is mainly Triassic quartz sandstone or lithic arkose and lutite

(Leaman, 1972).

The MM IV isoseismal in Figure 1 appears to be asymmetric. One possible explanation is that the epicentre is further north than it should be, due to a paucity of seismographs to the south. However, none of the instrumental locations of events in the West Tasman Sea Zone has put an epicentre far enough south to make the contour symmetrical. The other possibility is that the ground motion attenuation in Tasmania is less than in eastern Victoria.

Michael-Leiba (1992) derived a Tasmanian attenuation formula:

$$I = 4.94 + 1.45\ ML - 3.61 \log R$$

where I is Modified Mercalli intensity, R km is hypocentral distance (assuming a focal depth of 10 km), and ML is Richter magnitude using Michael-Leiba & Malafant's (1992) formula. The attenuation is based on 29 measurements on isoseismal maps of 14 Tasmanian earthquakes, 12 of which were not West Tasman Sea events. Michael-Leiba (1992) noted that this attenuation gives intensity estimates 0.6–0.7 intensity units higher than Gaull & others' (1990) southeastern Australian formula modified for the new ML scale (Michael-Leiba & Malafant, 1992, in press). The modified southeastern Australian formula is:

$$I = 4.35 + 1.5\ ML - 3.91 \log R$$

Thus, our preferred explanation for the asymmetry in the MM IV isoseismal is that Tasmanian attenuation is indeed lower.

Conclusions

The International Seismological Summary gives the epicentral coordinates of the earthquake as 40.2°S, 149.0°E, and the origin time as 19 hr 48 min 42 s. A relocation using arrivals from 25 stations including Melbourne gives an epicentre at 39.97°S, 149.35°E and an origin time of 19 hr 48 min 50 s. This is our preferred solution. It is only 39 km northeast of the International Seismological Summary epicentre which is remarkably good considering that the International Seismological Summary had no computers for earthquake location.

Based on amplitude readings from the Riverview and Melbourne seismograms, the duration on the latter, and our preferred intensity-based magnitude, we assign a Richter magnitude ML 6.0 to the event. This makes it the largest earthquake in southeastern Australia this century.

The 1946 event is in the West Tasman Sea Zone (Michael-Leiba & Gaull, 1989), the site of high seismic activity late last century. The earthquake is the largest in the zone since 26 January 1892. While activity there has declined this century, the occurrence of a magnitude 6.0 event in 1946 suggests that similar earthquakes may occur in the zone in future.

Macroseismic observations at Launceston and Hobart suggest that local site effects are due to amplification by Tertiary lake sediments.

The asymmetry in the MM IV isoseismal may be a result of lower strong ground motion attenuation in Tasmania.

Acknowledgements

We thank David Denham, Gary Gibson, Kevin McCue and Euan Smith for critically reading the manuscript, Ken Muirhead for relocating the earthquake with his program, and Rex Bates for drafting the figure.

References

British Association Seismological Committee, IUGG, 1955 — International Seismological Summary for 1946. *Kew Observatory, Richmond, Surrey.*

Gaull, B.A., Michael-Leiba, M.O. & Rynn, J.M.W., 1990 — Probabilistic earthquake risk maps of Australia. *Australian Journal of Earth Sciences* 37(2), 169–187.

Leaman, D., 1972 — Hobart. Geological Atlas 1:50,000 series. *Geological Survey of Tasmania, Department of Mines, Hobart.*

McCue, K.F., 1980 — Magnitude of some early earthquakes in southeastern Australia. *Search* 11(3), 78–80.

Michael-Leiba, M.O., 1989a — Macroseismic effects, locations and magnitudes of some early Tasmanian earthquakes. *BMR Journal of Australian Geology & Geophysics* 11(1), 89–99.

Michael-Leiba, M.O., 1989b — Estimation of earthquake magnitude from mean MM IV isoseismal radius. *New Zealand Journal of Geology and Geophysics* 32, 411–414.

Michael-Leiba, M.O., 1992 — Attenuation of strong earthquake ground motion in Tasmania. *Geological Society of Australia, Eleventh Australian Geological Convention, Ballarat, Abstract Volume.*

Michael-Leiba, M.O. & Malafant, K., 1992 — A new local magnitude scale for southeastern Australia. *BMR Journal of Australian Geology & Geophysics* 13(3), 201–205.

Michael-Leiba, M.O. & Gaull, B.A., 1989 — Probabilistic earthquake risk maps of Tasmania. *BMR Journal of Australian Geology & Geophysics* 11(1), 81–87.

Ripper, I.D., 1963 — Local and regional events recorded by the Tasmania seismic net. *Honours Thesis, University of Tasmania.*

BMR
GEOLOGY AND
GEOPHYSICS
AUSTRALIA

CONTENTS

9 780644 263092

B92/22900 Cat. No. 93 1065 9